NASA CR-121263
AiResearch 73-9488

HIGH-TIP-SPEED, LOW-LOADING TRANSONIC FAN STAGE

(Part 3 - Final Report)

(NASA-CR-121263) HIGH-TIP-SPEED, LOW-LOADING TRANSONIC FAN STAGE. PART 3: FINAL REPORT (AiResearch Mfg. Co., Los Angeles, Calif.) 200 p HC $13.00 CSCL 21E G3/28

N74-20442

Unclas 34960

February 1974

by T.C. Ware, R.J. Kobayashi, and R.J. Jackson

AIRESEARCH MANUFACTURING COMPANY,
A DIVISION OF
THE GARRETT CORPORATION
Los Angeles, California

Prepared for

NATIONAL AERONAUTICS AND SPACE ADMINISTRATION

Lewis Research Center

Contract NAS 3-13498

1. Report No.	2. Government Accession No.	3. Recipient's Catalog No.
NASA CR-121263		

4. Title and Subtitle	5. Report Date
HIGH-TIP-SPEED, LOW-LOADING TRANSONIC FAN STAGE (PART 3 - FINAL REPORT)	February 1974
	6. Performing Organization Code
7. Author(s)	8. Performing Organization Report No.
T. C. Ware, R. J. Kobayashi, and R. J. Jackson	73-9488
	10. Work Unit No.
9. Performing Organization Name and Address	11. Contract or Grant No.
AiResearch Manufacturing Company A Division of The Garrett Corporation Los Angeles, California 90509	NAS 3-13498
	13. Type of Report and Period Covered
12. Sponsoring Agency Name and Address	Contractor Report
National Aeronautics and Space Administration Washington, D.C. 20546	14. Sponsoring Agency Code

15. Supplementary Notes

Project Manager, E. E. Bailey, Fluid System Components Division, NASA-Lewis Research Center, Cleveland, Ohio 44135

16. Abstract

Tests were conducted on a high-tip-speed, low-loading transonic fan stage to determine the performance and inlet flow distortion tolerance of the design. The fan was designed for high efficiency at a moderate pressure ratio by designing the hub section to operate at minimum loss when the tip operates with an oblique shock. The design objective was an efficiency of 86 percent at a pressure ratio of 1.5, a specific flow (flow per unit annulus area) of 42 lb/sec-ft^2 (205.1 kgm/sec-m^2), and a tip speed of 1600 ft/sec (488.6 m/sec). During testing, a peak efficiency of 84 percent was achieved at design speed and design specific flow. At the design speed and pressure ratio, the flow was 4 percent greater than design, efficiency was 81 percent, and a stall margin of 24 percent was obtained. The stall line was improved with hub radial distortion but was reduced when the stage was tested with tip radial and circumferential flow distortions. Blade-to-blade values of static pressures were measured over the rotor blade tips.

17. Key Words (Suggested by Author(s))	18. Distribution Statement
Transonic Fan Stage Low Loading, High Tip Speed	Unclassified-unlimited

19. Security Classif. (of this report)	20. Security Classif. (of this page)	21. No. of Pages	22. Price*
Unclassified	Unclassified	200	

* For sale by the National Technical Information Service, Springfield, Virginia 22151

NASA-C-168 (Rev. 6-71)

PRECEDING PAGE BLANK NOT FILMED

TABLE OF CONTENTS

TABLE OF CONTENTS (Continued)

LIST OF TABLES

LIST OF ILLUSTRATIONS

LIST OF ILLUSTRATIONS (Continued)

LIST OF ILLUSTRATIONS (Continued)

LIST OF ILLUSTRATIONS (Continued)

LIST OF ILLUSTRATIONS (Continued)

LIST OF ILLUSTRATIONS (Continued)

LIST OF ILLUSTRATIONS (Continued)

SUMMARY

A high-tip-speed, low-pressure-ratio transonic fan stage without inlet guide vanes was designed and tested to 110 percent of design speed to determine overall, blade element, and mechanical performance with uniform inlet flow, radially distorted inlet flow, and circumferentially distorted inlet flow. The design rotor relative Mach numbers were supersonic over 85 percent of the span at the inlet and 30 percent of the span at the exit. To achieve this condition, the rotor was designed to accommodate weak oblique shocks in the tip region of the blades. The stator design was conventionally subsonic with the primary role of turning the flow to axial and was configured with double-circular-arc airfoils. The stage was designed for a specific flow (flow per unit of annulus area) of 42 lb/sec-ft^2 (205.1 kgm/sec-m^2) to deliver a pressure ratio of 1.5 at an efficiency of 86 percent and an equivalent tip speed of 1600 ft/sec (488.6 m/sec).

All testing was performed with the stator closed 3 deg from its nominal setting (greater stagger angle), which slightly improved stall margin and efficiency over the values obtained from other settings tested at design speed. With uniform inlet flow at design speed and pressure ratio, the stage efficiency was 81 percent, specific flow was 4 percent greater than design, and stall margin was 24 percent. The peak efficiency obtained at design speed was 84 percent, which corresponded to a pressure ratio of 1.67, 103 percent of design equivalent flow, and a stall margin of 10.5 percent. The design level of stage efficiency was achieved at the design specific flow, but at 95 percent of design speed and at a pressure ratio of 1.6. Rotor-only efficiency exceeded design goals, both at design speed and design flow rates, but at pressure ratios higher than design. The level of peak efficiency decayed rather uniformly as speed was increased to 90 percent of design speed, then abruptly increased by 3 points when speed was increased to 95 percent of design speed indicating the transition between the "unstarted" and "started" modes. These results, therefore, substantiate the quasi-three-dimensional characteristic procedure used in the design.

Shock patterns were not easily discernable from the static pressure contour plots derived from high-frequency-response instrumentation over the rotor blade tips. Tip leakage vortices, wall boundary layers, and the designed weakness of the tip shock system, all inferred from the plots, complicate the isolation of shock fronts. Holograms taken utilizing this fan stage under separate NASA Contract NAS 3-15336, however, showed shock patterns throughout the entire outer span of the blading. The shock system for the 100 percent design speed condition showed four major shock waves; (1) a leading edge shock. (2) a midspan damper shock, (3) a second damper shock, and (4) a trailing edge shock. The original design considered only the leading and trailing edge shocks.

The stall limit line was improved with hub-radial distortion, but was reduced when the stage was tested with circumferential and tip-radial flow distortions. Stage peak efficiency levels were decreased with all distortions tested. Over-attenuation resulted when the stage was subjected to hub radial distortion; however, amplification was obtained with tip radial distortion. With circumferential distortion, amplification occurred in the hub region and attenuation occurred in the mid passage and tip region.

INTRODUCTION

A low-loading, high-tip-speed transonic fan stage was designed, fabricated, and tested. A fan stage of this type would allow the drive turbine to operate at a higher rotational speed than would be suitable for fans having higher loading characteristics. Accordingly, turbine efficiency would be improved or the number of stages could be reduced, resulting in an engine having better performance and/or less weight and volume. The rotor design objective was, therefore, to deliver good efficiency at low work input by elimination of strong shock losses and shock-inducted separation in the high-Mach-number tip region.

The rotor design, as reported herein, is actually a redesign of the rotor described in ref. 1 and also reported upon in refs. 2 and 3. The midspan dampers of the original design failed in initial testing to 110 percent of design speed possibly as a result of classical blade flutter. Design speed performance resulting from this test was encouraging, and only minimal modifications were considered to be necessary to relieve the structural problem while retaining the original aerodynamic features. Dampers with increased thickness and revised contact surfaces and altered thickness distribution of the blading immediately adjacent to the dampers were incorporated into a redesign, herein referred to as "the design." The blade thickness distribution was altered immediately adjacent to the midspan damper to provide a less marginal flutter parameter. The midspan damper was redesigned to (1) reduce the vibratory stress by increasing thickness and removing the notches to make the interlock a single plane and (2) reduce the steady-state loading by changing the contact angle. This rotor followed the same design procedures as outlined in ref. 1. The stator vanes from the initial test were not damaged and were retained.

Aerodynamic and mechanical design results for the rotor are presented in Appendix A. The stator was varied to arrive at the best stage operating characteristics. This report also presents the experimental data obtained from uniform and distorted inlet flows and compares these data to the design values. Tabulations of these data are presented in ref. 4. Symbols and performance parameter definitions used in this report are presented in Appendix B.

Holograms of the rotor flow field were made under Contract NAS 3-15336. The results of this holographic study are reported in ref. 5.

APPARATUS AND PROCEDURES

Test Facility

The fan stage was tested in the sea level compressor test cell shown in fig. 1. A single-stage, radial-inflow turbine driven by heated facility air provides power to the fan through a 1.477-to-1 gearbox. Filtered air enters the fan through a calibrated bellmouth, which also serves to check total flow measurement. An open-mesh, conical screen shrouds the bellmouth for protection against damage by foreign objects. The airflow exiting the fan is diffused and exhausted to a double-walled plenum and then to two separate discharge ducts: one of 35.38 in. (89.85 cm) inside diameter and one of 23.50 in. (59.69 cm) inside diameter. These large-diameter discharge ducts were necessary to minimize system pressure losses and thereby extend the range of performance mapping. Each discharge duct contains a butterfly valve for back-pressure control and an ASME* square-edge orifice plate for primary flow measurement.

Distortion tests were accomplished by series stacking screens of various porosities attached to a support grid with 2 in. (5.08 cm) square openings. This support grid is capable of rotating through 360 deg in 5 min for circumferential distortion testing. The support grid was not rotated during radial distortion testing and was removed durir uniform inlet flow testing. Fig. 2 shows the hub-radial, tip-radial, and circumferential distortion screens mounted to the support grid.

Stage Configuration

The test configuration, shown in fig. 3, consists of an axial-flow fan with a single-exit-row, continuous-span stator and no inlet guide vanes. A detailed description of the stage appears in the design report (ref. 1). A redesigned rotor blade was necessitated by midspan damper failure that occurred on the original design during initial testing at 110 percent of design speed. The aerodynamic and mechanical details of this redesign appear in Appendix A of this report.

The stage was designed to deliver a total pressure ratio of 1.5 with an adiabatic efficiency of 86 percent at an inlet specific flow (flow per unit annulus area) of 42 lb/sec-ft^2 (205.1 kgm/sec-m^2). The rotor was designed to operate at a tip speed of 1600 ft/sec (488.6 m/sec) to accomplish these objectives. To satisfy the range of test requirements, however, the rotor was mechanically designed to operate at 110 percent of the design speed or at a rotor tip speed of 1760 ft/sec (537.2 m/sec).

---

*American Society of Mechanical Engineers.

The rotor contained 40 blades of 2.64 aspect ratio with midspan dampers located at 30 percent of the span from the tip. The rotor inlet hub-to-tip radius ratio was 0.46. Design relative Mach numbers were supersonic over 85 percent of span at the inlet and 30 percent of span at the exit of the rotor. Nominal running tip clearance at design speed was 0.045 in. (0.114 cm) and 0.035 in. (0.089 cm) at 110 percent of design speed. Two views of the rotor blade are shown in fig. 4, and the bladed disc assembly is shown in fig. 5.

The stator consisted of 45 vanes of 3.10 aspect ratio. The vanes could be remotely controlled to rotate about their centers of gravity on the span-wise stacking line such as to vary the stagger angle by ±10 deg from the design setting. Double-circular-arc airfoil sections were chosen for the design. At the design point, the maximum inlet Mach number occurs at the hub and was only 0.811 with a corresponding diffusion factor of 0.43. The stator vane leading edge was located axially 1.42 in. (3.61 cm) downstream of the rotor hub trailing edge. All performance testing was accomplished with the stator closed 3 deg from the as-designed setting (increasing the stagger angle.)

Instrumentation

Aerodynamic instrumentation.--Aerodynamic evaluation of the overall stage performance, rotor performance, blade element, and vane element data of the transonic fan stage required highly accurate sensing elements and utilized a computer-controlled data acquisition system. Accordingly, the types and designs of fixed sensing elements were carefully selected to provide the necessary accuracy, and the proper locations and distribution of all fixed instrumentation were determined to minimize blockage effects. Three categories of aerodynamic instrumentation were needed to provide three basic sets of data: (1) fixed instrumentation for evaluating overall stage performance, (2) traverses for determining rotor and stator element performance, and (3) high-response pressure transducers and stall sensors for evaluating transient and dynamic characteristics. A schematic of the test stage identifying the designated instrumentation stations and their corresponding axial locations is shown in fig. 6. A summary of the instrumentation station designations is shown below, and a schematic indicating the type of instrumentation and circumferential location of each station appears in fig. 7. Fig. 8 shows the fully instrumented test stage.

Station number	Location
0	Inlet bellmouth screen
1	Bellmouth instrumentation plane
2	Distortion screen plane
3, 4, 4.3, 4.6	Inlet duct instrumentation
5	Rotor inlet instrumentation plane

5.5	Rotor inlet traverse plane
6	Rotor leading edge
7	Rotor casing instrumentation
8	Rotor trailing edge
9	Rotor exit traverse plane
10	Stator leading edge
11	Stator trailing edge
12	Stage exit instrumentation plane
13	Plenum inlet plane
14	Downstream temperature mixing plane

The primary airflow measurement system consisted of ASME standard thin plate, square edged orifices located downstream in two straight pipe measuring sections. The orifice sizes were chosen to provide the largest orifice-to-pipe diameter ratio for which accurate coefficients are available in the ASME power test code of ref. 6. Accordingly, an 18.30-in. (46.48-cm) orifice was used in the 23.50-in. (59.69-cm) diameter pipe and a 27.13-in. (68.90-cm) orifice was used in the 35.38-in. (89.85-cm) diameter pipe. Two diametrically opposed sets of flange taps for each orifice were used. Each orifice temperature was measured by dual thermocouples located in accordance with ASME standards. Transverse (cruciform) pitot-static rakes located in the calibrated bellmouth section (station 1) provided a secondary check of the flow measurement. Station 1 instrumentation contained 29 elements located at centers of equal annular areas. The sum of the orifice flows agreed with that obtained from the bellmouth measurement to within ±0.5 percent.

Speed was monitored and compared with two independent inductively coupled monopole electromagnetic pickups and counters. Overall system accuracy was ±0.2 percent.

The inlet total temperature was measured at station 0 by fourteen chromel-constantan type E thermocouples of 0.020-in. (0.051-cm) wire diameter. Stator exit total temperatures (fig. 9a) were measured by six radial rakes with shielded high-recovery thermocouples. These rakes were circumferentially indexed to obtain readings evenly distributed across the stator vane at 0, 20, 40, 60, 80, and 100 percent gap. The seventh rake, which measured temperature at mid-gap, was located approximately 180 deg from the 40 and 60 percent gap thermocouples. These vane exit thermocouples were chromel-constantan, Type E, using 0.010-in. (0.025-cm) wire diameter. The thermocouple lead wires were calibrated for each temperature element. In addition, stage downstream temperatures (after radial and circumferential mixing) were measured in each exhaust duct at station 14, which gave a check to the station 12 measurements. All thermocouples were channeled through constant-temperature ovens for reference. To check overall system performance and assure data validity, two standard temperatures (the melting point of ice and the boiling point of water) were monitored through each reference junction. These temperatures generally were maintained to within ±0.5°F (±0.1°K) of their standard.

The inlet total pressure was measured by the bellmouth cruciform pitot-static rake during uniform inlet flow testing and by two radial rakes located at station 5 during circumferential distortion testing. The station 5 rakes were removed for uniform inlet flow testing. The stator exit total pressures were measured by 11-element wake rakes (fig. 9b) evenly distributed circumferentially across the vane passage. Two wake rakes, 180 deg opposed, were used at each immersion. Wall static pressure tap locations are shown in fig. 7. A schematic of the stator channel static tap locations is shown in fig. 10. Pneumatic switches utilizing one calibrated pressure transducer per 45 pressures were used for most pressure measurements. To check system performance and assure data validity, two reference pressures for each transducer were supplied by dead weights at 0 and 80 percent of transducer full scale and monitored to maintain a recording accuracy of 0.3 percent of full range.

Radial rakes (fig. 11a), located at station 10 and midway between stator gaps, contained high-frequency-response pressure transducers for the detection of rotating stall. The rakes, separated by 180 deg, each had immersions that corresponded to 10, 47, and 90 percent of span.

Three different types of wedge probes (shown in figs. 11b, 11c, and 11d) were used for obtaining blade and vane element data. Total pressure, static pressure, absolute air angle, and temperature were measured with 60-deg and 30-deg wedge probes; static pressure and absolute air angle also were measured with an 8-deg wedge probe. During uniform inlet flow and radial distortion testing, stations 5.5 and 9 each were equipped with one 60-deg wedge probe and one 8-deg wedge probe, while two 60-deg wedge probes were located at station 12. During circumferential distortion testing, however, two 60-deg wedge probes and one 30-deg wedge probe were located at both stations 5.5 and 9. Wedge probes were calibrated for Mach number as a function of indicated static-to-total pressure ratio. Stator angles, discharge valve settings, and distortion screen angular positions were visually displayed and manually recorded by the data acquisition system.

Ten high-frequency-response pressure transducers were flush-mounted in two axial lines over the rotor blade tip. As shown in fig. 12, these transducers were located in two rows spanning one rotor passage along with ten corresponding wall static pressure taps that provided a reference level for each high-frequency-response transducer. A proximity detector, sensing a target on the front shaft assembly, provided a one-per-rotor-revolution pulse to locate a known blade passage and position relative to the transducer positions. The transducers have a linearity of one percent and rise time of less than two microseconds. A shock tube calibration of each transducer and a matching source follower was made and photographed prior to test to verify pressure level response.

The nine immersions of fixed instrumentation were defined by the intersection of the axial station and the design streamlines that pass through 5, 10, 15, 28.2, 47, 68.9, 85, 90, and 93.7 percent of the passage height measured from the tip at the rotor trailing edge.

All aerodynamic data except those from high-frequency-response instrumentation were obtained in millivolts by an automatic data acquisition system and recorded, in counts, on magnetic tape. The data acquisition system used for recording fixed instrumentation displayed all measured parameters on a cathode ray tube in real time at 30-sec intervals. The data acquisition system used for recording blade element data and stall transient flow data recorded in 1-sec intervals. The high-frequency-response data were recorded on wide-band, multichannel magnetic tape recorders.

Mechanical instrumentation.--Rotor blade vibrations were measured with dynamic strain gages located at four different positions (established from bench testing) on the blade and midspan damper and monitored through a slip ring. Stator vane vibration was similarly measured with strain gages located in two basic positions.

Shaft dynamics and bearing mechanical conditions were monitored with accelerometers located in the bearing housings on vertical and horizontal planes. In addition, bearing housing temperatures were measured with chromel-alumel thermocouples. The structure dynamic response was measured with velocity pickups located on the front frame in the vertical and horizontal positions.

Five capacitance-type calibrated clearanceometers were utilized to monitor rotor blade running tip clearances and untwist. Four clearanceometers spaced 90 deg apart were located at the rotor leading edge, and the fifth was placed at the trailing edge on a projection of the tip chord line from one leading edge probe.

Data from the mechanical instrumentation were monitored visually on oscilloscopes and recorded on wide-band magnetic tape recorders.

Test Procedure

Shakedown test.--Shakedown tests were conducted with the following objectives.

(1) Establish mechanical integrity of the test vehicle.

(2) Evaluate stress and vibration levels throughout the required test operating range.

(3) Determine a stator setting at design speed that results in minimal influence on rotor stall.

(4) Thoroughly check out instrumentation and data reduction programs.

Initially, a mechanical check-out to only 60 percent of design speed was conducted for procedure and vehicle familiarization. The test stage was fitted with Plexiglas windows contoured to the outer shroud adjacent to the rotor to check out the system required for the flow visualization program. (The windows were replaced with metal plugs for the shakedown test and all performance testing.) The flow visualization program was scheduled to be conducted following completion of the uniform inlet flow testing to make the most efficient use of available test time.

For the shakedown test, the fan stage was slowly accelerated to design speed with wide-open discharge valves and the stator stagger angle set at the nominal (design) position. Rotor and stator vibratory stresses, vibration levels on critical components, and rotor blade tip clearances were monitored and recorded during this acceleration. All stress and vibration levels were well within acceptable limits. Data at two design speed points (wide-open throttle and design pressure ratio) for overall and blade element performance were recorded to check instrumentation and data reduction programs. The stage was then stalled. The stall-created overspeed activated a facility safety valve in the drive turbine, resulting in a shutdown. Inspection after shutdown revealed that three rotor blades had sustained minor damage from foreign objects. The damage was caused by several pieces of braze material that had broken off at the junctions of the protective screen on the bellmouth. The screen was repaired, the three damaged blades replaced, the rotor disc reinstrumented, and the test resumed. Shakedown testing was concluded with the stator optimization test, wherein the stators were varied ±5 deg from their nominal setting at design speed with flows from wide-open throttle to near-stall. A 3-deg-closed stator setting (increased stagger angle) was used for all performance testing because it slightly improved stall margin and efficiency over the values obtained from other settings tested at design speed.

Uniform inlet flow test.--Thirty-one overall and blade element performance data points were obtained with uniform inlet flow at speeds of 60, 70, 80, 90, 95, 100, and 110 percent of design speed. Four data points were taken at 60, 70, 80, and 110 percent of design speed, while 5 data points were taken at the other speeds. Stall flows were obtained at all speeds except at 110 percent design speed. High overspeed stall (110 percent of design speed) was deleted from the test program as a safety precaution to ensure successful completion of the flow visualization program. Because stall occurred abruptly during the shakedown test with nominal stators, the design speed stall was deferred until just prior to distortion testing. Near stall, only overall performance data points were taken at 80 and 100 percent speed. To maintai- a measure of safety, the traversing wedge probes were retracted out of the flow path as stall was approached. High-frequency-response rotor casing transducer data were record for fifteen points: two at 80, three at 90, and five each at 95 and 100 percent of design speed. These data were utilized for developing blade tip static pressure contours.

Following completion of testing with uniform inlet flow and prior to distortion testing, the fan stage was configured for the flow visualization program. This was accomplished by removal of the traversing wedge probes and installation of contoured Plexiglas windows in the outer shroud. All fixed instrumentation was retained.

Distorted inlet flow test.--Prior to distortion testing, the rotatable distortion support grid was installed 17.2 in. (43.7 cm) upstream of the rotor leading edge; Plexiglas windows in the outer shroud were replaced with metal plugs; traversing wedge probes were reinstalled; and rotor inlet total pressure radial rakes were placed at station 5. Sixteen overall performance data points for the predistortion baseline configuration were obtained at 70, 90, and 100 percent of design speed at flows from wide-open throttle to stall. Five readings at 70, six at 90, and five at 100 percent speed were taken. This predistortion configuration was evaluated to establish baseline data prior to distortion testing in the event that performance with the distortion screen support grid would be substantially different than for uniform inlet flow.

Three layers of screens of open area ratio 0.585, 0.602, and 0.560 (varying from upstream to downstream) were attached to the distortion support grid to create the hub-radial, tip-radial, and circumferential distortion patterns at the rotor inlet. The radial distortion screens were sized to create a distortion pattern extending over 40 percent of the annulus area at the rotor inlet plane. The circumferential distortion screen was sized to create a 90-degree continuous segment of low pressure area at the rotor inlet plane.

Overall performance and blade element performance or flow distribution data were taken at twelve readings for hub-radial distortion, eleven readings for tip-radial distortion, and twelve readings for circumferential distortion. These data were obtained at speeds of 70, 90, and 100 percent of design speed and flows between wide-open throttle and stall. A data point was taken at 97 percent design speed with tip radial distortion to establish the distortion level at design flow. At design speed with hub-radial distortion, a facility system-induced instability was encountered prior to stall and was characterized by a low-frequency acoustic test cell resonance. An overall performance data point reading for circumferential distortion consisted of seven separate scans of data, wherein the distortion screen was indexed by 45 deg between scans (270 deg of total movement) referenced to the screen centerline. Flow distribution data were recorded for circumferential distortion while continuously rotating the distortion screen through 360 deg.

Rotor blade and stator vane vibrations were monitored for all testing, and stress levels were well within established limits. Rotor tip high-frequency-response instrumentation was not recorded during distortion testing.

Data Reduction Methods

Raw digitized data for determination of overall and blade element performance were measured in millivolts, converted to counts, recorded on magnetic tape, and transferred to printed output in engineering units corrected to standard day conditions. Analog data recorded on magnetic tape for analysis of stress and vibration levels, stall probe signals, tip clearanceometers, and rotor casing high-response transducers were transferred to oscillograph traces for interpretation.

Overall performance.--The two total pressure elements corresponding to the same stator gap position and radial location were arithmetically averaged and the resultant eleven values circumferentially mass averaged. A constant circumferential static pressure, obtained by linearly interpolating an arithmetic average of the wall static pressures, was assumed. Stage exit total pressure was then calculated by radially mass averaging the nine immersion circumferential mass averages.

The circumferentially and radially mass-averaged stage exit total temperatures were obtained in the same manner as that used for calculating total pressures except for the added interpolation required to satisfy a one-to-one correspondence between the seven available temperature elements and the eleven pressure elements at the same immersion.

For circumferential distortion testing, seven separate data scans were recorded for distortion screen positions indexed by 45 deg over a 270-deg segment. An eighth scan was developed wherein the individual element exit pressures (both static and total) and temperatures were set equal to the arithmetic average of the previous seven scans. The stage exit total pressure and temperature were then circumferentially and radially mass averaged as previously described for uniform and radially distorted inlet flow testing.

Inlet total pressure for uniform inlet flow was set equal to the arithmetic average of the pitot-static elements downstream of the inlet bellmouth. For radially distorted inlet flow, an arithmetic average of radially mass-flow averaged pressures from the two fixed rakes at the rotor inlet was used as the inlet total pressure.

Circumferential distortion inlet total pressure was determined from the two fixed rakes at the rotor inlet in the following manner. Separation of both total and static pressures was maintained while under the influence of the distortion screen (±45 deg from the screen centerline angular position) from that instrumentation located in the remaining 270-deg undistorted region for each data scan. The arithmetic average of these pressures taken over seven scans (seven different screen positions constituting a data point) for each immersion was then radially mass-averaged separately for both the distorted (minimum pressure region) and undistorted (maximum pressure region) rotor inlet segments. (These minimum and maximum radially mass-averaged pressures were used as the measure or index of the distortion.) Finally, the inlet total pressure was computed by circumferentially weighting the minimum pressure value over one-fourth the inlet annulus and the maximum pressure value over the remaining three-fourths of the inlet annulus.

Blade element performance.--Continuous traversing wedge probes at the rotor inlet plane, rotor exit plane, and stator exit plane were used to measure total pressure, total temperature, air angle, and static pressure for uniform and radially distorted inlet flow testing. Primary measurements of static pressure were obtained with the 8-deg wedge probes, while primary angle measurements were obtained with the 30-deg wedge probes. Angle-only measurements obtained from wedge probes were used at the stator exit plane for evaluating stator vane element performance; the pressure and temperature data were taken from the circumferentially mass-averaged values determined from the fixed instrumentation.

All blade element parameters determined for the blade and vane leading and trailing edge positions were translated from the measuring planes accounting for continuity and radial equilibrium and assuming design streamline slopes. Rotor-only performance was based on the mass-averaged total pressures as measured by the radial surveys and the fixed temperature rakes at the stator exit plane. For near-stall data points, for which traverse data were not taken, the arithmetic average of the peak values of circumferential total pressure at the same immersion was used as the rotor exit radial pressure distribution.

Three fixed-position (30-deg and 60-deg) wedge probes calibrated for Mach number at each of the rotor inlet and rotor exit planes were used to measure flow distribution data at the measuring planes only (not translated to blade and vane leading and trailing edges) during a continuous 360-deg rotation of the distortion screen. Stator exit vector diagram parameters at the selected radial positions were based on the arithmetic average of the stage exit wake rake pressures as a function of the particular rake mean angular position, local temperature, and a linear interpolation of the localized wall static pressures.

Rotor casing static pressure contours.--Static pressure contours over the rotor blade tips were obtained by using continuously recorded variable pressure data measured by ten high-frequency-response transducers distributed axially and by correspondingly located wall static pressure taps for measurements of the average static pressure level. The transducer data were recorded at 120 in./sec (304.8 cm/sec) tape speed in the frequency modulation mode double extended. Also recorded and superimposed on these transducer signals were the one-per-revolution pulse for accurate positioning of a known blade passage, a 10 000-Hz reference signal for speed checks, and an Inter-range Instrumentation Group (IRIG) time code to provide a time reference. These recorded signals were reproduced at a tape speed of 1.875 in./sec (4.763 cm/sec) and inserted directly into an oscillograph and traced at 80 in./sec (203.2 cm/sec) paper speed. Each transducer trace was then referenced to the same point in time (instant of the one-per-revolution pulse). A computer program then converted manual measurements taken from the oscillograph traces over a one-blade-passing period plus the average pressure obtained from the wall static taps into isobaric values of pressure between a blade passage.

RESULTS AND DISCUSSION

Shakedown Tests

The shakedown tests were accomplished with uniform inlet flow and established that vibratory stress levels for the blades and vanes were well within acceptable limits over the required operating range. A stator setting of 3-deg closed was selected as a result of stator optimization tests and was used for all further testing.

Fig. 13 presents relevant efficiency and flow data obtained during stator optimization tests wherein the stator setting was varied between 5-deg open and 5-deg closed at design speed for two separate levels of pressure ratio. The data show that open (negative) settings reduce efficiency at both the design pressure ratio and the pressure ratio adjacent to stall, while reducing flow only at the near-stall pressure ratio. The closed (positive) settings, however, showed the opposite trend of increasing efficiency for both the lower and higher pressure ratios and increased flow at the near-stall pressure ratio. (It was felt that a significant flow rate reduction with increasing pressure ratio at design speed would result in reduced stall-margin at part speed.)

The stagger setting also was found to have a significant effect on the stator vane vibration, but the effect on rotor blade vibration was negligible. The measured rotor blade stress did not exceed ±3 ksi (±20.68 x 10^6 N/m^2). The stator vane stress approached ±30 ksi (±206.8 x 10^6 N/m^2) for the 5-deg-open setting and decreased to ±4 ksi (±27.57 x 10^6 N/m^2) with vibration levels becoming less random as the vanes were closed. The stator vanes responded at a predominant frequency of 620 Hz, which is the fundamental flexural natural frequency. The random character of the vibration at the open stator angles was indicative of separated flow. No regular modulation was seen that would have been indicative of rotating stall.

During shakedown testing, three rotor blades sustained minor damage from foreign objects (braze material from the bellmouth inlet screen) and had to be replaced prior to completion of the test. Check points of data taken prior to the blade replacements indicated no change in performance.

Uniform Inlet Flow

Rotor and stage overall performance.--Overall performance of the rotor and stage with the 3-deg-closed stator setting is tabulated in table 1 and shown in figs. 14 and 15. Stall was approached gradually such that stall transient flow data (1-sec intervals) was correlated with the slower responding overall performance data (30-sec intervals) to establish the stall-limit data point.

At design speed, the rotor achieved a peak efficiency of 89.7 percent at a pressure ratio of 1.724 and an equivalent flow 3 percent in excess of design. A pressure ratio of 1.512 and efficiency of 88 percent were the design objectives for the rotor. At design speed and pressure ratio, the rotor efficiency was 85.4 percent, but the flow rate was 4 percent greater than design.

The peak stage efficiency achieved at design speed was 83.7 percent at a pressure ratio of 1.669, whereas the design intent was 86.2 percent at a pressure ratio of 1.500. At this design pressure ratio and speed, an efficiency of 81.2 percent, and a stall margin of 24 percent were achieved. On the basis of a constant-throttle line passing through the design pressure ratio at design speed, stall margins of 23.2 percent at 90 percent speed and 32.8 percent at 70 percent speed were obtained.

The rotor efficiency exceeded 90 percent, and the stage met the design intent, but this occurred at 95 percent of design speed and a pressure ratio higher than design. Although the rotor was capable of producing efficiency levels higher than design at design speed, the efficiency loss across the stator was over twice the design prediction.

The level of peak efficiency decayed rather uniformly from 60 percent to 90 percent of design speed, then abruptly increased by 5.5 points for the rotor and 3 points for the stage when speed was increased to 95 percent of design speed indicating the transition between the "unstarted" and "started" operating modes. At 90 percent of design speed, the wide-open-throttle, rotor-only efficiency was 88.5 percent for a pressure ratio of 1.352 and then abruptly decayed to 85.8 percent for a pressure ratio of 1.429 with only a 1.3-percentage point reduction in flow. The remainder of the efficiency characteristic was continuous to stall. (The stage efficiency characteristic did not reflect this abrupt change in efficiency, however, because of compensating stator losses.) A thorough investigation of this rotor passage starting development is detailed in ref. 5. A summary of this material is included in this report together with pertinent holographic data.

Minimal data obtained on the original design prior to failure indicated a 2 percent over-design flow at design speed. The 4 percent over-design flow at design speed with the redesigned rotor results from a combination of two effects:

(1) The start margin (defined in ref. 1) applied to this design was over-conservative.

(2) The geometric throat area for the blading was 4 percent greater than for the original design.

A start margin varying from 5 percent for section 1 to approximately 2.5 percent for section 8 was thought to be required to ensure passage starting at design speed for the original design and was retained for the redesign. A review of these data coupled with the extensive study of rotor passage starting development indicated that starting occurred at wide-open throttle and 90 percent of design speed, which corresponds to 98.4 percent of design flow, or approximately 6 percent less flow than delivered at design speed and at a considerably lower relative Mach number than design. Using the methods presented in ref. 1, the design start margin could have been reduced.

Although the aerodynamic throat areas, i.e., start margin, of the original design were incorporated in the redesigned rotor blading, the added structural safety margins of the redesign, as reflected in axial and tangential tilts and pretwist to counteract steady-state stresses, resulted in a 4 percent larger throat area for the as-manufactured blade. If the steady-state stresses (not measured) were less than predicted and allowance is made for increased blockage of a 70 percent thicker midspan damper on the redesign, a flow 2 percent higher than that of the original design is reasonable. It can therefore be seen that a reduction in throat area required to pass design flow at design speed could result in insufficient start margin.

The rotor blade was mechanically e for all operating conditions. At the highest pressure ratio of 1.67 inve ted and 110 percent of design speed, the rotor strain gages indicated the ma... stress level of ±3 ksi (20.69 x 10^6 N/m^2) at a frequency of 1270 Hz. This frequency was close to the calculated first torsional natural frequency, but does not correspond to an integral order of rotational speed, possibly indicating that the blade was approaching a flutter condition. The analytically derived natural frequencies were considerably higher than those measured at any operating condition, probably because of the variation in fixity assumed at the midspan damper in the calculation.

An oscillograph trace from the high-frequency-response instrumentation used for detecting rotating stall is shown in fig. 16 for 90 percent of design speed and is typical of all speeds. The stall, although abrupt, is seen to originate in the tip region and then become a full span stall. The stall pulse had a frequency of recurrence of approximately 5.8 percent of rotor speed. The pressure amplitude is approximately 10.5 psi (7.24 N/cm^2).

Blade element data.--Rotor spanwise pressure ratio and efficiency at the design speed and design stage pressure ratio is compared to the design prediction in fig. 17. The pressure ratio is significantly higher than design in both the tip region and the area adjacent to 70 percent span. The hub and region close to the midspan damper met design levels. The efficiency was moderately less than design at the end walls, but was significantly below design at the damper. The three-dimensional shock patterns seen in the hologram could account for the high losses in the midspan damper region.

Fig. 18 is the rotor spanwise distribution of total loss coefficient, diffusion factor, deviation angle, and suction surface incidence at the design speed and stage pressure ratio compared to design predictions. The span-wise distribution of total loss coefficient parallels the design intent if the integrated loss associated with the midspan damper was equally distributed radially as practiced in the design method of ref. 1. The resultant loss would match the design levels from mid-passage to 85 percent span, but exceeds the design values in the tip and end-wall regions. Except for these end-wall regions, the loss is greatest at mid-passage, which substantiates the design assumptions of ref. 1. The diffusion factor was slightly higher throughout the span, with the largest discrepancy from design occurring at the hub (0.5 compared to 0.3). The deviation angle was approximately 2 deg less than design throughout most of the span, reaching almost 5 deg at 70 percent span and exceeding design .y at the hub. Since this data point was 4 percent over design flow, the suction surface incidence was less than design, varying from approximately 1 deg less at the tip to over 6 deg less at the hub.

The inlet and exit relative Mach number spanwise distributions are compared to the design values in fig. 19. The inlet relative Mach number is in agreement with the design intent even with the 4 percent over design flow -- this affects the inlet relative Mach number by only 0.6 percent. The exit relative Mach number was less than predicted in the supersonic region, thereb hing sonic velocity slightly outboard of the desired midspan damper locati ef. 1).

The stator spanwise total loss coefficient, diffusion factor, deviation angle, and suction surface incidence are compared to the design values for the design speed and stage pressure ratio in fig. 20. Of note are the severe endwall losses at moderate diffusion factors and the significantly higher incidence near 30 percent span as influenced by the midspan damper.

Fig. 21 compares the spanwise stage element pressure ratio, temperature ratio, and resulting adiabatic efficiency at the design speed and pressure ratio to the design intent. The temperature ratio exceeds the design goal to 40 percent span and satisfies the design levels for the remainder of the span. The efficiencies of the end-wall and midspan damper regions ar below design predictions.

Blade element performance at nine radial positions is tabulated in ref. 4. These data are presented in figs. 22a through 22i for the rotor and 23a through 23i for the stator in terms of total loss coefficient, diffusion factor, and deviation angle versus suction surface incidence angle. The design values are indicated in the figures. In general, these data show similar trends to the spanwise design speed and pressure ratio data previously presented.

Rotor blade tip static pressure contours.--The axial distribution of steady-state static pressures at the design speed and pressure ratio for both the hub and shroud is shown in fig. 24 compared to the design intent. Steady-state values of static pressure in the outer shroud over the rotor blade tips between stations 6 and 8 shown in the figure were coupled to high-frequency-response measurements to develop static-pressure contours within the rotor blade passage. Figs. 25 and 26 show typical high-frequency-response oscillograph traces. Fig. 25, obtained at design speed from wide-open throttle to near-stall, indicates the change in amplitude response through the blade passage at varying back pressures. The design shock system is superimposed on the blade tip (streamline 1) passage conical development in fig. A-4 of Appendix A.

The steady-state (time-averaged) axial distribution of static pressure along with the contours developed from the oscillograph traces are shown in figs. 27 through 41 for a range of operating conditions at 80, 90, 95, and 100 percent of design speed. Interpretation of these contour plots for defining shock pattern, strength, and location is complicated by several factors such as wall boundary layers, tip leakage vortices, and, primarily, by the large-diameter sensing surface of the transducer relative to the small dimensions to be resolved. A study of the figures, for example, reveals that most of the static pressure contours are normal, rather than parallel, to the predicted shock directions. Therefore, the contour plots should be viewed as a measure of qualitative, rather than of quantitative, value.

Figs. 27 and 28 obtained at 80 percent of design speed show steep gradients in static pressure upstream of the blade leading edge indicating the presence of a strong bow shock. This conclusion is substantiated by the holograms obtained at this condition and reported upon in ref. 5 wherein a strong detached bow shock was observed at the 80 percent of design speed, mid-throttle condition. When speed was increased to 86 percent of design speed, the bow shock detachment distance was reduced and at 90 percent of design speed, a strong, normal shock was recorded attached to the blade leading edge. A weak oblique shock system, as per design intent and indicative of passage starting, was not developed within the blade passage until 92 percent speed was reached. These strong bow shocks are, therefore, representative of the steep gradients in static pressures recorded through 90 percent of design speed as shown in figs. 30 and 31. The shock patterns as detected and included in ref. 5 are shown by dashed lines superimposed on fig. 31 for reading 106. Fig. 30, which corresponds to a lesser back pressure, shows steeper gradients in static pressure in the leading edge region, but these gradients do not influence the complete blade passage as for the higher back pressure condition shown in fig. 31.

The static pressure contours for wide-open throttle, 90 percent of design speed presented in fig. 29 from reading 103 show that static pressure gradients do not extend upstream of the leading edge, but are contained essentially within the passage. Holograms were obtained at this condition. The shock system and tip leakage vortex is shown superimposed in dashed lines on the contour plot. The leading-edge shock is seen to be oblique.

The rotor efficiency characteristic for 90 percent of design speed was previously shown (overall performance section) to decay abruptly from the wide-open throttle condition (reading 103) to the adjacent back-pressure condition corresponding to reading 101 indicating the effect between "started" and "unstarted" operating conditions. This started-to-unstarted transition is further substantiated by the extension of the static pressure gradients at the leading edge shown on the contour plots and the holograms recorded at this condition. This transition also is shown by the large passage-to-passage variations (primarily in the leading-edge region) of the oscillograph recordings of the high-frequency-response transducers over the rotor tip. A portion of this oscillograph record appears in fig. 26 and was obtained during the transient between wide-open throttle and the next highest back-pressure condition. The peak-to-peak amplitude variation is shown to vary abruptly from 4.0 psi (2.8 N/cm^2) for one passage to approximately 16.0 psi (11.0 N/cm^2) for an adjacent passage. This is evident in the transducer signal just inside the blade leading edge (channel 3). A large variation also can be seen in the transducer signal just upstream of the blade leading edge (channel 2). The traces in the trailing-edge region (channels 8, 9, and 10), however, show reasonable passage-to-passage repeatability. The transition region was not approached from the low-flow end of the characteristic to determine hysteresis.

Figs. 32 through 36 are the contours obtained at 95 percent of design speed. Fig. 35 appears to be typical of the contours obtained at this speed, and shows the shock pattern (dashed lines) as determined from the holograms. The oblique shock at the leading edge is seen to curve sharply as it intersects the tip leakage vortex to become perpendicular to the suction surface. The next downstream shock was determined from ref. 5 to emanate from the midspan damper and is termed as such. The furthest downstream shock shown is identified as a second damper shock. Any trailing-edge shock was partially obscured by the midspan damper and, therefore, was not shown. The shock system is defined, however, at inboard streamlines to the midspan damper in ref. 5. The near-stall data point (reading 119) obtained at 95 percent of design speed indicates the progression of the contours forward of the leading edge, which may be indicative of passage unstarting.

Static-pressure passage contours at design speed are shown in figs. 37 through 41 in order of ascending pressure ratio. These contours are all similar to the more open throttle setting contours obtained at 95 percent of design speed. The shock pattern obtained from the holograms at the condition of wide-open throttle is superimposed on fig. 37 (reading 107) in dashed lines indicating that the pressure contours do not explicitly define shock fronts. The trailing-edge shock is shown at the intersection of the leading-edge oblique shock and the suction surface. Fig. 39, the design stage pressure ratio, also contains the superimposed shock patterns derived from ref. 5 shown by dashed lines. The shock system at design pressure ratio and speed showed four major shock waves (1) a leading edge shock, (2) a midspan damper shock, (3) a second damper shock, and (4) a trailing edge shock. Tip leakage vortices were also seen along the suction surface on the blade. A weak oblique shock extended from the blade leading edge to the suction surface near the trailing edge at the outer wall. The shock was bent sharply to become nearly perpendicular at the intersection of the suction surface. A segment of this shock appeared to continue obliquely and intersect the blade further along the chord away from the tip region. Details of this shock near the suction surface were obscured, however, by the coalescence of the midspan damper and trailing edge shock fringes as well as the tip vortices; the leading edge shock became visible outboard of the midspan damper shock, where it intersected the shock from the midspan damper. The midspan damper shock appeared to be a conically shaped shock emanating from the intersection of the leading edge of the midspan damper on the suction surface. The shock extended across the passage and the forward portion intersected the pressure surface of the opposite blade well forward of the midspan damper leading edge. The shock extended radially outward and intersected the pressure surface immediately behind the blade leading edge. The shock extended across the passage and intersected the suction surface of the trailing edge near the outer wall. Further back in the passage, a second damper shock was observed, which emanated from the intersection of the midspan damper and pressure side of the blade. This shock was a highly warped surface nearly coinciding with the midspan damper and trailing edge shock at the blade trailing edge. The trailing edge shock appeared as a single bright fringe at the blade trailing edge. This shock was similar to the design trailing edge shock but was displaced slightly forward of the trailing edge. The shock intersected the suction surface of the blade slightly downstream of the leading edge shock. The four shock fronts appeared to coalesce near the blade trailing edge.

Predistortion Baseline Test

A distortion screen support grid was installed at station 3, rotor inlet total pressure rakes were installed at station 5, and the fan stage was tested from wide-open throttle to stall at 70, 90, and 100 percent of design speed. The purpose of this test was to evaluate the influence of the configuration changes on overall performance, since inlet total pressure was now measured and defined at station 5 rather than at station 1 as it was for uniform inlet flow.

A summary of the rotor-only and stage overall performance data is presented in table 2. These data are superimposed on the uniform inlet flow performance characteristics previously obtained for the rotor in fig. 42 and for the stage in fig. 43. Comparison of these data with that obtained for uniform inlet flow showed that repeatability was excellent. The only unexplained discrepancy was the 1.5 percent higher peak stage efficiency obtained at design speed. The abrupt decay in rotor efficiency from wide-open throttle to the adjacent lower flow condition at 90 percent of design speed was repeated. The agreement obtained for these data, therefore, established baseline data for comparing the results of distortion testing.

Hub-Radially Distorted Inlet Flow

Series stacking of annular screens on the distortion screen support grid suppressed the inner 40 percent of the rotor inlet area producing a distortion index $(P_{max} - P_{min})/P_{max}$ of 0.158 at design flow, which occurred at design speed. The equivalent inlet total pressure spanwise profile obtained is shown by the lower curve of fig. 44.

Rotor and stage overall performance.--The rotor-only and stage overall data summary with hub radial distortion appears in table 3. These data are superimposed on the uniform inlet flow performance (dashed lines) in figs. 45 and 46 for the rotor and stage, respectively. The level of distortion index obtained versus design equivalent flow ratio is shown in fig. 47. This index ranged from 0.158 at design flow to approximately 0.05 at 60 percent of design flow. The wide-open throttle flow decreased by 7 percent at 70 percent of design speed, 2.5 percent at 90 percent of design speed, and 1.5 percent at design speed. A significant decay in pressure ratio occurred at all speeds evaluated, resulting in a flat pressure ratio-flow characteristic when compared to that obtained with uniform inlet flow. A 4.5 point loss in peak efficiency resulted at design speed and a 6 point loss resulted at 70 percent of design speed.

The stall limit line was improved at 70 and 90 percent of design speed over that obtained with uniform inlet flow. Stall margins (as referenced from the constant throttle line developed with uniform inlet flow) of 44.3 and 50.4 percent were obtained at 90 percent and 70 percent of design speed, respectively. The general character of the stall is shown by the high-frequency-response stall probe oscillograph traces of fig. 48 for 90 percent of design speed. As for uniform inlet flow, the stall originated at the tip and progressed to the hub. The typical stall pulse had a frequency of recurrence of 6.7 percent of rotor speed and an amplitude of 6 psi (4.14 N/cm^2). The design speed line stall flow was not obtained however, because of the onset of an apparent facility-induced instability characterized by a test cell acoustic resonance. This phenomenon has been experienced in the past with similar test configurations. With throttling, the design speed characteristic increased to a pressure ratio of 1.59. Further throttling resulted in a flow reduction at constant pressure ratio until the facility instability was heard. Rotating stall was not detected, and rotor blade and stator vane vibratory stress levels remained within acceptable limits. The vibratory stress on the rotor blades reached only ±4.5 ksi (±31.0 x 10^6 N/m^2) and the stator vanes reached a fluctuating ±7.0 ksi (±48.3 x 10^6 N/m^2).

Blade element data.--Blade element performance at 9 radial positions for hub-radially distorted inlet flow in terms of total loss coefficient, diffusion factor, and deviation angle versus suction surface incidence is presented in figs. 49a through 49i for the rotor and 50a through 50i for the stator. A detailed tabulation of these data with additional performance parameters is contained in ref. 4.

Rotor tip incidence was approximately 2 deg less than that obtained with uniform inlet flow. Levels of diffusion factor and deviation were similar, however. Design values of rotor hub incidence with uniform inlet flow ranged from 2 deg to 4 deg less than design values at design speed. Rotor hub diffusion factors exceeded 0.65 (the highest seen in the testing of this stage), but losses were less than with uniform inlet flow at design speed. At design pressure ratio and speed, the local pressure ratio was higher at the hub and lower in the tip region, indicating that hub-radial distortion was over-attenuated in the hub region and amplified in the top region.

Stator end-wall losses were as severe as measured with uniform inlet flow. Measured hub incidence of the stator exceeded design values by as much as 16 deg.

Tip-Radially Distorted Inlet Flow

Series stacking of annular screens of the same open area ratio as used for generating hub-radial distortion suppressed the outer 40 percent of the rotor inlet area producing a distortion index $(P_{max} - P_{min})/P_{max}$ of 0 153 at design flow and 97 percent of design speed. The resulting equivalent inlet total pressure spanwise profile is shown by the upper curve of fig. 44.

Rotor and stage overall performance.--The rotor-only and stage overall data summary with tip-radially distorted inlet flow appears in table 4. These data are superimposed on the uniform inlet flow performance (dashed lines) in fig. 51 for the rotor and fig. 52 for the stage. The range of distortion index obtained versus design equivalent flow ratio is shown in fig. 47 and is identical to that obtained with hub-radially distorted inlet flow. The wide-open throttle flow at design speed decreased by approximately 2 percent from that obtained with uniform inlet flow, a 2.5 percent flow reduction was recorded at 90 percent speed, and virtually no difference was noted at 70 percent. A loss of 5 points in peak stage efficiency was evident, both at design speed and 70 percent of design speed. The level of peak rotor efficiency at 90 percent of design speed was approximately that obtained with uniform inlet flow, but stage efficiency was lower by 3 points, indicating higher stator losses.

The stall limit line was reduced from that obtained with uniform inlet flow. The stall margins as referenced from the constant throttle line developed with uniform inlet flow were 19.4, 12.1, and 13.0 percent at 100, 90, and 70 percent of design speed, respectively. A typical oscillograph trace of the high-frequency-response stall probes taken at design speed is shown in fig. 48. The stall progressed from tip to hub as with uniform inlet flow. The frequency of recurrence of the stall pulse was 6.02 percent of rotor speed. This stall pulse had a pressure amplitude of 9.0 psi (6.21 N/cm^2). The highest levels of vibratory stress measured with tip-radial distortion were ± 3 ksi ($\pm 20.7 \times 10^6$ N/m^2) for the rotor blades and ± 4.5 ksi ($\pm 31.0 \times 10^6$ N/m^2) for the stator vanes, which occurred at design speed just prior to stall. These levels were less than that seen during hub-radial distortion testing.

Blade element data.--Blade element performance at 9 radial positions for tip-radially distorted inlet flow in terms of total loss coefficient, diffusion factor, and deviation angle versus suction surface incidence angle is shown in figs. 53a through 53i for the rotor and 54a through 54i for the stator. These data and additional performance parameters are tabulated in ref. 4.

Rotor incidence angles were about 3 deg higher in the tip region and 3 deg lower adjacent to the hub than the angles obtained with uniform inlet flow. Stator incidence angles, however, were approximately the same, for comparable speeds, as seen during uniform inlet flow testing. The levels of deviation, loss, and loading throughout the span for both rotor and stator are not appreciably different that were seen with uniform inlet flow. At design pressure ratio and speed, the local pressure ratio was higher at the tip, whereas the hub pressure ratio was lower, indicating that tip-radial distortion was over-attenuated at the tip and amplified at the hub.

Circumferentially Distorted Inlet Flow

A 100-degree, full-span screen segment of the identical arrangement and open area ratio as previously used for radial distortion testing suppressed approximately 90 degrees of the rotor inlet measuring plane and produced a distortion index of 0.138 at design speed and flow.

Stage overall performance.--A stage overall data summary for 70, 90, and 100 percent of design speed is presented in table 5 for circumferential distortion. These data are superimposed on the uniform inlet flow performance (dashed lines) in fig. 55. The level of distortion index obtained versus design equivalent flow ratio appears in fig. 47, indicating that a distortion level range from 0.147 at 102 percent of design flow to 0.050 at 64 percent of design flow was covered. These distortion levels were lower than those resulting from radial distortion. The flow at wide-open throttle was reduced by approximately 2 percent at all speeds from that obtained with uniform inlet flow. A 3-point peak efficiency loss also resulted at all speeds evaluated.

The stall limit line with circumferentially distorted inlet flow was reduced from that obtained with uniform inlet flow, but not as severely as that obtained with tip-radial distortion. The stall margins as referenced from the constant throttle line developed with uniform inlet flow were 19.7, 20.9, and 27.9 percent at 100, 90, and 70 percent design speed, respectively. Fig. 48 shows a typical oscillograph trace of the stall instrumentation for design speed. The stall originated in the tip region with a stall pulse of 6.0 percent of rotor speed and a pressure amplitude of 12 psi (8.27 N/cm^2), higher than was seen during all other testing. This design speed stall also resulted in the highest vibratory stresses measured on the rotor of ±20 ksi (±137.9 x 10^6 N/m^2). The stator vibratory stress level remained low, however, at ±4.5 ksi (31.0 x 10^6 N/m^2).

Circumferential variations of flow distribution parameters.--Typical hub and shroud wall static pressure circumferential distributions at five axial stations between the distortion screen and rotor inlet planes are shown in fig. 56 for design speed (reading 284), wherein a static pressure decay behind the screen is indicated at all axial planes. Fig. 57 shows the total pressure distribution at design speed for 10, 47, and 90 percent of span obtained at the rotor inlet, rotor exit, and stage exit measuring planes. At design speed, the exit pressure distortion was amplified in the hub region, but attenuated in the midspan and tip regions. Only a small spanwise gradient in static pressure exists at the stage exit plane as seen in fig. 58. The circumferential distributions of absolute Mach number resulting from the static and total pressure distributions is shown in fig. 59. A significant feature is the low value of Mach number at the screen centerline adjacent to the hub at the stage exit plane.

The stage exit total temperature circumferential distribution obtained from fixed instrumentation is presented in fig. 60 for design speed data point reading 284. Fig. 61 presents the absolute velocity distribution showing the low value near the hub at station 12. Fig. 62 presents the measured flow angle distributions at the rotor inlet and exit plane for this design speed reading.

Rotor inlet preswirl (positive angles in the direction of rotor rotation) is created from 180 through 360 deg (viewed aft looking forward), while counterswirl is created from zero to 180 deg. A 10-deg error, suspected to be due to an offset during calibration in rotor inlet angle, was experienced. The angle-changes are, however, consistent with those of the other two immersions. Fig. 63 presents the circumferential distribution of rotor inlet and rotor exit axial velocity for reading 284, which reflects what was previously seen in the distributions of absolute Mach number and absolute velocity.

Design speed circumferential distributions of relative Mach number, relative velocity, and relative flow angle at the rotor inlet and exit planes for 10, 47, and 90 percent span from the tip are presented in figs. 64, 65, and 66. The influence of the screen on these relative parameters is more severe in the streamline adjacent to the hub than in the midspan and tip regions. Tabulations of additional data showing circumferential variations of flow distribution parameters are presented in ref. 4.

CONCLUDING REMARKS

With uniform inlet flow, the fan stage produced a peak efficiency of 84 percent at the design tip speed of 1600 ft/sec (488.6 m/sec), but a higher-than-design flow and pressure ratio. The design stage efficiency goal of 86 percent was obtained at the design specific flow of 42 lb/sec-ft^2 (205.1 kgm/sec-m^2), but at a pressure ratio of 1.6 instead of 1.5, and only 95 percent of design speed. A stall margin of 24 percent was achieved at the design speed and pressure ratio.

The rotor blade sections in the outboard, supersonic region exceeded design efficiency levels, thereby substantiating the method of characteristics design procedure and the assumption of oblique shocks. The subsonic sections adjacent to the hub, however, were moderately deficient because design incidence was not achieved. Inlet flow was shifted toward the hub resulting in rotor hub incidences considerably less than design. The st[illegible]r vane incurred large end-wall losses, thereby preventing the stage from reaching the efficiency goal at design speed.

The transition between rotor-tip-passage "started" and "unstarted" operating modes was seen to occur as low as 90 percent of design speed, wherein an abrupt decay in rotor efficiency was obtained from wide-open throttle with only a small increase in back pressure. Data from the high-frequency-response instrumentation over the rotor tips and from holograms obtained under separate contract also substantiate this minimum speed of transition. The highest speed at which the passage was seen to unstart was at 95 percent of design speed, near stall, as indicated by the rotor tip high-frequency-response data. Holograms show the leading-edge shock to be oblique and attached for the started condition and detached and near normal to the passage for the unstarted condition.

Holograms taken at and near design speed show not only the leading-edge and trailing-edge shocks that were considered in the design of the fan stage, but also a conical shock emanating from the intersection of the midspan damper leading edge and blade suction surface and a second damper shock, neither of which were considered in the design analysis. Some of the high losses in the midspan damper region may be due to this shock system.

The stall limit line was reduced by both tip-radial and circumferential inlet distortion. Reduction in wide-open throttle flow, stall pressure ratio, and peak efficiency level resulted from all types of distortion tested.

TABLE 1

UNIFORM INLET FLOW PERFORMANCE DATA SUMMARY

$\frac{N/\sqrt{\theta}}{(N/\sqrt{\theta})_{des}}$	Reading	$\frac{W\sqrt{\theta}/\delta}{(W\sqrt{\theta}/\delta)_{des}}$	$\frac{T_{T12}-T_{T5}}{T_{T5}}$	Rotor			Stage		
				P_{T9}/P_{T5}	η_{ad}	η_{poly}	P_{T12}/P_{T5}	η_{ad}	η_{poly}
0.60	59	0.686	0.0444	1.152	0.927	0.929	1.145	0.889	0.891
0.60	61	0.650	0.0548	1.185	0.908	0.910	1.179	0.880	0.883
0.60	62	0.618	0.0608	1.203	0.892	0.894	1.197	0.866	0.869
0.60	63	0.565	0.0695	1.223	0.853	0.857	1.213	0.816	0.821
0.60	64	0.499	0.0801	1.245	0.807	0.813	1.221	0.733	0.740
0.70	67	0.793	0.0627	1.210	0.891	0.894	1.196	0.835	0.839
0.70	69	0.764	0.0744	1.262	0.921	0.924	1.250	0.882	0.886
0.70	70	0.731	0.0833	1.289	0.904	0.907	1.277	0.869	0.873
0.70	71	0.656	0.0997	1.328	0.847	0.853	1.307	0.798	0.805
0.70	74	0.590	0.1095	1.347	0.811	0.819	1.310	0.732	0.742
0.80	75	0.881	0.0825	1.274	0.867	0.872	1.250	0.736	0.802
0.80	76	0.869	0.0991	1.338	0.876	0.881	1.324	0.841	0.847
0.80	80	0.842	0.1106	1.396	0.903	0.907	1.371	0.853	0.859
0.80	81	0.801	0.1236	1.440	0.888	0.894	1.415	0.842	0.850
0.80	83	0.742	0.1345	1.457	0.844	0.852	1.428	0.795	0.805
0.80	85	0.699	0.1438	1.468	0.806	0.816	1.424	0.738	0.750
0.90	103	0.984	0.1016	1.352	0.885	0.890	1.320	0.811	0.818
0.90	100	0.971	0.1252	1.429	0.858	0.865	1.414	0.830	0.838
0.90	101	0.957	0.1426	1.500	0.861	0.868	1.479	0.828	0.837
0.90	106	0.942	0.1530	1.545	0.865	0.873	1.524	0.834	0.844
0.90	115	0.887	0.1721	1.612	0.850	0.850	1.580	0.809	0.821
0.90	116	0.863	0.1764	1.621	0.840	0.850	1.574	0.782	0.795
0.95	104	1.019	0.1136	1.396	0.879	0.885	1.348	0.784	0.793
0.95	105	1.016	0.1353	1.490	0.892	0.898	1.449	0.825	0.834
0.95	117	1.008	0.1523	1.583	0.921	0.926	1.540	0.861	0.869
0.95	118	0.995	0.1665	1.640	0.900	0.907	1.604	0.855	0.864
0.95	119	0.952	0.1914	1.711	0.867	0.876	1.656	0.808	0.821
0.95	120	0.918	0.1966	1.709	0.842	0.853	1.658	0.788	0.803
1.00	107	1.040	0.1261	1.429	0.851	0.858	1.369	0.743	0.754
1.00	108	1.044	0.1462	1.510	0.854	0.863	1.475	0.803	0.813
1.00	128	1.041	0.1524	1.545	0.867	0.875	1.505	0.812	0.822
1.00	125	1.035	0.1677	1.623	0.884	0.892	1.572	0.821	0.83[illegible]
1.00	126	1.031	0.1877	1.724	0.897	0.905	1.669	0.837	0.849
1.00	127	1.016	0.2060	1.770	0.860	0.871	1.738	0.827	0.840
[a]1.00	210	0.986	0.2201	1.806	0.836	0.849	1.763	0.796	0.812
1.10	109	1.079	0.1493	1.491	0.809	0.820	1.413	0.695	0.709
1.10	110	1.081	0.1589	1.522	0.802	0.814	1.475	0.738	0.752
1.10	113	1.082	0.1854	1.653	0.833	0.844	1.597	0.770	0.784
1.10	114	1.083	0.2049	1.736	0.832	0.845	1.582	0.779	0.794

[a] Obtained during predistortion baseline testing.

TABLE 2

PREDISTORTION BASELINE PERFORMANCE DATA SUMMARY

$\frac{N/\sqrt{\theta}}{(N/\sqrt{\theta})_{des}}$	Reading	$\frac{W\sqrt{\theta}/\delta}{(W\sqrt{\theta}/\delta)_{des}}$	$\frac{T_{T12}-T_{T5}}{T_{T5}}$	Rotor P_{T9}/P_{T5}	Rotor η_{ad}	Rotor η_{poly}	Stage P_{T12}/P_{T5}	Stage η_{ad}	Stage η_{poly}
0.70	195	0.791	0.0627	1.211	0.897	0.900	1.199	0.849	0.853
0.70	196	0.759	0.0744	1.258	0.911	0.914	1.246	0.872	0.876
0.70	197	0.737	0.0837	1.288	0.896	0.900	1.276	0.862	0.866
0.70	198	0.656	0.0989	1.330	0.858	0.864	1.311	0.814	0.821
0.70	199	0.581	0.1111	1.342	0.789	0.798	1.303	0.706	0.717
0.90	200	0.985	0.1033	1.356	0.880	0.885	1.329	0.818	0.825
0.90	201	0.967	0.1238	1.426	0.862	0.869	1.408	0.828	0.837
0.90	202	0.954	0.1426	1.505	[illegible]	0.876	1.485	0.837	0.846
0.90	203	0.943	0.1537	1.552	0.871	0.878	1.530	0.839	0.848
0.90	211	0.908	0.1652	1.593	0.861	0.870	1.565	0.824	0.835
0.90	204	0.865	0.1722	1.607	0.843	0.853	1.571	0.798	0.810
1.00	205	1.040	0.1284	1.437	0.850	0.857	1.395	0.777	0.787
1.00	206	1.040	0.1538	1.536	0.848	0.857	1.511	0.813	0.823
1.00	207	1.041	0.1691	1.610	0.862	0.871	1.583	0.827	0.838
1.00	208	1.035	0.1862	1.704	0.883	0.892	1.676	0.852	0.862
1.00	210	0.986	0.2201	1.806	0.836	0.849	1.763	0.796	0.812

TABLE 3

HUB RADIAL DISTORTION PERFORMANCE DATA SUMMARY

$\frac{N/\sqrt{\theta}}{(N/\sqrt{\theta})_{des}}$	Reading	$\frac{W\sqrt{\theta}/\delta}{(W\sqrt{\theta}/\delta)_{des}}$	$\frac{T_{T12}-T_{T5}}{T_{T5}}$	Rotor			Stage		
				P_{T9}/P_{T5}	η_{ad}	η_{poly}	P_{T12}/P_{T5}	η_{ad}	η_{poly}
0.70	224	0.739	0.0663	1.217	0.872	[illegible]	1.200	0.806	0.811
0.70	225	0.706	0.0783	1.254	0.854	0.859	1.243	0.817	0.823
0.70	226	0.670	0.0840	1.275	0.856	0.861	1.258	0.805	0.811
0.70	227	0.594	0.0979	1.310	0.820	0.826	1.273	0.728	0.737
0.70	271	0.509	0.1221	1.330	0.695	0.707	1.284	0.605	0.619
[a] 0.70	228	0.493							
0.90	229	0.953	0.1091	1.365	0.852	0.858	1.333	0.782	0.791
0.90	230	0.923	0.1296	1.454	0.870	0.877	1.416	0.805	0.814
0.90	231	0.872	0.1437	1.484	0.831	0.840	1.447	0.773	0.784
0.90	232	0.828	0.1549	1.500	0.793	0.804	1.465	0.742	0.756
0.90	233	0.800	0.1589	1.509	0.785	0.797	1.470	0.730	0.745
0.90	271	0.679	0.1895	1.547	0.701	0.718	1.479	0.622	0.642
[a] 0.90	235	0.660							
1.00	223	1.022	0.1319	1.434	0.822	0.831	1.390	0.746	0.757
1.00	220	1.002	0.1604	1.560	0.845	0.854	1.517	0.787	0.799
1.00	221	0.991	0.1766	1.658	0.880	0.888	1.583	0.792	0.805
1.00	222	0.962	0.1832	1.661	0.852	0.862	1.589	0.769	0.784
1.00	237	0.921	0.1918	1.622	0.773	0.788	1.585	0.730	0.747

[a] Stall flow only obtained.

TABLE 4

TIP RADIAL DISTORTION PERFORMANCE DATA SUMMARY

$\frac{N/\sqrt{\theta}}{(N/\sqrt{\theta})_{des}}$	Reading	$\frac{W\sqrt{\theta}/\delta}{(W\sqrt{\theta}/\delta)_{des}}$	$\frac{T_{T12}-T_{T5}}{T_{T5}}$	Rotor			Stage		
				P_{T9}/P_{T5}	η_{ad}	η_{poly}	P_{T12}/P_{T5}	η_{ad}	η_{poly}
0.70	242	0.782	0.0693	1.236	0.900	0.903	1.217	0.832	0.836
0.70	242	0.748	0.0817	1.276	0.883	0.887	1.259	0.8[illegible]1	0.836
0.70	244	0.716	0.0897	1.299	0.865	0.870	1.281	0.817	0.823
0.70	245	0.677	0.0974	1.315	0.835	0.842	1.291	0.776	0.784
0.90	246	0.956	0.1160	1.377	0.825	0.833	1.336	0.743	0.753
0.90	248	0.948	0.1345	1.463	0.85[illegible]	0.861	1.426	0.791	0.802
0.90	249	0.937	0.1526	1.538	0.858	0.866	1.500	0.804	0.814
0.90	272	0.920	0.1573	1.547	0.844	0.853	1.513	0.797	0.809
[a]0.90	250	0.910							
0.97	241	0.997	0.1595	1.544	0.828	0.839	1.498	0.766	0.779
1.00	251	1.021	0.1365	1.452	0.824	0.833	1.395	0.730	0.742
1.00	252	1.022	0.1604	1.552	0.834	0.844	1.500	0.764	0.777
1.00	253	1.023	0.1713	1.592	0.829	0.840	1.546	0.771	0.784
1.00	254	1.019	0.1795	1.635	0.840	0.851	1.585	0.781	0.795
1.00	272	1.004	0.2044	1.720	0.820	0.833	1.664	0.763	0.779
[a]1.00	255	0.984							

[a] Stall flow only obtained.

TABLE 5

CIRCUMFERENTIAL DISTORTION PERFORMANCE DATA SUMMARY

$\frac{N/\sqrt{\theta}}{(N/\sqrt{\theta})_{des}}$	Reading	$\frac{W\sqrt{\theta}/\delta}{(W\sqrt{\theta}/\delta)_{des}}$	$\frac{T_{T12}-T_{T5}}{T_{T5}}$	Stage		
				P_{T9}/P_{T5}	η_{ad}	η_{poly}
0.70	263	0.768	0.0664	1.208	0.834	0.838
0.70	264	0.736	0.0773	1.249	0.846	0.851
0.70	265	0.707	0.0848	1.267	0.824	0.830
0.70	266	0.635	0.0989	1.286	0.753	0.761
[a]0.70	267	0.591				
0.90	276	0.963	0.1124	1.350	0.795	0.803
0.90	278	0.940	0.1343	1.432	0.804	0.813
0.90	279	0.904	0.1492	1.469	0.777	0.789
0.90	280	0.859	0.1648	1.498	0.741	0.756
[a]0.90	281	0.833				
1.00	283	1.027	0.1374	1.412	0.753	0.764
1.00	284	1.021	0.1645	1.534	0.789	0.801
1.00	285	1.002	0.1836	1.586	0.765	0.780
1.00	286	0.979	0.1946	1.610	0.746	0.763
[a]1.00	287	0.940				

[a] Stall flow only obtained.

Note: rotor-only values not computed.

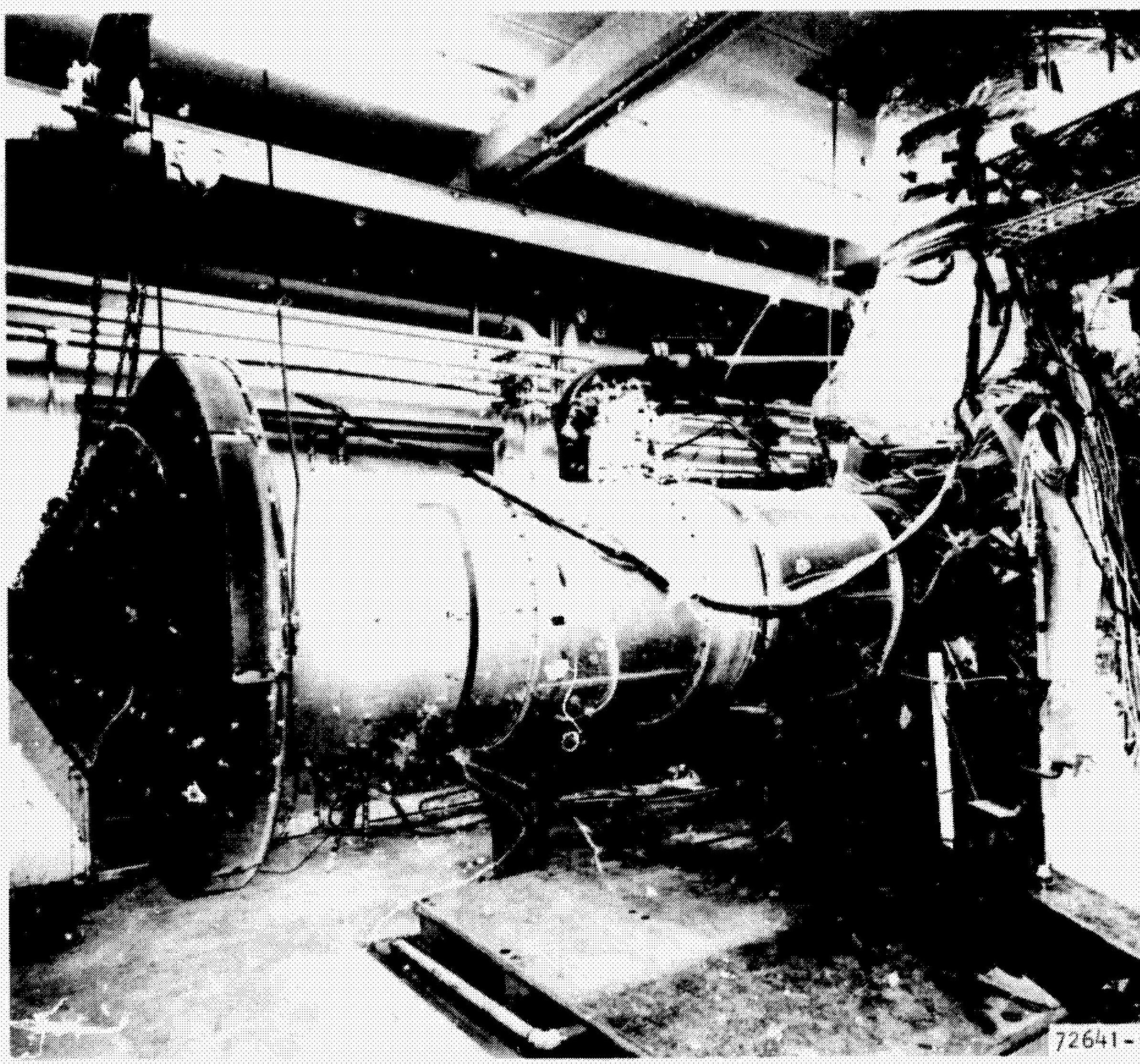

Figure 1.--Sea Level Compressor Test Cell.

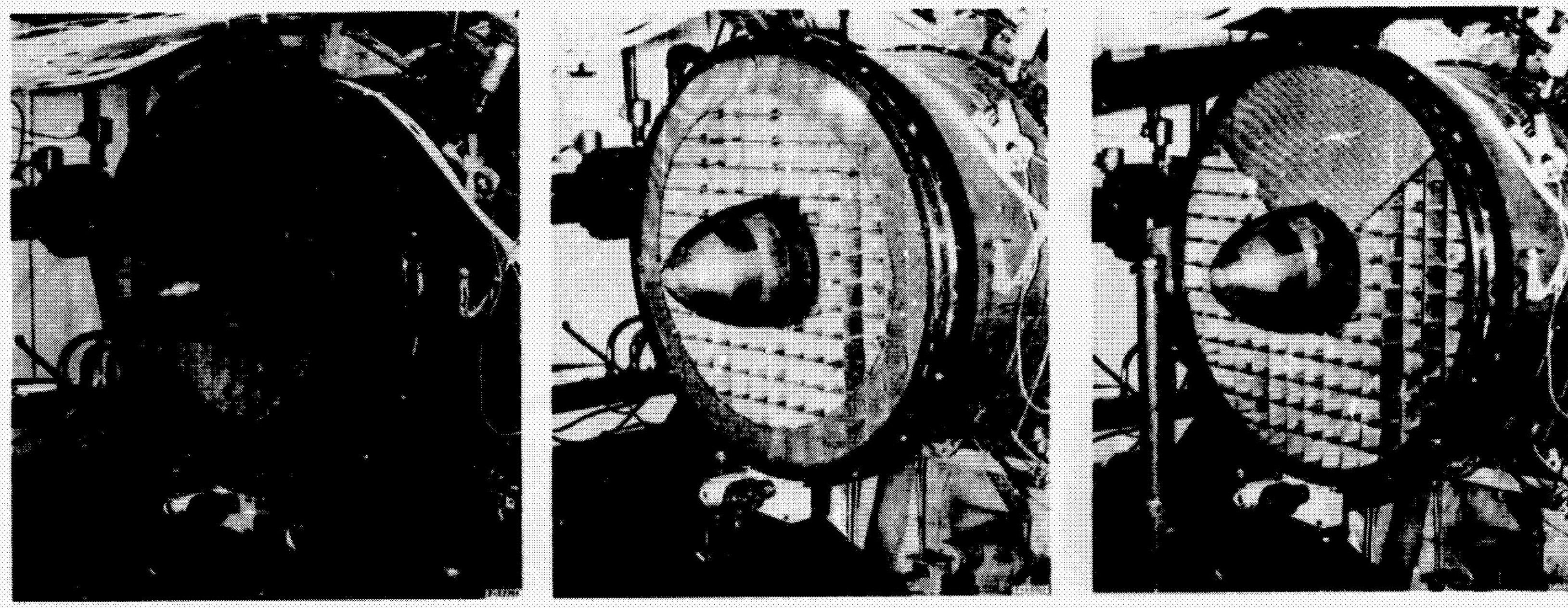

(a) Hub-radial distortion screen.

(b) Tip-radial distortion screen.

(c) Circumferential distortion screen.

F-18625

Figure 2.--Distortion Screens.

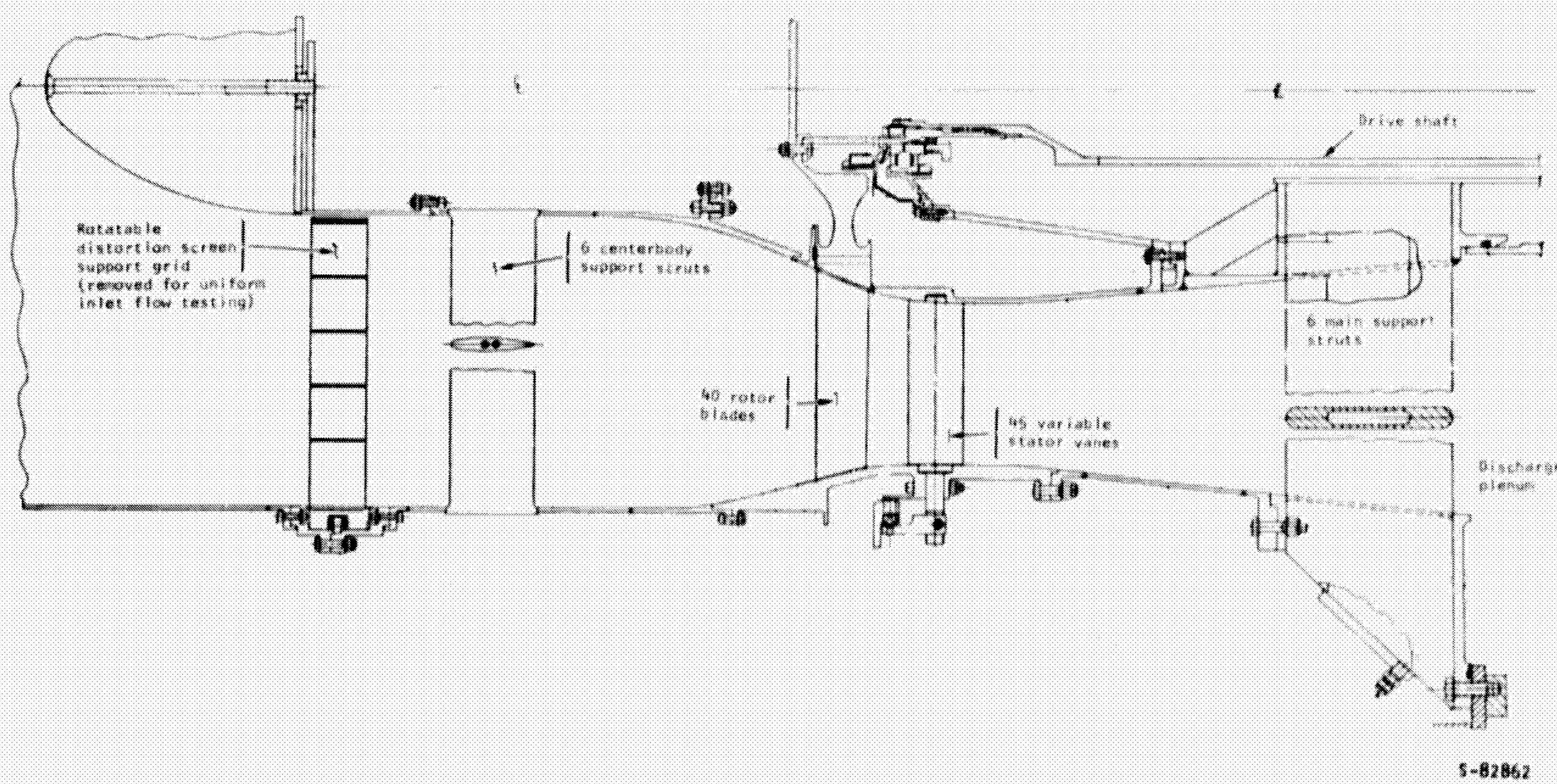

Figure 3.--Fan Cross Section.

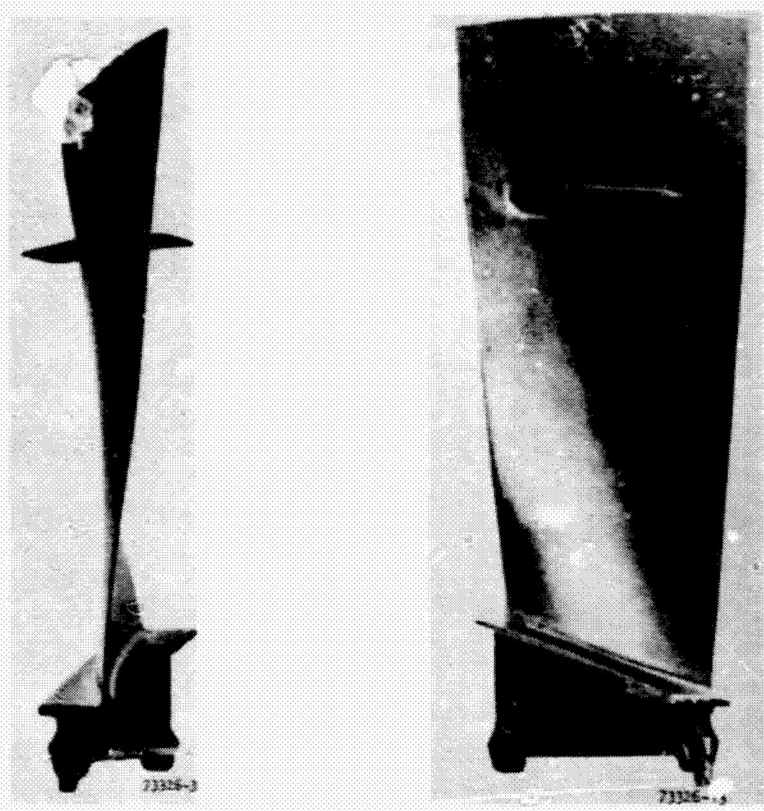

Figure 4.--Rotor Blade.

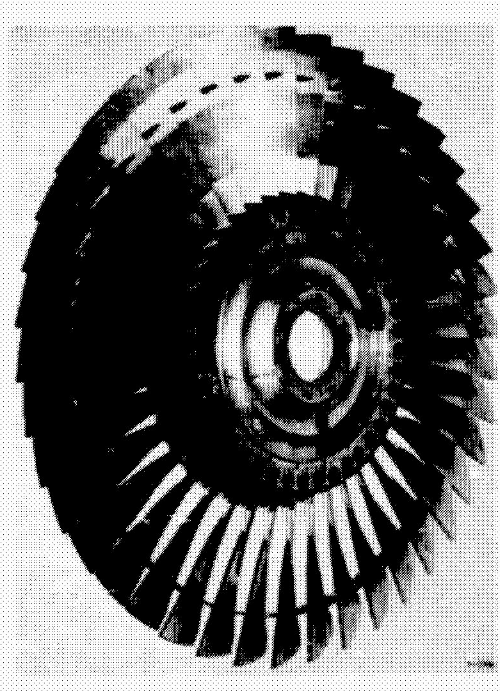

F-19102

Figure 5.--Bladed Disc Assembly.

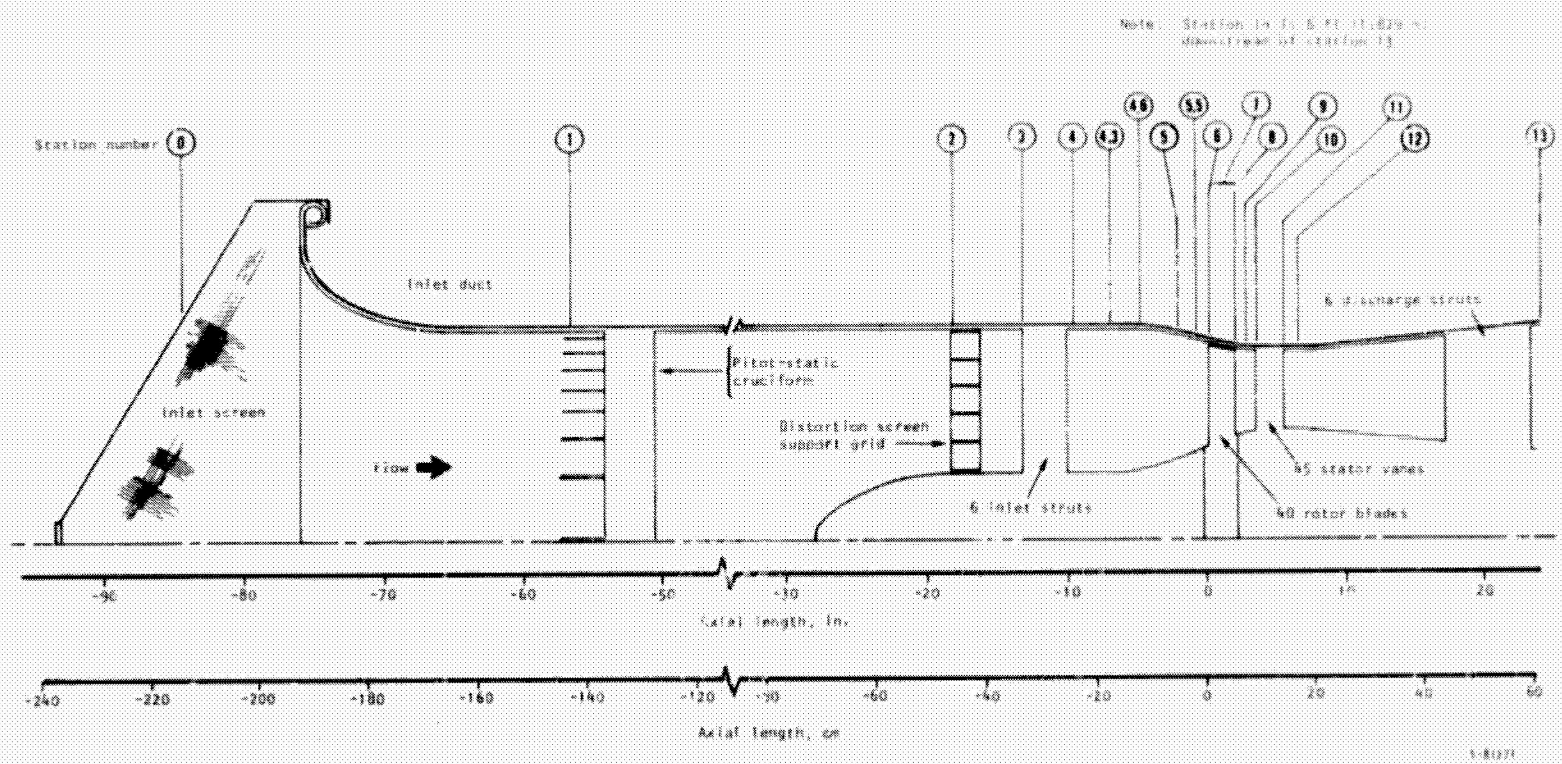

Station number	Location	Station number	Location
0	Inlet bellmouth screen	7	Rotor casing instrumentation
1	Bellmouth instrumentation plane	8	Rotor trailing edge
2	Distortion screen plane	9	Rotor exit traverse plane
3, 4, 4.3, 4.6	Inlet duct instrumentation	10	Stator leading edge
5	Rotor inlet instrumentation plane	11	Stator trailing edge
5.5	Rotor inlet traverse plane	12	Stage exit instrumentation plane
6	Rotor leading edge	13	Plenum inlet plane

Figure 6.--Axial Station Designations.

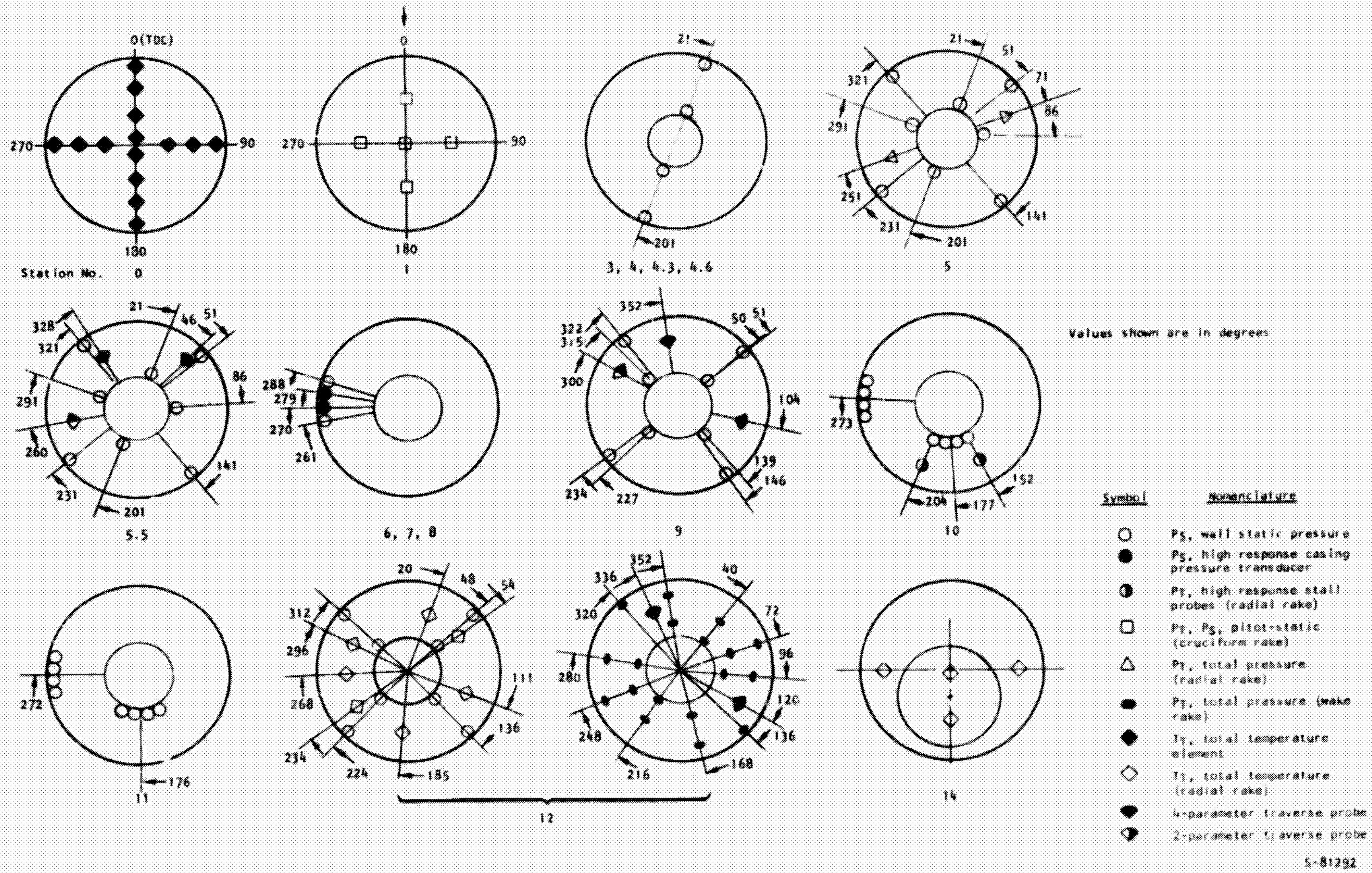

Figure 7.--Circumferential Position of Instrumentation Viewed Aft, Looking Forward.

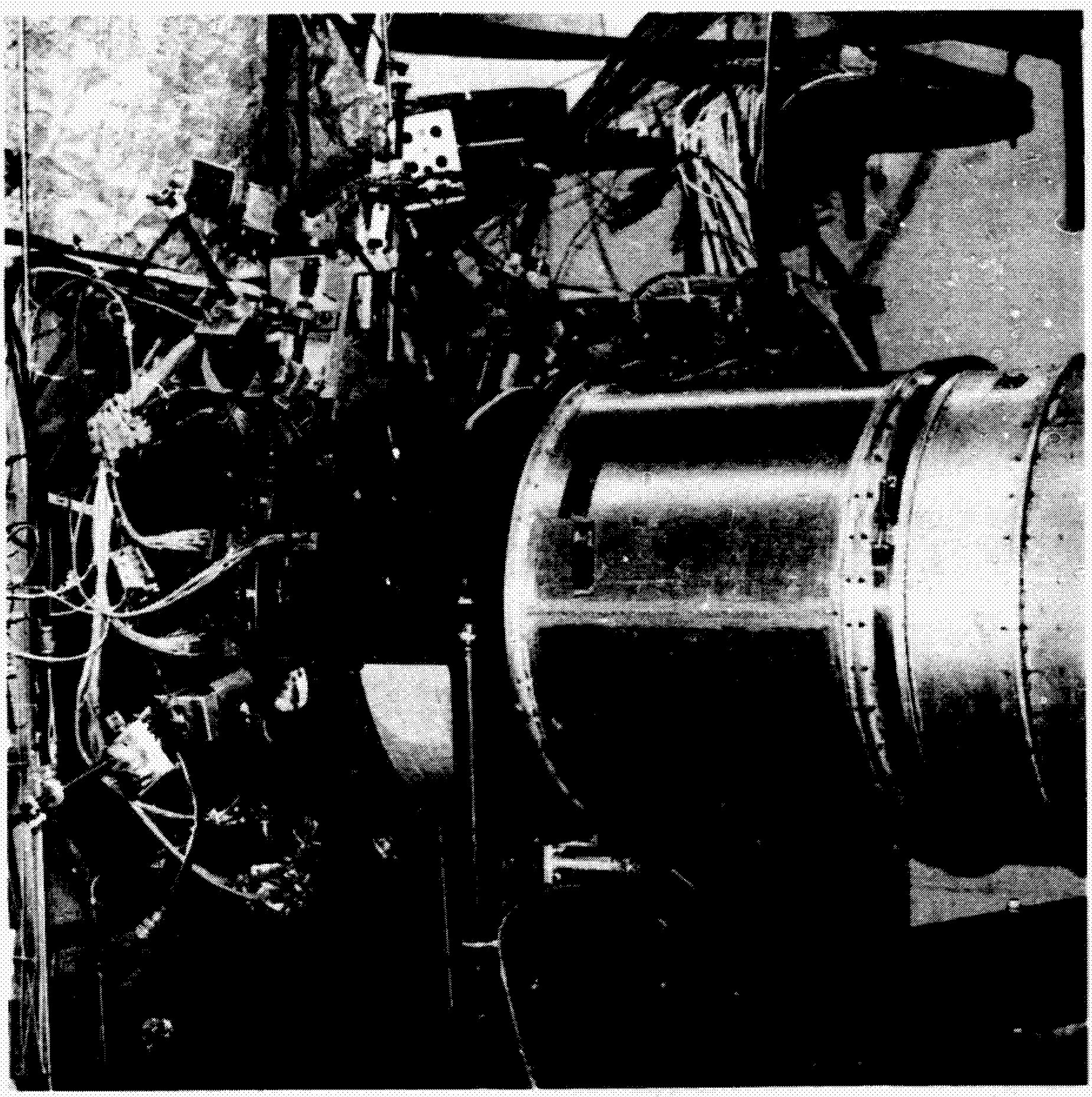

F-18623

Figure 8.--Instrumented Test Compressor.

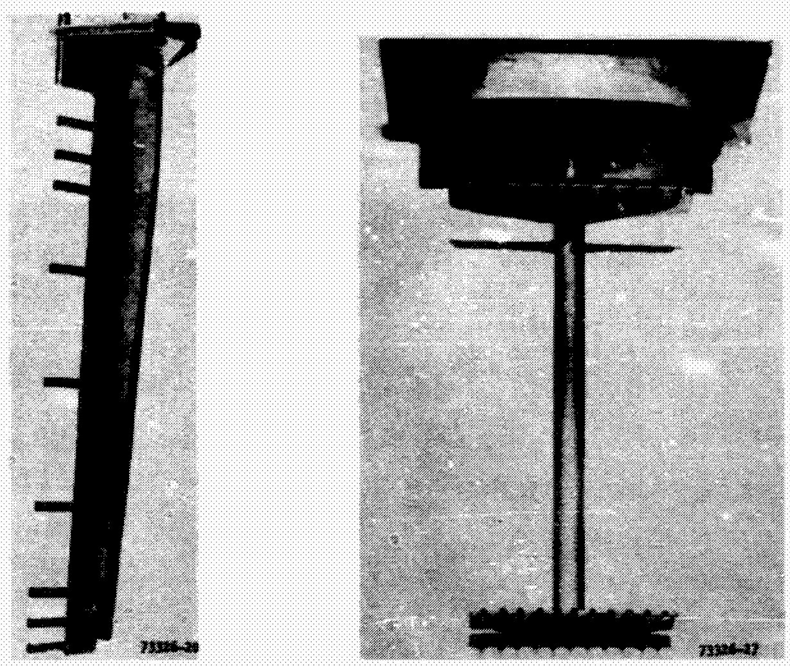

(a) Temperature Rake. (b) Total Pressure Rake.

Figure 9.--Stage Exit Temperature and Total Pressure Rakes.

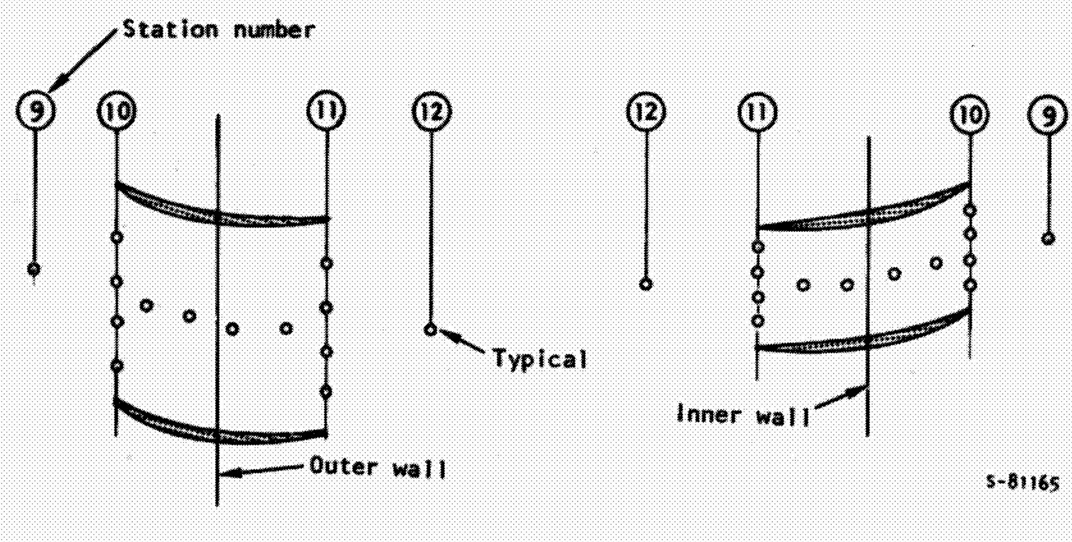

F-19137

Figure 10.--Stator Channel Static Pressure Schematic.

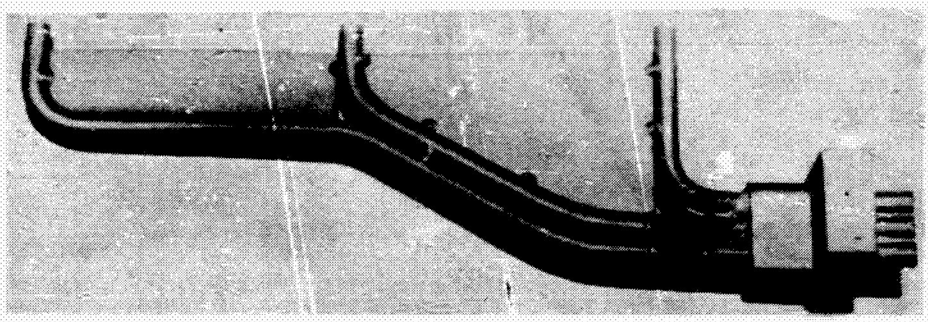

73326-21

(a) Stall Sensing Radial Rake.

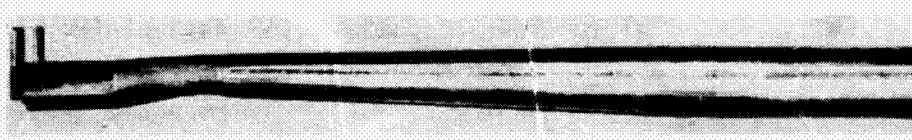

73326-25

(b) 60-Deg Wedge Probe.

73326-19

(c) 30-Deg Wedge Probe.

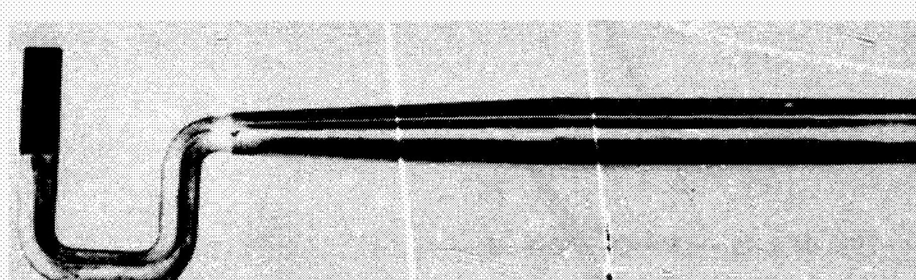

73326-18

(d) 8-Deg Wedge Probe.

F-18621

Figure 11.--Radial Rake and Wedge Probes.

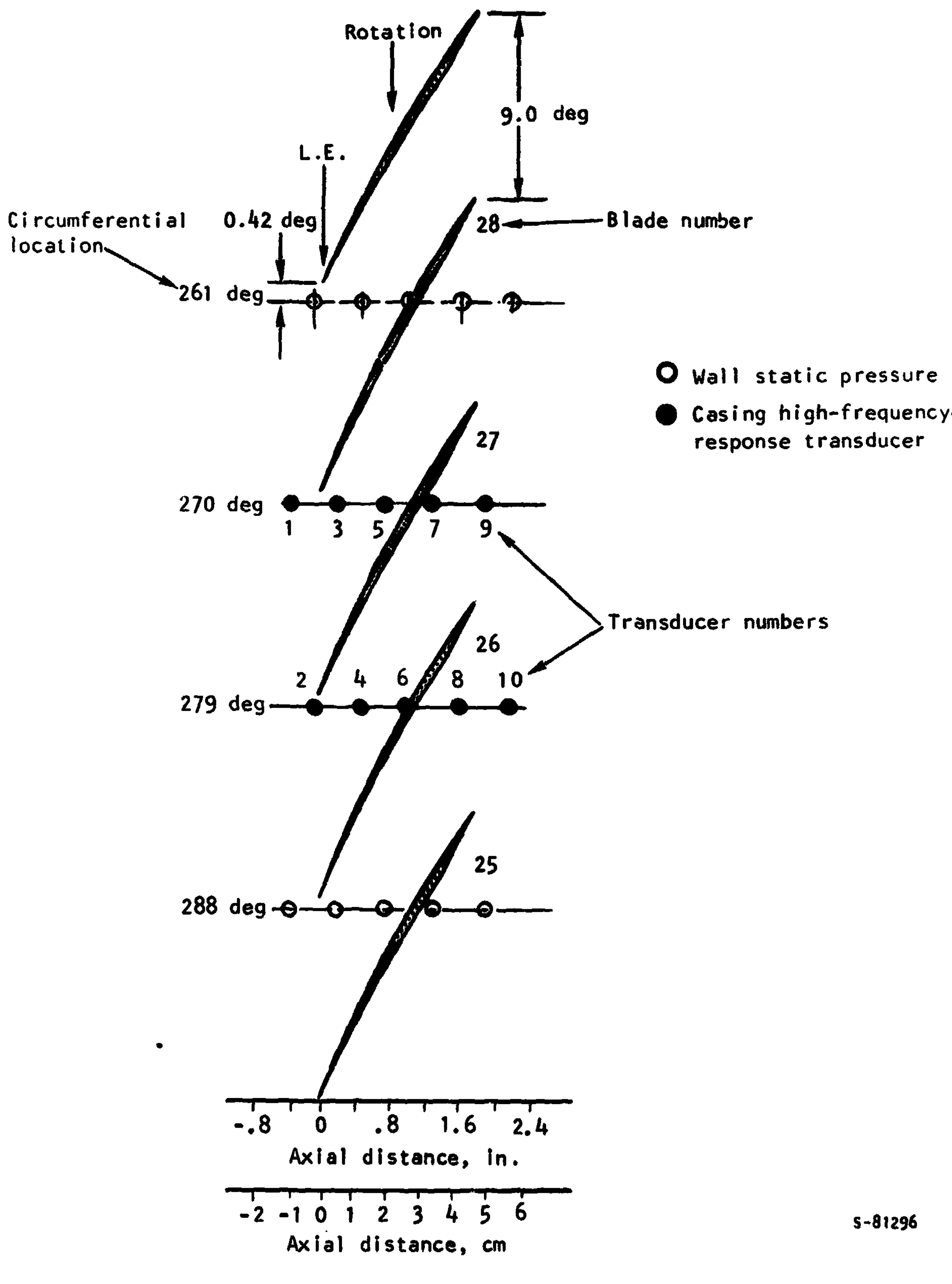

Figure 12.--High-Response Casing Pressure Transducer Locations.

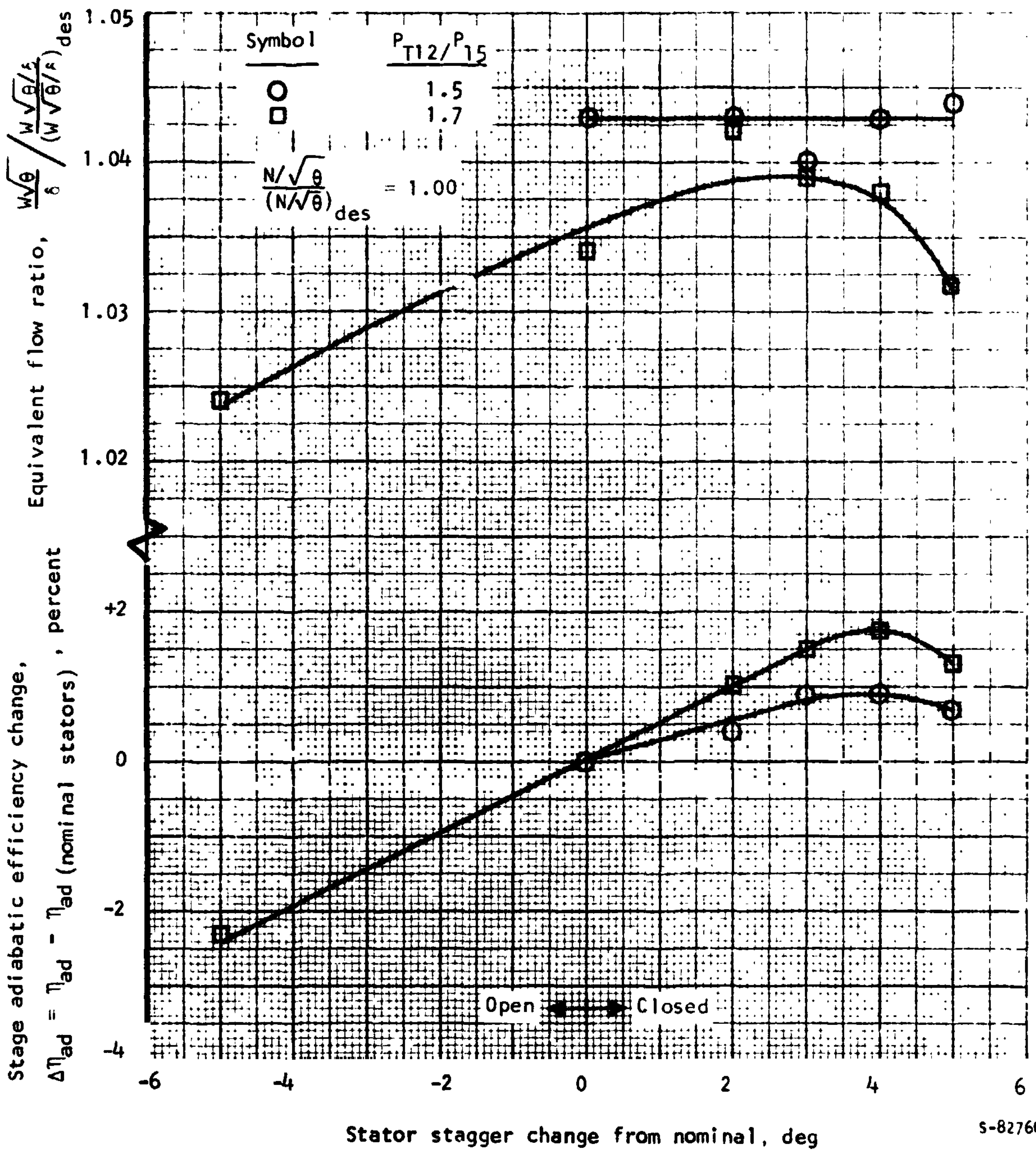

Figure 13.--Effect of Vane Stagger Settings on Stage Performance.

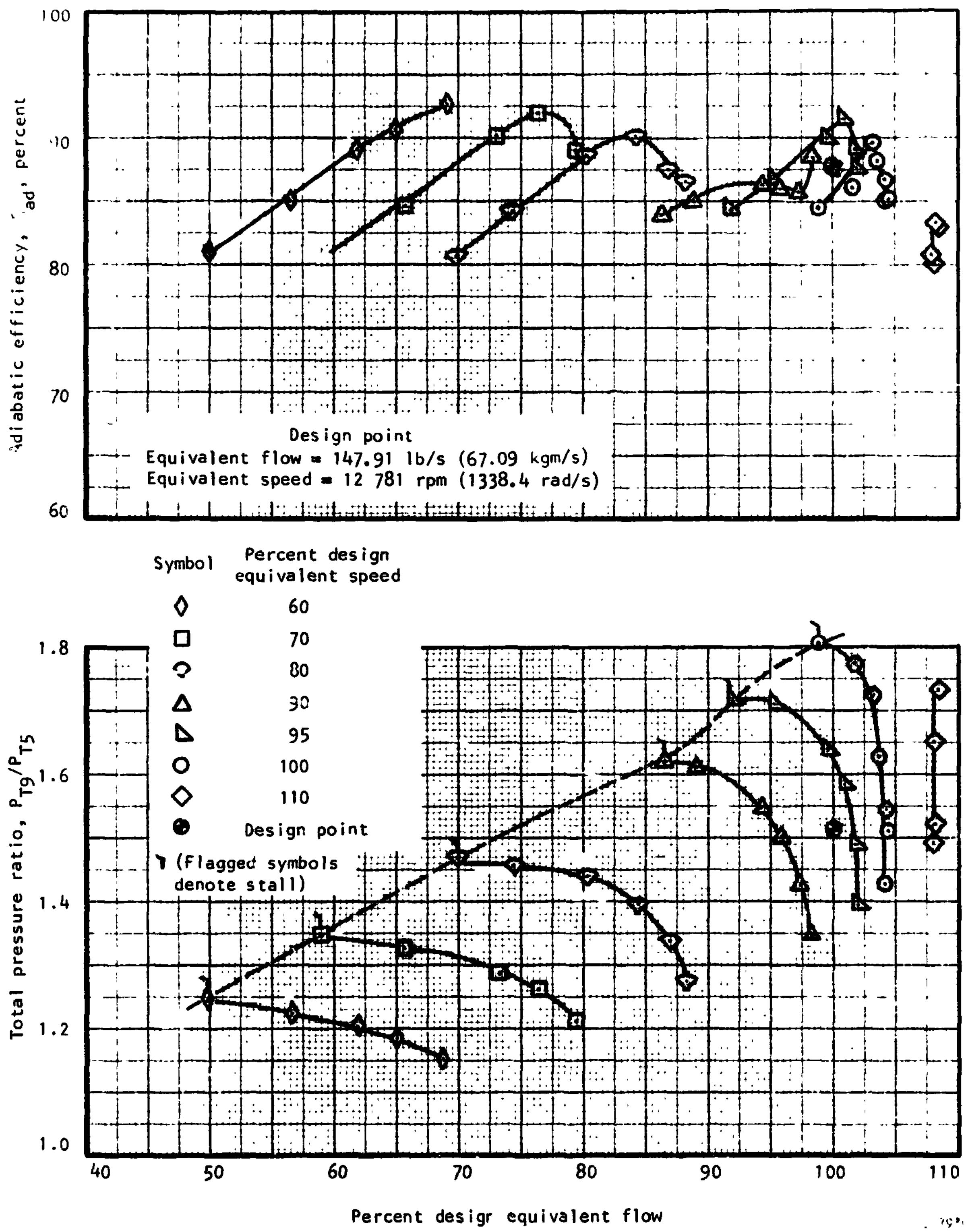

Figure 14.--Rotor Performance, Uniform Inlet Flow.

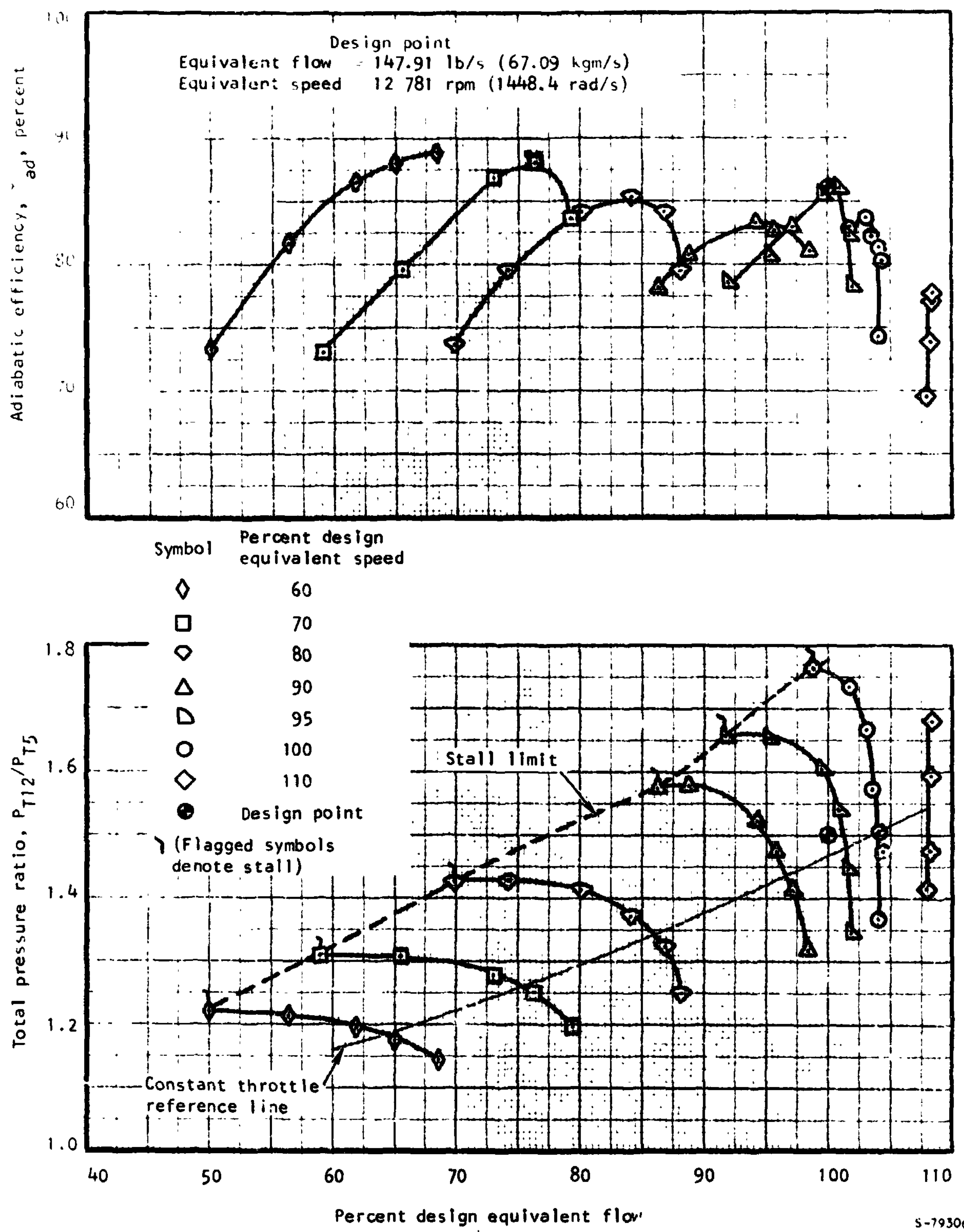

Figure 15.--Stage Performance, Uniform Inlet Flow.

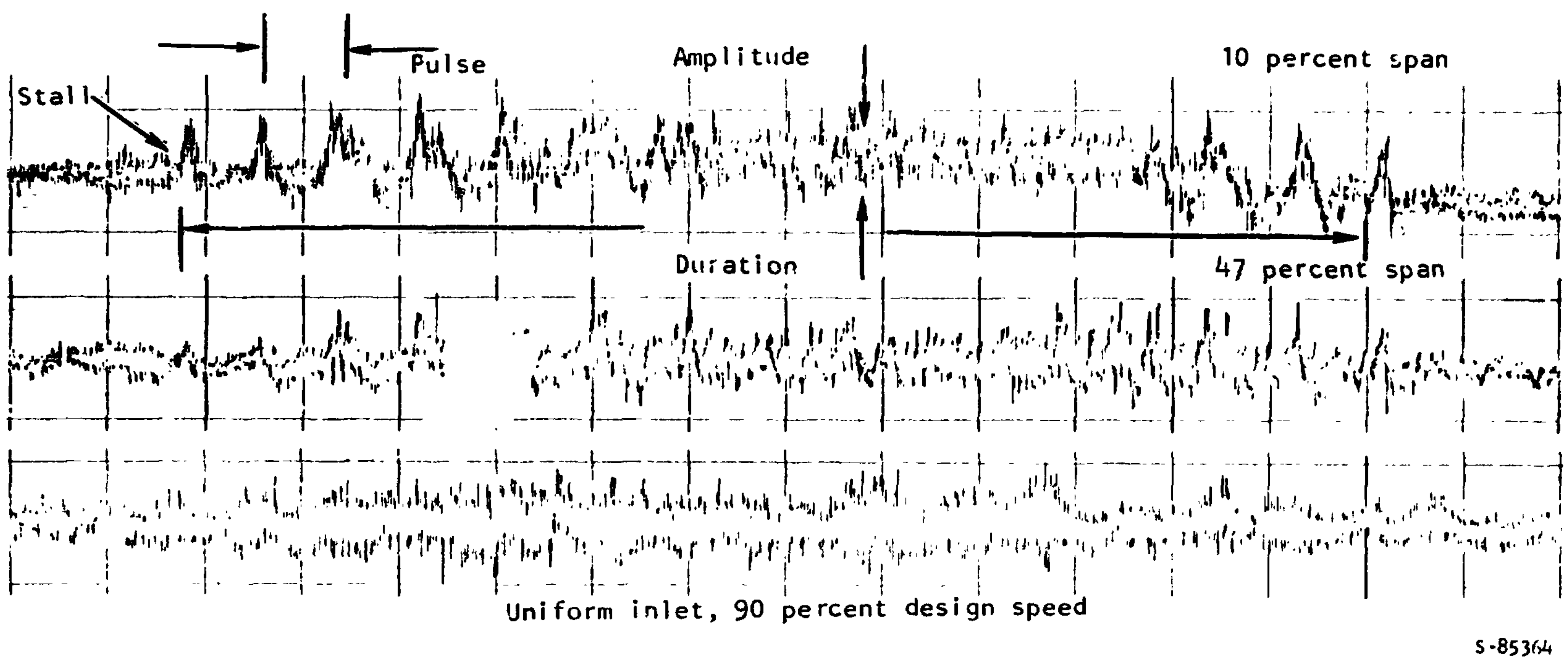

Figure 16.--Uniform Inlet Flow Stall Oscillograph Trace at 90 Percent Design Speed.

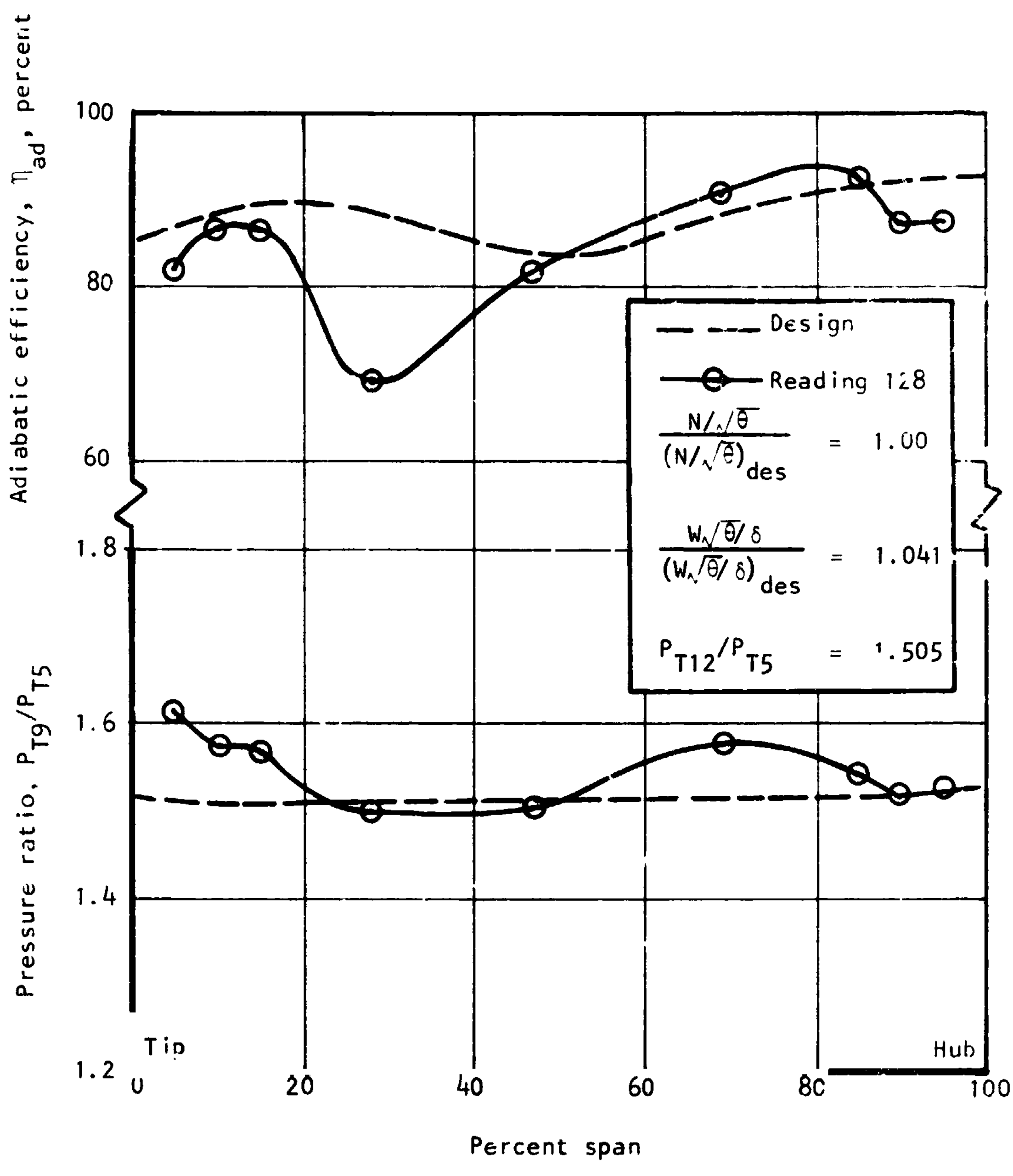

Figure 17.--Rotor Blade Element Performance, Uniform Inlet Flow.

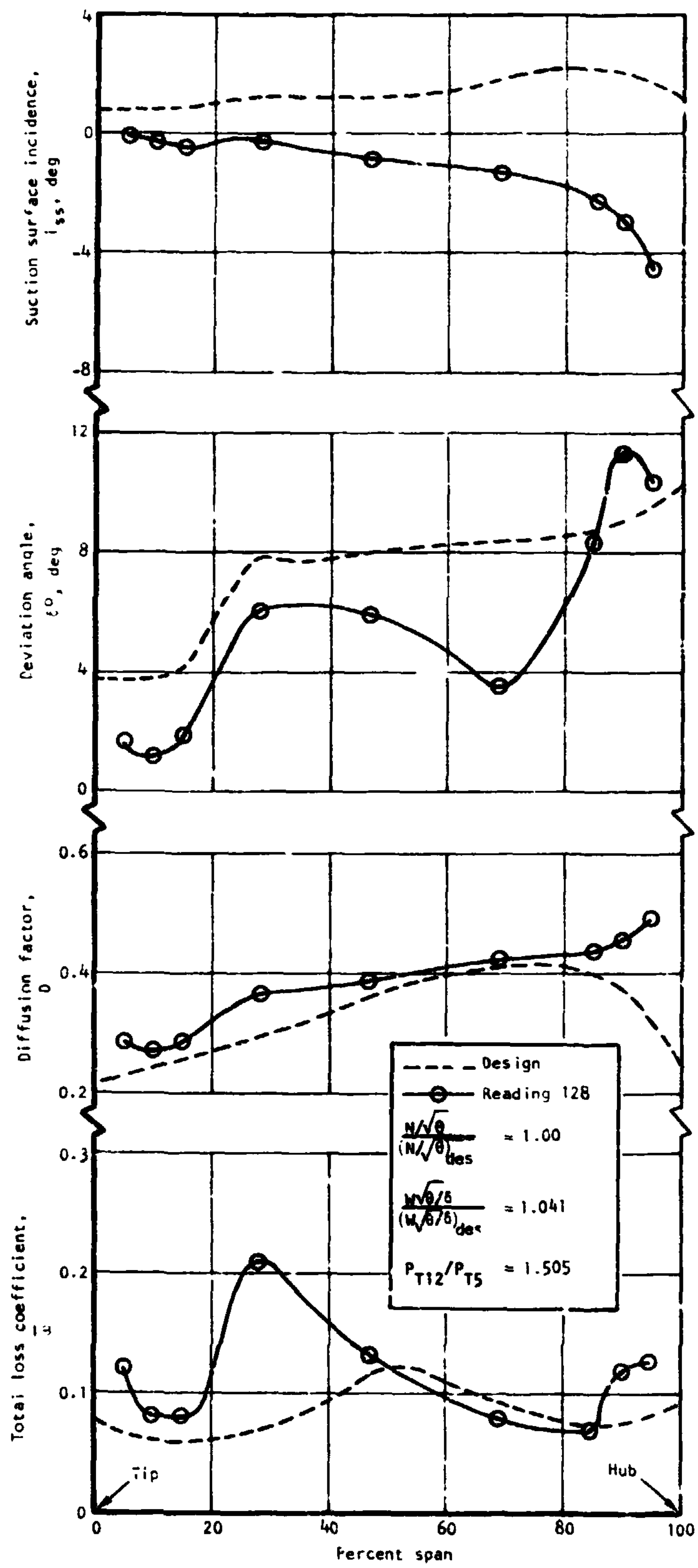

S-81796

Figure 18.--Rotor Blade Element Performance, Uniform Inlet Flow.

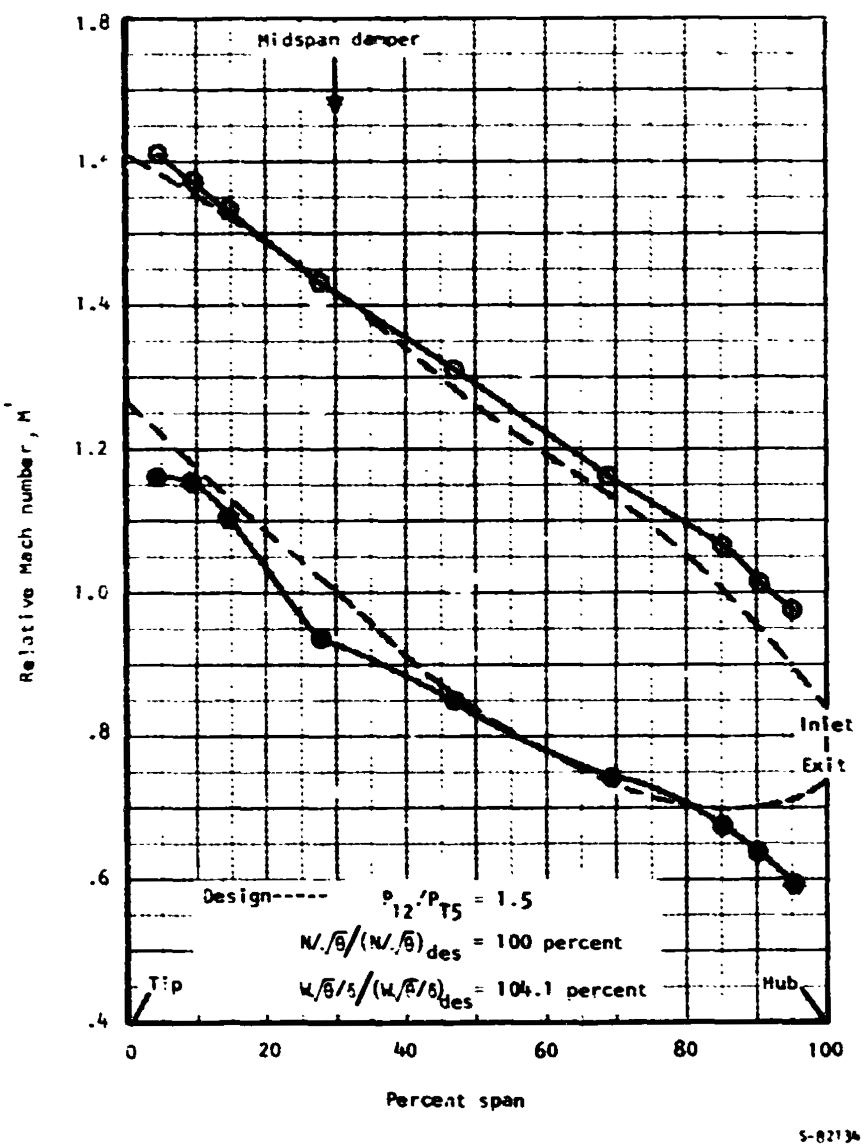

Figure 19.--Rotor Relative Mach Number, Design Speed and Design Pressure Ratio.

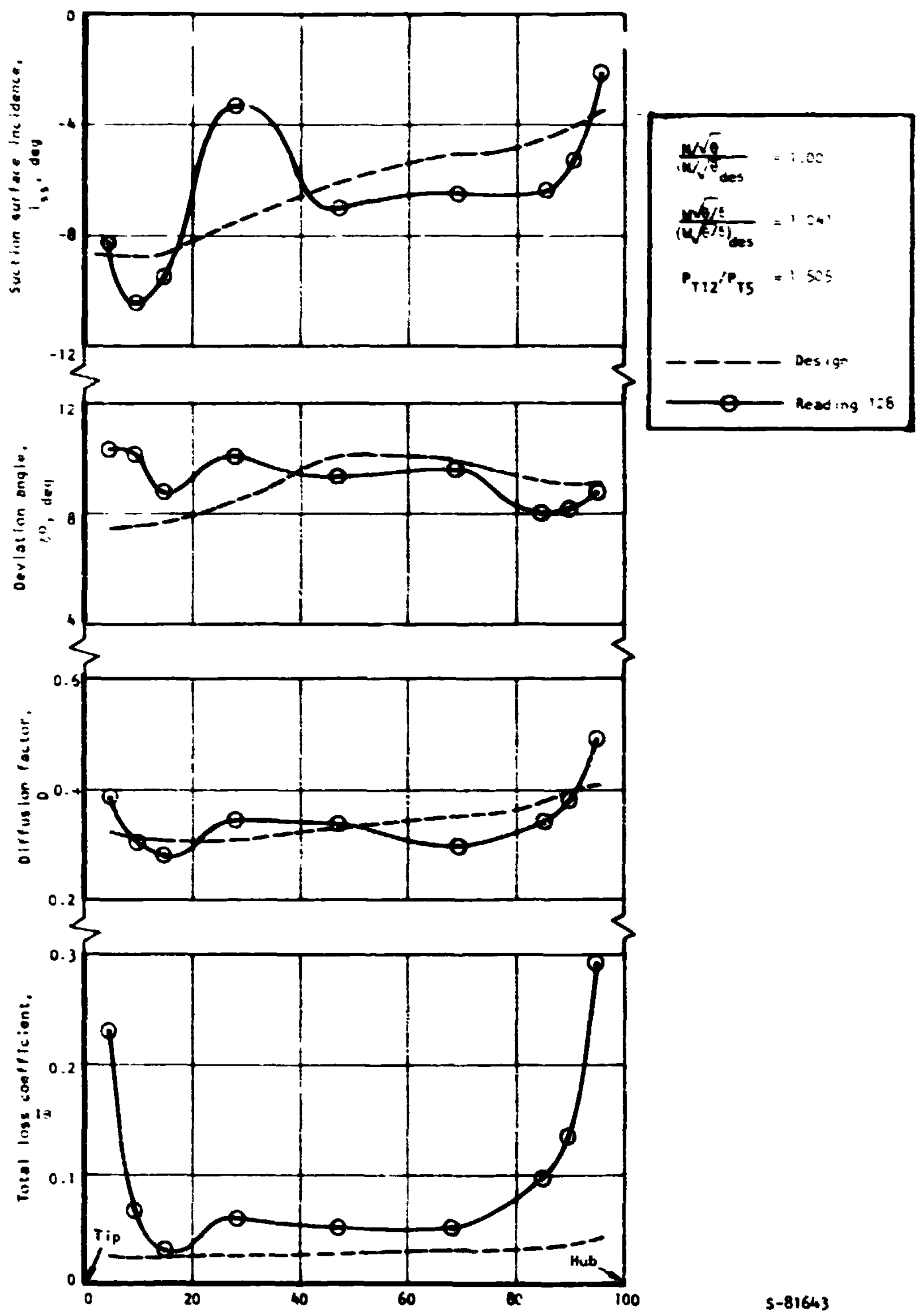

Figure 20.--Stator Vane Element Performance, Uniform Inlet Flow.

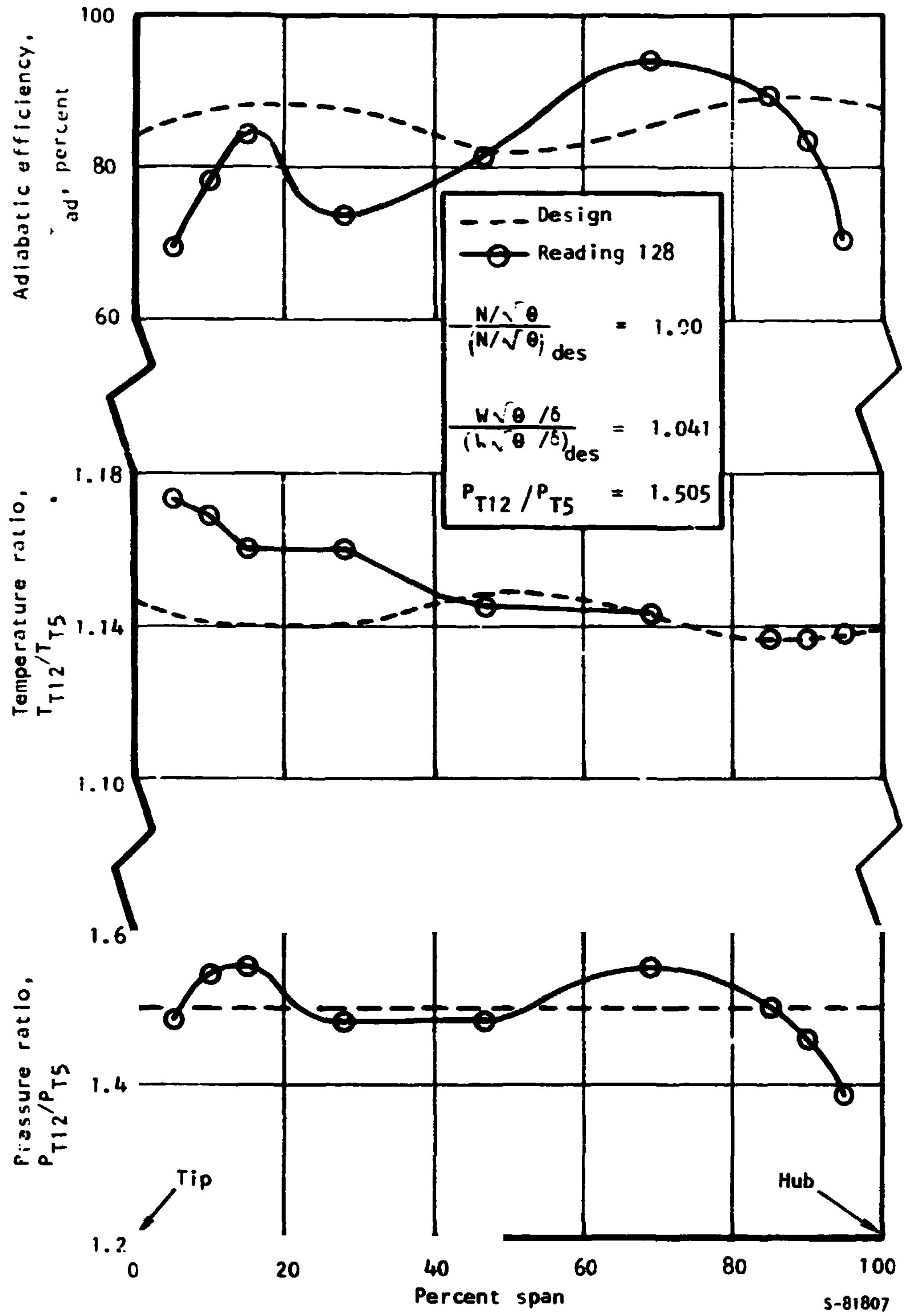

Figure 21. -- Stage Element Performance, Uniform Inlet Flow.

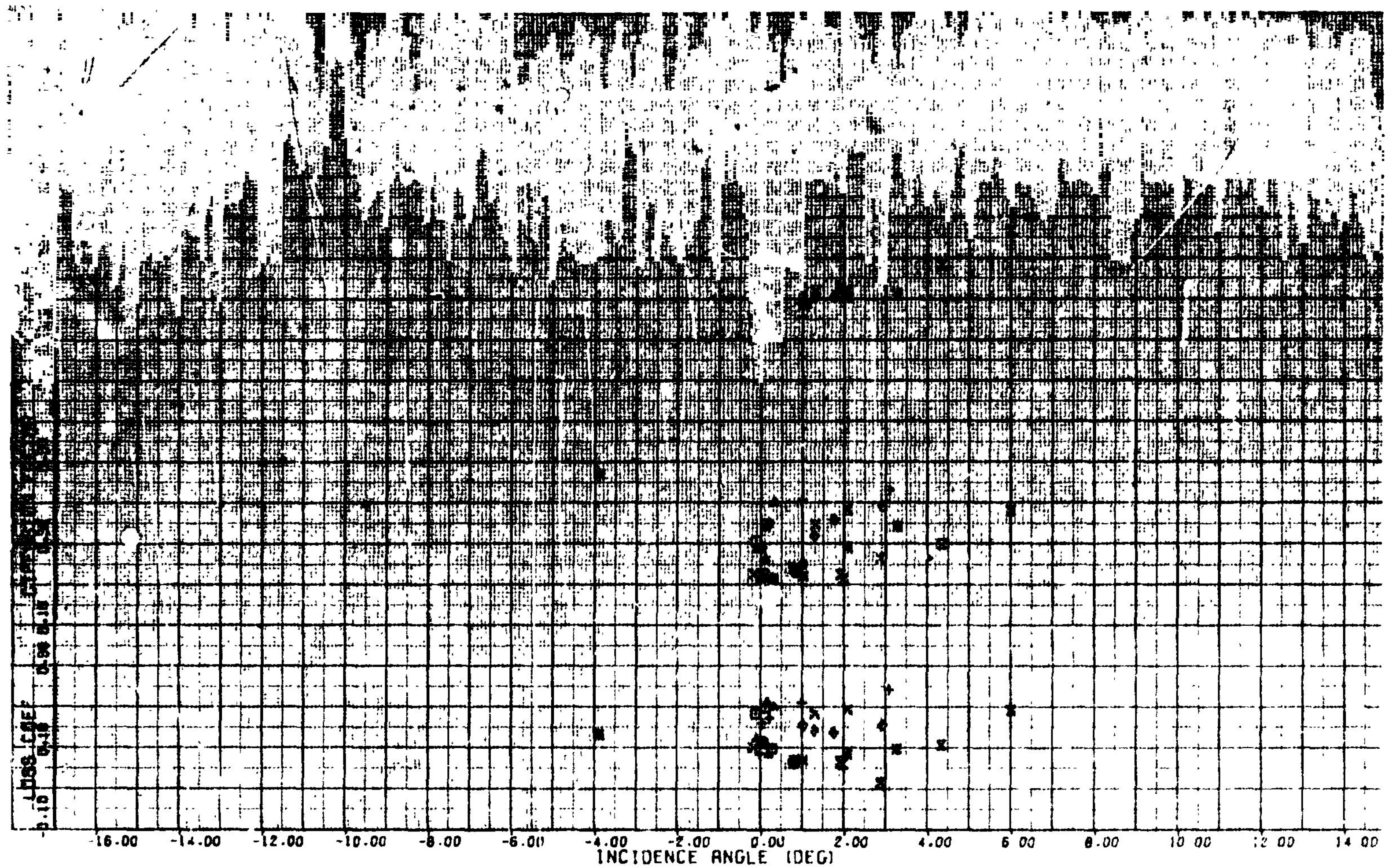

Figure 22a.--Rotor Blade Element Performance, Uniform Inlet Flow, 5 Percent Span from Tip.

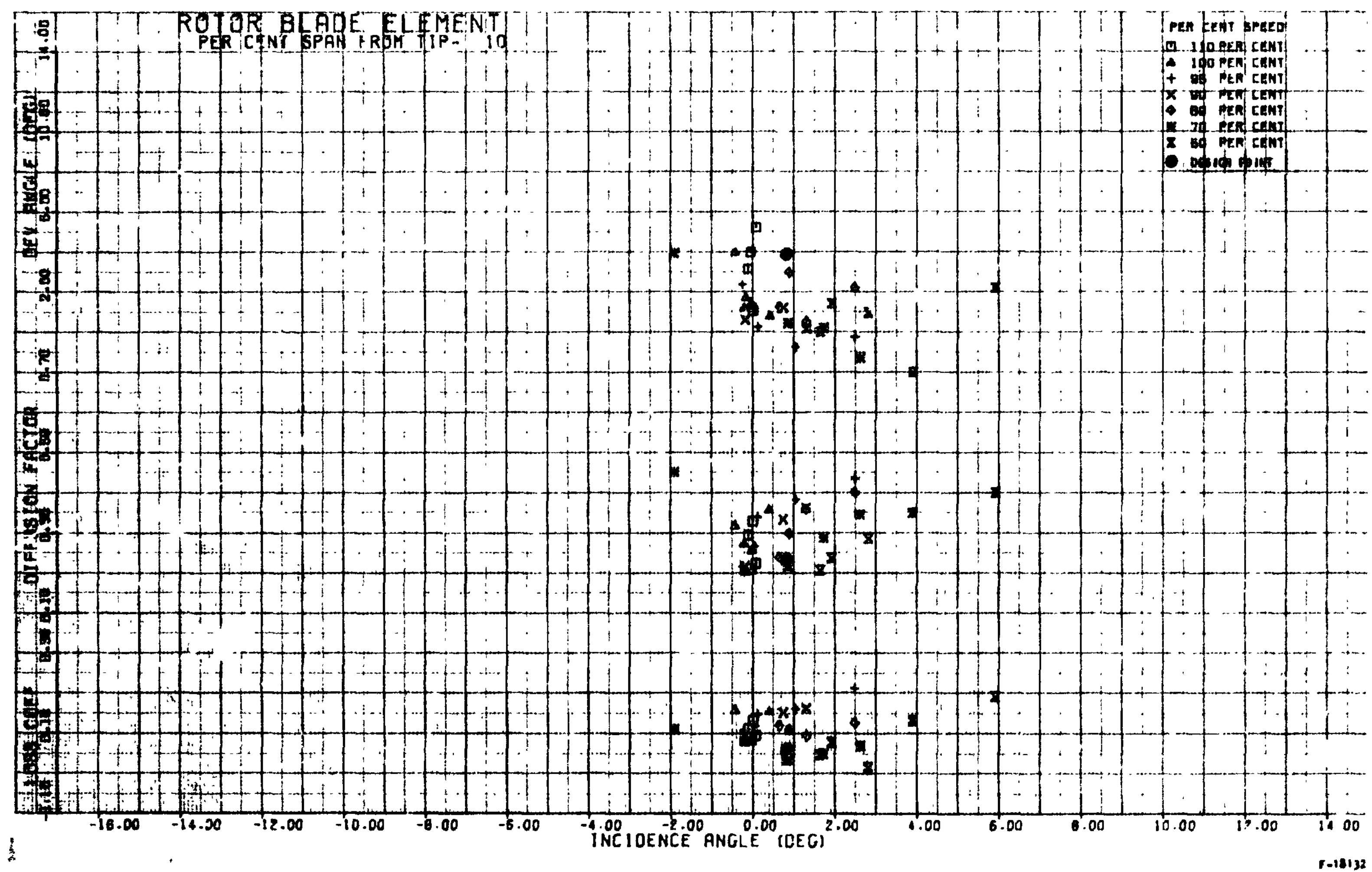

Figure 22b.--Rotor Blade Element Performance, Uniform Inlet Flow, 10 Percent Span from Tip.

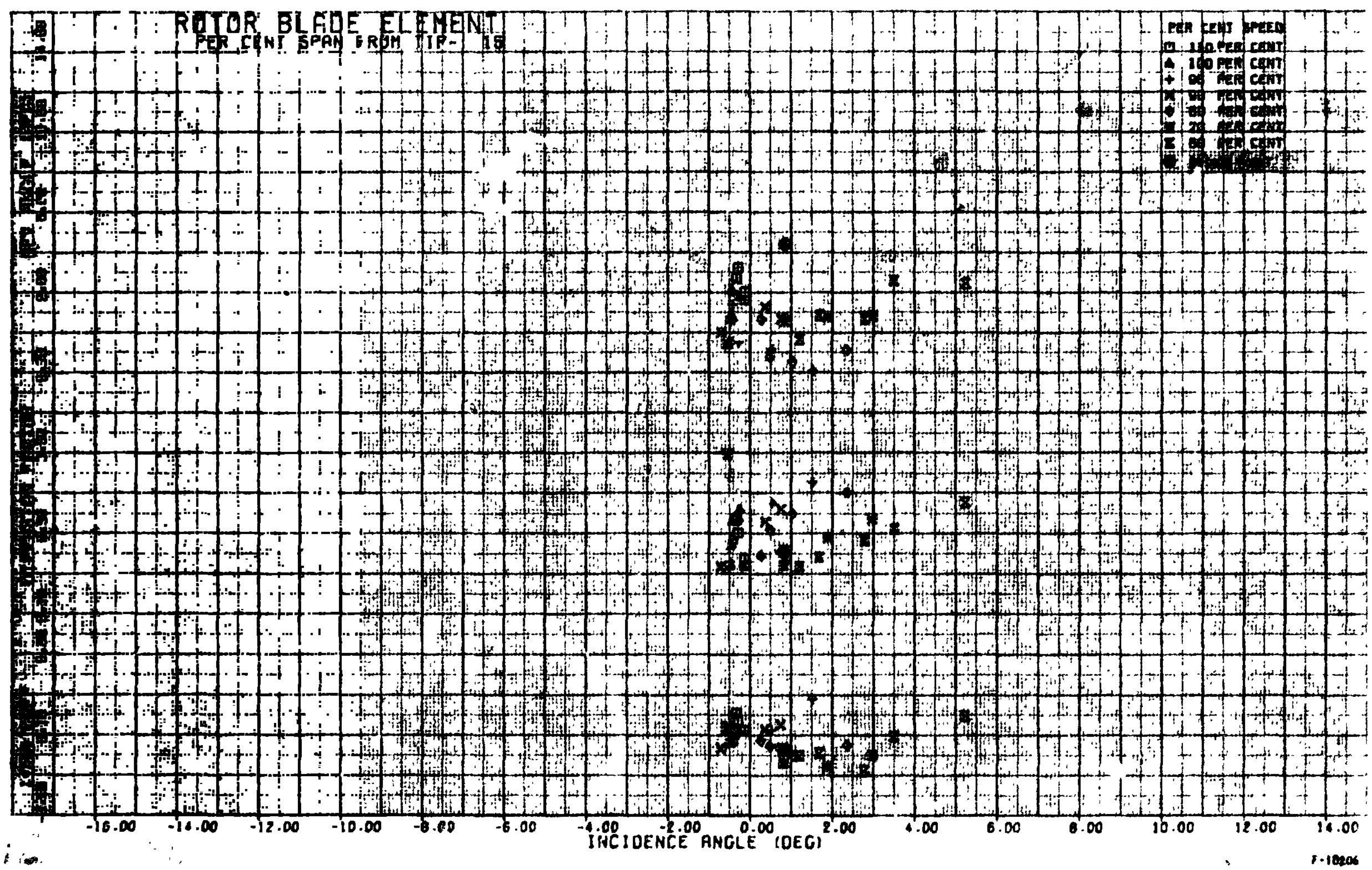

Figure 22c.--Rotor Blade Element Performance, Uniform Inlet Flow, 15 Percent Span from Tip.

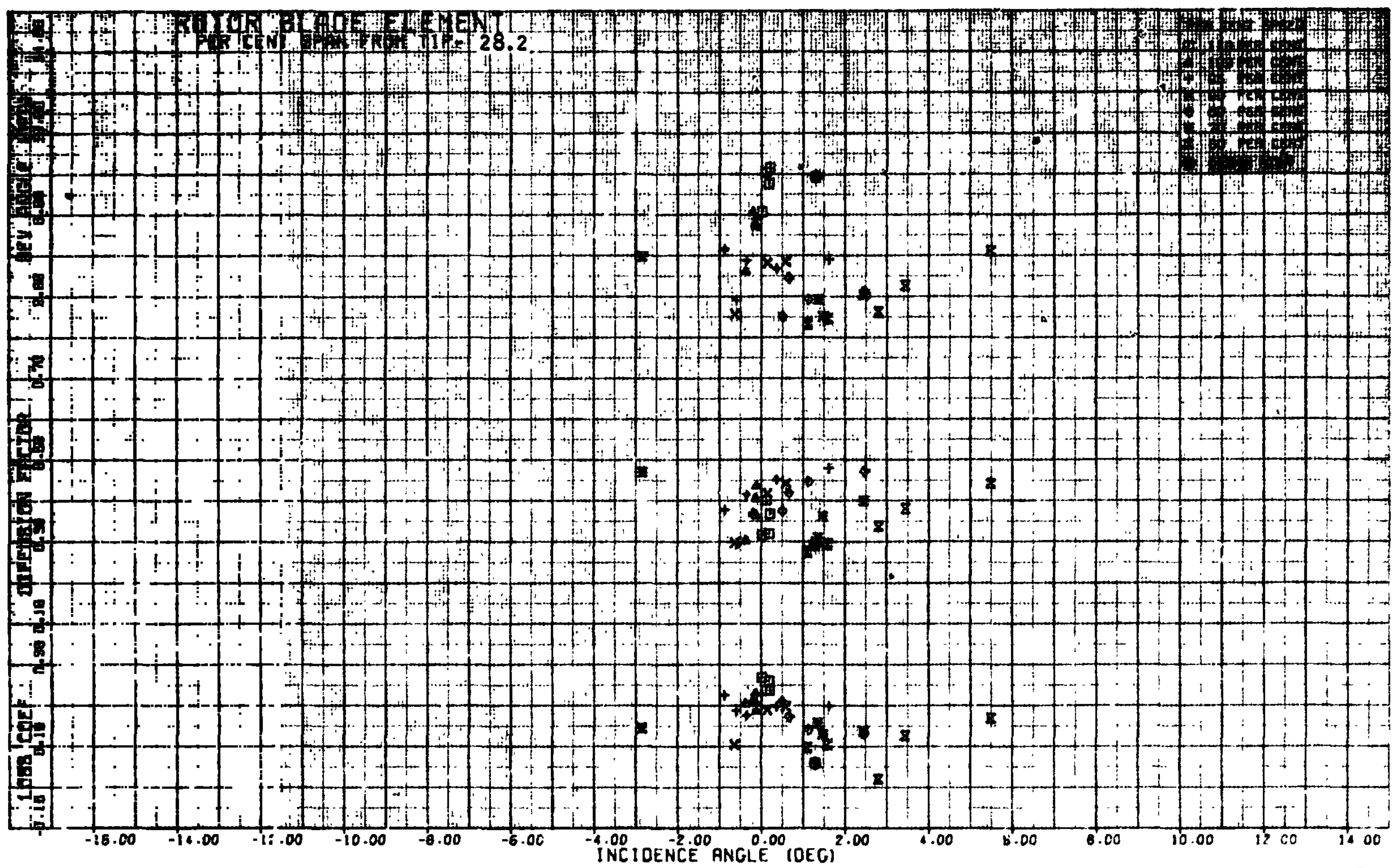

Figure 22d.--Rotor Blade Element Performance, Uniform Inlet Flow, 28.2 Percent Span from Tip.

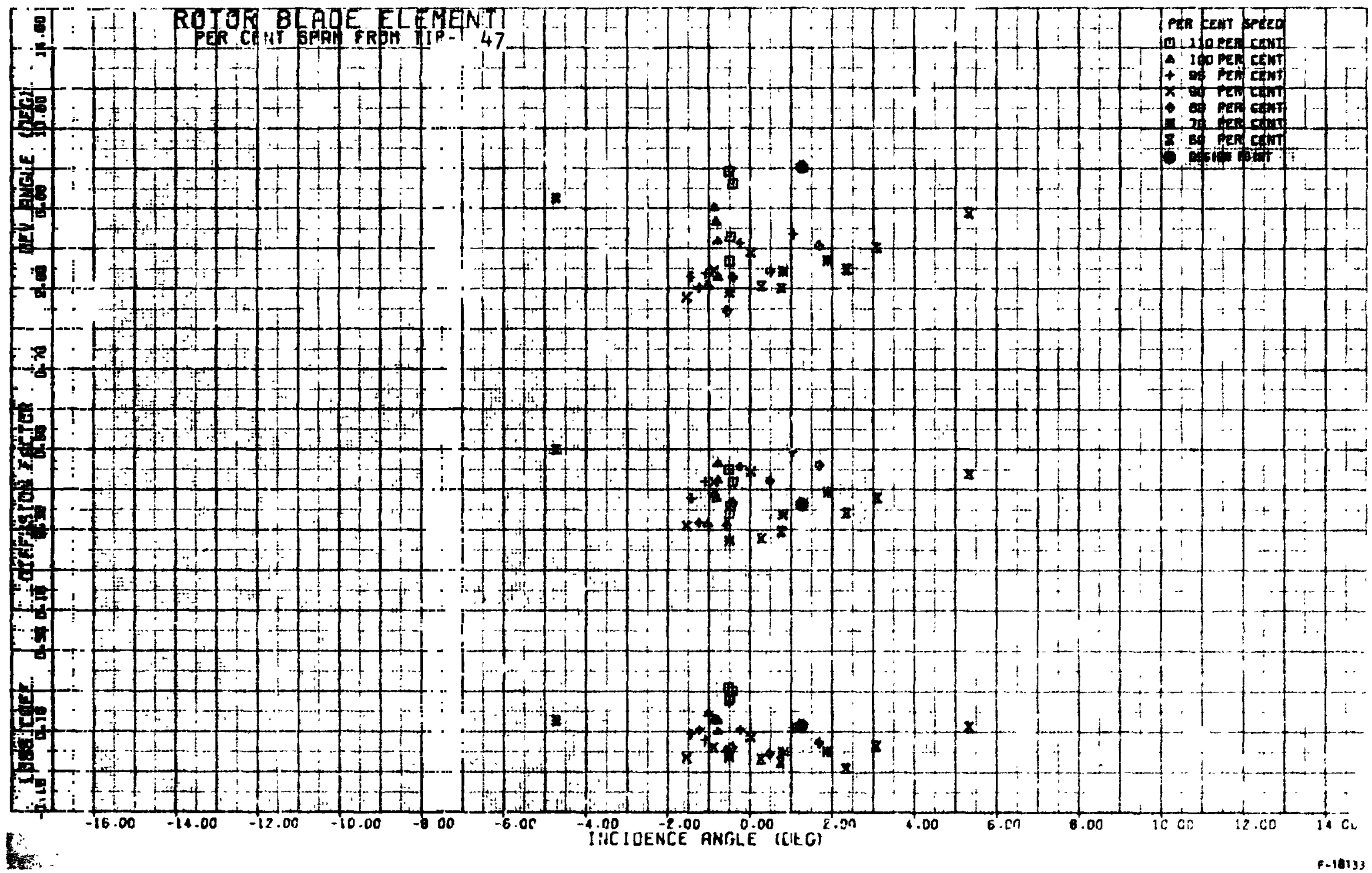

Figure 22e.--Rotor Blade Element Performance, Uniform Inlet Flow, 47 Percent Span from Tip.

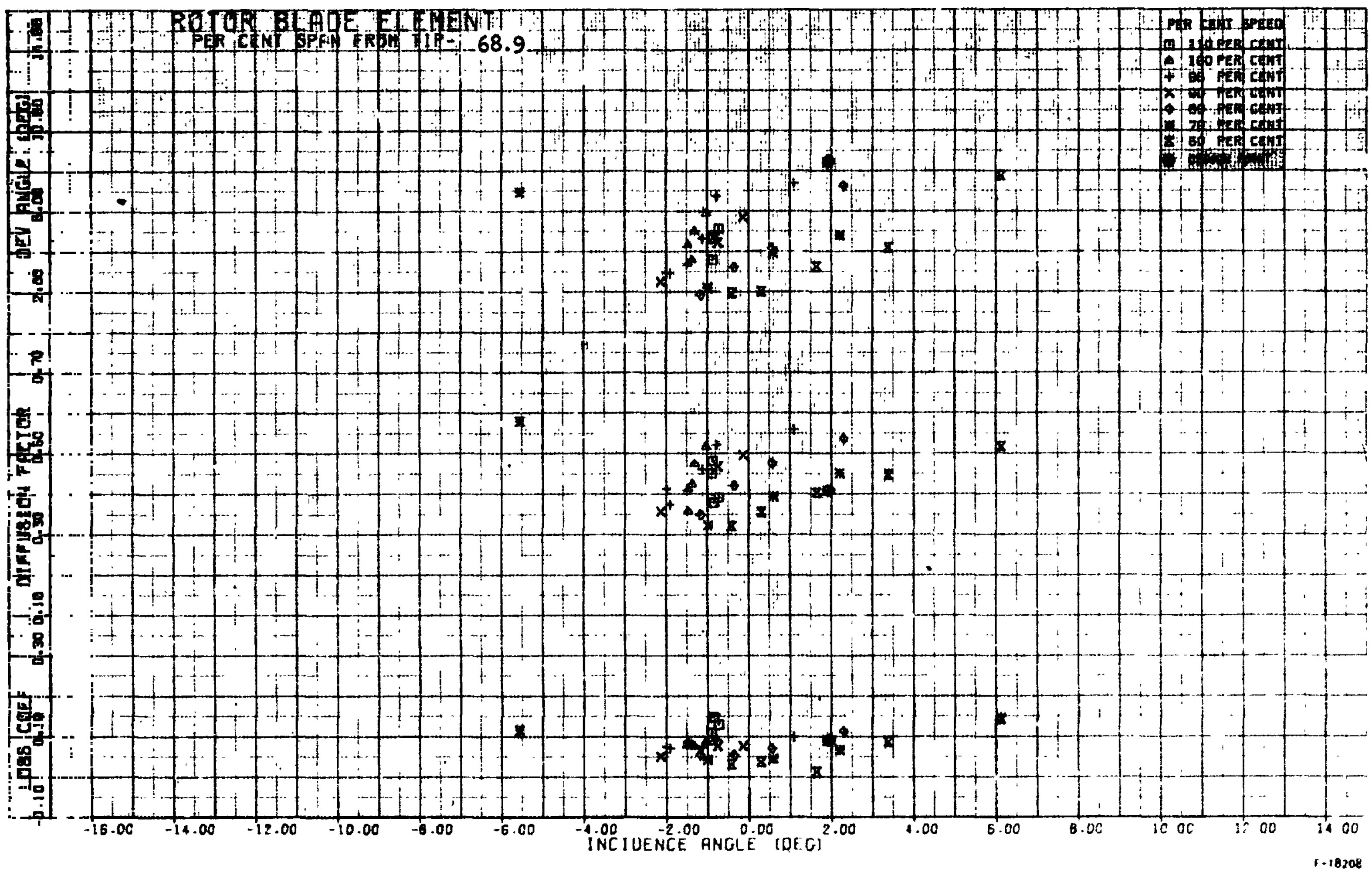

Figure 22f.--Rotor Blade Element Performance, Uniform Inlet Flow, 68.9 Percent Span from Tip.

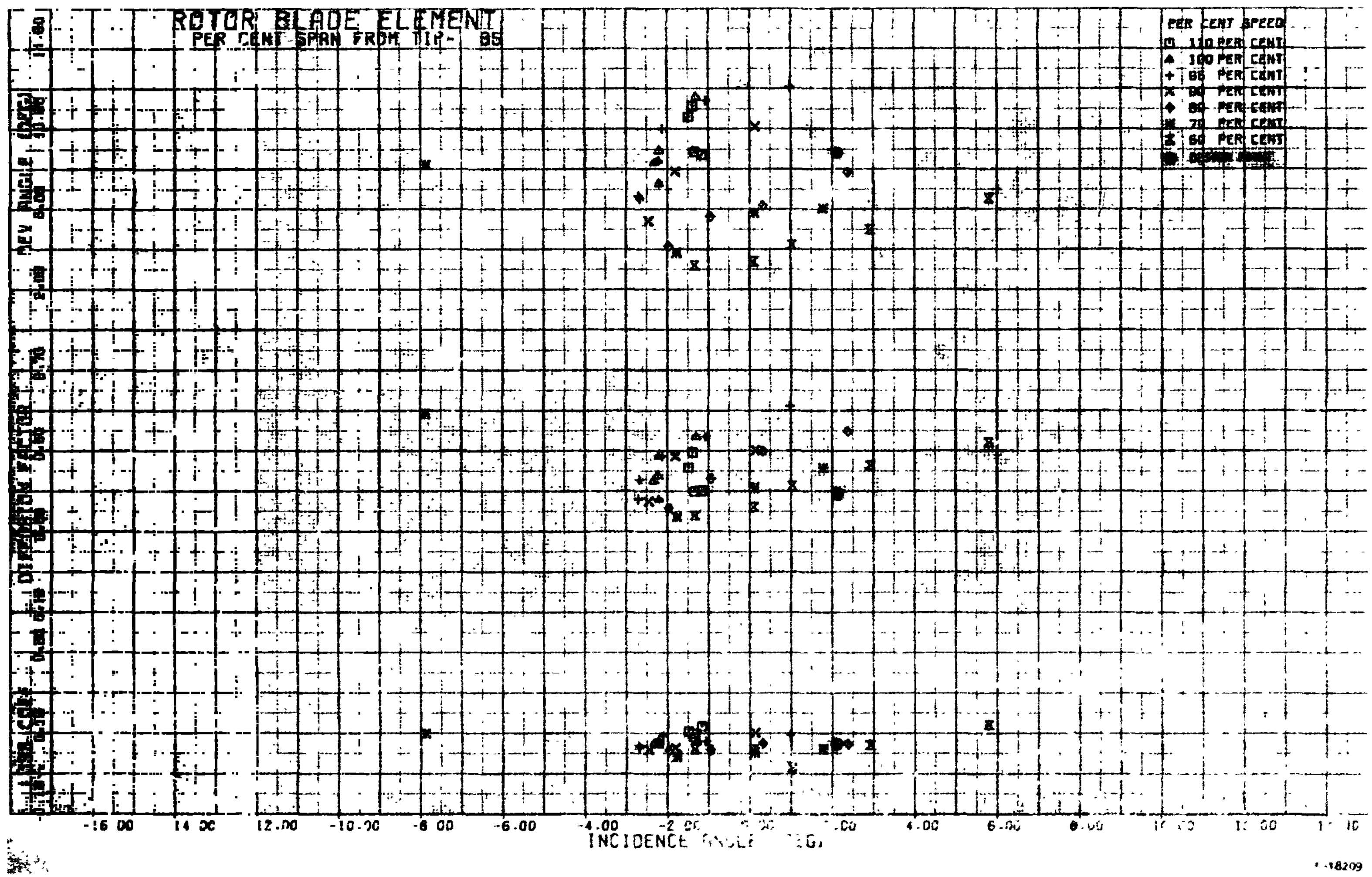

Figure 22g.--Rotor Blade Element Performance, Uniform Inlet Flow, 85 Percent Span from Tip.

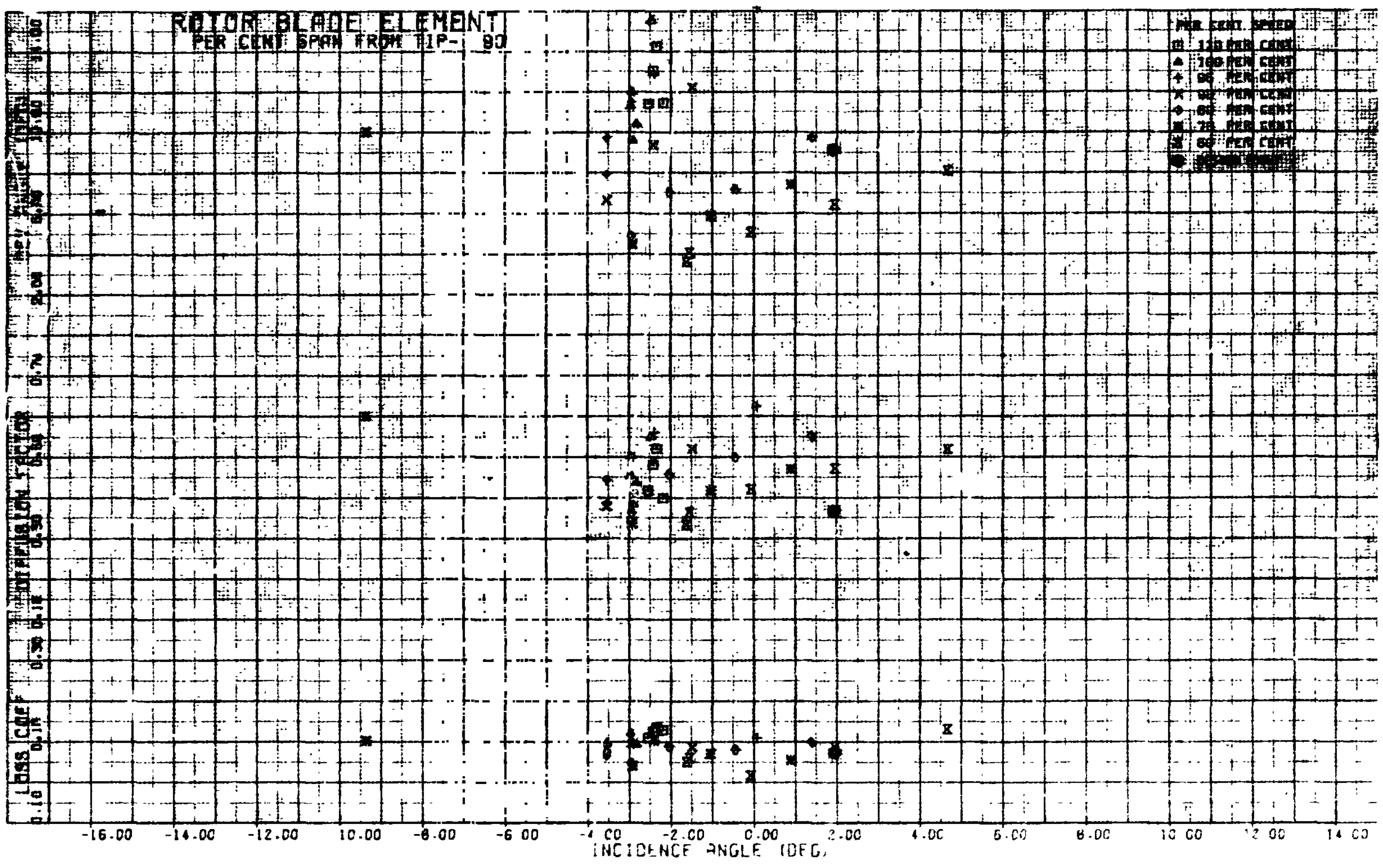

Figure 22h.--Rotor Blade Element Performance, Uniform Inlet Flow, 90 Percent Span from Tip.

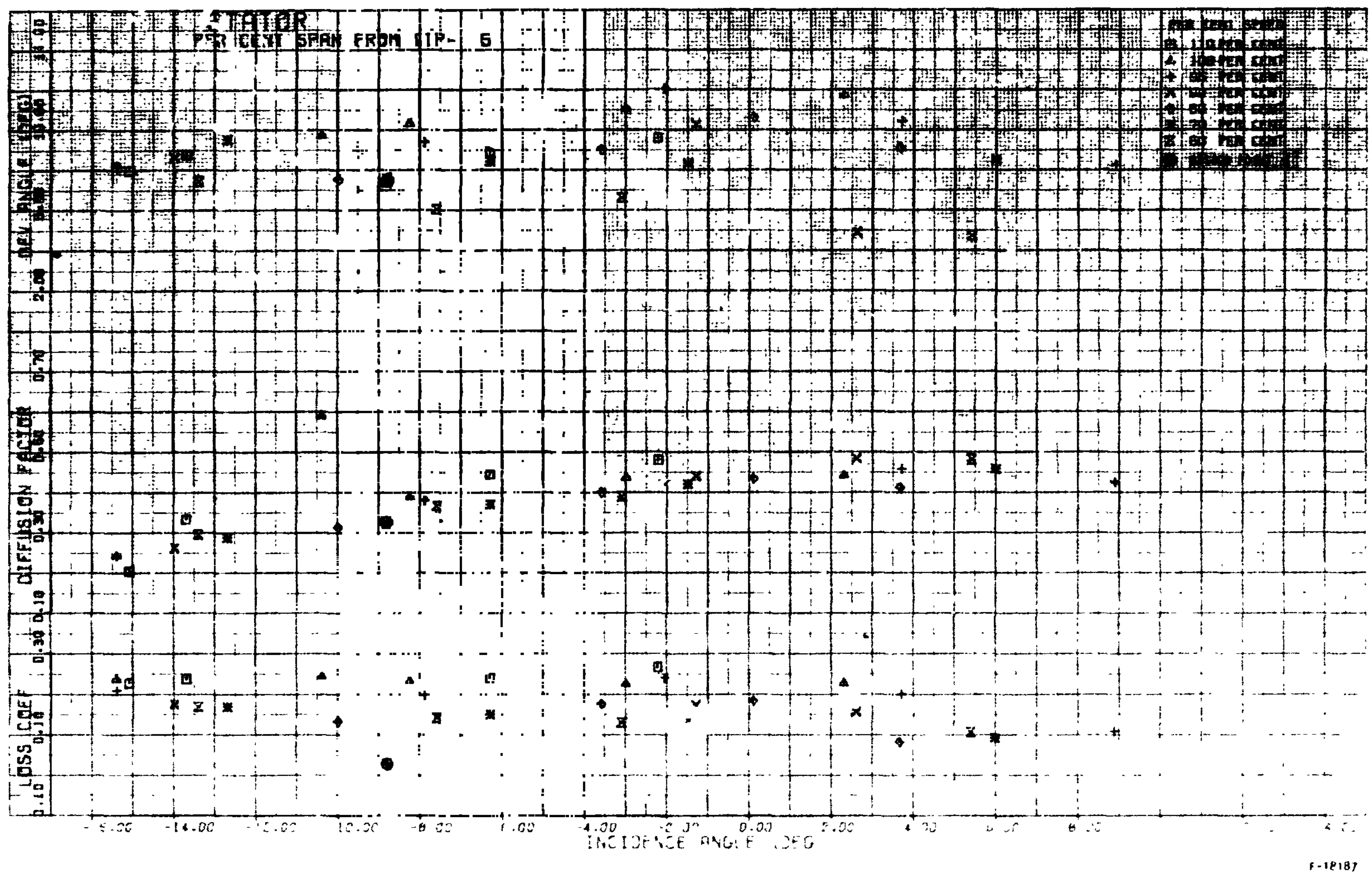

Figure 22i.--Rotor Blade Element Performance, Uniform Inlet Flow, 93.7 Percent Span from Tip.

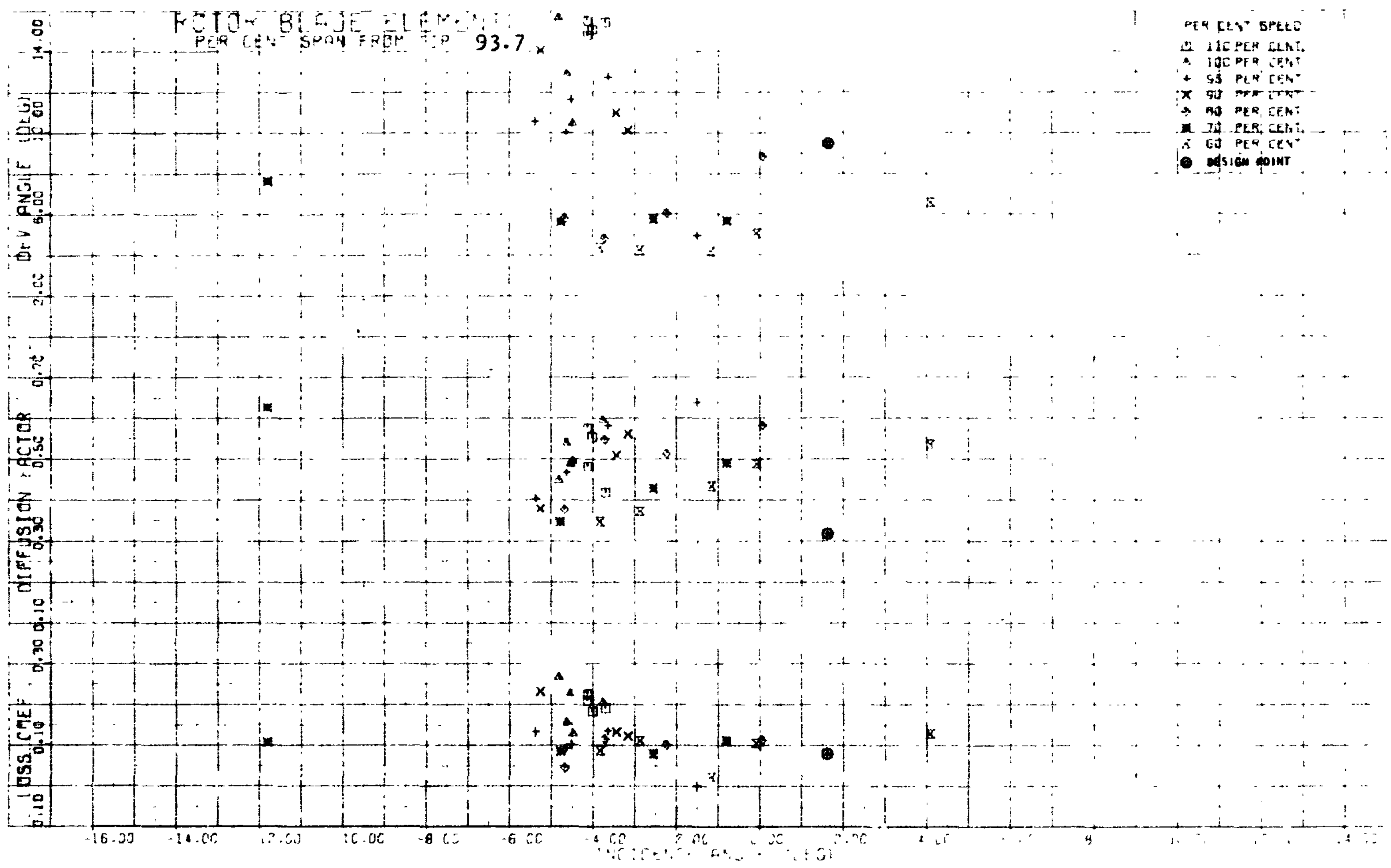

Figure 23a.--Stator Vane Element Performance, Uniform Inlet Flow, 5 Percent Span from Tip.

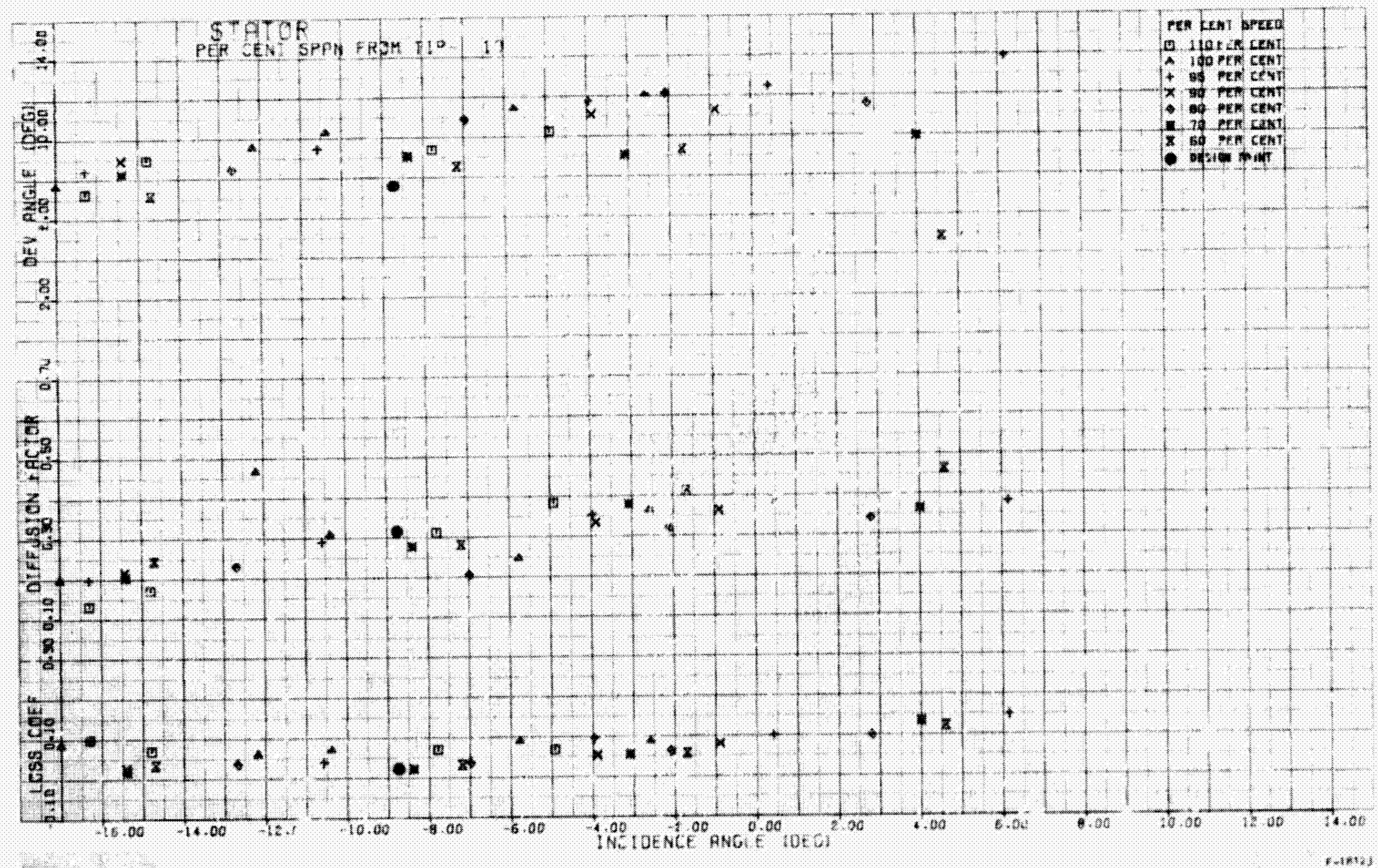

Figure 23b.--Stator Vane Element Performance, Uniform Inlet Flow, 10 Percent Span from Tip.

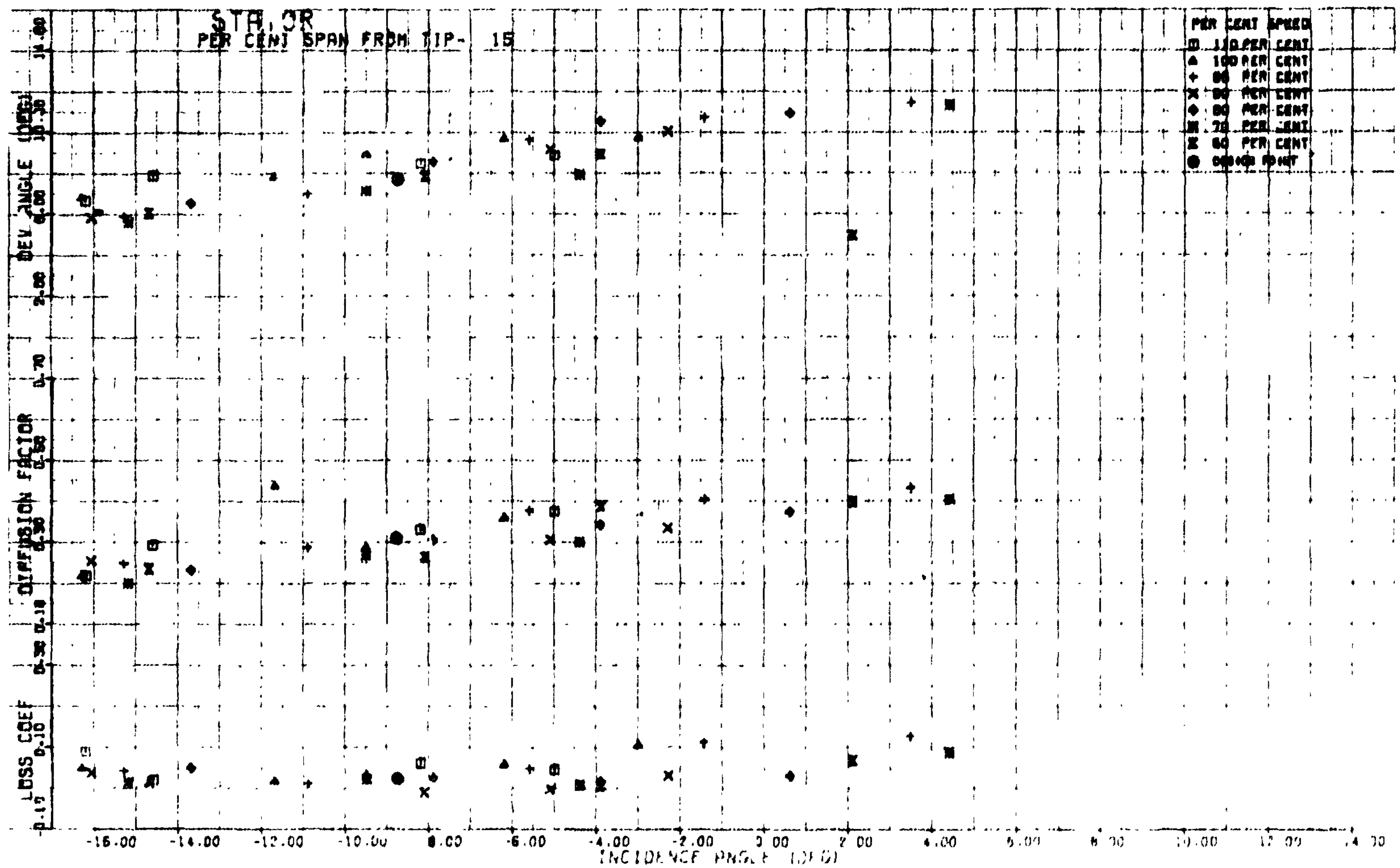

Figure 23c.--Stator Vane Element Performance, Uniform Inlet Flow, 15 Percent Span from Tip.

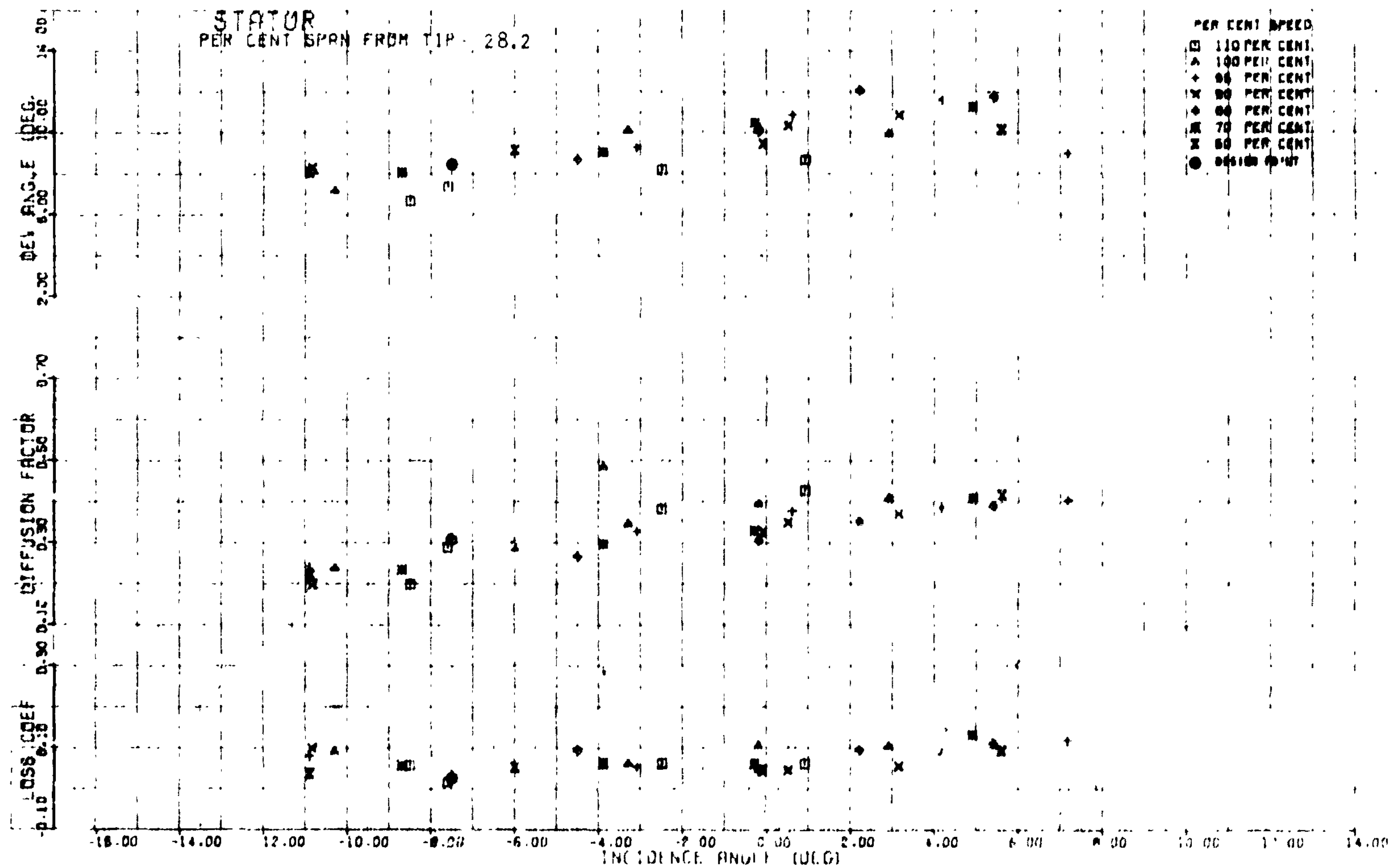

Figure 23d.--Stator Vane Element Performance, Uniform Inlet Flow, 28.2 Percent Span from Tip.

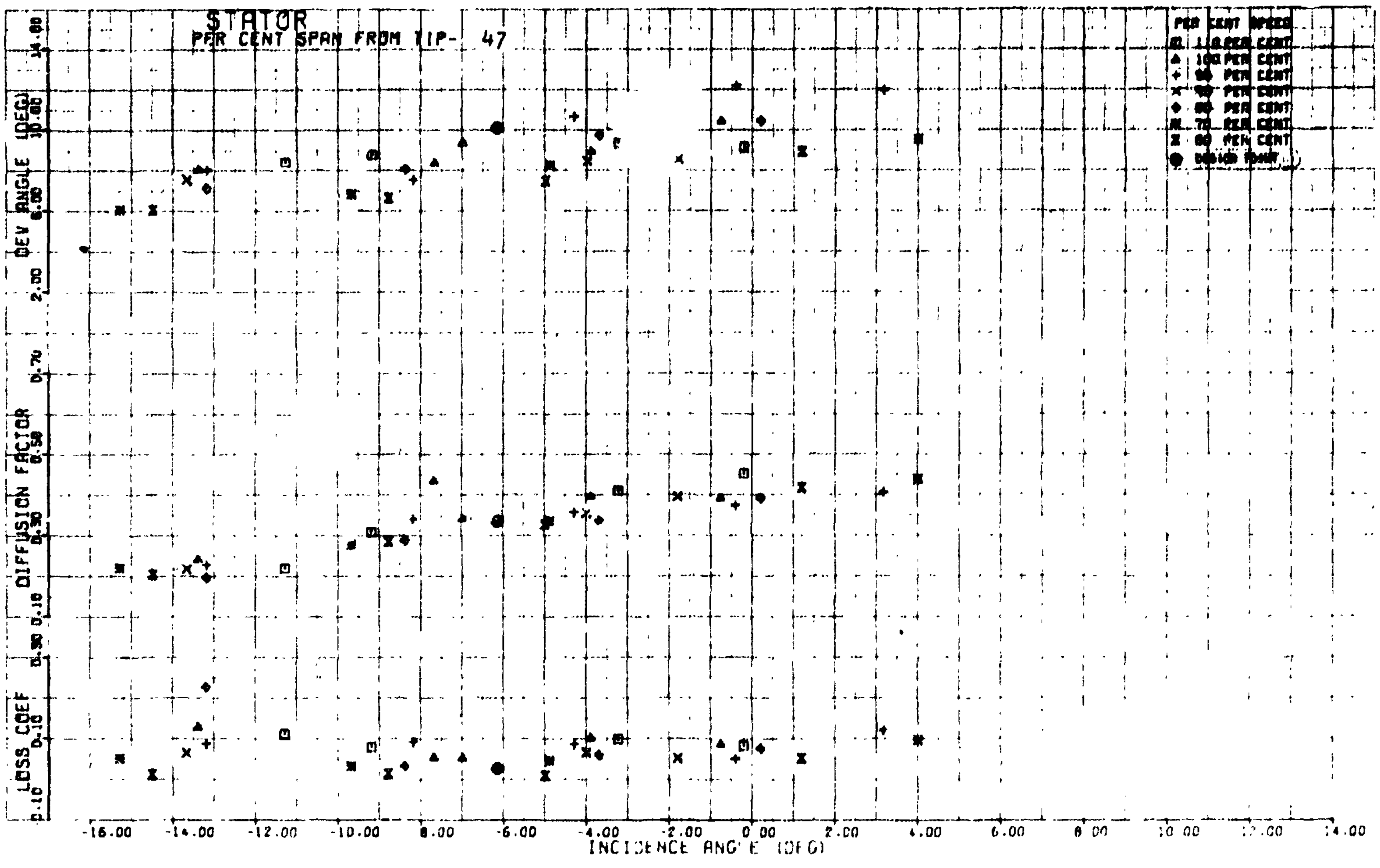

Figure 23e.--Stator Vane Element Performance, Uniform Inlet Flow, 47 Percent Span from Tip.

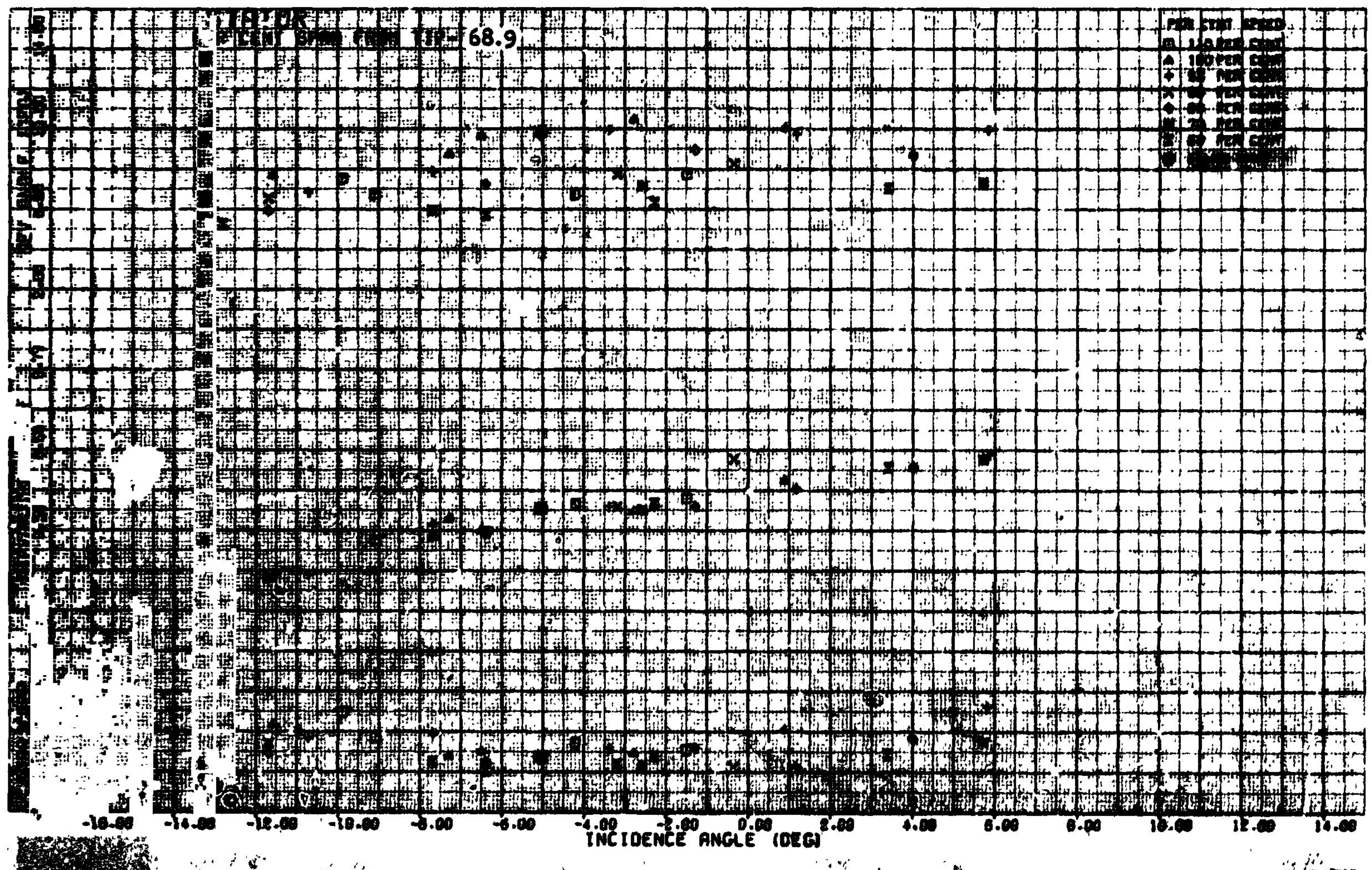

Figure 23f.--Stator Vane Element Performance, Uniform Inlet Flow, 68.9 Percent Span from Tip.

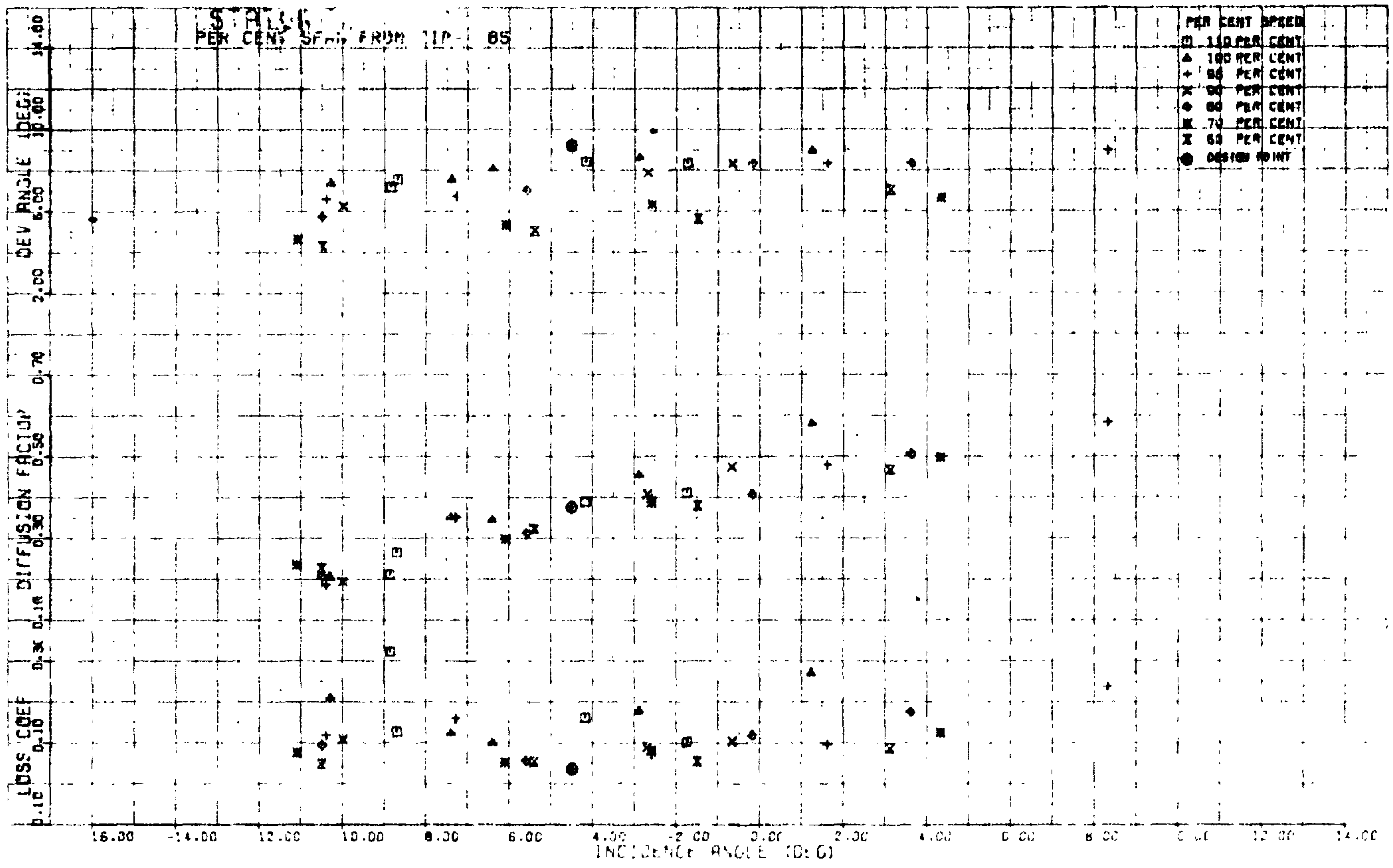

Figure 23c.--Stator Vane Element Performance, Uniform Inlet Flow, 85 Percent Span from Tip.

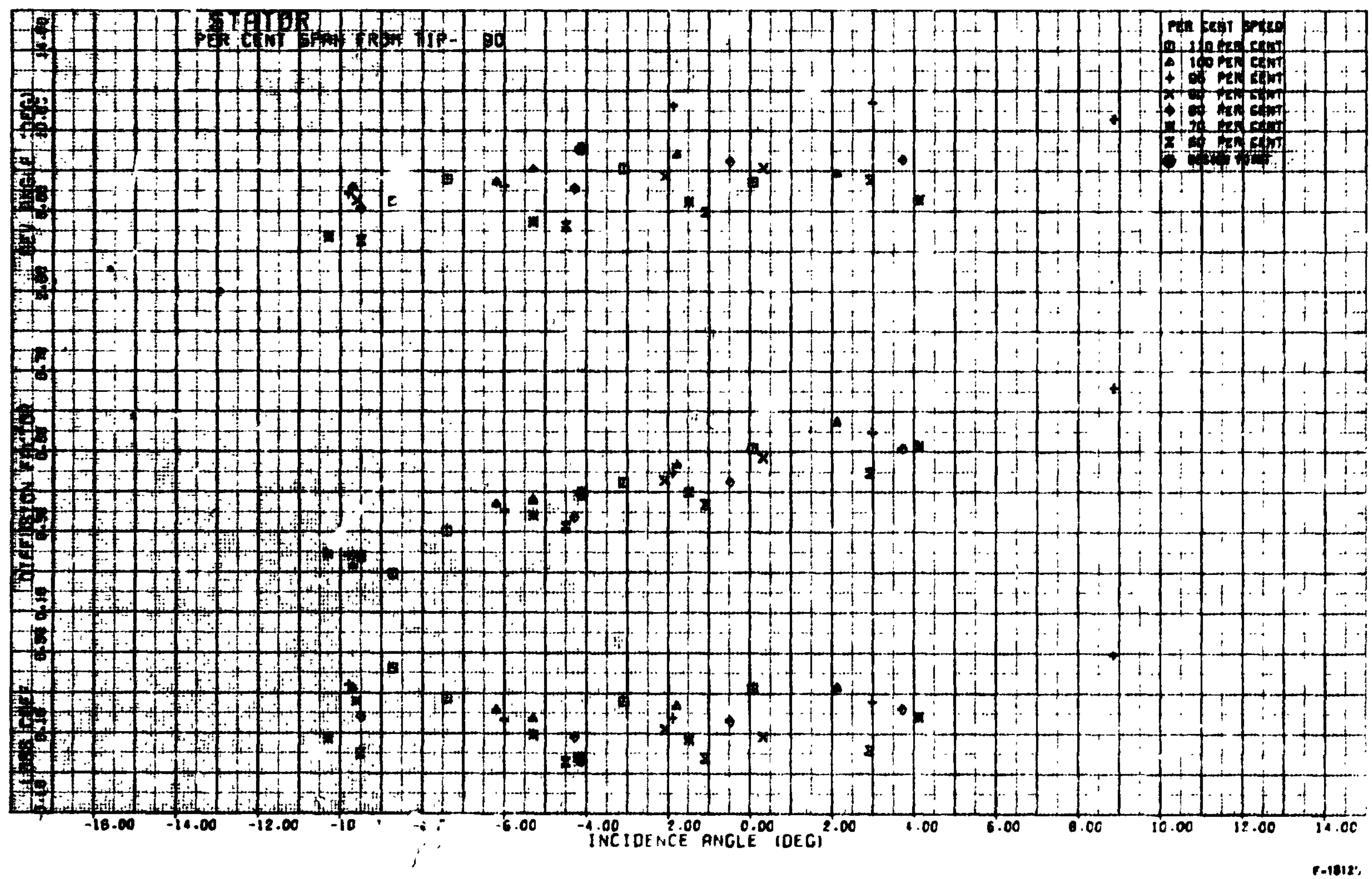

Figure 23h.--Stator Vane Element Performance, Uniform Inlet Flow,
90 Percent Span from Tip.

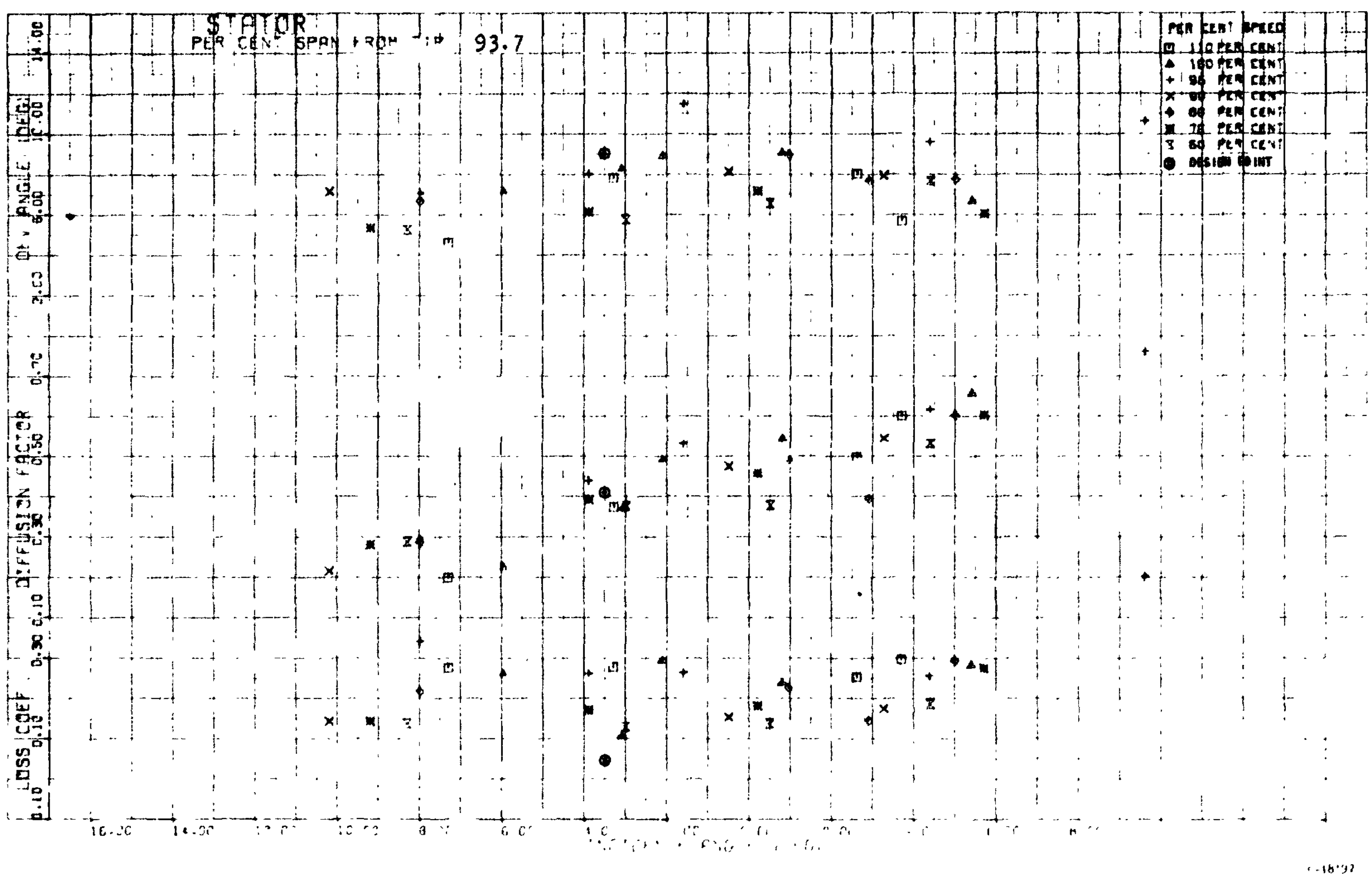

Figure 23i.--Stator Vane Element Performance, Uniform Inlet Flow, 93.7 Percent Span from Tip.

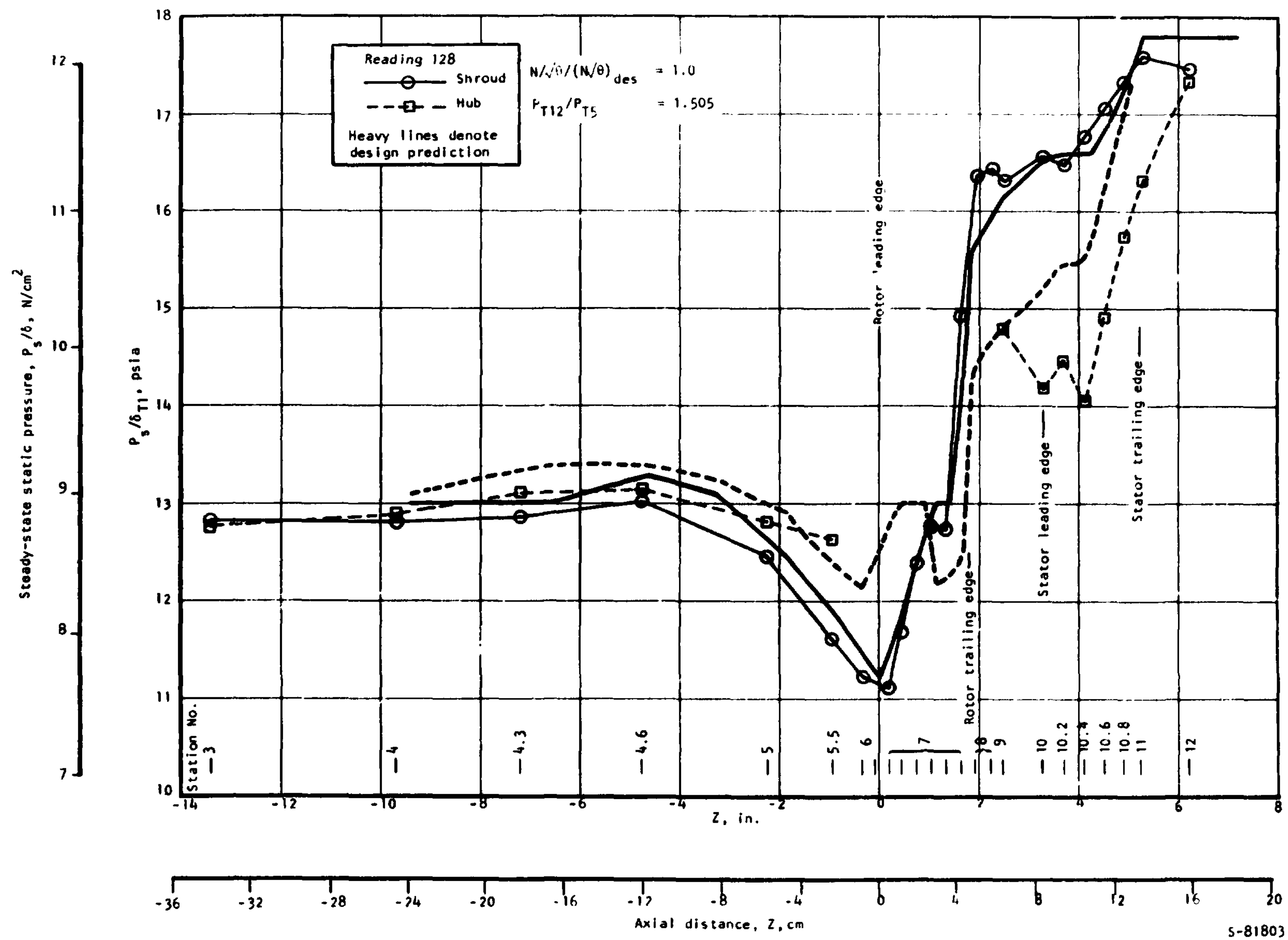

Figure 24. Axial Static Pressure Distribution, Uniform Inlet Flow.

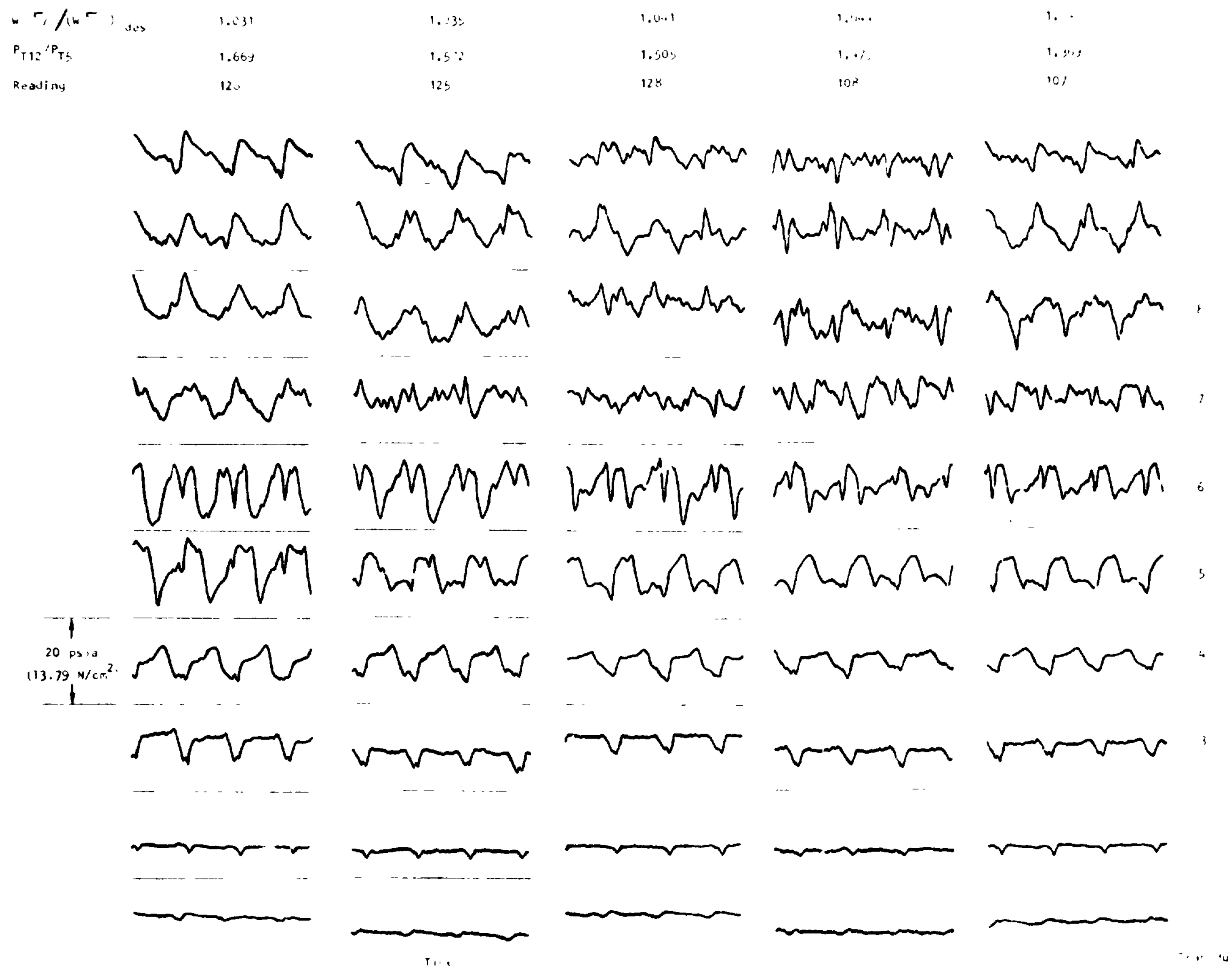

Figure 25.--Typical Rotor Casing High-Frequency-Response Oscillograph Traces at Design Speed.

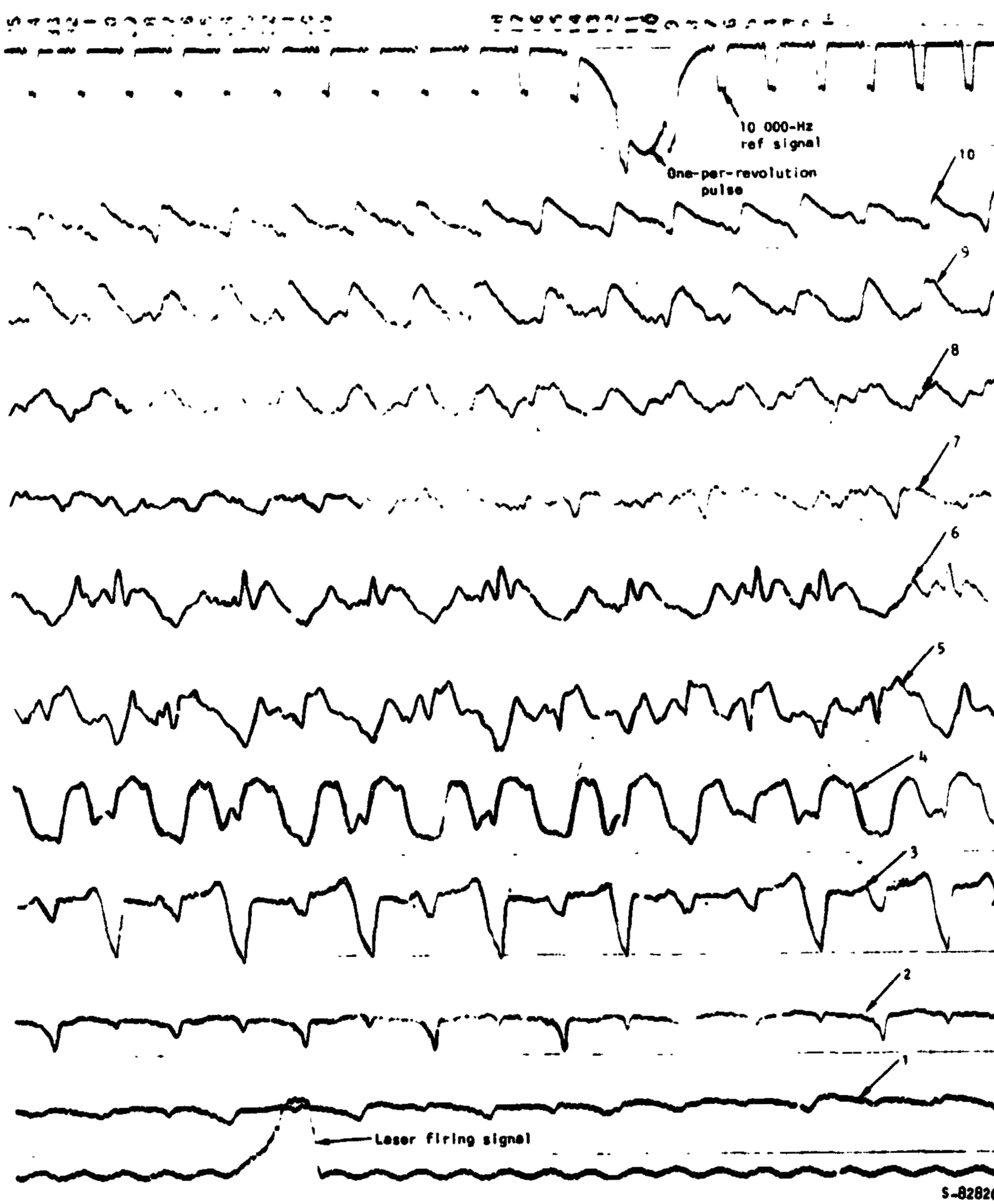

Figure 25.--Rotor Casing High-Frequency-Response Oscillograph Traces at 90 Percent of Design Speed Showing Transition from Started to Unstarted Conditions.

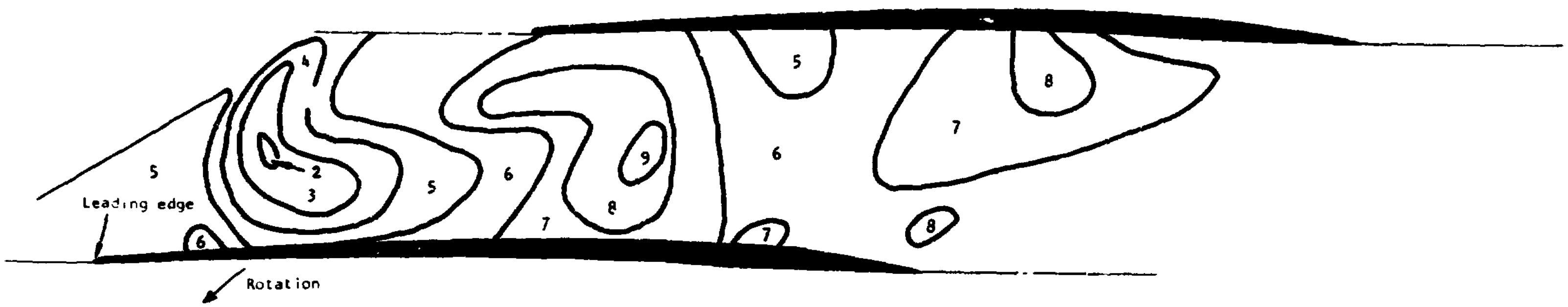

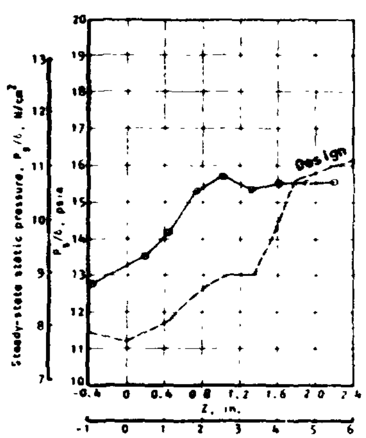

Reading	75
$\frac{N/\sqrt{\theta}}{N/\sqrt{\theta}_{des}}$	0.80
$\frac{W\sqrt{\theta}/\delta}{W\sqrt{\theta}/\delta_{des}}$	= 0.869
P_{T12}/P_{T5}	= 1.324

Static pressure contour code		
Code number	Static pressure range	
	psia	N/cm²
1	3 to 5	2.07 to 3.45
2	5 to 7	3.45 to 4.83
3	7 to 9	4.83 to 6.21
4	9 to 11	6.21 to 7.58
5	11 to 13	7.58 to 8.96
6	13 to 15	8.96 to 10.34
7	15 to 17	10.34 to 11.72
8	17 to 19	11.72 to [illegible]
9	19 to 21	13.10 to [illegible]
10	21 to 23	[illegible] to [illegible]
11	23 to 25	[illegible] to [illegible]

S-81376

Figure 27.--Rotor Blade Tip Static Pressure Contours, 80 Percent Design Speed, Pressure Ratio 1.324.

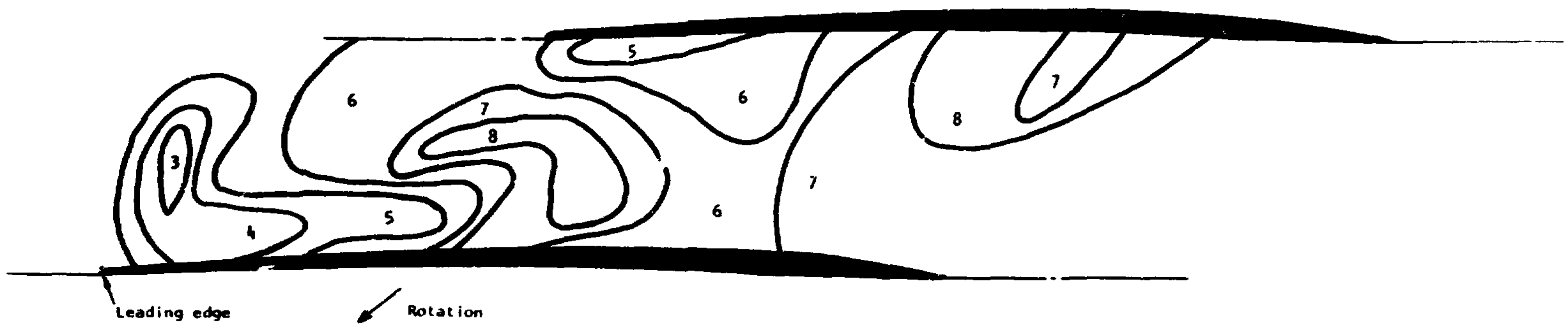

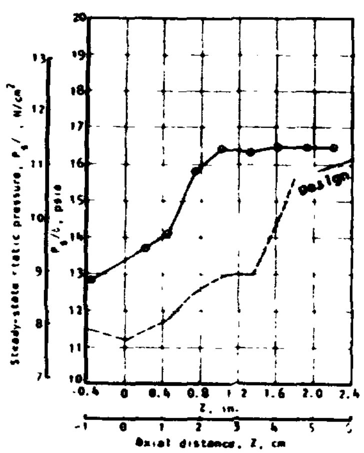

Reading	80
$\frac{N/\sqrt{\theta}}{N/\sqrt{\theta}_{des}}$	= 0.80
$\frac{W\sqrt{\theta}/\delta}{W\sqrt{\theta}/\delta_{des}}$	= 0.842
P_{T12}/P_{T5}	= 1.371

Static pressure contour code		
Code number	Static pressure range	
	psia	N/cm²
1	3 to 5	2.07 to 3.45
2	5 to 7	3.45 to 4.83
3	7 to 9	4.83 to 6.21
4	9 to 11	6.21 to 7.58
5	11 to 13	7.58 to 8.96
6	13 to 15	8.96 to 10.34
7	15 to 17	10.34 to 11.[illegible]
8	17 to 19	11.72 to 13.10
9	19 to 21	13.10 to 14.48
10	21 to 23	14.48 to 15.8[illegible]
11	23 to 25	15.8[illegible] to 17.[illegible]

S-81877

Figure 28.--Rotor Blade Tip Static Pressure Contours, 80 Percent Design Speed, Pressure Ratio 1.371.

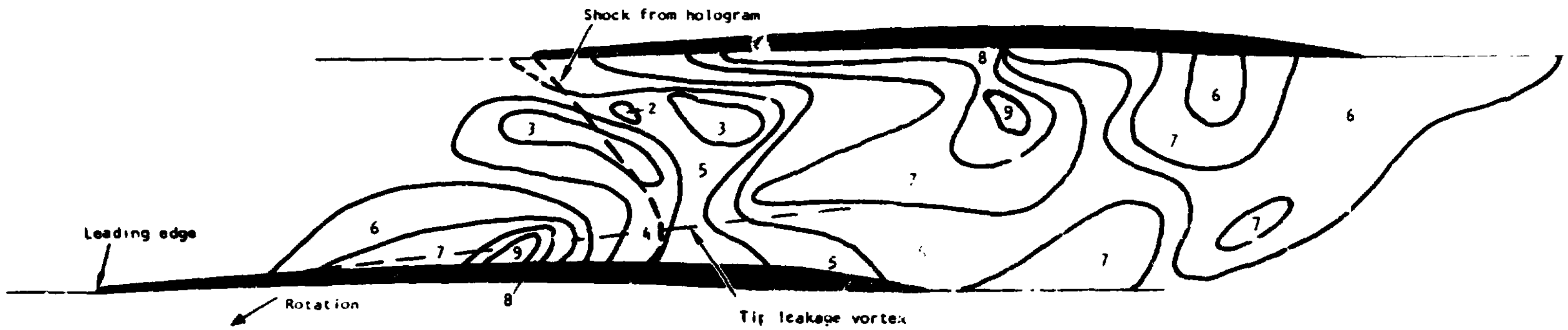

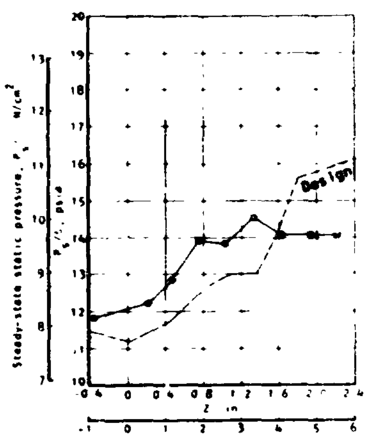

Reading	103
$\frac{N/\sqrt{\theta}}{N/\sqrt{\theta}_{des}}$	= 0.90
$\frac{W\sqrt{\theta}/\delta}{W\sqrt{\theta}/\delta_{des}}$	0.984
P_{T12}/P_{T5}	= 1.320

Static pressure contour code		
Code number	Static pressure range	
	psia	N/cm²
1	3 to 5	2.07 to 3.45
2	5 to 7	3.45 to 4.83
3	7 to 9	4.83 to 6.21
4	9 to 11	6.21 to 7.58
5	11 to 13	7.58 to 8.96
6	13 to 15	8.96 to 10.34
7	15 to 17	10.34 to 11.[illegible]
8	17 to 19	[illegible]
9	19 to 21	[illegible]
10	21 to 23	[illegible]
11	23 [illegible]	[illegible]

S-81P80

Figure 29.--Rotor Blade Tip Static Pressure Contours, ,0 Percent Design Speed, Pressure Ratio 1.320.

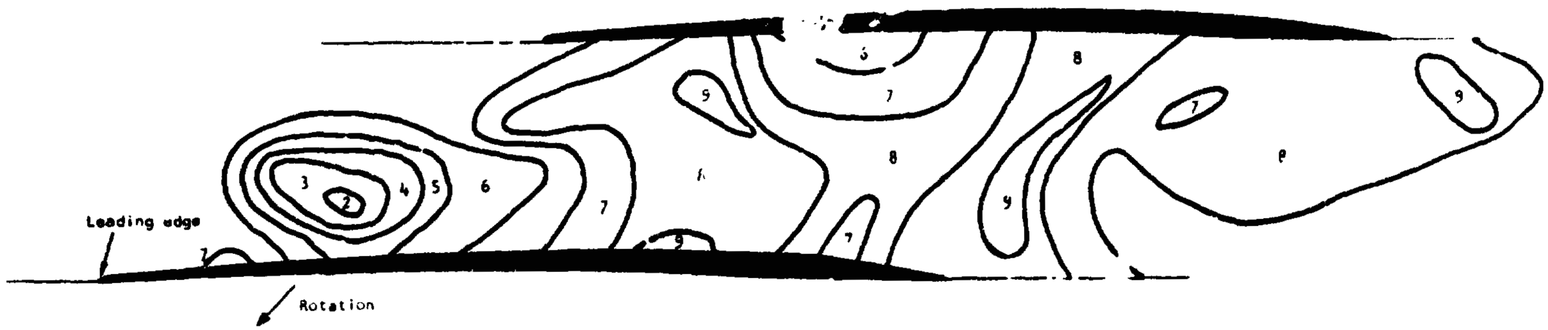

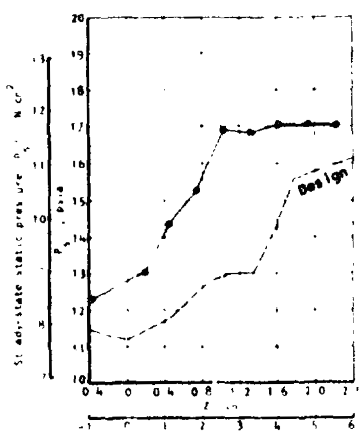

Reading 101

$\frac{N/\sqrt{\theta}}{N/\sqrt{\theta}_{des}}$ = [illegible]

$\frac{W\sqrt{\theta}/\delta}{W\sqrt{\theta}/\delta_{des}}$ = 0.4[illegible]7

P_{T17}/P_{T5} = 1.479

Static pressure contour code		
Code number	Static pressure range	
	psia	N/cm²
1	3 to 5	2.07 to 3.45
2	5 to [illegible]	3.45 [illegible] .83
3	7 to 9	4.83 to [illegible].21
4	9 to 1[illegible]	6.[illegible] to 7.58
5	11 to 13	7.58 [illegible] 8.96
6	[illegible] to 15	8.9[illegible] [illegible] 10.3[illegible]
7	15 to 17	[illegible]
8	17 to 19	[illegible] 13.1
9	19 to 2[illegible]	[illegible] 14.[illegible]
10	21 [illegible] 23	[illegible] 15.8[illegible]
11	23 [illegible]	[illegible].8[illegible] [illegible]

5-818/E

Figure 30.--Rotor Blade Tip Static Pressure Contours, 90 Percent Design Speed, Pressure Ratio 1.479.

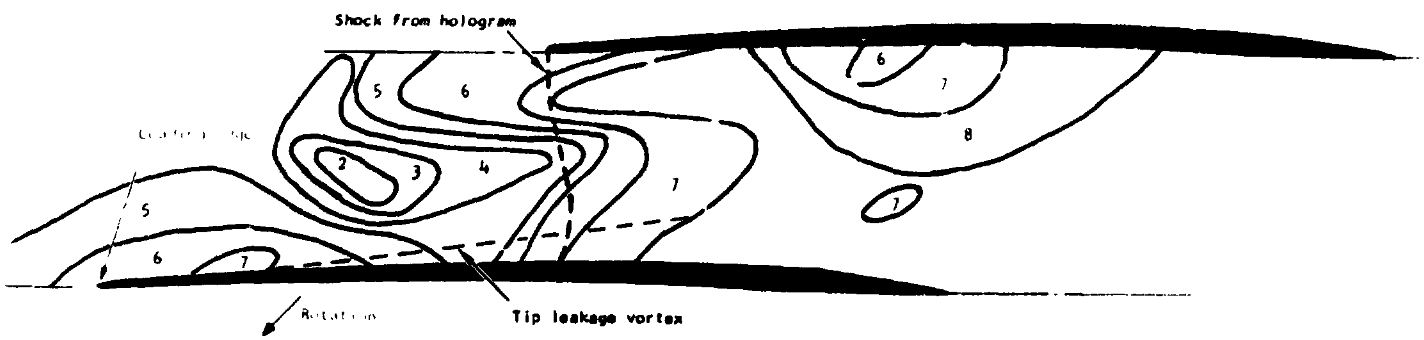

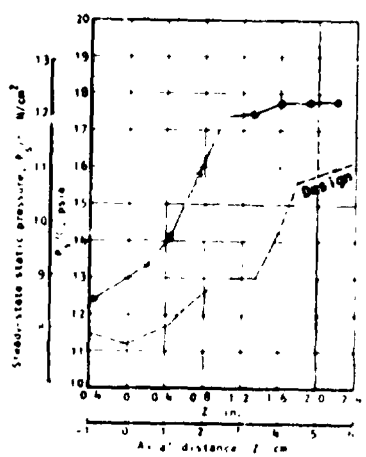

Reading	106
$\frac{N/\sqrt{\theta}}{N/\sqrt{\theta}_{des}}$	0.90
$\frac{W\sqrt{\theta}/\delta}{W\sqrt{\theta}/\delta_{des}}$	0.[illegible]42
P_{T12}/P_{T5}	1.5[illegible]

Static pressure contour code		
Code number	Static pressure range, psia	Static pressure range, N/cm²
1	3 to 5	2.07 to 3.45
2	5 to 7	[illegible]
3	7 [illegible]	[illegible]
4	[illegible] to 11	[illegible]
5	11 to 13	[illegible]
6	13 to 15	[illegible]
7	15 to 17	[illegible]
8	17 to [illegible]	[illegible]
9	[illegible]	[illegible]
10	[illegible]	[illegible]
11	[illegible]	[illegible]

S-81879

Figure 31.--Rotor Blade Tip Static Pressure Contours, 90 Percent Design Speed, Pressure Ratio 1.524.

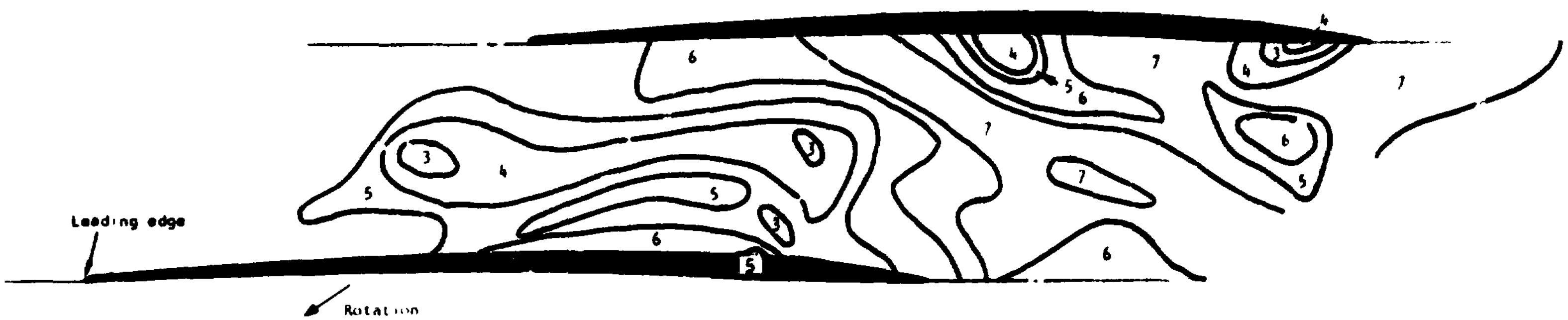

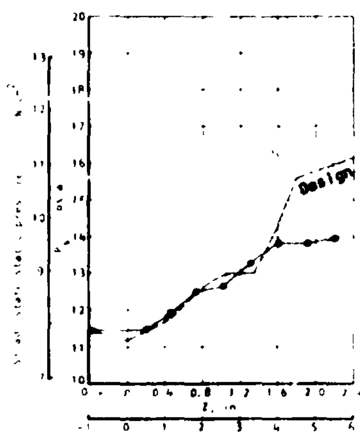

Reading	104
$\frac{N/\sqrt{\theta}}{N/\sqrt{\theta}_{des}}$	= 0.95
$\frac{W\sqrt{\theta}/\delta}{W\sqrt{\theta}/\delta_{des}}$	= 1.019
P_{T12}/P_{T5}	= 1.348

Static pressure contour code		
Code number	Static pressure range	
	psia	N/cm^2
1	3 to 5	2.07 to 3.45
2	5 to 7	3.45 to 4.83
3	7 to 9	4.83 to 6.21
4	9 to 11	6.21 to 7.58
5	11 to 13	7.58 to 8.96
6	13 to 15	8.96 to 10.34
7	15 to 17	10.34 to 11.[illegible]
8	17 to 19	11.72 to 13.[illegible]
9	19 to 21	13.10 to 14.[illegible]
10	21 to 23	14.48 to 15.86
11	23 to 25	15.86 [illegible]

S-81881

Figure 32.--Rotor Blade Tip Static Pressure Contours, 95 Percent Design Speed, Pressure Ratio 1.348.

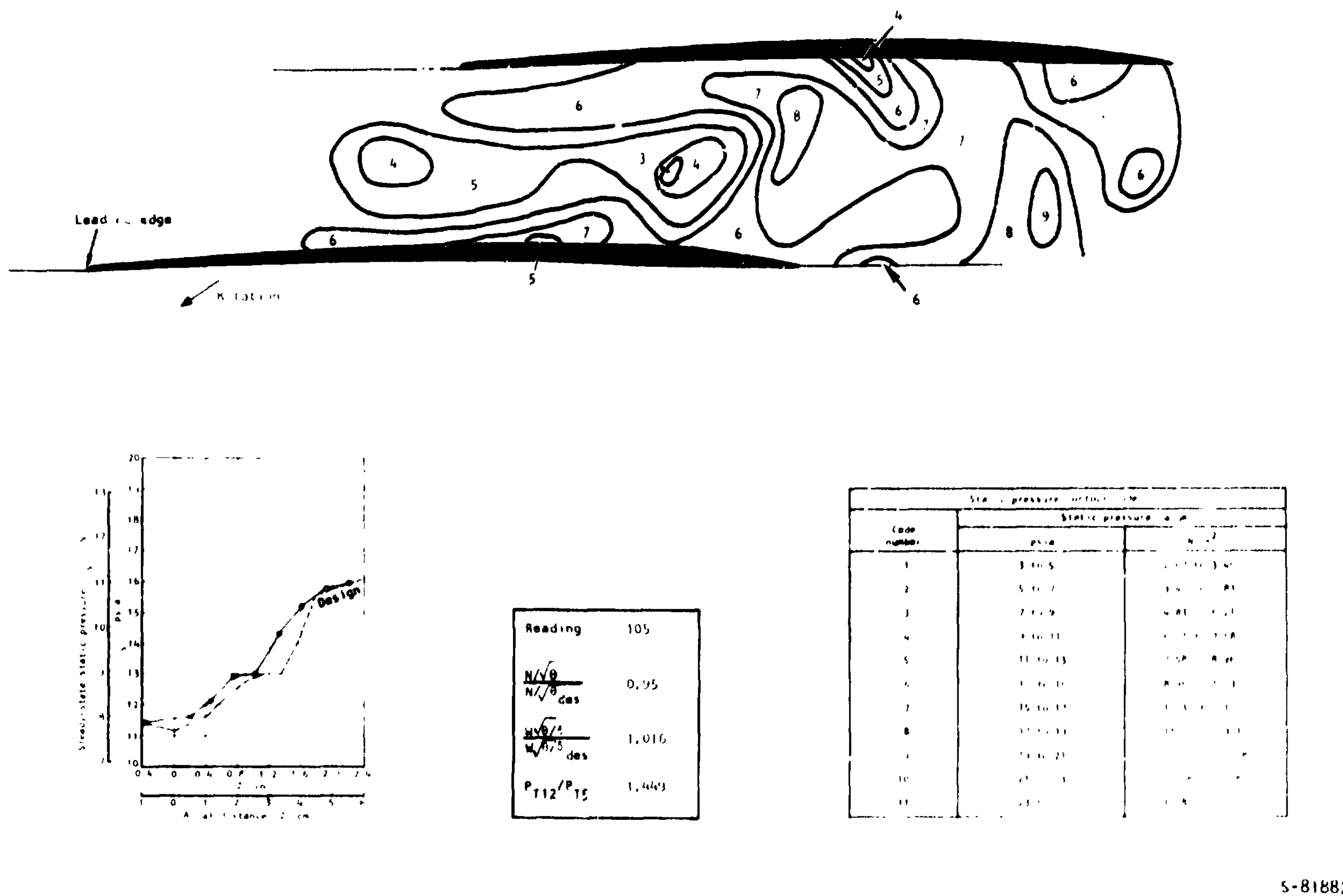

Figure 33.--Rotor Blade Tip Static Pressure Contours, 95 Percent Design Speed, Pressure Ratio 1.449.

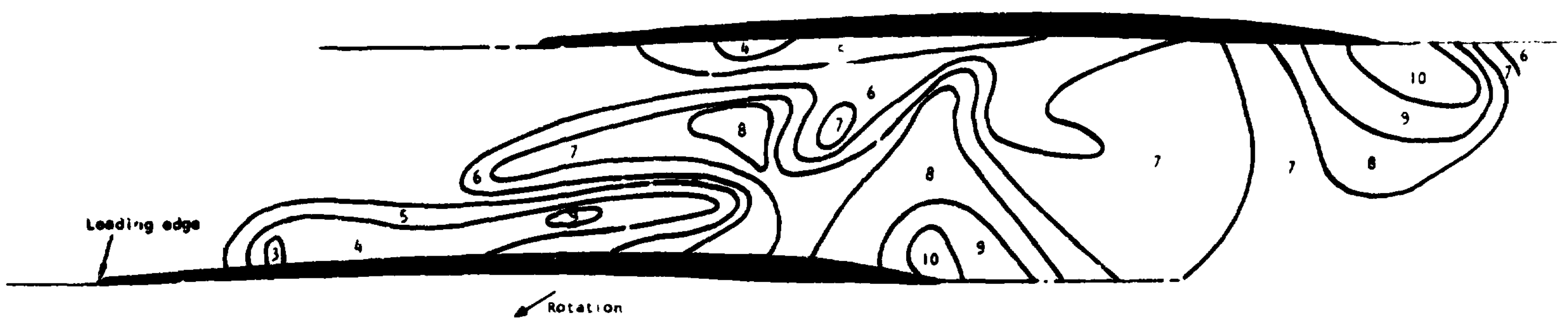

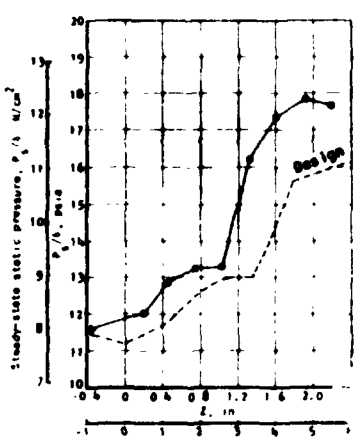

Reading	117
$\frac{N/\sqrt{\theta}}{N/\sqrt{\theta}_{des}}$	= 0.95
$\frac{W\sqrt{\theta}/\delta}{W\sqrt{\theta}/\delta_{des}}$	= 1.008
P_{T12}/P_{T5}	= 1.540

Static pressure contour code		
Code number	Static pressure range	
	psia	N/cm²
1	3 to 5	2.07 to 3.45
2	5 to 7	3.45 to 4.83
3	7 to 9	4.83 to 6.21
4	9 to 11	6.21 to 7.58
5	11 to 13	7.58 to 8.96
6	13 to 15	8.96 to 10.34
7	15 to 17	10.34 to 11.72
8	17 to 19	11.72 to 13.10
9	19 to 21	13.10 to 14.48
10	21 to 23	14.48 to 15.86
11	23 to 25	15.86 to 17.24

S-81883

Figure 34.--Rotor Blade Tip Static Pressure [illegible], 95 Percent Design Speed, Pressure Ratio 1.540.

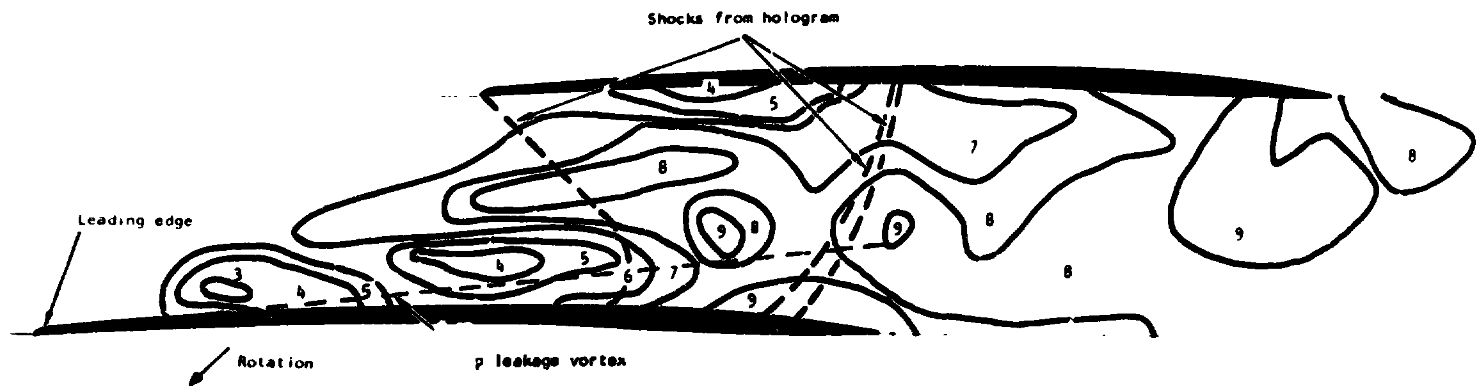

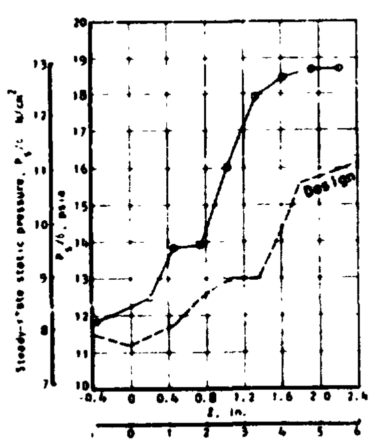

Reading	118
$\frac{N/\sqrt{\theta}}{N/\sqrt{\theta}_{des}}$	= 0.95
$\frac{W\sqrt{\theta}/\delta}{W\sqrt{\theta}/\delta_{des}}$	= 0.995
P_{T12}/P_{T5}	= 1.604

Static pressure contour code		
Code number	Static pressure range	
	psia	N/cm²
1	3 to 5	2.07 to 3.45
2	5 to 7	3.45 to 4.83
3	7 to 9	4.83 to 6.21
4	9 to 11	6.21 to 7.58
5	11 to 13	7.58 to 8.96
6	13 to 15	8.96 to 10.34
7	15 to 17	10.34 to 11.72
8	17 to 19	11.72 to 13.10
9	19 to 21	13.10 to 14.48
10	21 to 23	14.48 to 15.86
11	23 to 25	15.86 to 17.24

S-81875

Figure 35.--Rotor Blade Tip Static Pressure Contours, 95 Percent Design Speed, Pressure Ratio 1.604.

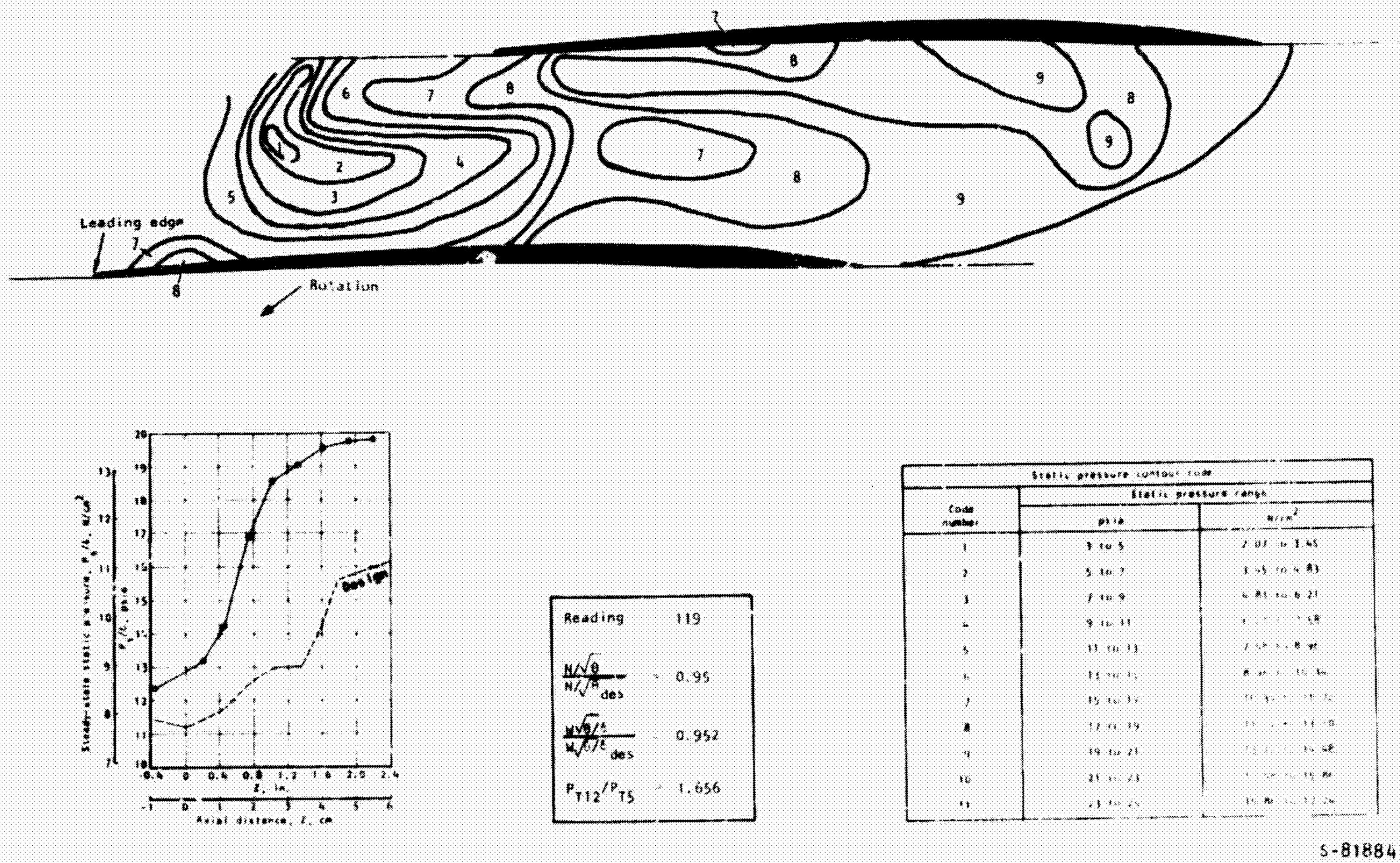

Figure 36.--Rotor Blade Tip Static Pressure Contours, 95 Percent Design Speed, Pressure Ratio 1.656.

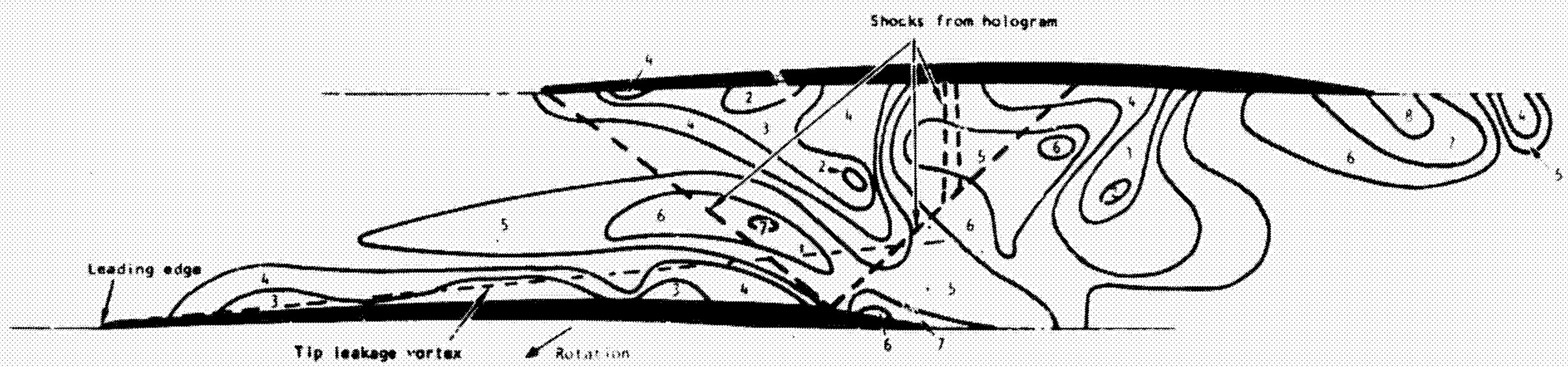

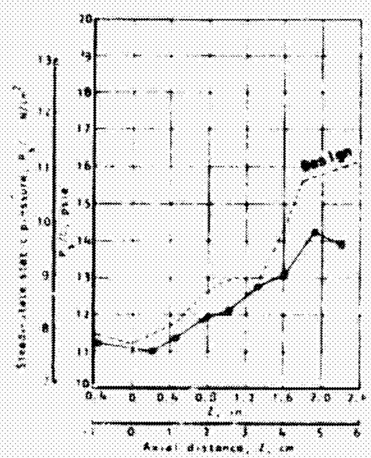

Reading 107

$\frac{N/\sqrt{\theta}}{N/\sqrt{\theta}_{des}} = 1.00$

$\frac{W\sqrt{\theta}/\delta}{W\sqrt{\theta}/\delta_{des}} = 1.040$

$P_{T12}/P_{T5} = 1.369$

Static pressure contour code		
Code number	Static pressure range	
	psia	N/cm²
1	3 to 5	2.07 to 3.45
2	5 to 7	3.45 to 4.83
3	7 to 9	4.83 to 6.21
4	9 to 11	6.21 to 7.58
5	11 to 13	7.58 to 8.96
6	13 to 15	8.96 to 10.34
7	15 to 17	10.34 to 11.72
8	17 to 19	11.72 to 13.10
9	19 to 21	13.10 to 14.48
10	21 to 23	14.48 to 15.86
11	23 to 25	15.86 to 17.24

S-8188 7

Figure 37.--Rotor Blade Tip Static Pressure Contours, Design Speed, Pressure Ratio 1.369.

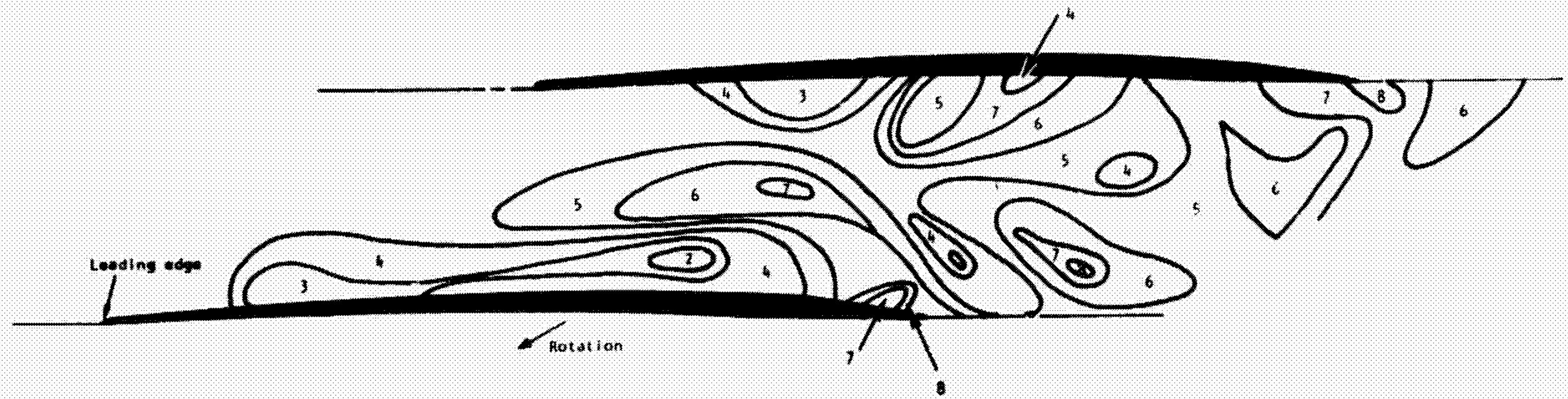

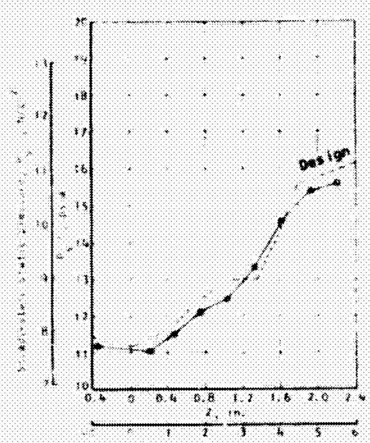

Reading	108
$\frac{N/\sqrt{\theta}}{N/\sqrt{\theta}_{des}}$	= 1.00
$\frac{W\sqrt{\theta}/\delta}{W\sqrt{\theta}/\delta_{des}}$	= 1.044
P_{T12}/P_{T5}	= 1.475

Static pressure contour code		
Code number	Static pressure range	
	psia	N/cm²
1	3 to 5	2.07 to 3.45
2	5 to 7	[illegible]
3	7 to 9	[illegible]
4	9 to 11	[illegible]
5	11 to 13	[illegible]
6	13 to 15	[illegible]
7	15 to 17	[illegible]
8	17 to 19	[illegible]
9	19 to 21	[illegible]
10	21 to 23	[illegible]
11	23 to 25	[illegible]

S-81885

Figure 38.--Rotor Blade Tip Static Pressure Contours, Design Speed, Pressure Ratio 1.475.

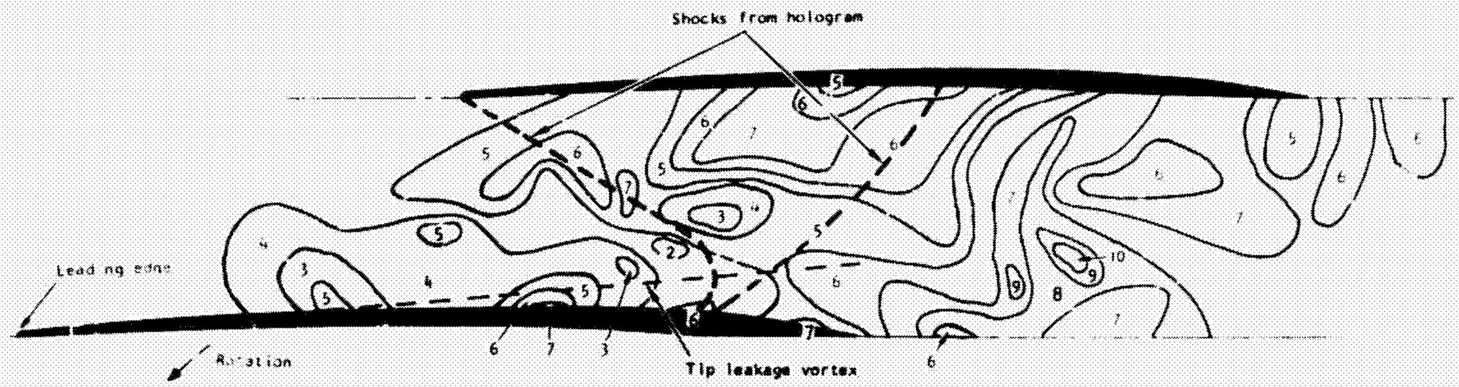

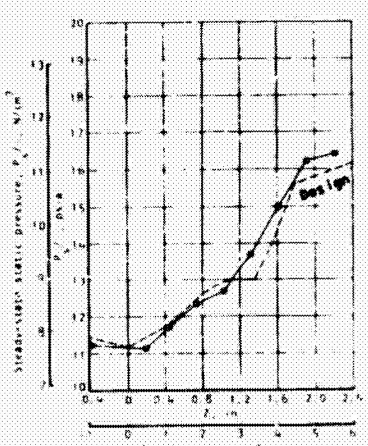

Reading	128
$\frac{N/\sqrt{\theta}}{N/\sqrt{\theta}_{des}}$	= 1.00
$\frac{W\sqrt{\theta}/\delta}{W\sqrt{\theta}/\delta_{des}}$	= 1.041
P_{T12}/P_{T5}	= 1.505

Static pressure contour code

Code number	Static pressure range, psia	Static pressure range, N/cm²
1	3 to 5	2.07 to 3.45
2	5 to 7	3.45 to 4.83
3	7 to 9	4.81 to 6.21
4	9 to 11	6.21 to 7.58
5	11 to 13	7.58 to 8.[illegible]
6	13 to 15	[illegible]
7	15 to 17	[illegible]
8	17 to 19	[illegible]
9	19 to 21	[illegible]
10	21 to 23	[illegible]
11	23 to [illegible]	[illegible]

S-81873

Figure 39.--Rotor Blade Tip Static Pressure Contours, Design Speed, Pressure Ratio 1.505.

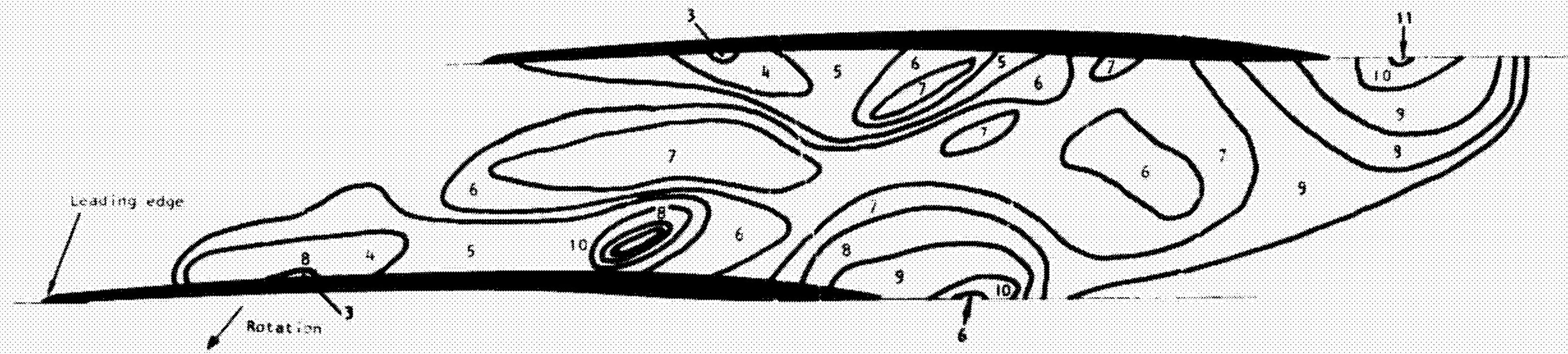

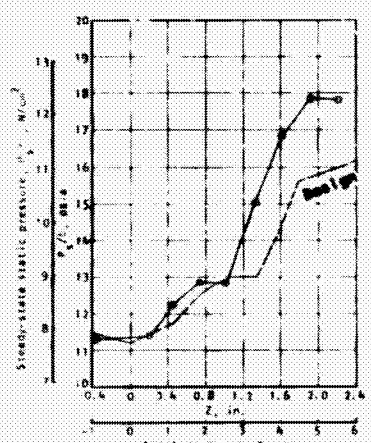

Reading	125
$\frac{N/\sqrt{\theta}}{N/\sqrt{\theta}_{des}}$	= 1.00
$\frac{W\sqrt{\theta}/\delta}{W\sqrt{\theta}/\delta_{des}}$	= 1.035
P_{T12}/P_{T5}	= 1.623

Static pressure contour code		
Code number	Static pressure range	
	psia	N/cm²
1	3 to 5	2.07 to 3.45
2	5 to 7	3.45 to 4.83
3	7 to 9	4.83 to 6.21
4	9 to 11	6.21 to 7.58
5	11 to 13	7.58 to 8.96
6	13 to 15	8.96 to 10.34
7	15 to 17	10.34 to 11.72
8	17 to 19	11.72 to 13.10
9	19 to 21	13.10 to 14.48
10	21 to 23	14.48 to 15.86
11	23 to 25	15.86 to 17.24

S-81874

Figure 40.--Rotor Blade Tip Static Pressure Contours, Design Speed, Pressure Ratio 1.623.

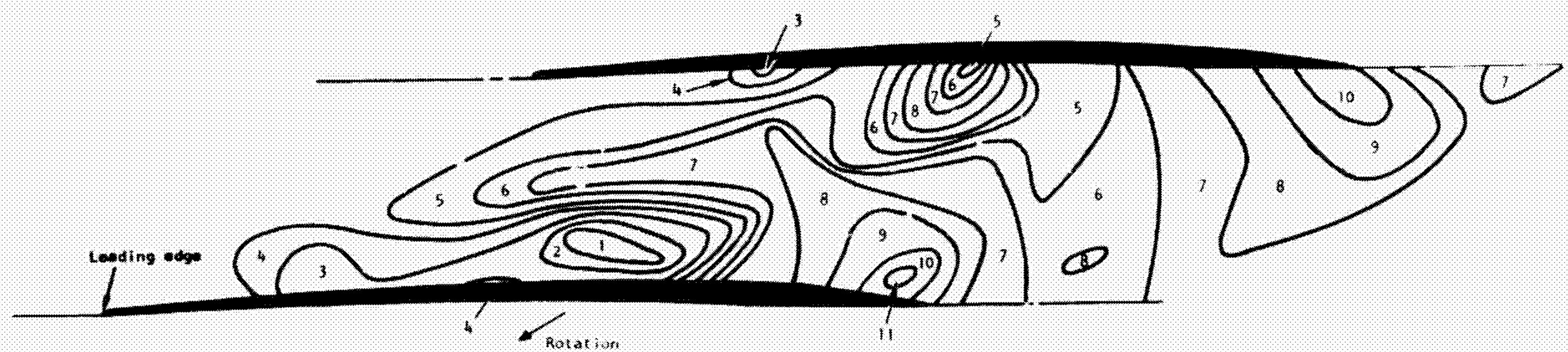

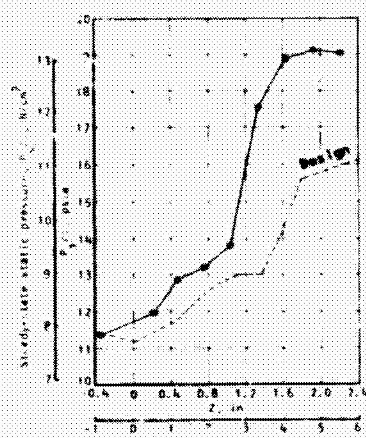

Reading 126

$\frac{N/\sqrt{\theta}}{N/\sqrt{\theta}_{des}} = 1.00$

$\frac{W\sqrt{\theta}/\delta}{W\sqrt{\theta}/\delta_{des}} = 1.031$

$P_{T12}/P_{T5} = 1.669$

Static pressure contour code		
Code number	Static pressure range	
	psia	N/cm²
1	3 to 5	2.07 to 3.45
2	5 to 7	3.45 to 4.83
3	7 to 9	4.83 to 6.21
4	9 to 11	6.21 to 7.58
5	11 to 13	7.58 to 8.96
6	13 to 15	8.96 to 10.34
7	15 to 17	10.34 to 11.72
8	17 to 19	11.72 to 13.10
9	19 to 21	13.10 to 14.48
10	21 to 23	14.48 to 15.86
11	23 to 25	15.86 to 17.24

S-8188c

Figure 41.--Rotor Blade Tip Static Pressure Contours, Design Speed, Pressure Ratio 1.669.

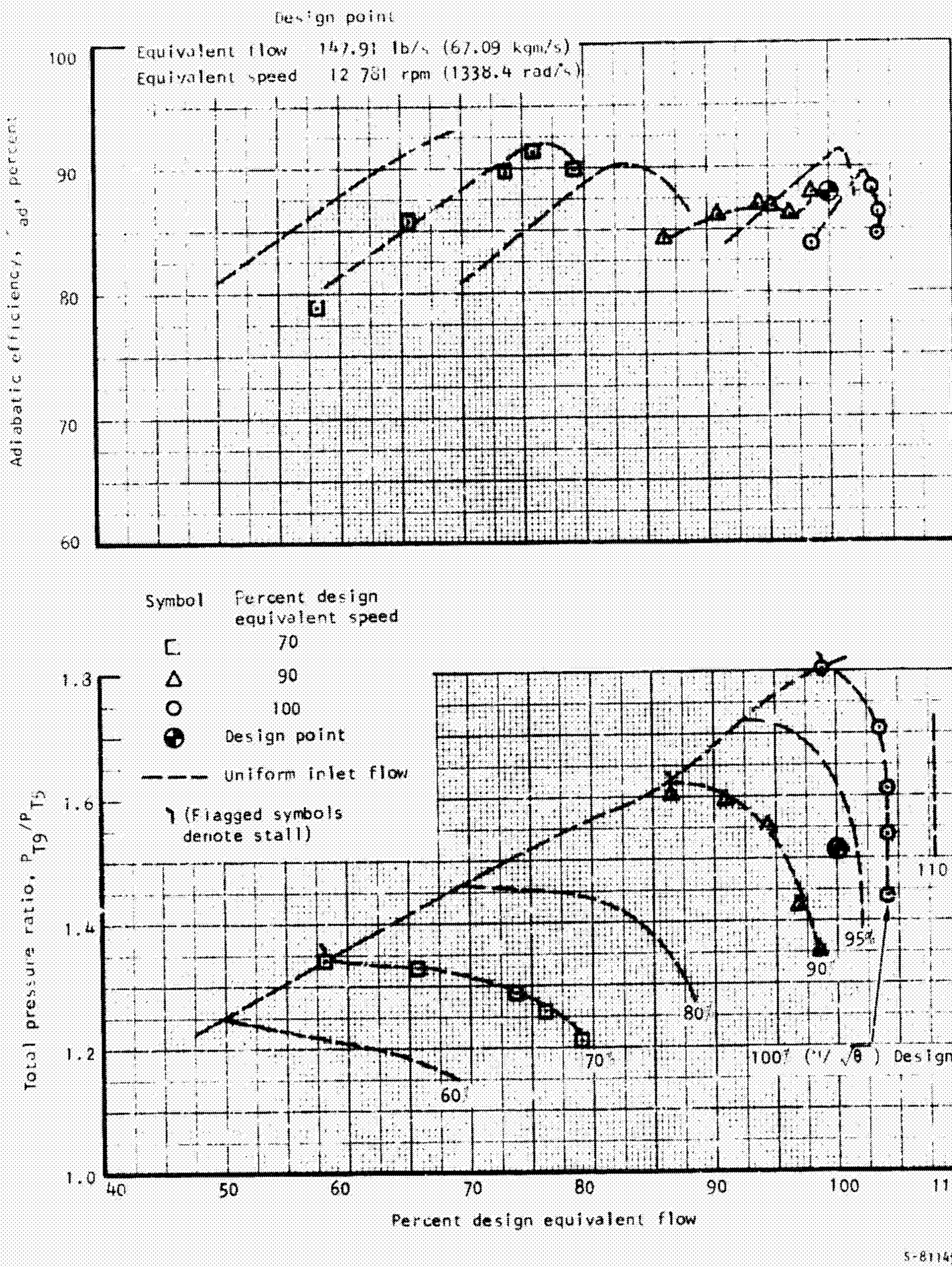

Figure 42.--Rotor Performance, Predistortion Baseline.

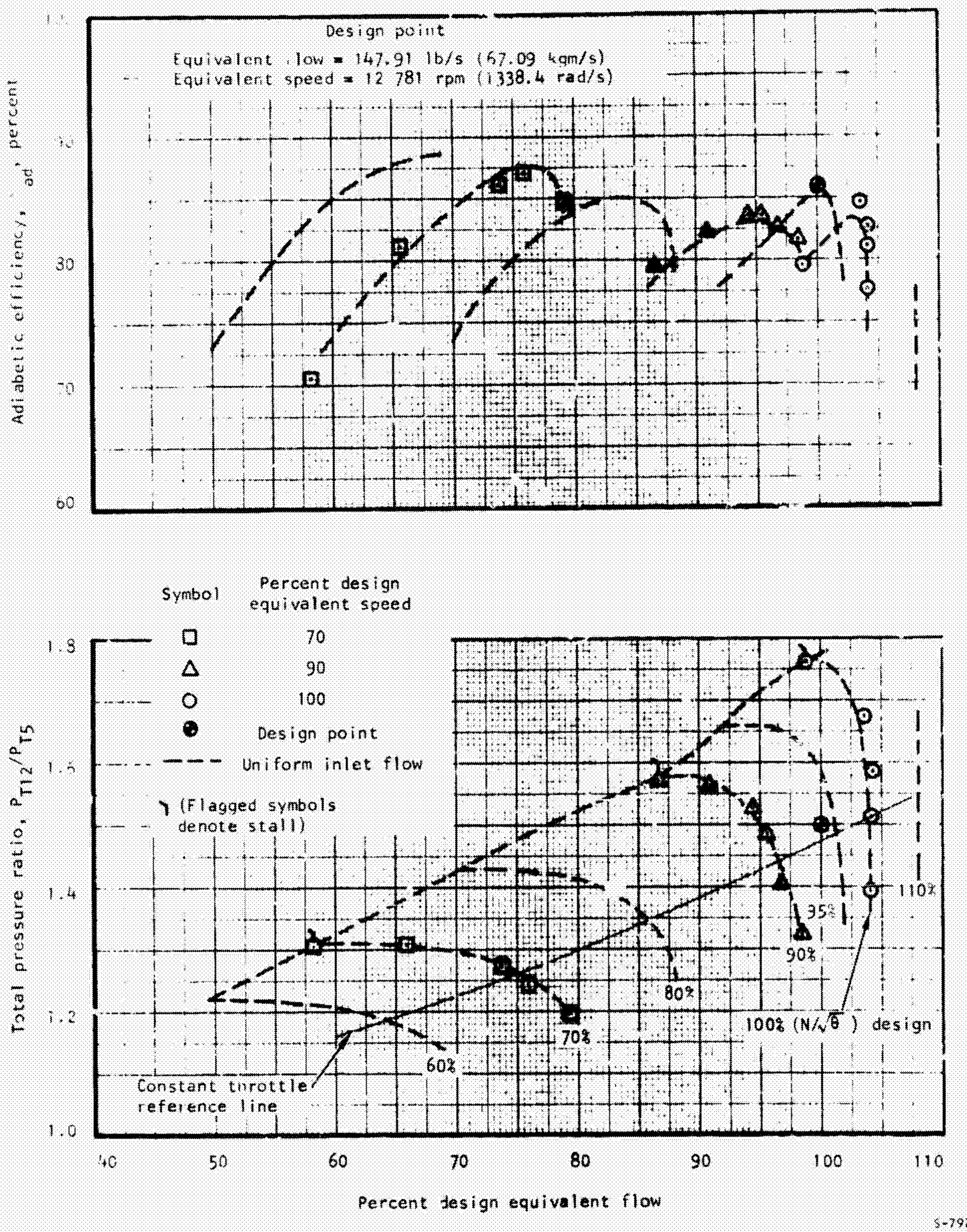

Figure 43.--Stage Performance, Predistortion Baseline.

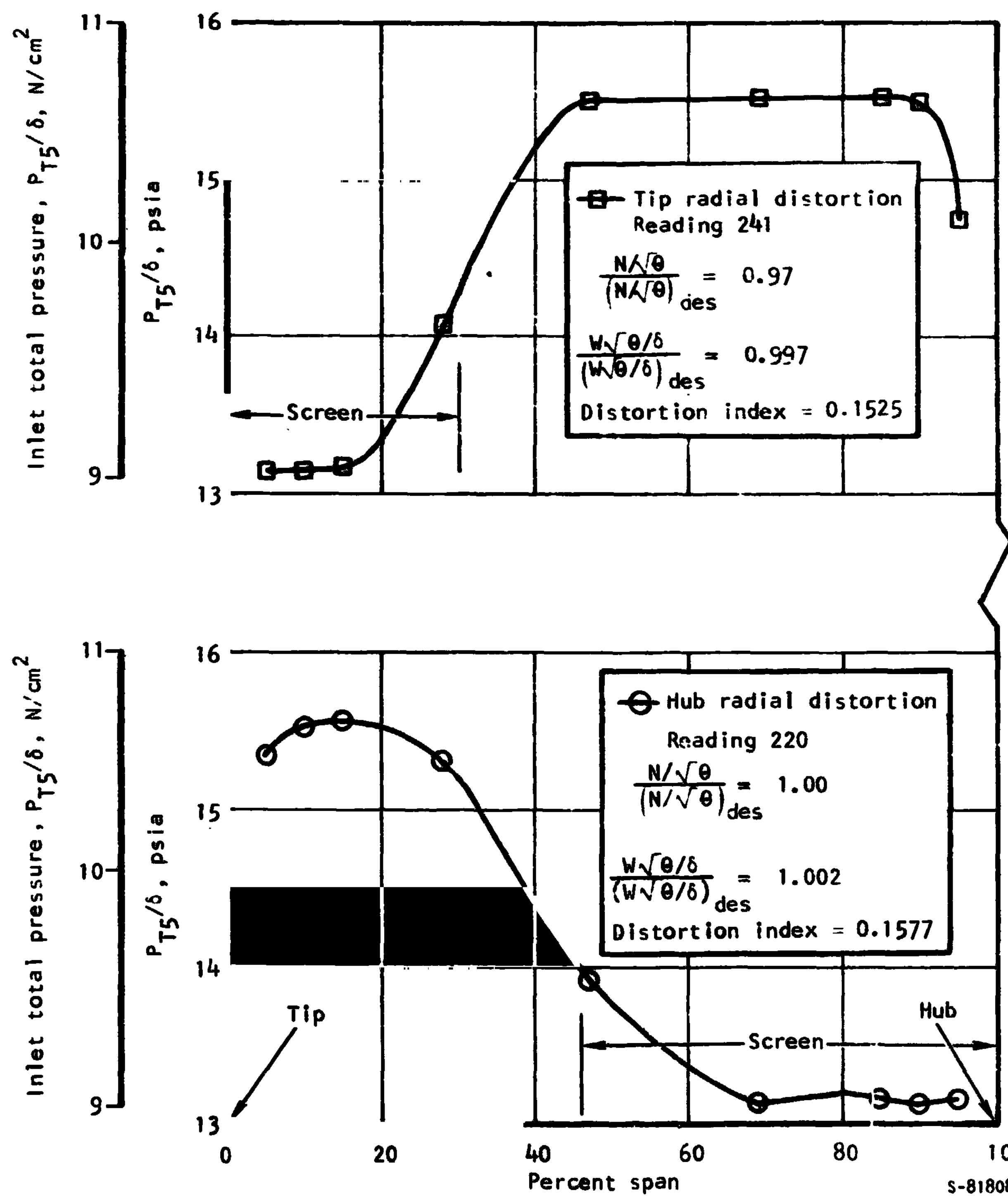

Figure 44.--Radial Distortion Total Pressure Profiles for Design Equivalent Flow.

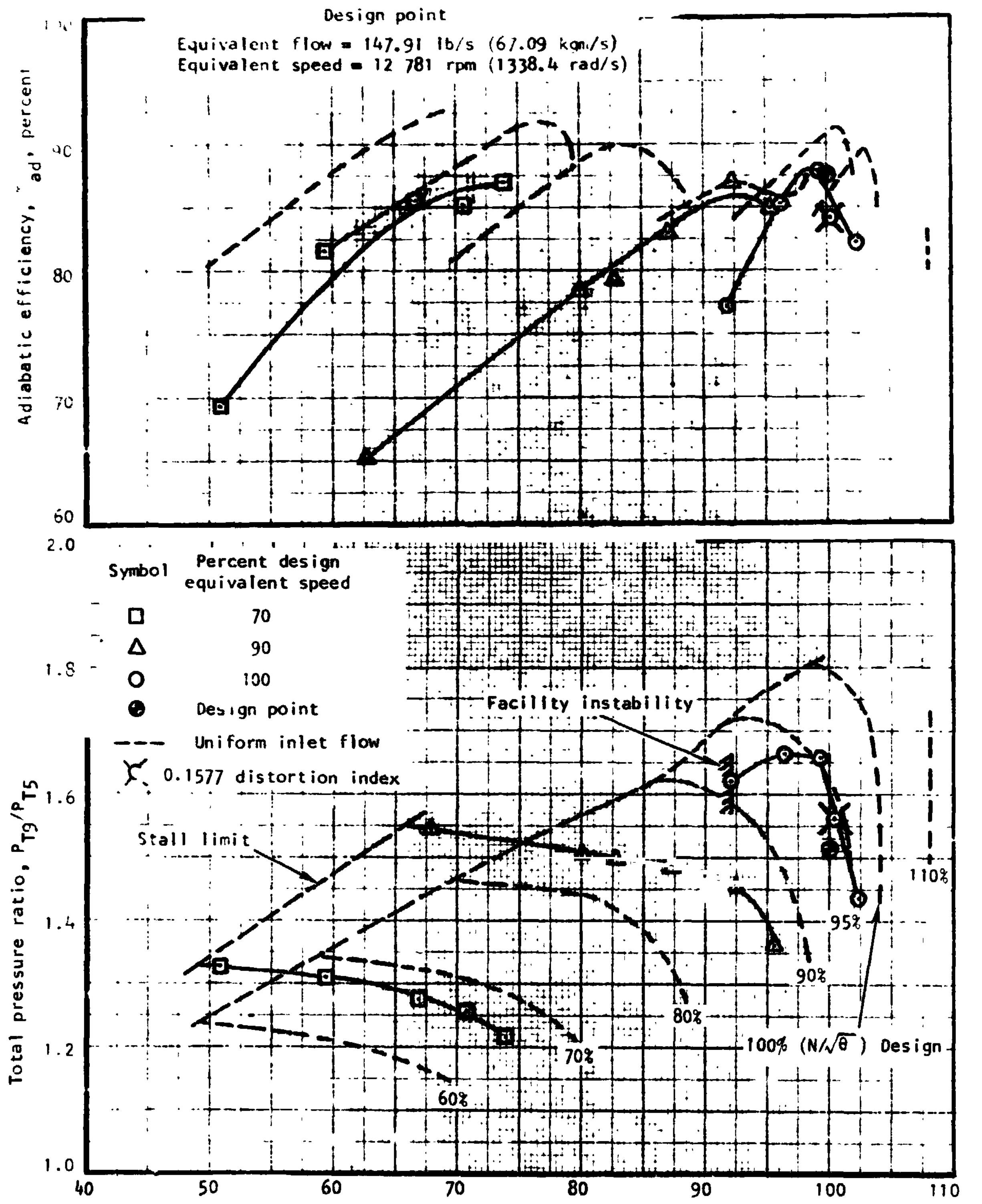

Figure 45.--Rotor Performance, Hub-Radial Distortion.

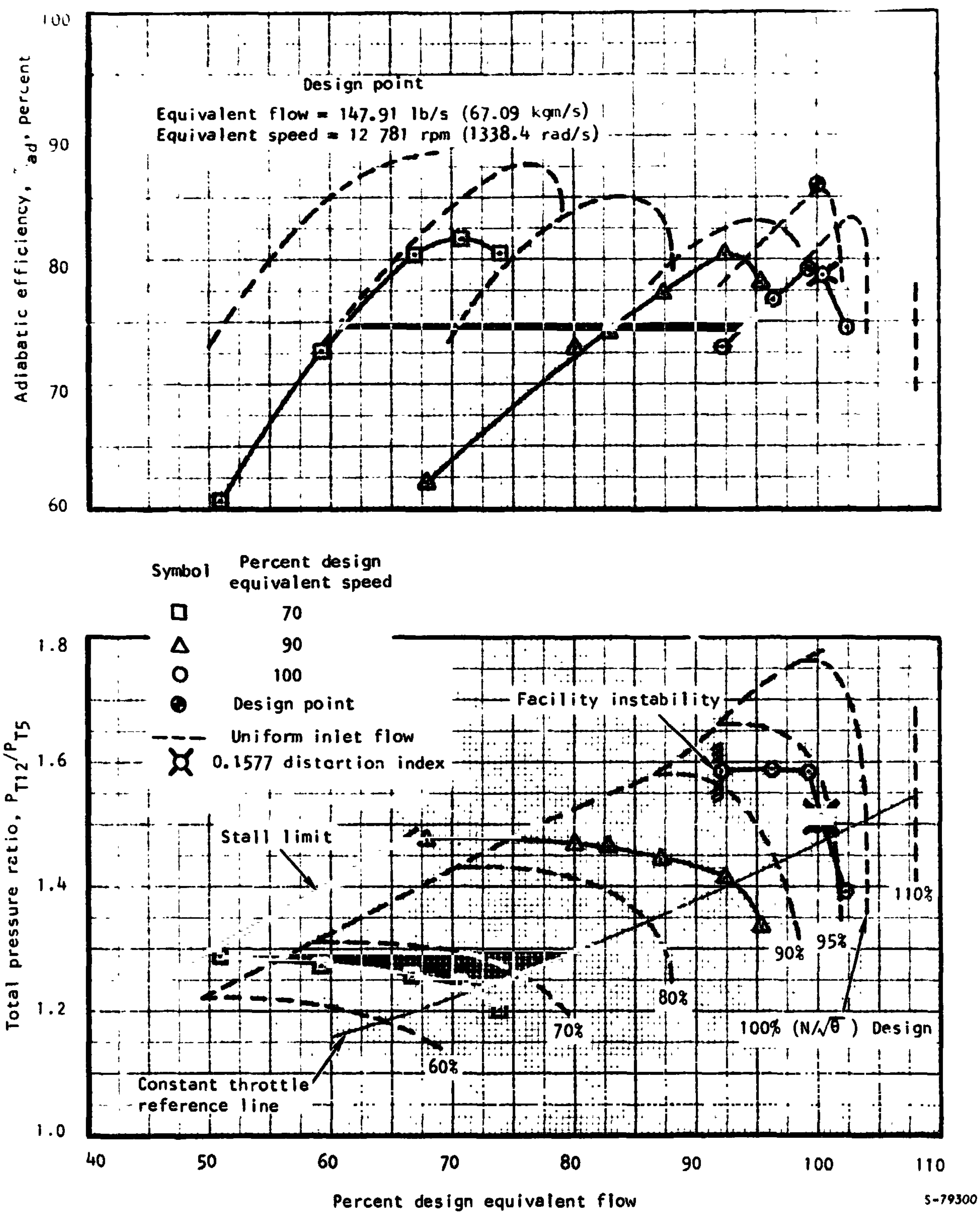

Figure 46.--Stage Performance, Hub-Radial Distortion.

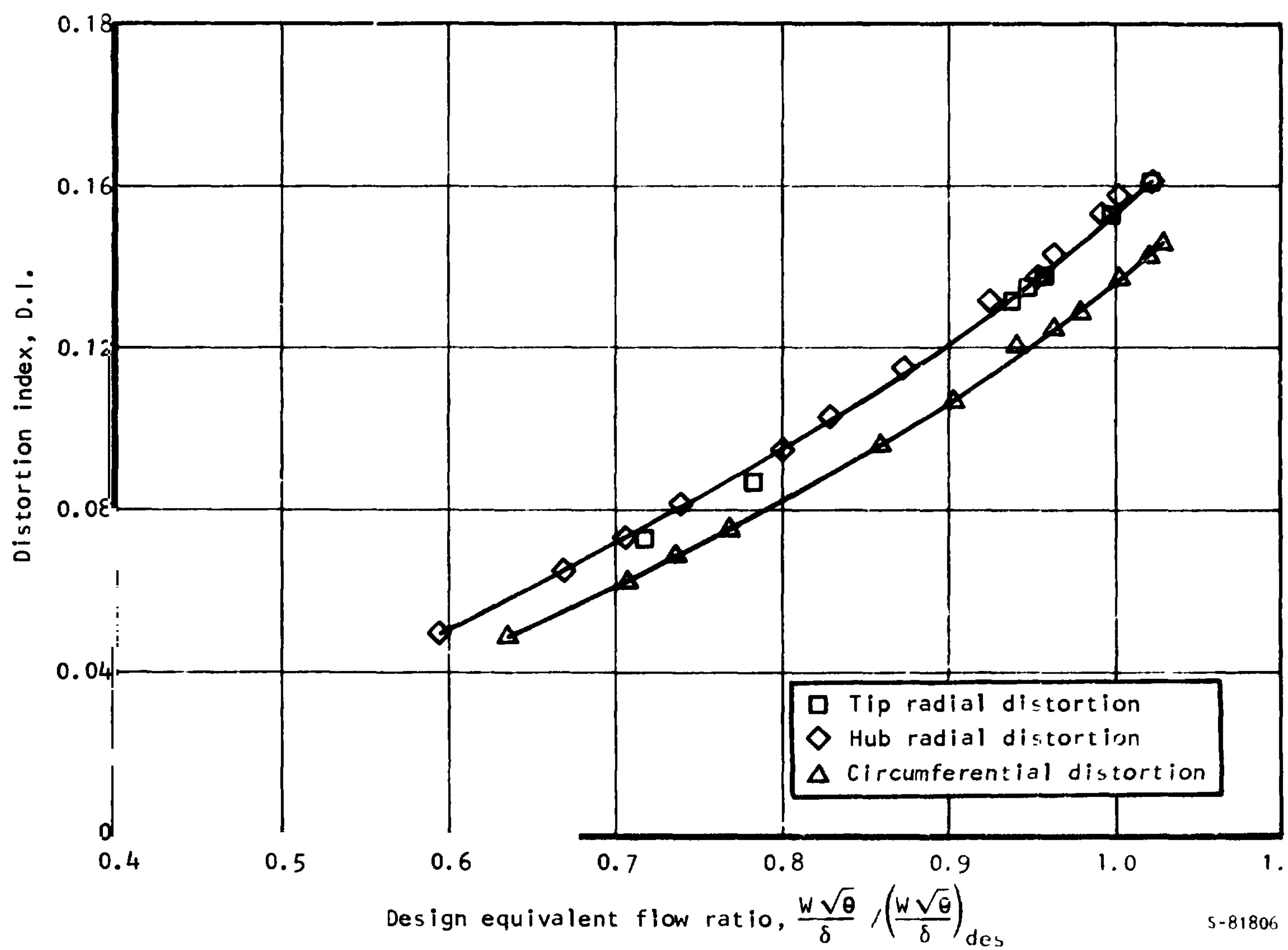

Figure 47.--Distortion Index vs Design Equivalent Flow Ratio.

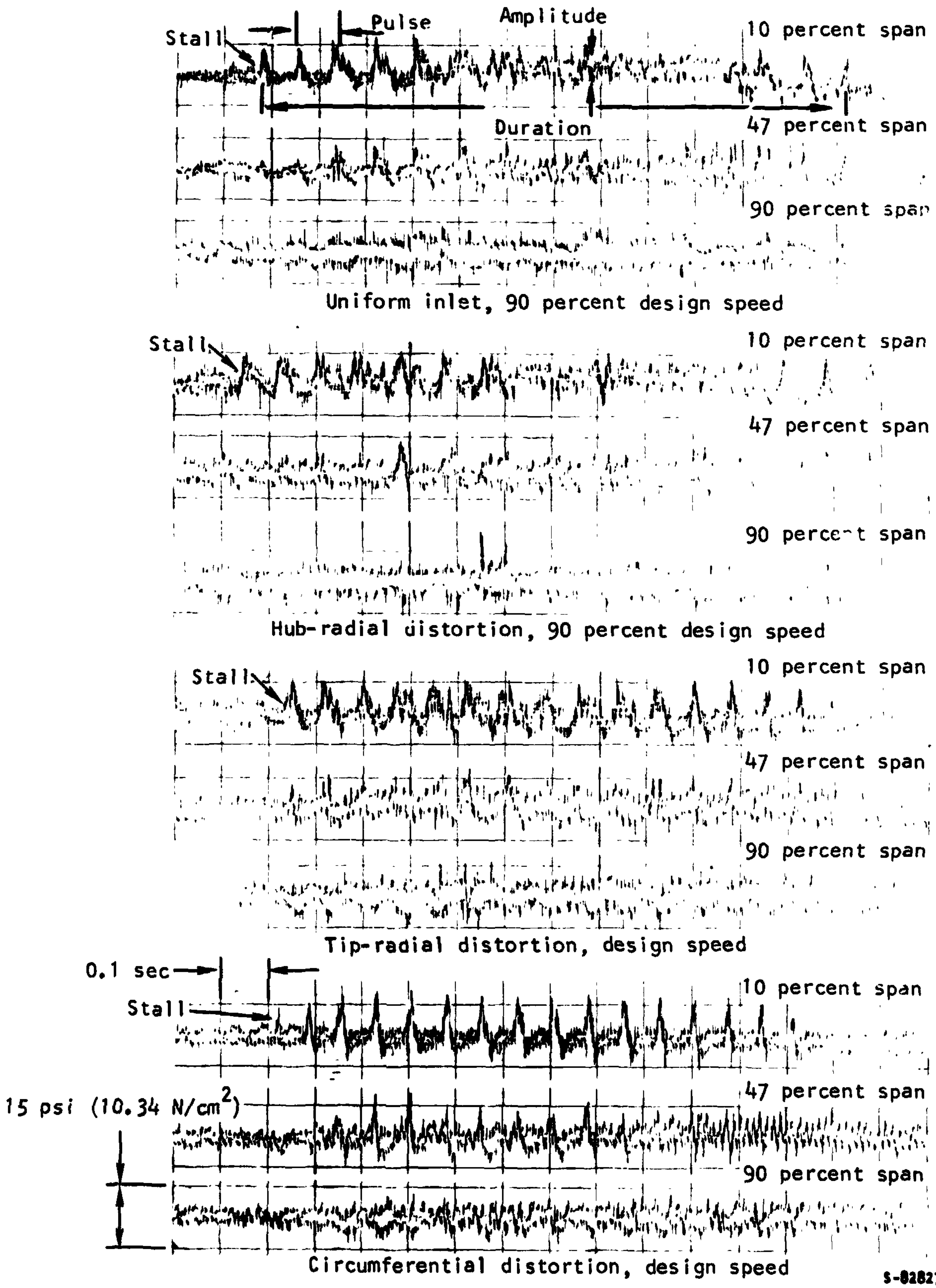

Figure 48.--Distorted Inlet Flow Stall Oscillograph Traces.

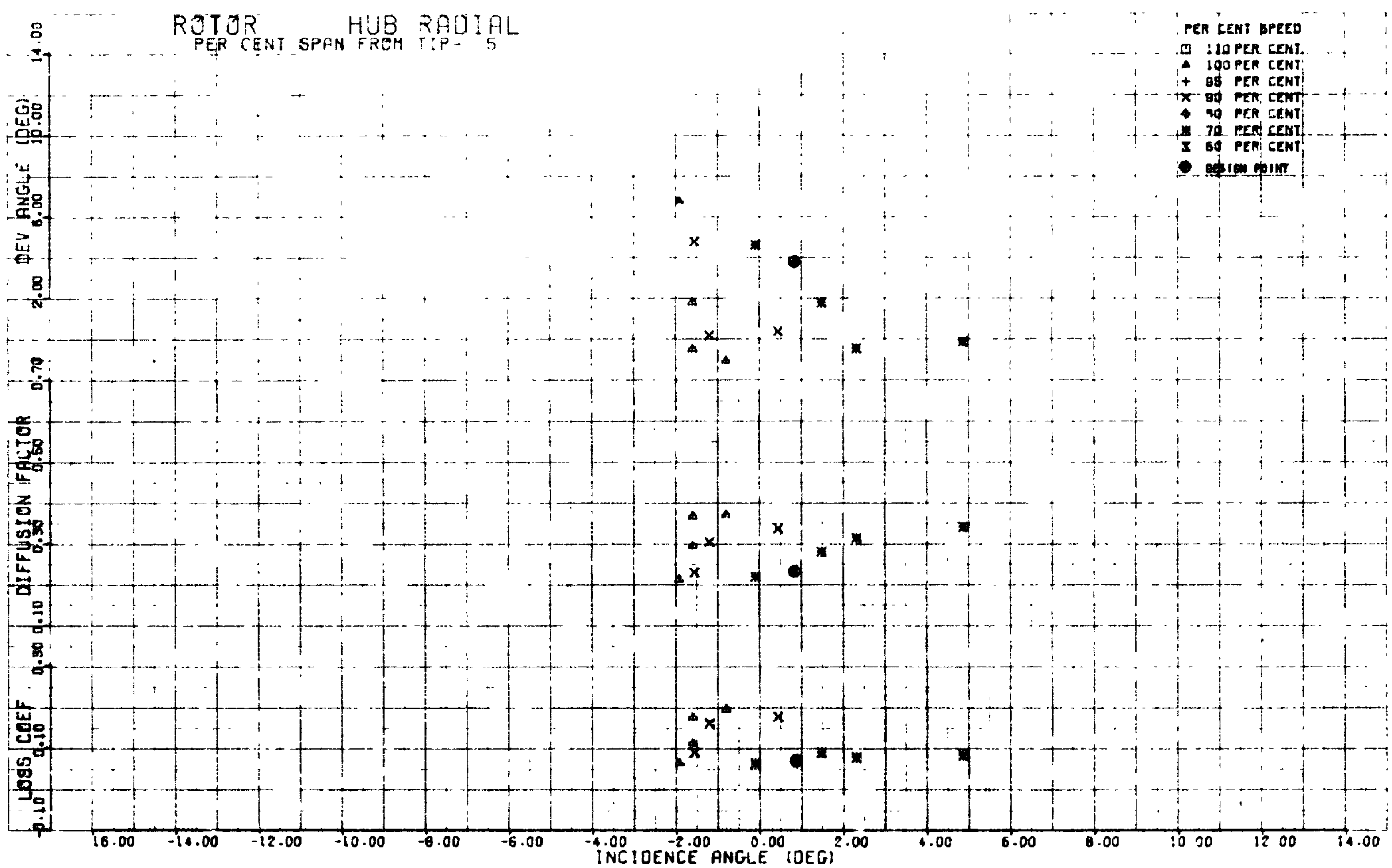

Figure 49a.--Rotor Blade Element Performance, Hub-Radially Distorted Inlet Flow, 5 Percent Span from Tip.

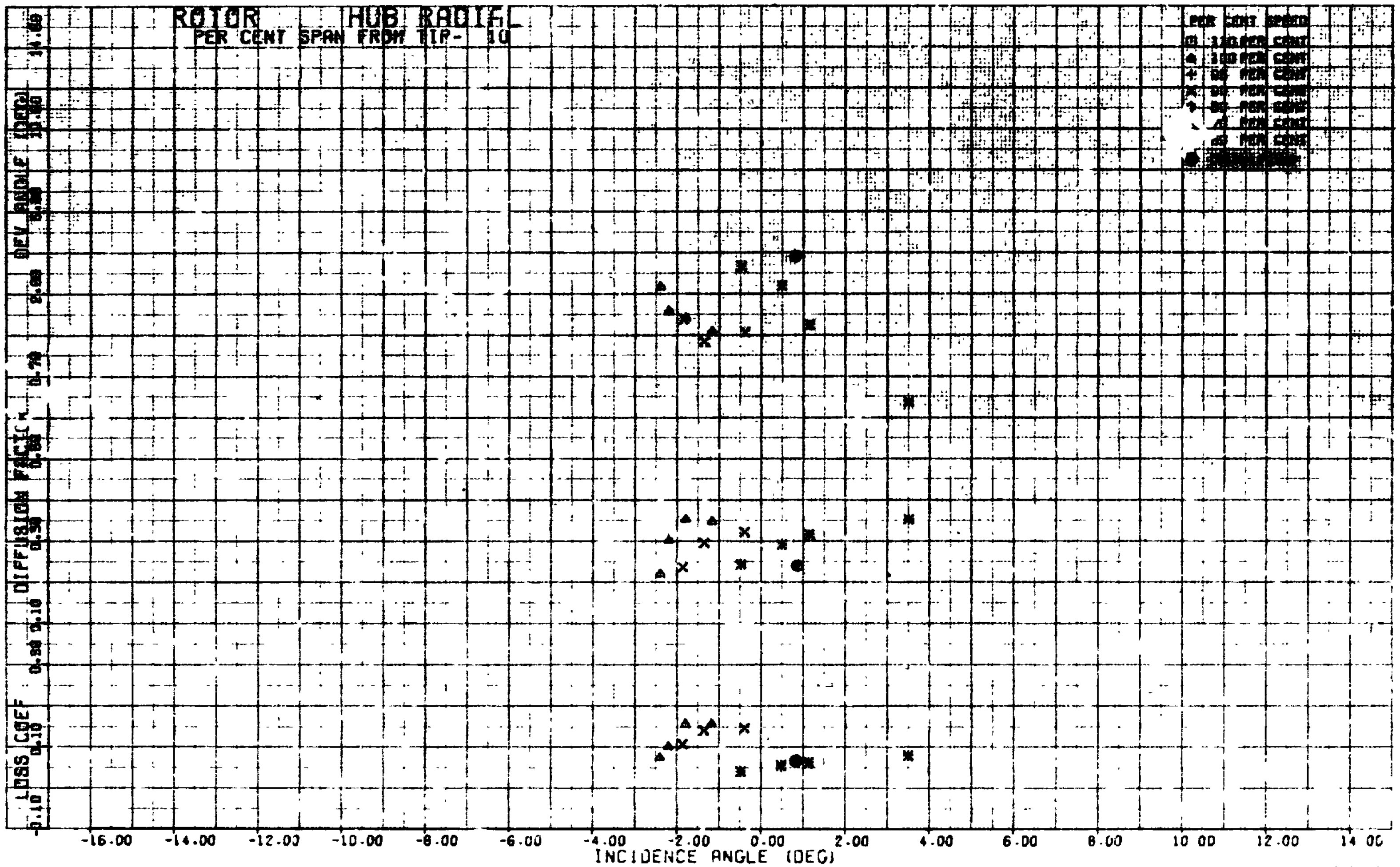

Figure 49b.--Rotor Blade Element Performance, Hub-Radially Distorted Inlet Flow, 10 Percent Span from Tip.

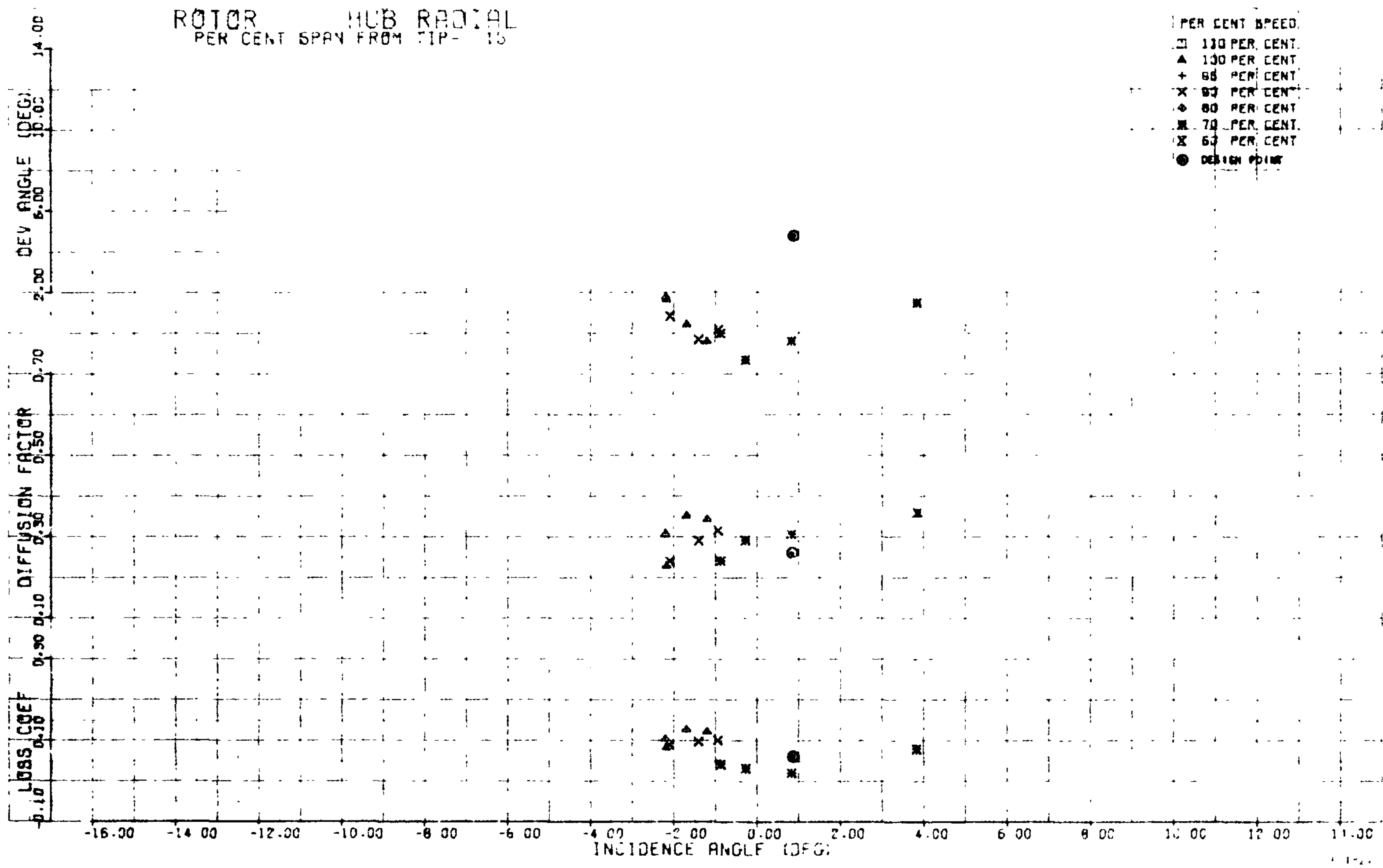

Figure 49c.--Rotor Blade Element Performance, Hub-Radially Distorted Inlet Flow, 15 Percent Span from Tip.

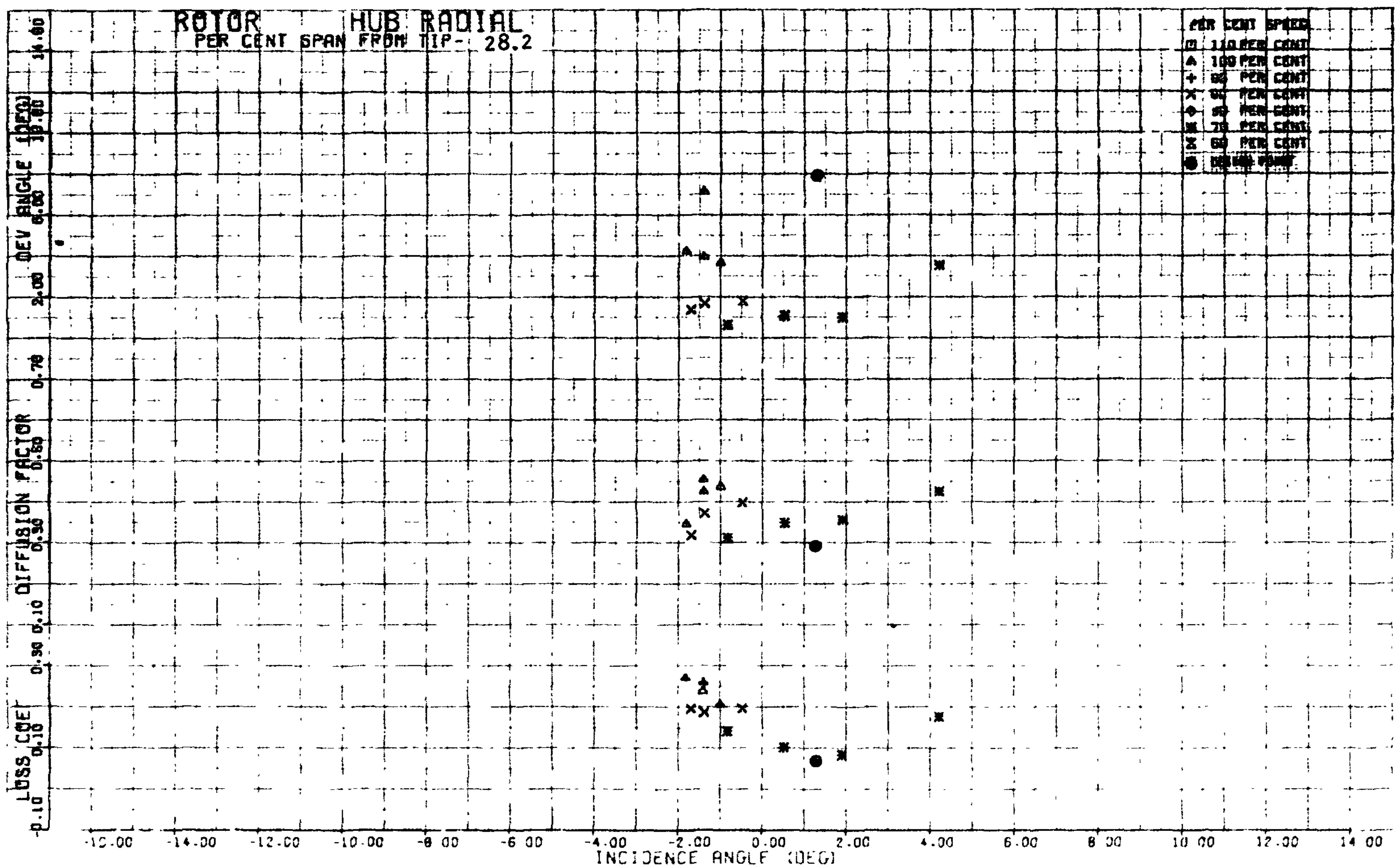

Figure 49d.--Rotor Blade Element Performance, Hub-Radially Distorted Inlet Flow, 28.2 Percent Span from Tip.

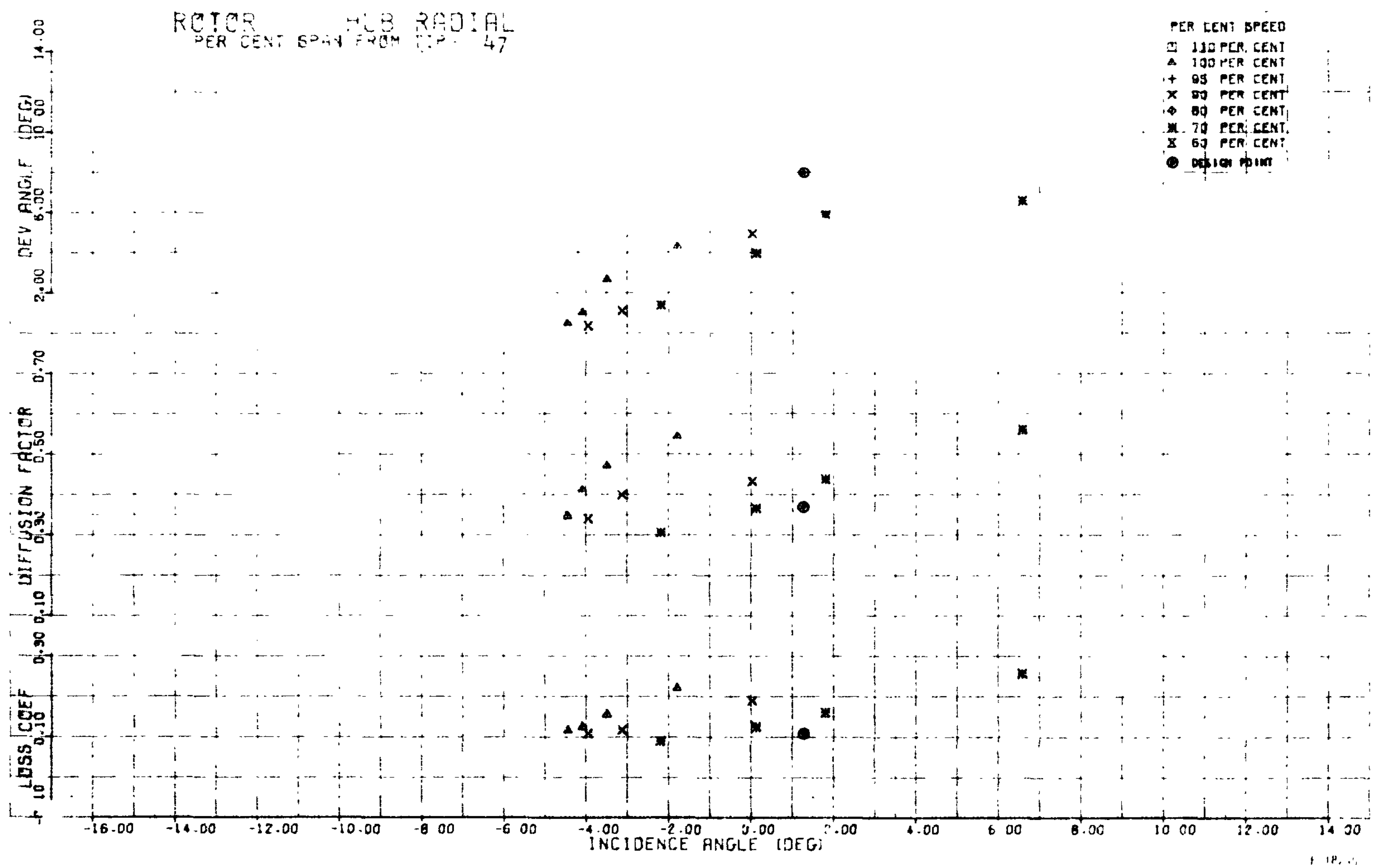

Figure 49e.--Rotor Blade Element Performance, Hub-Radially Distorted Inlet Flow, 47 Percent Span from Tip.

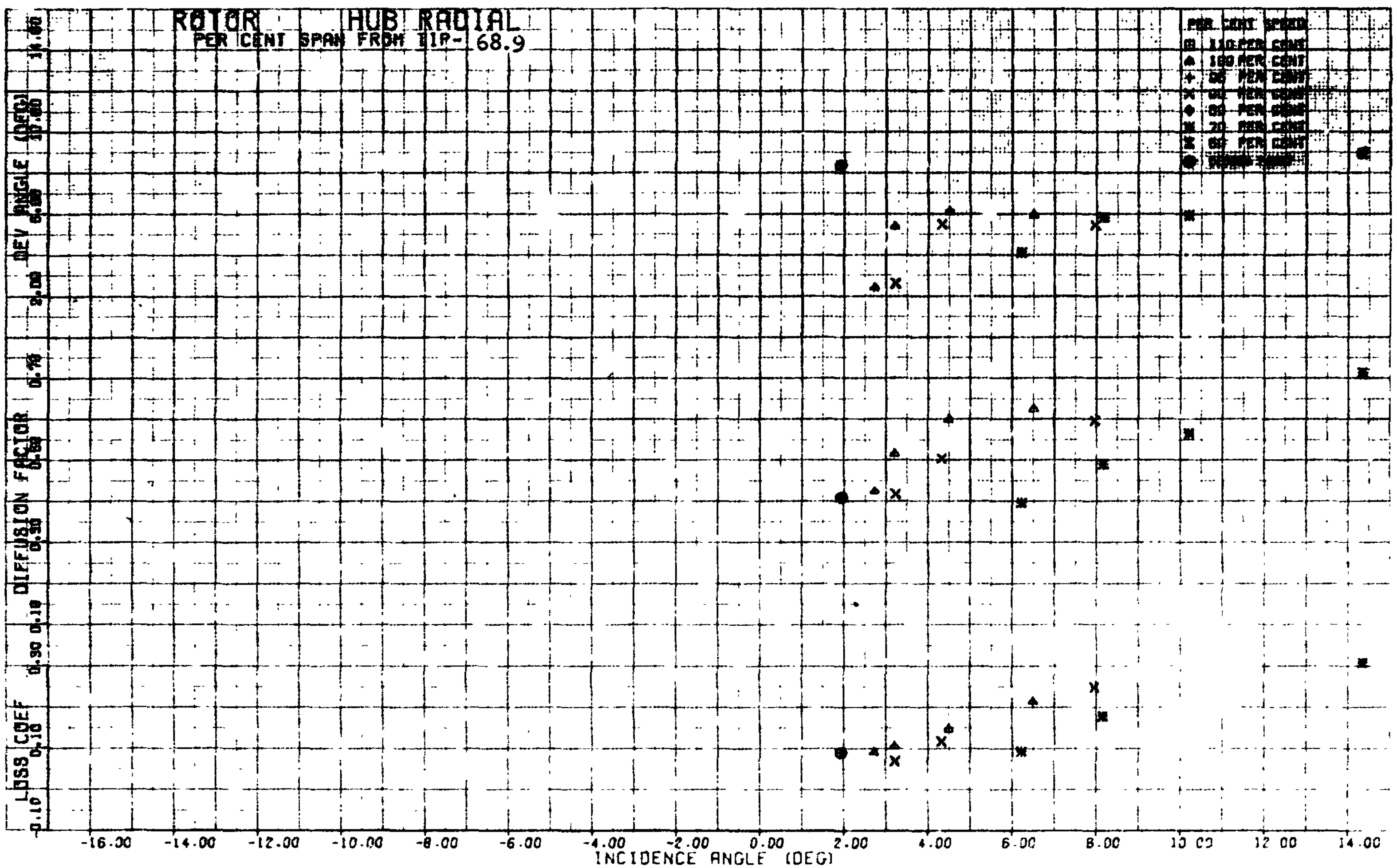

Figure 49f.--Rotor Blade Element Performance, Hub-Radially Distorted Inlet Flow, 68.9 Percent Span from Tip.

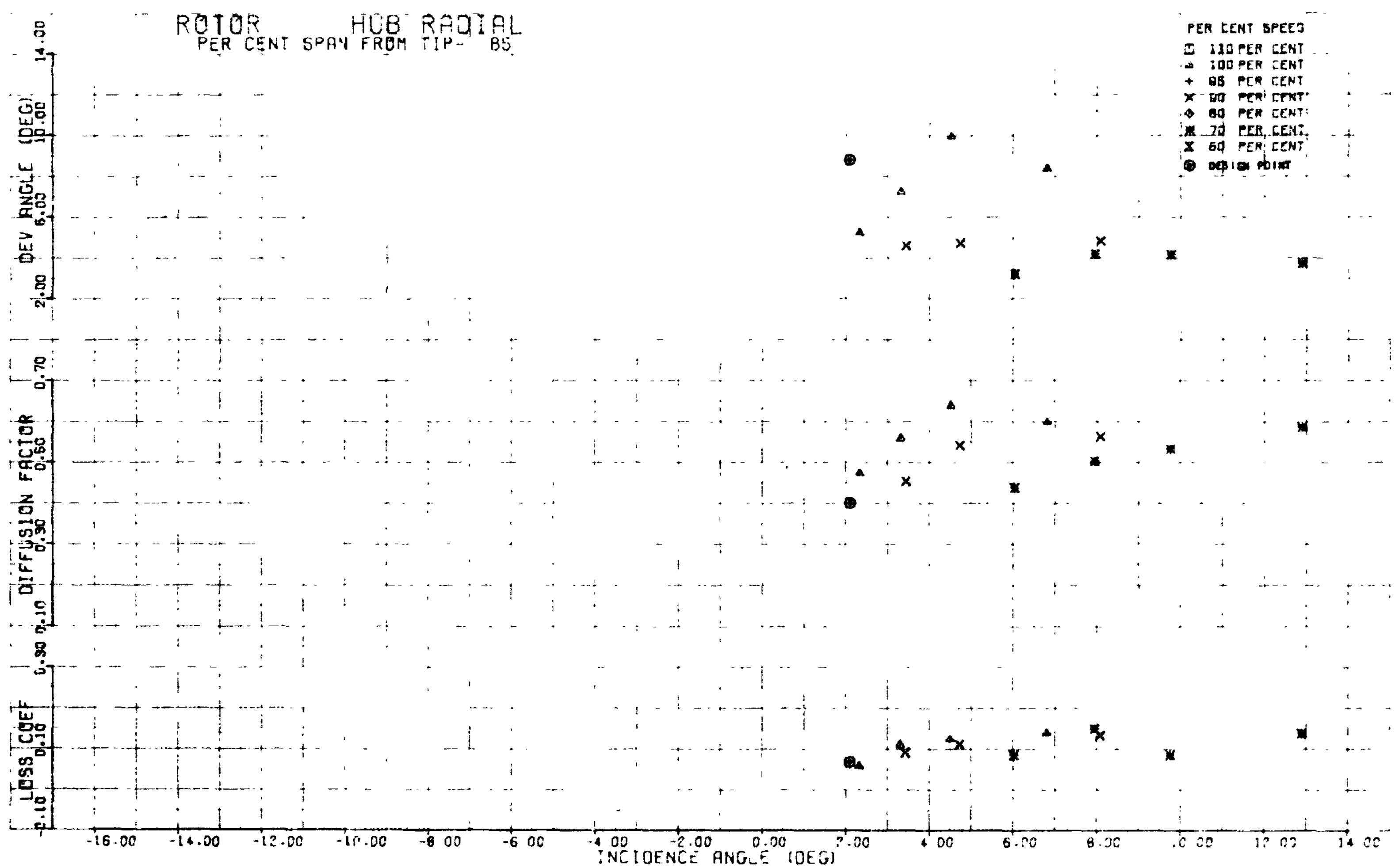

Figure 49g.--Rotor Blade Element Performance, Hub-Radially Distorted Inlet Flow, 85 Percent Span from Tip.

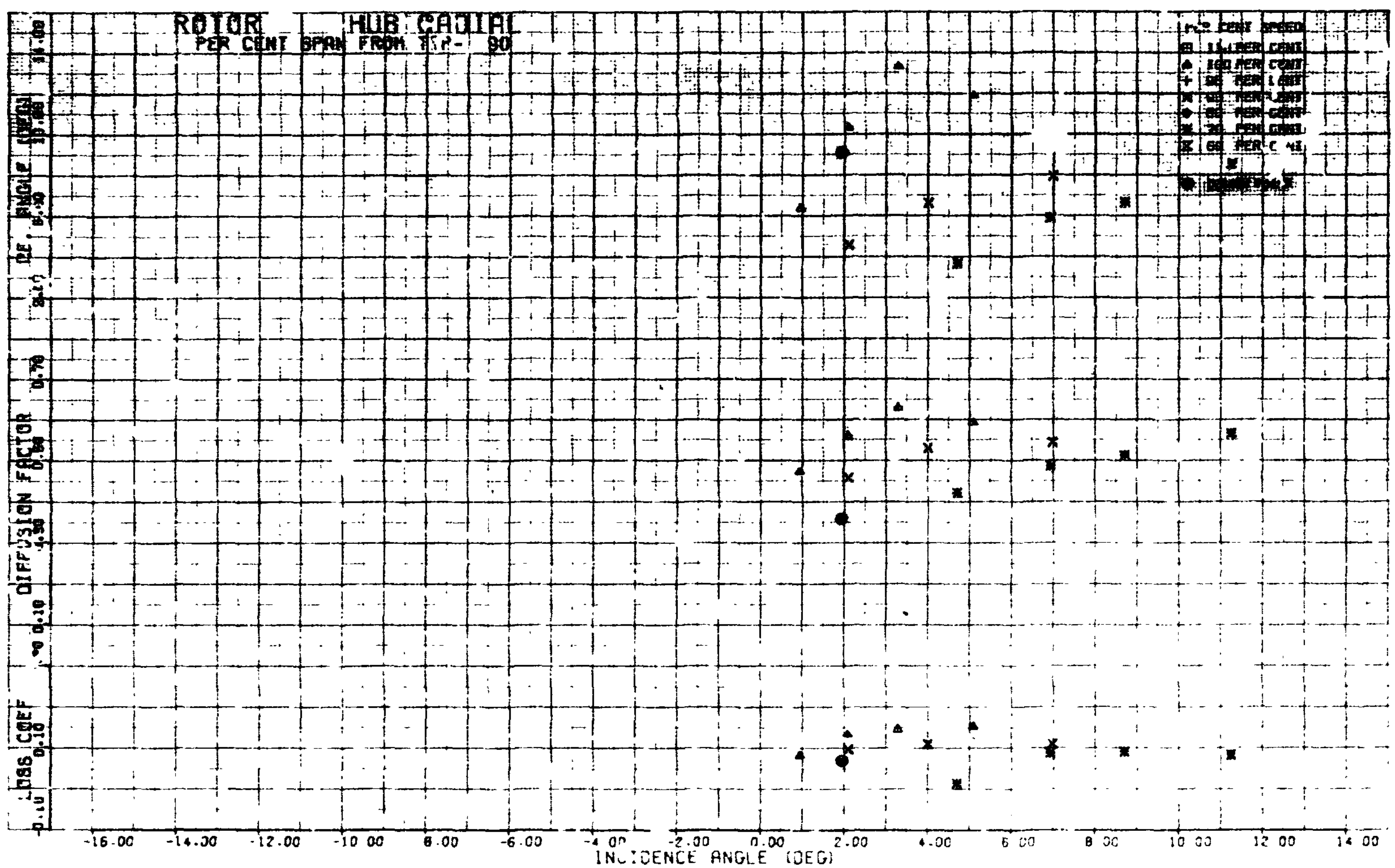

Figure 49h.--Rotor Blade Element Performance, Hub-Radially Distorted Inlet Flow, 90 Percent Span from Tip.

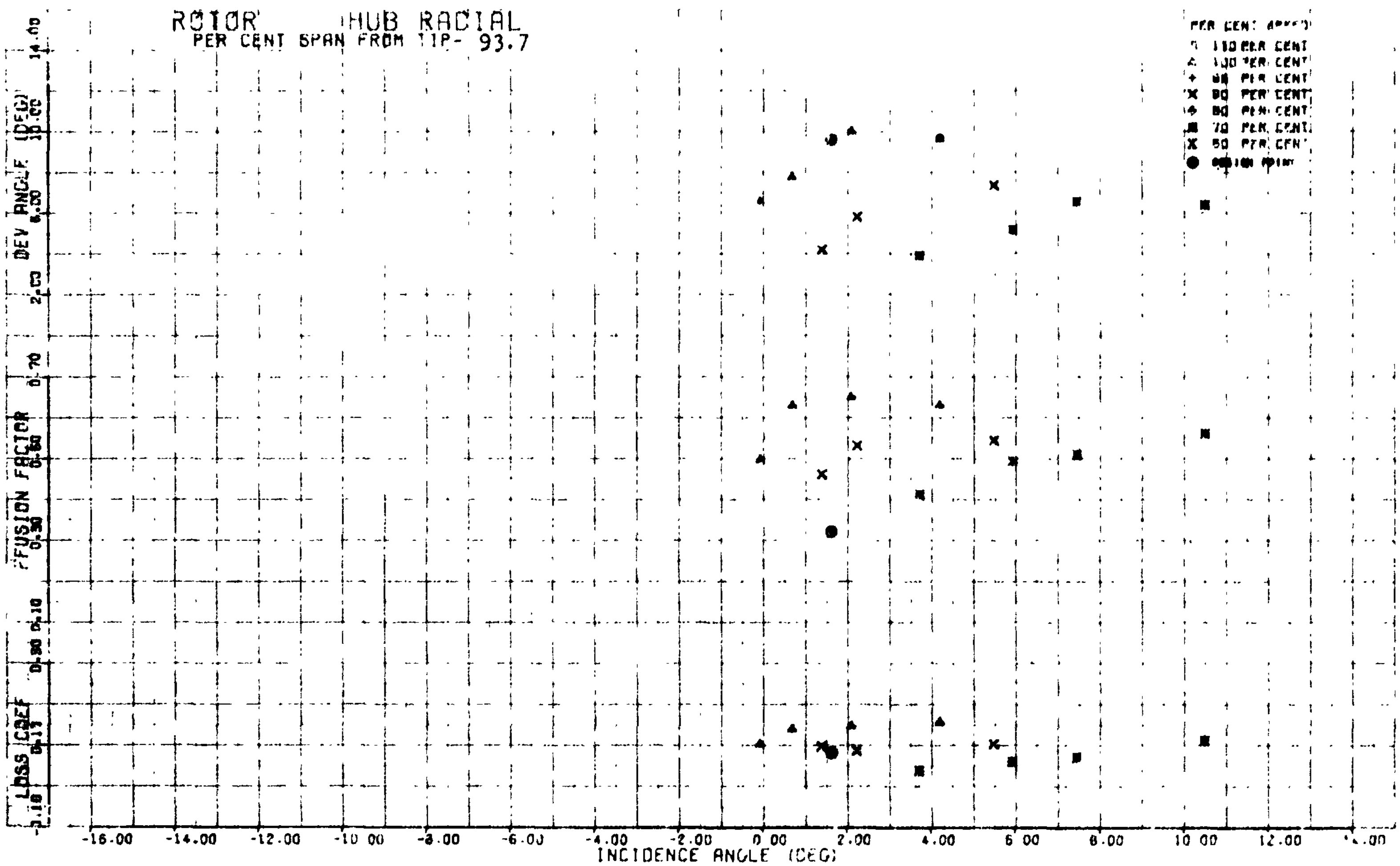

Figure 49i.--Rotor Blade Element Performance, Hub-Radially Distorted Inlet Flow, 93.7 Percent Span from Tip.

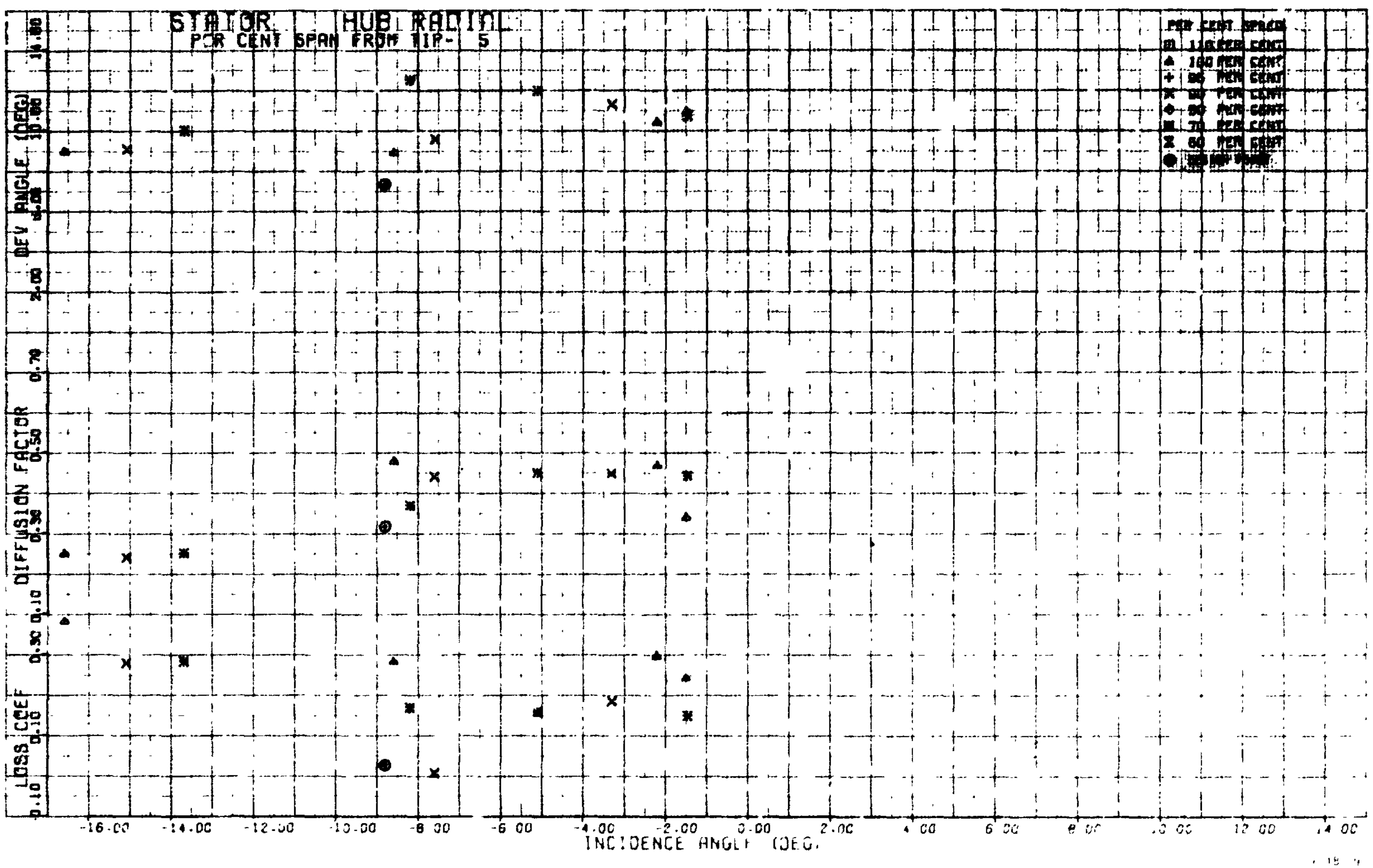

Figure 50a.--Stator Vane Element Performance, Hub-Radially Distorted Inlet Flow, 5 Percent Span from Tip.

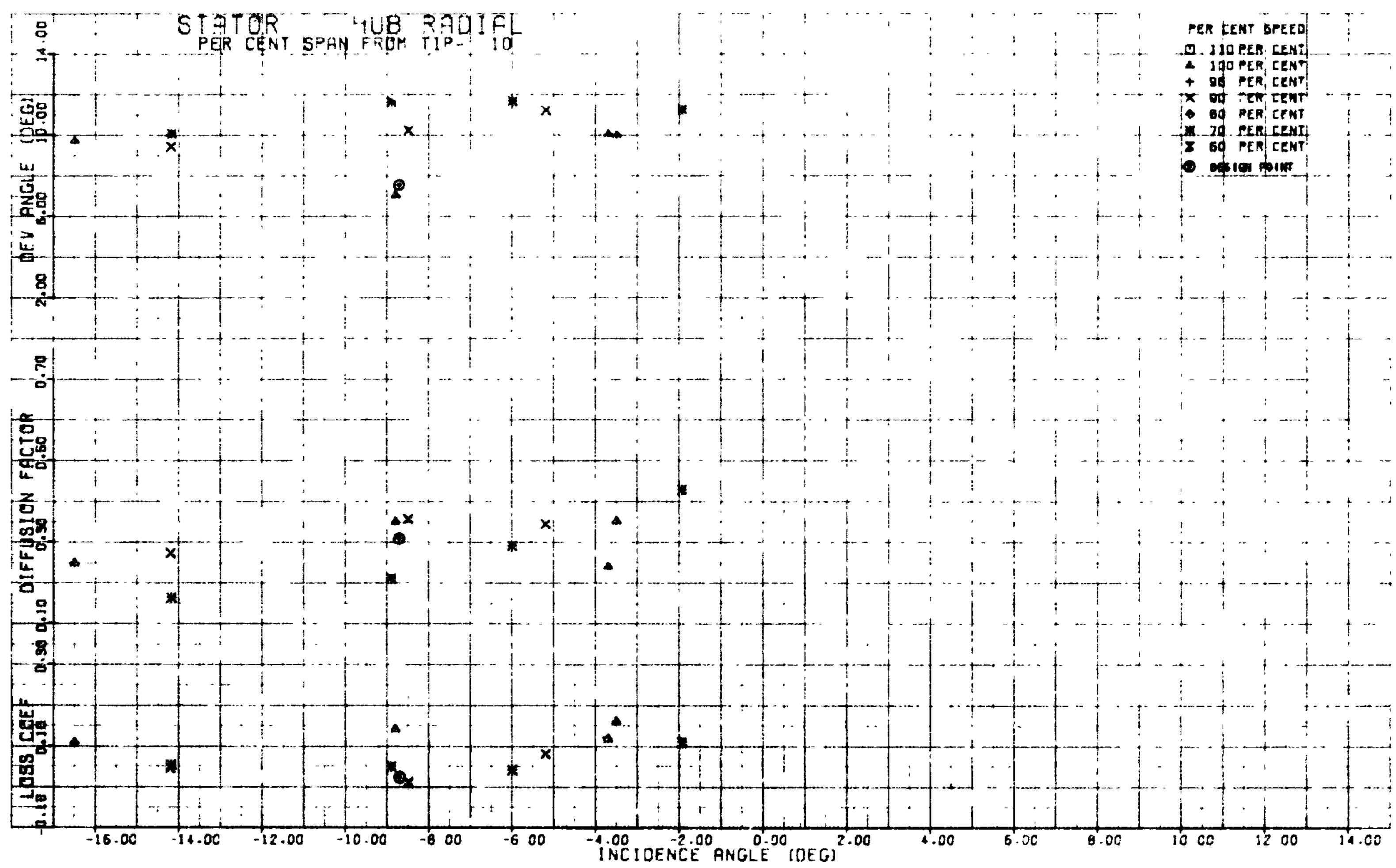

Figure 50b.--Stator Vane Element Performance, Hub-Radially Distorted Inlet Flow, 10 Percent Span from Tip.

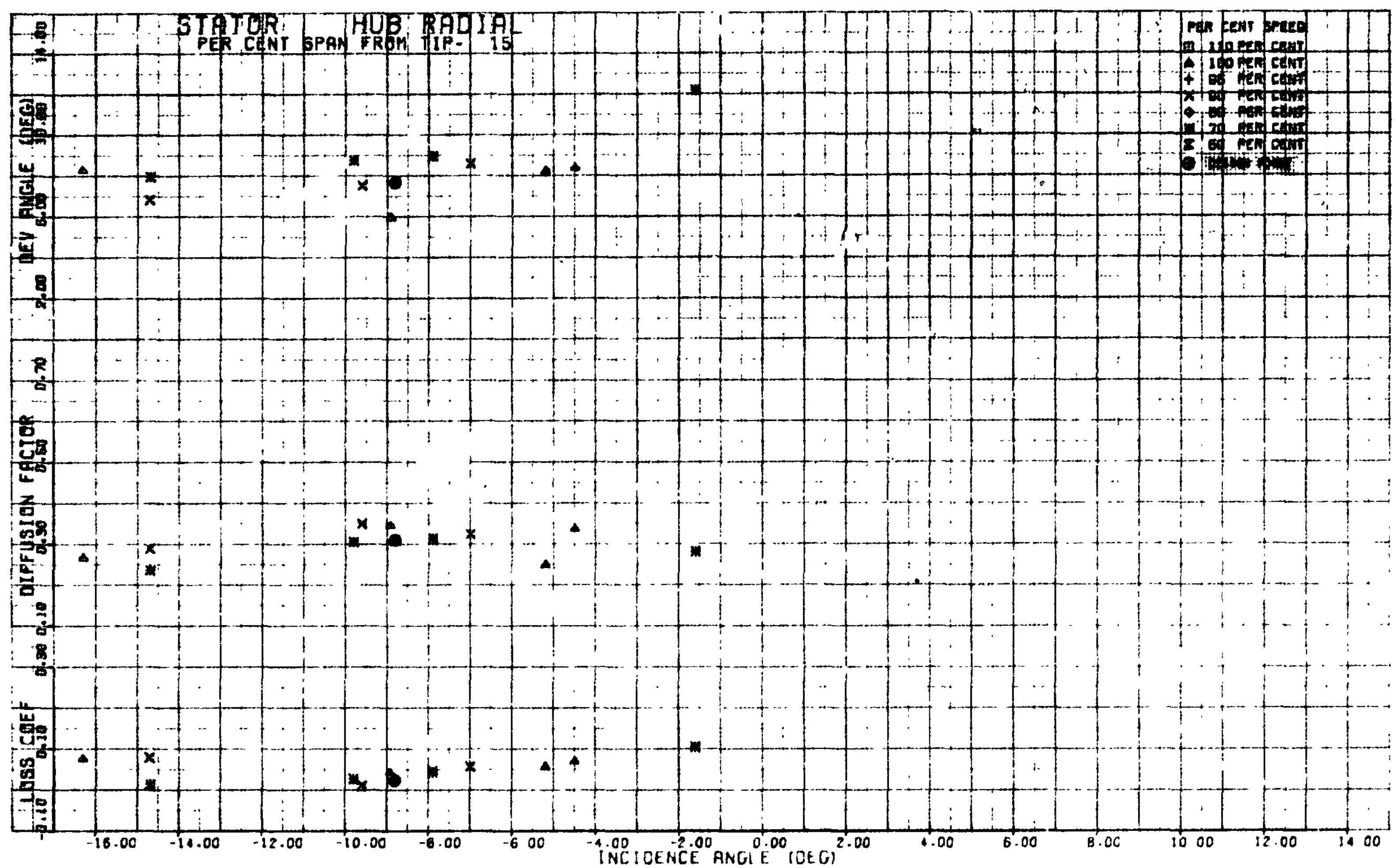

Figure 50c.--Stator Vane Element Performance, Hub-Radially Distorted Inlet Flow, 15 Percent Span from Tip.

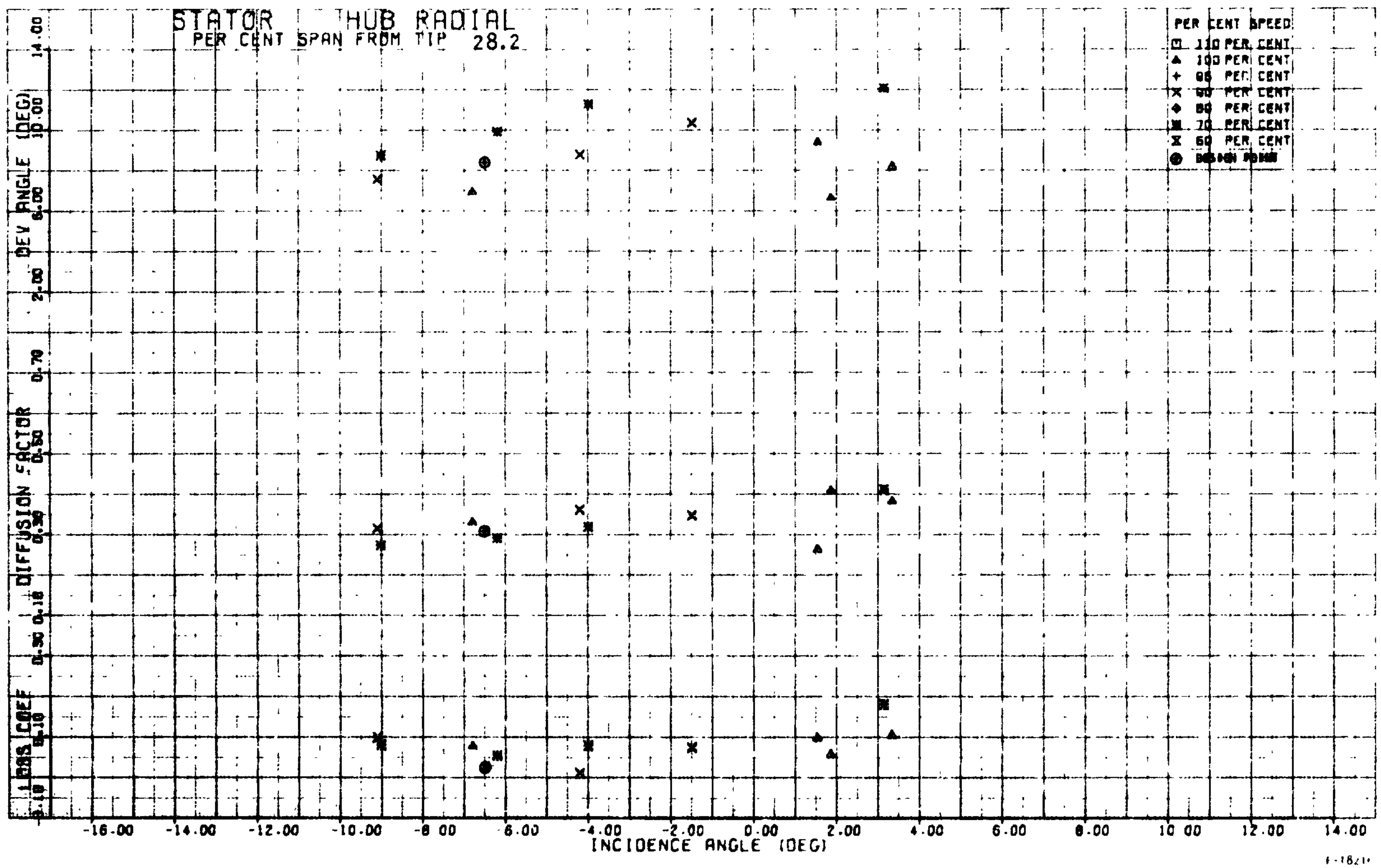

Figure 50d.--Stator Vane Element Performance, Hub-Radially Distorted Inlet Flow, 28.2 Percent Span from Tip.

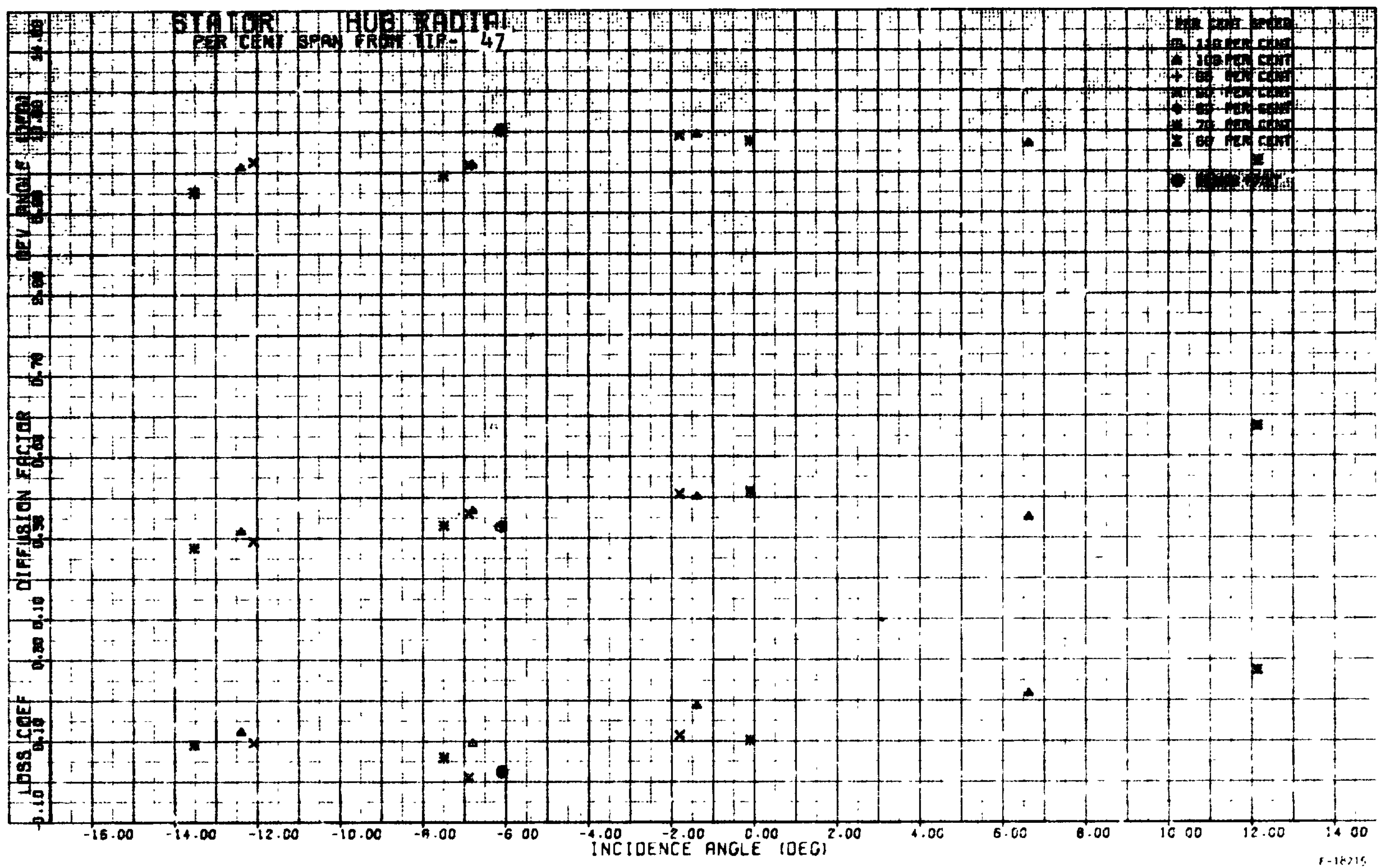

Figure 50e.--Stator Vane Element Performance, Hub-Radially Distorted Inlet Flow, 47 Percent Span from Tip.

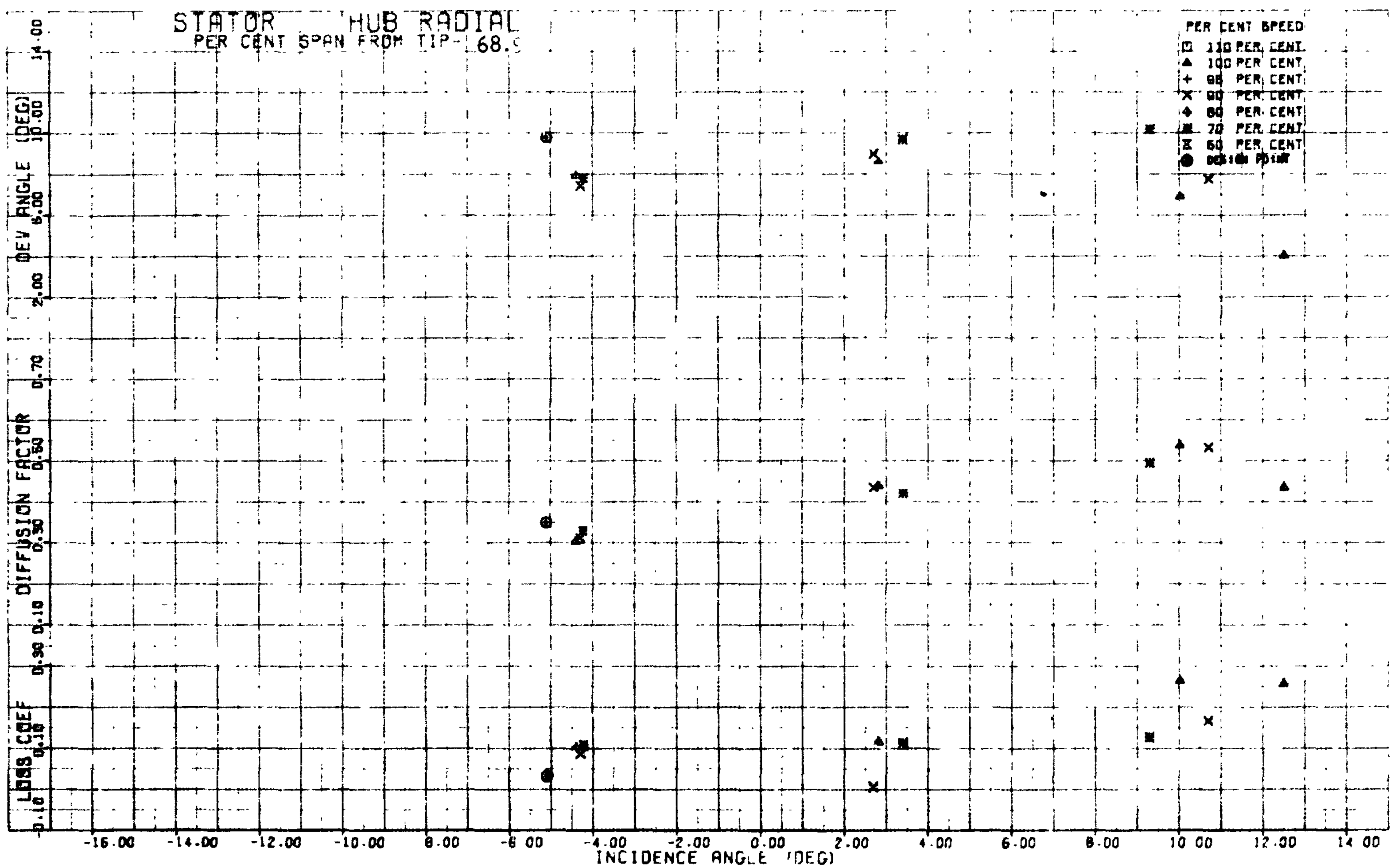

Figure 50f.--Stator Vane Element Performance, Hub-Radially Distorted Inlet Flow, 68.9 Percent Span from Tip.

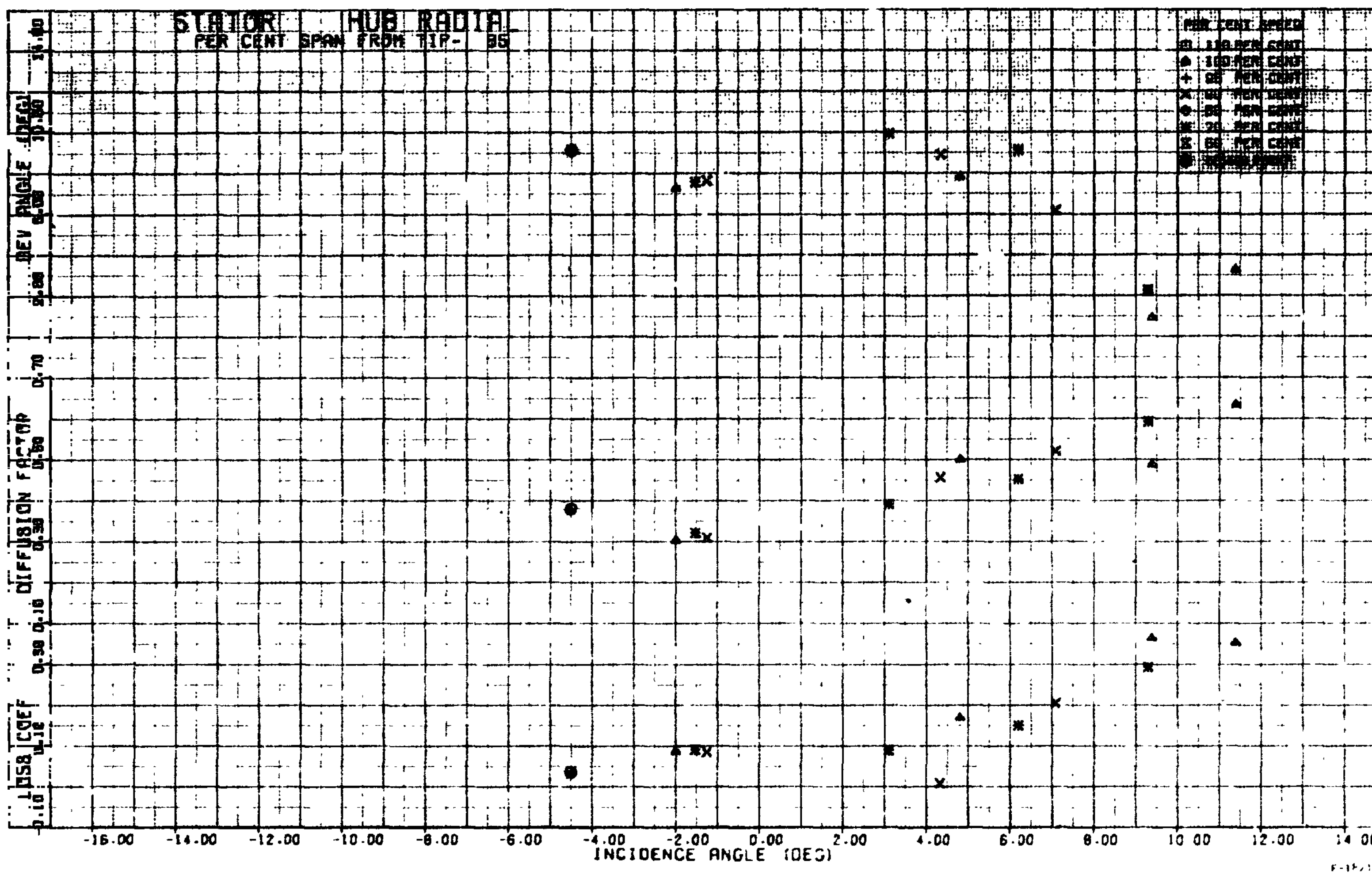

Figure 50g.--Stator Vane Element Performance, Hub-Radially Distorted Inlet Flow, 85 Percent Span from Tip.

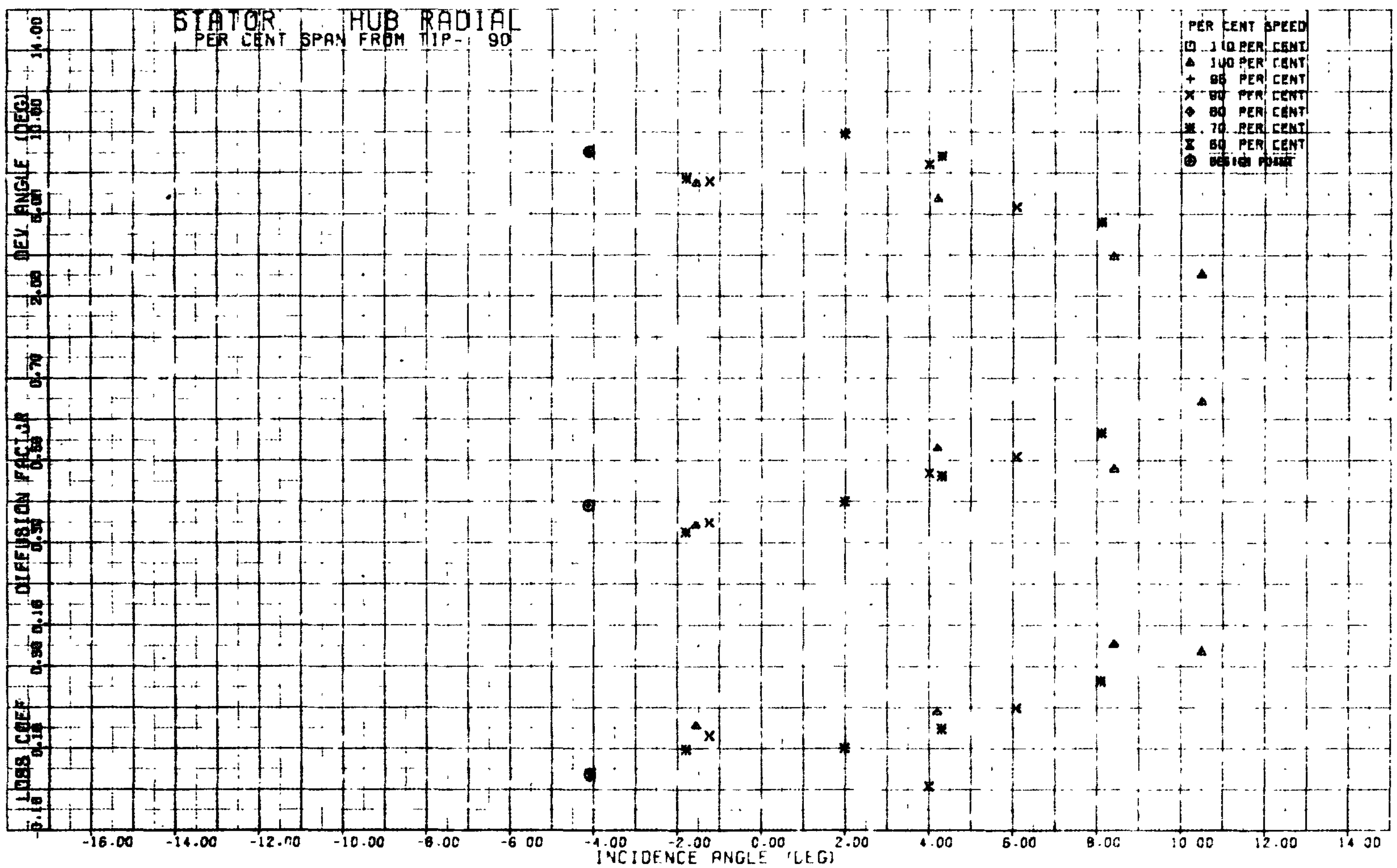

Figure 50h.--Stator Vane Element Performance, Hub-Radially Distorted Inlet Flow, 90 Percent Span from Tip.

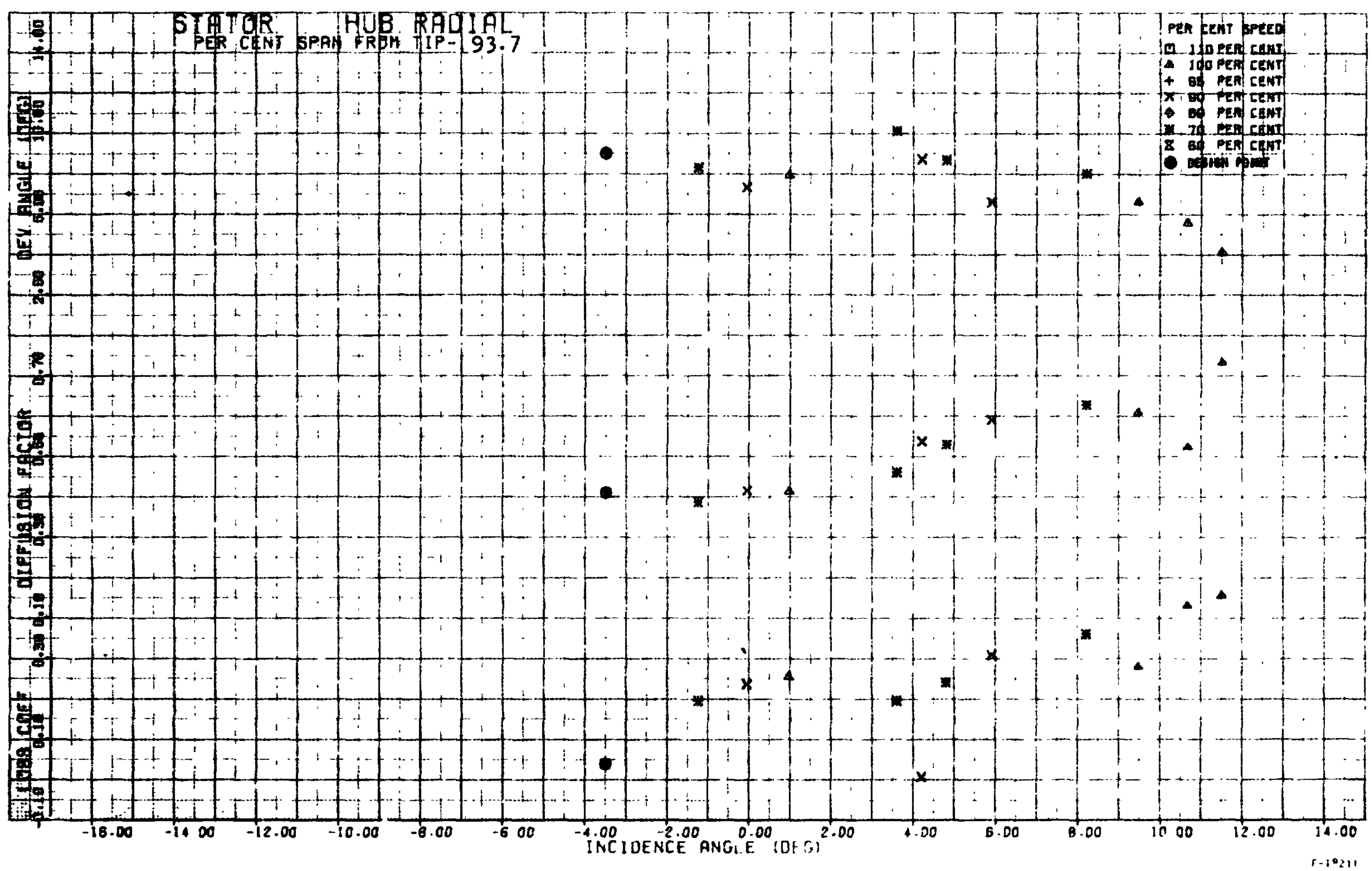

Figure 50i.--St tor Vane Element Performance, Hub-Radially Distorted Inlet Flow, 93.7 Percent Span from Tip.

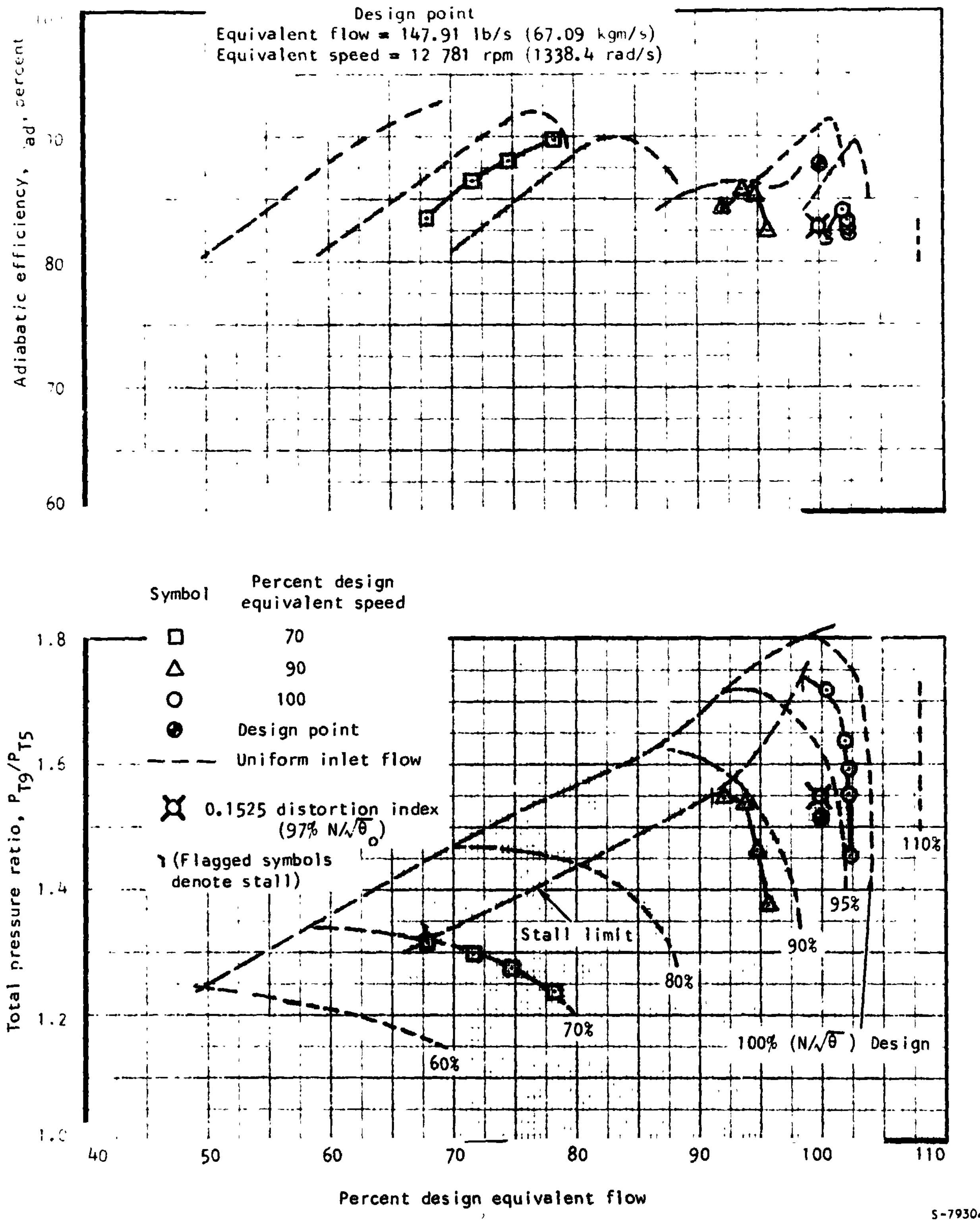

Figure 51.--Rotor Performance, Tip-Radial Distortion.

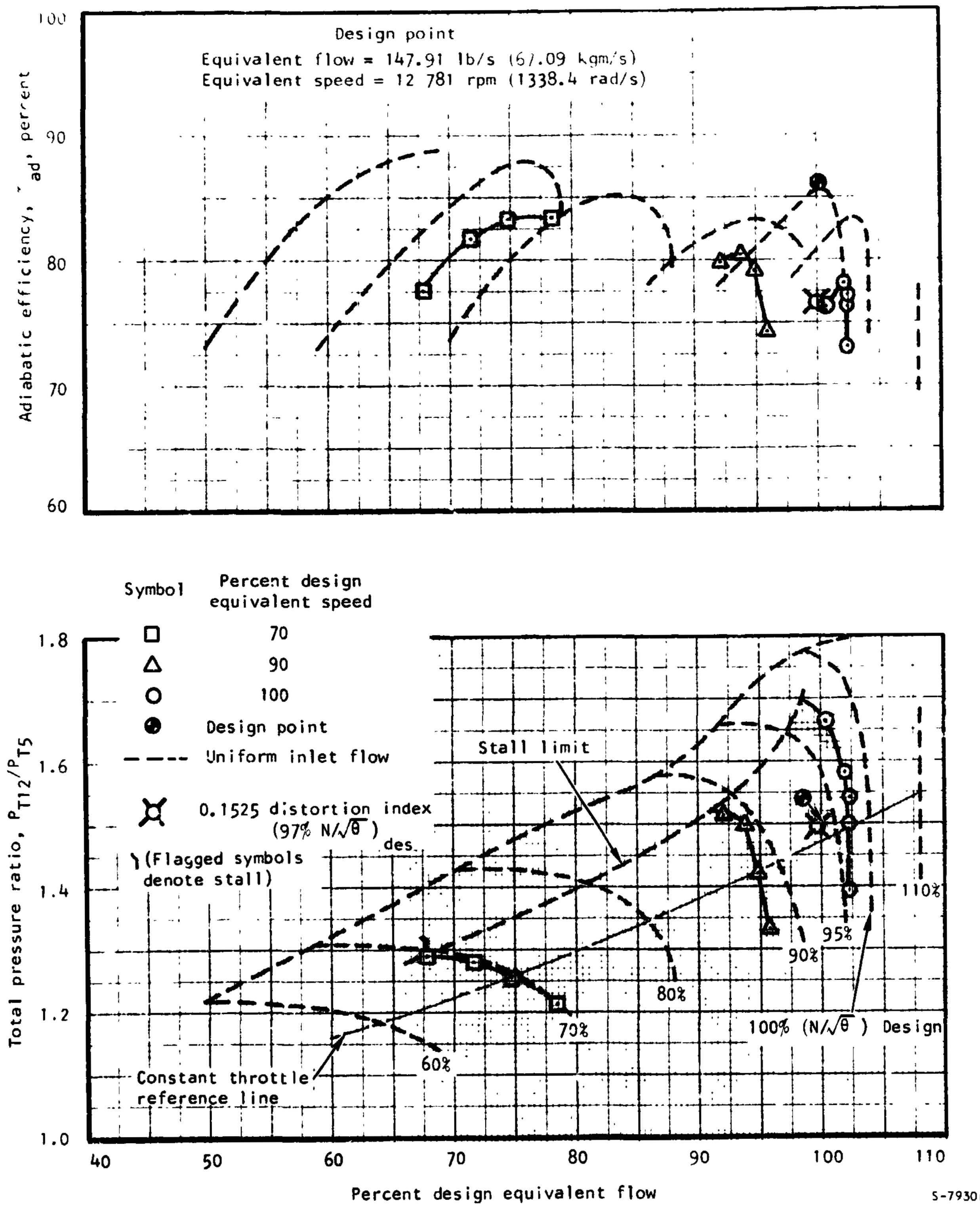

Figure 52.--Stage Performance, Tip-Radial Distortion.

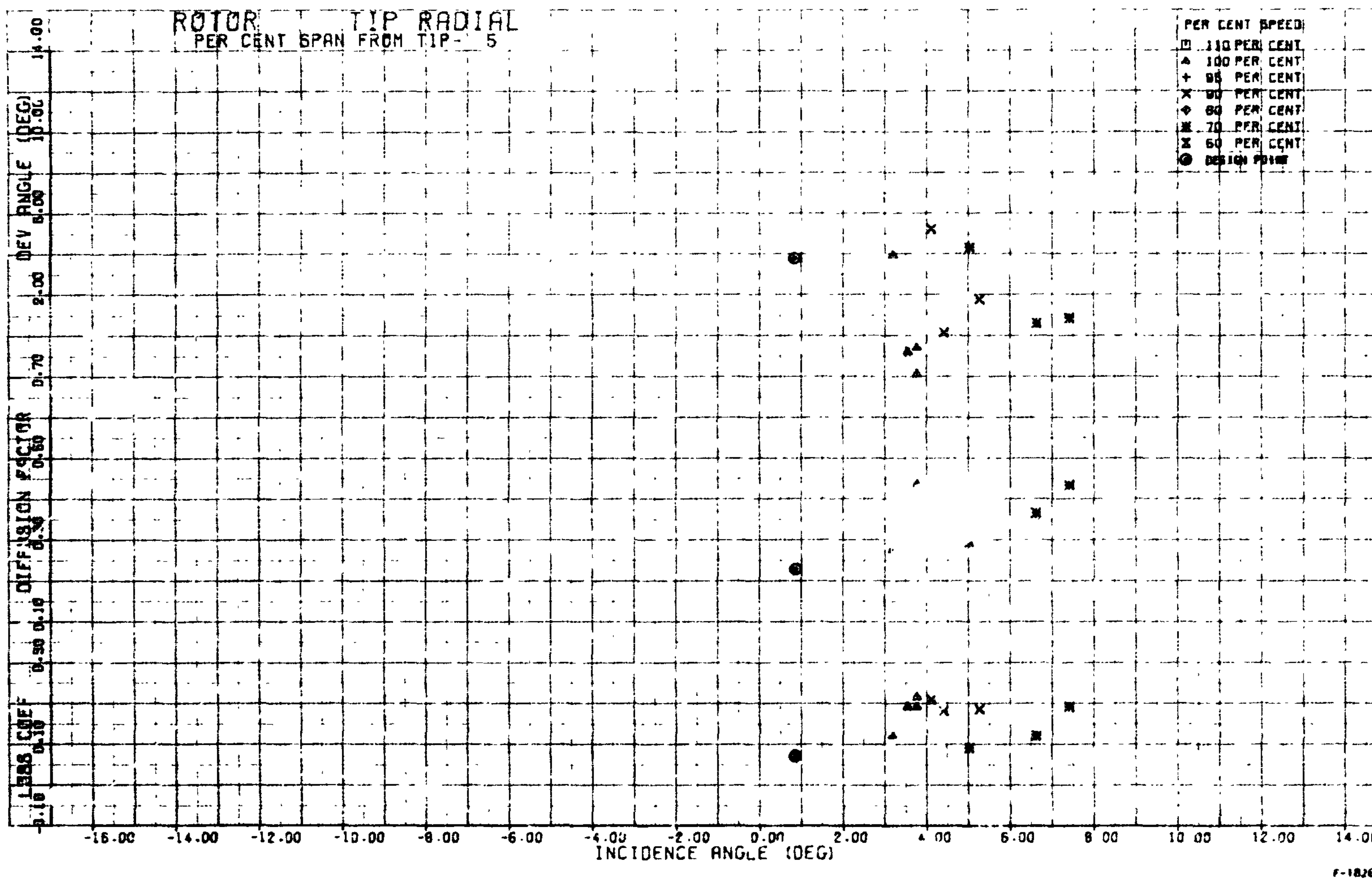

Figure 53a.--Rotor Blade Element Performance, Tip-Radially Distorted Inlet Flow, 5 Percent Span from Tip.

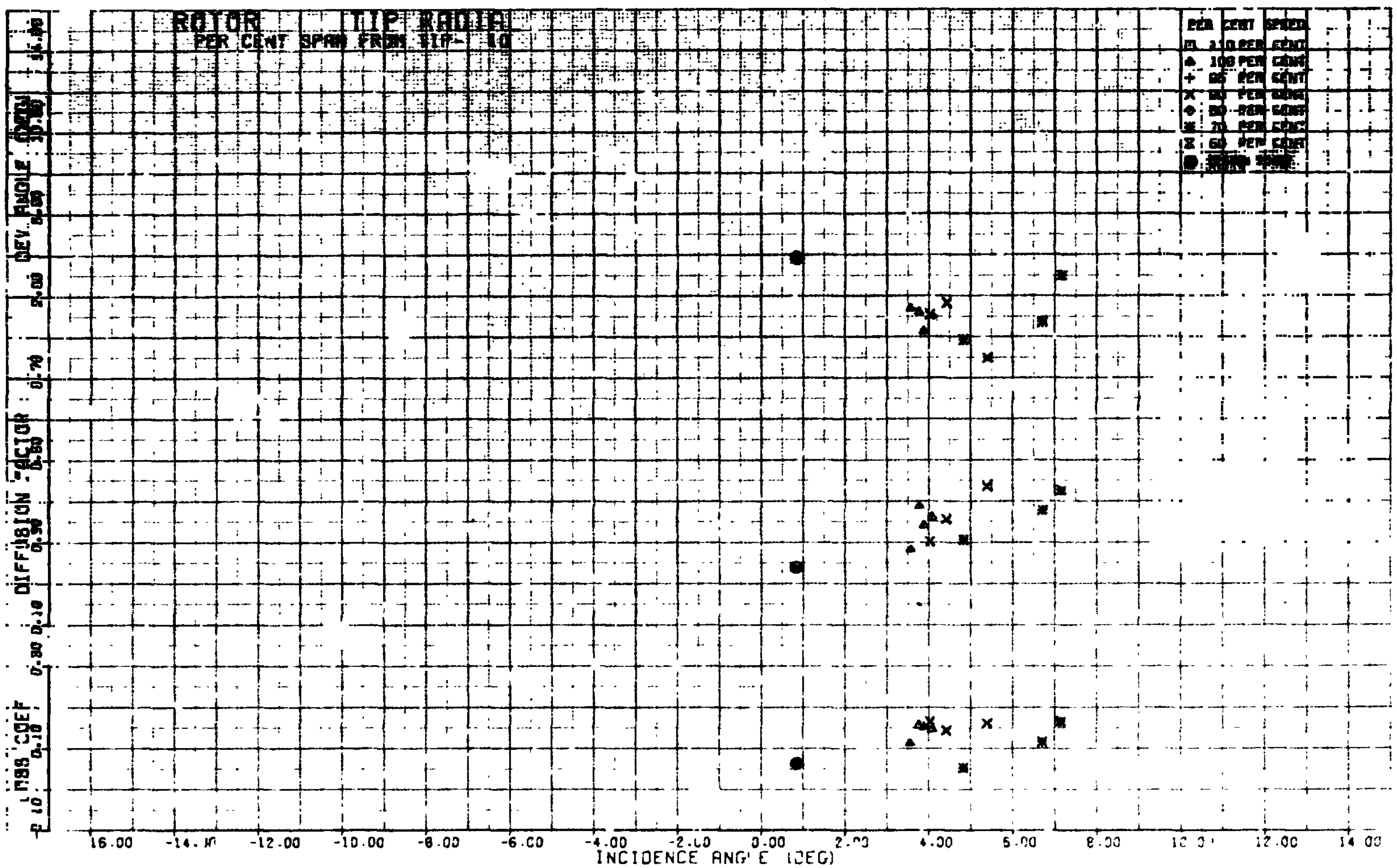

Figure 53b.--Rotor Blade Element Performance, Tip-Radially Distorted Inlet Flow, 10 Percent Span from Tip.

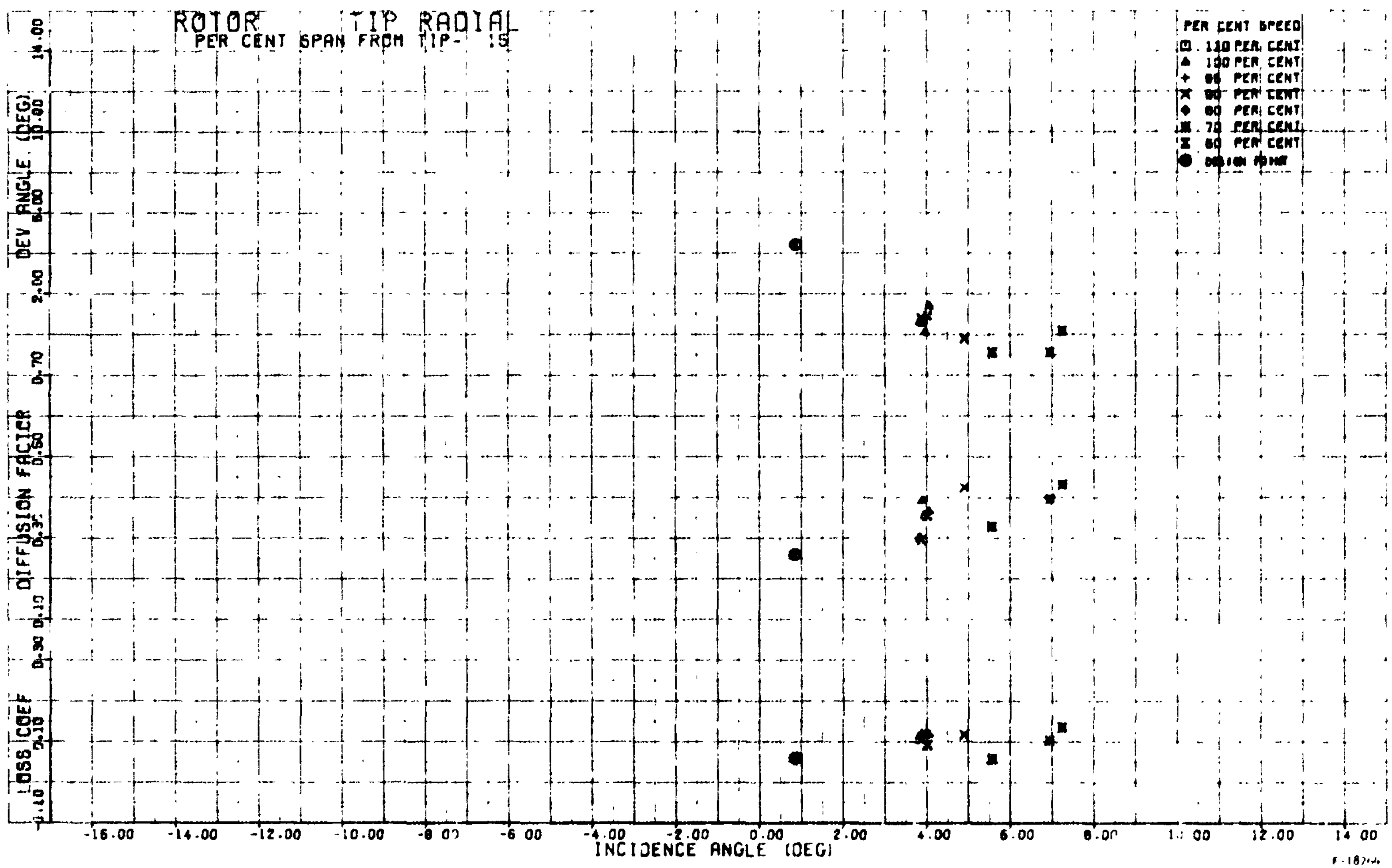

Figure 53c.--Rotor Blade Element Performance, Tip-Radially Distorted Inlet Flow, 15 Percent Span from Tip.

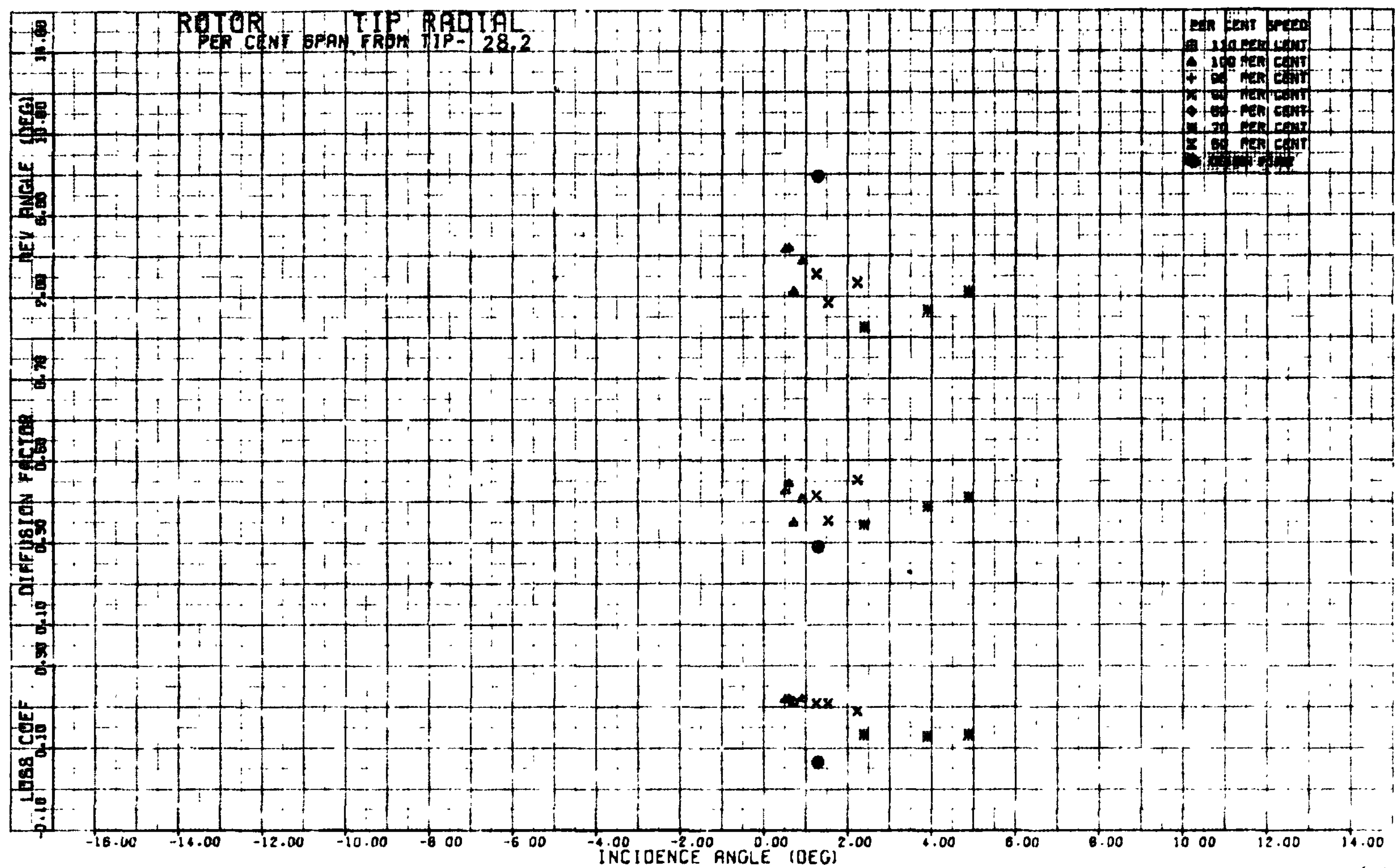

Figure 53d.--Rotor Blade Element Performance, Tip-Radially Distorted Inlet Flow, 28.2 Percent Span from Tip.

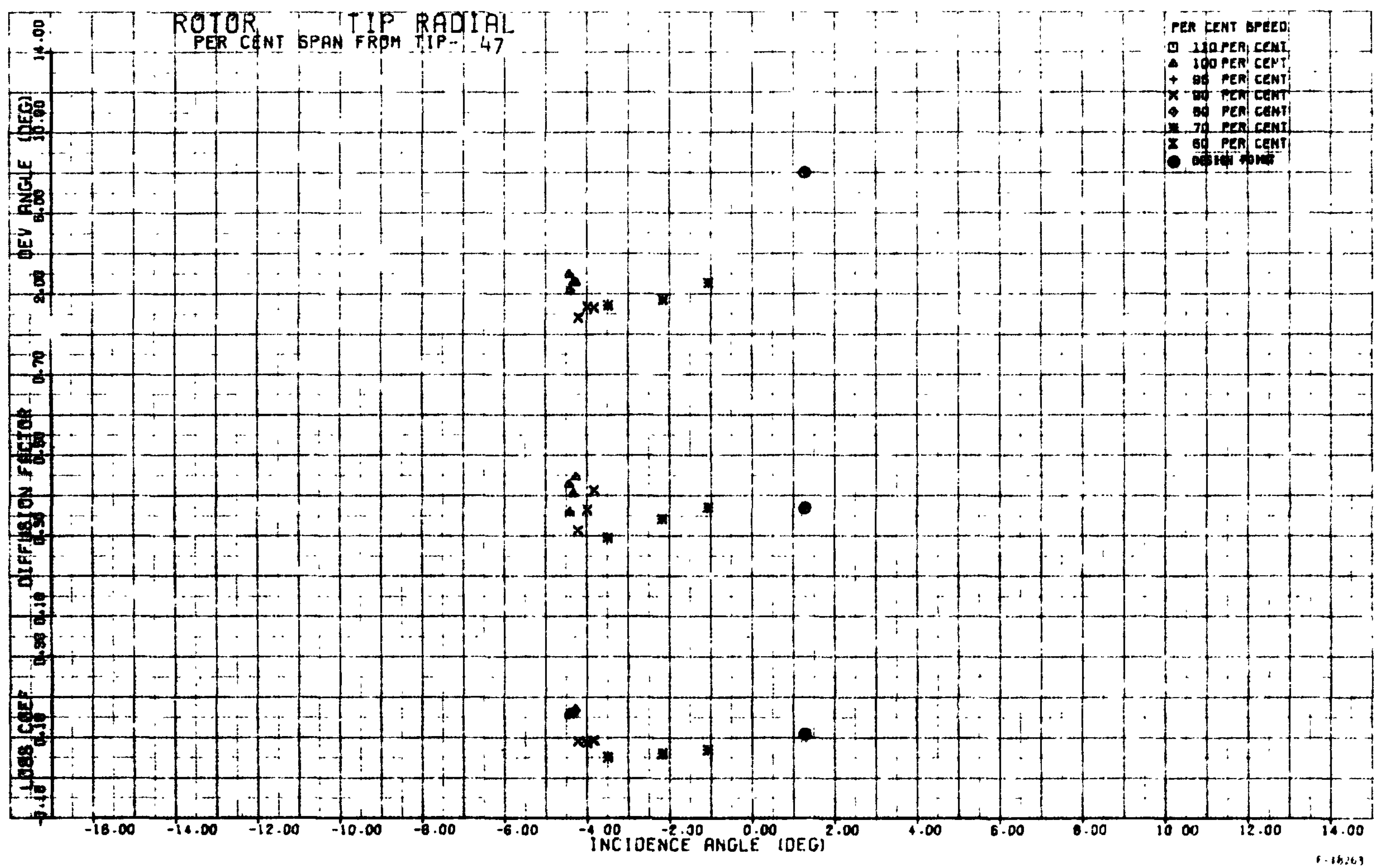

Figure 53e.--Rotor Blade Element Performance, Tip-Radially Distorted Inlet Flow, 47 Percent Span from Tip.

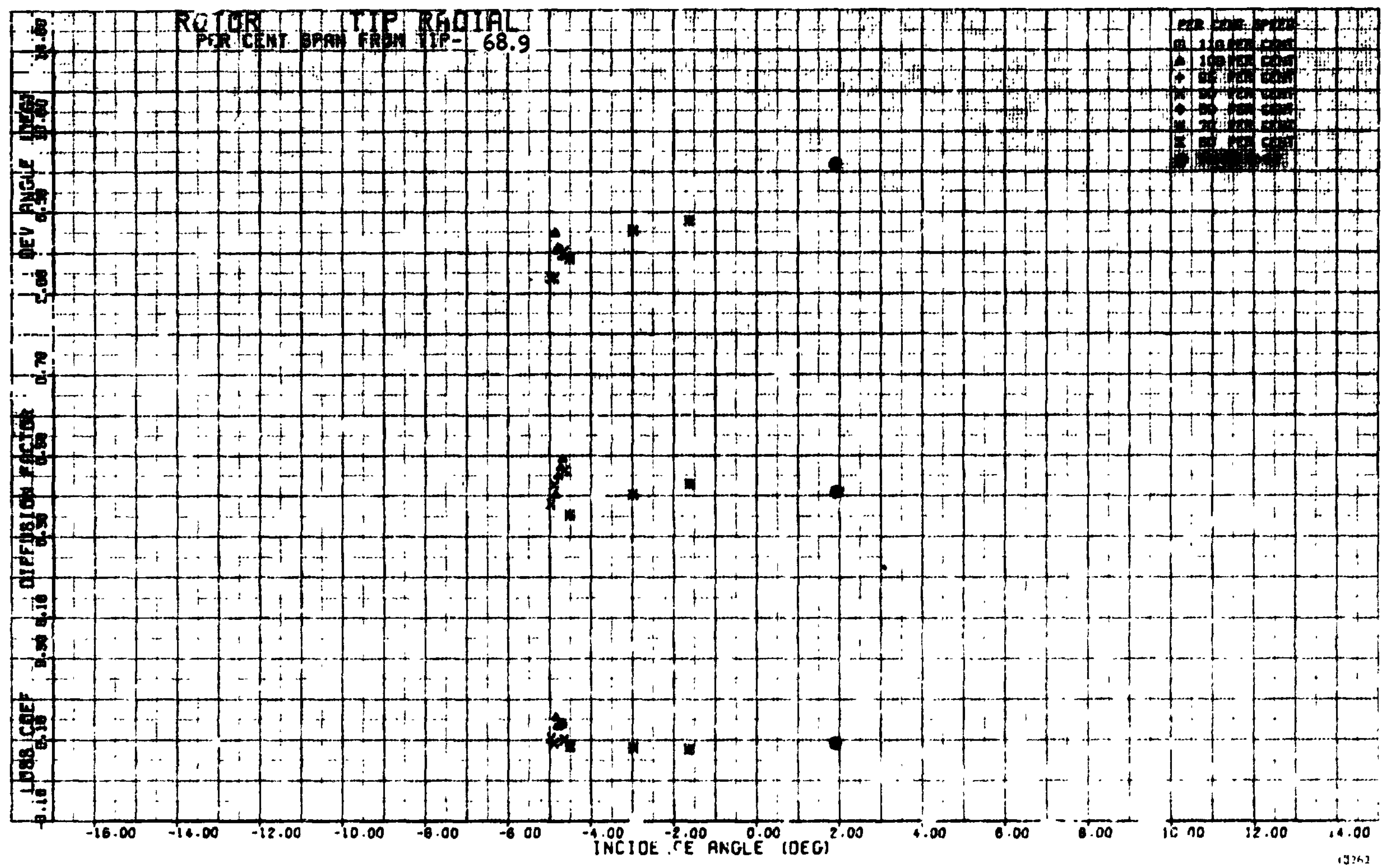

Figure 53f.--Rotor Blade Element Performance, Tip-Radially Distorted Inlet Flow, 68.9 Percent Span from Tip.

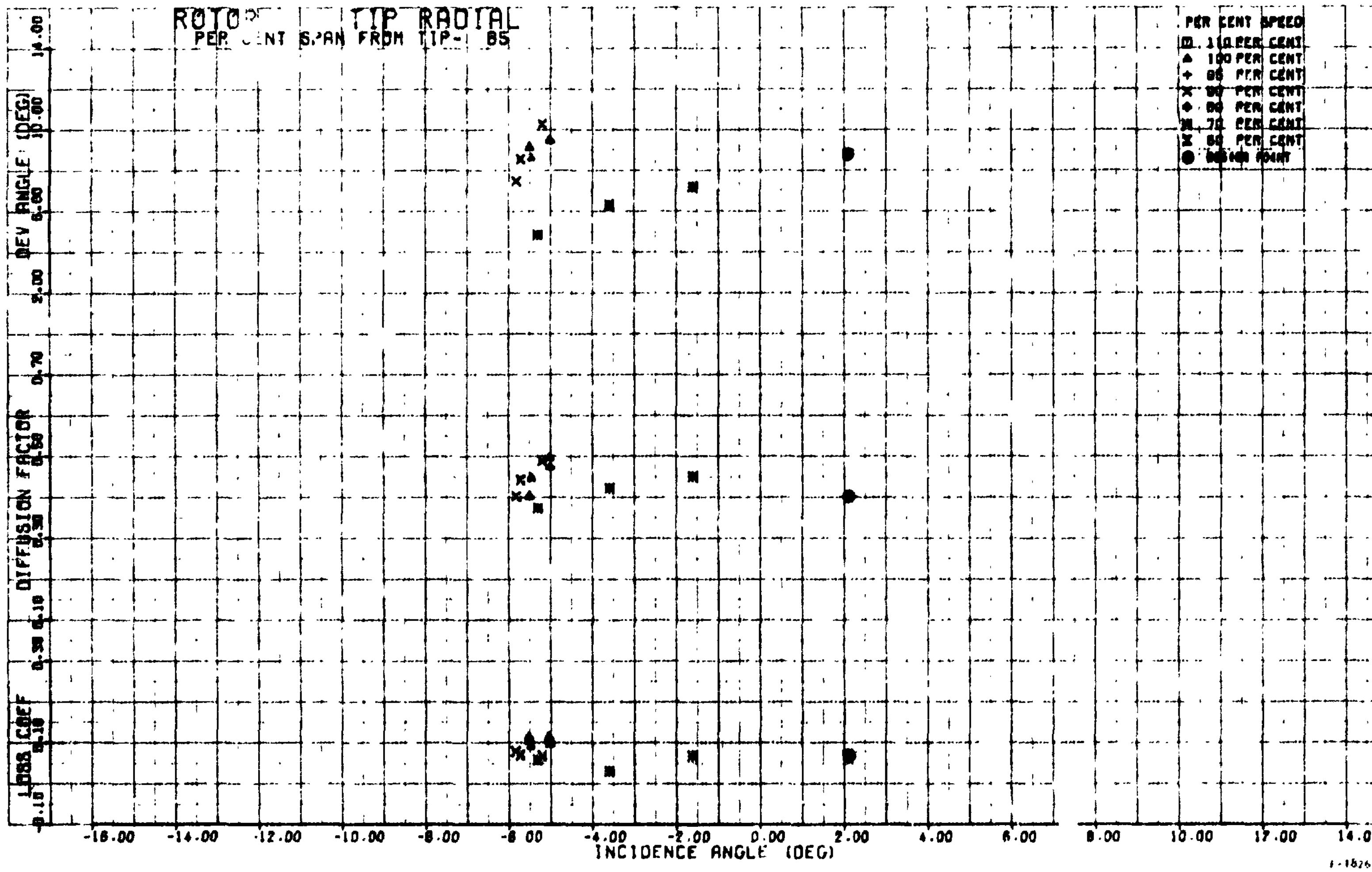

Figure 53g.--Rotor Blade Element Performance, Tip-Radially Distorted Inlet Flow, 85 Percent Span from Tip.

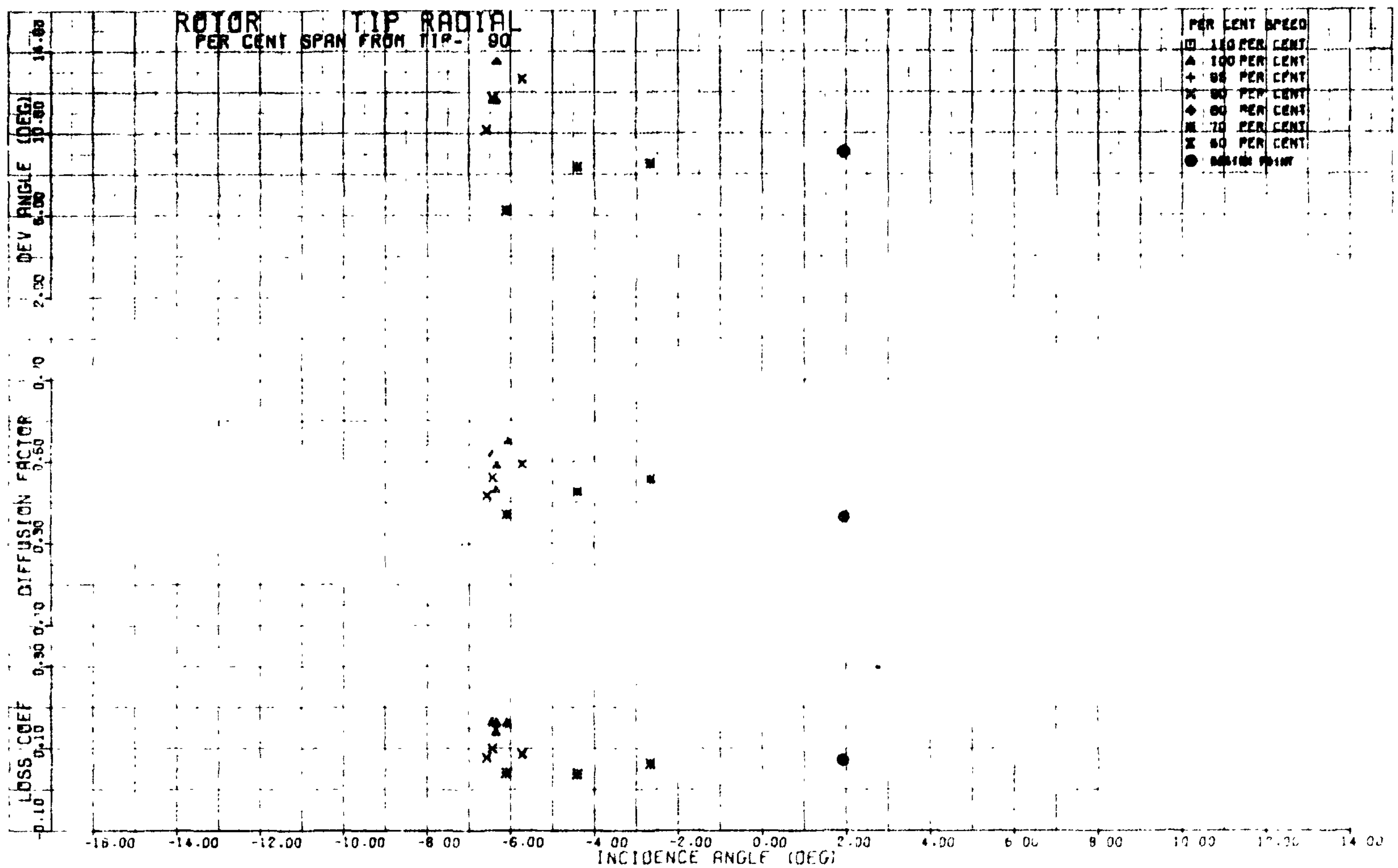

Figure 53h.--Rotor Blade Element Performance, Tip-Radially Distorted Inlet Flow, 90 Percent Span from Tip.

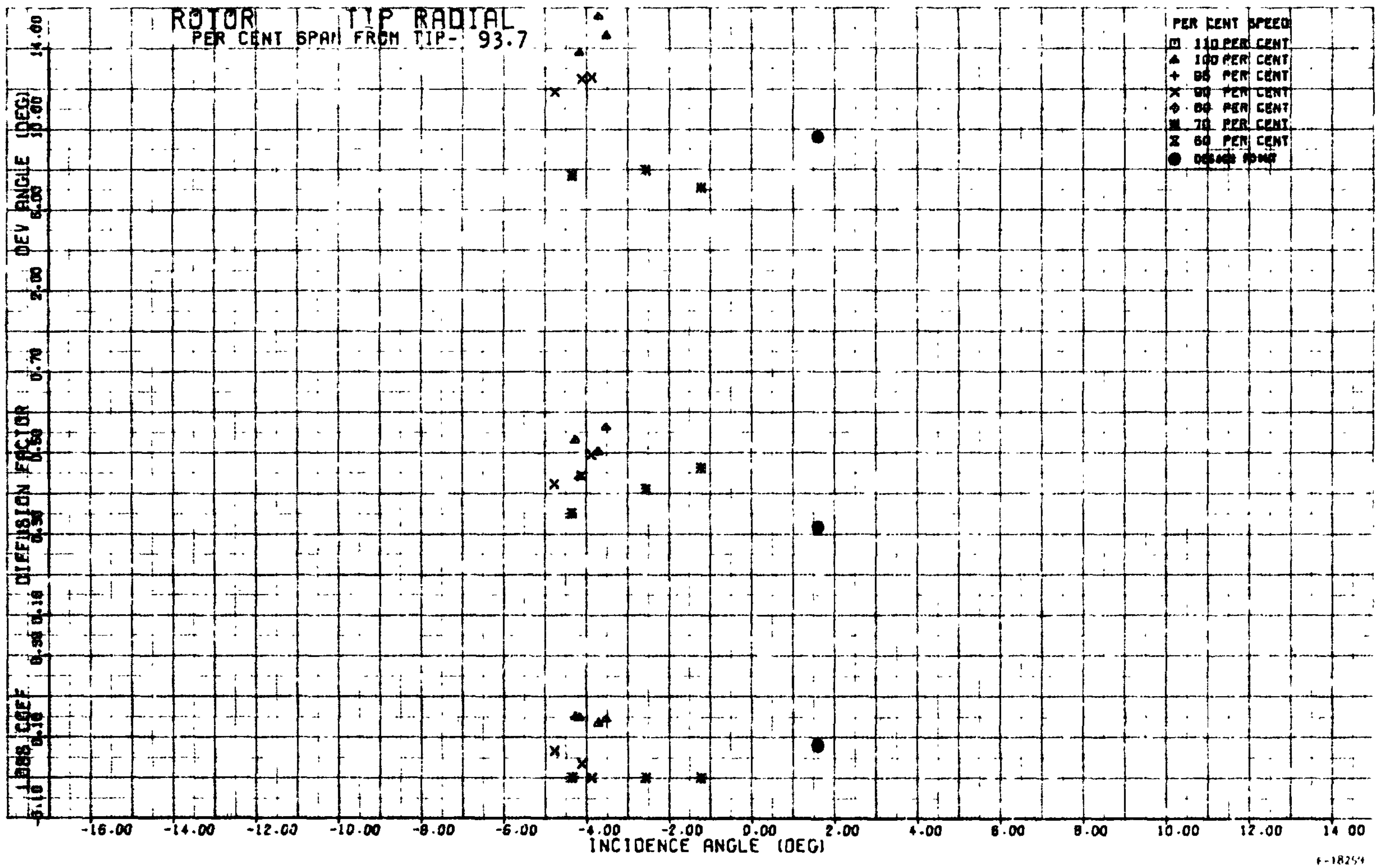

Figure 53i.--Rotor Blade Element Performance, Tip-Radially Distorted Inlet Flow, 93.7 Percent Span from Tip.

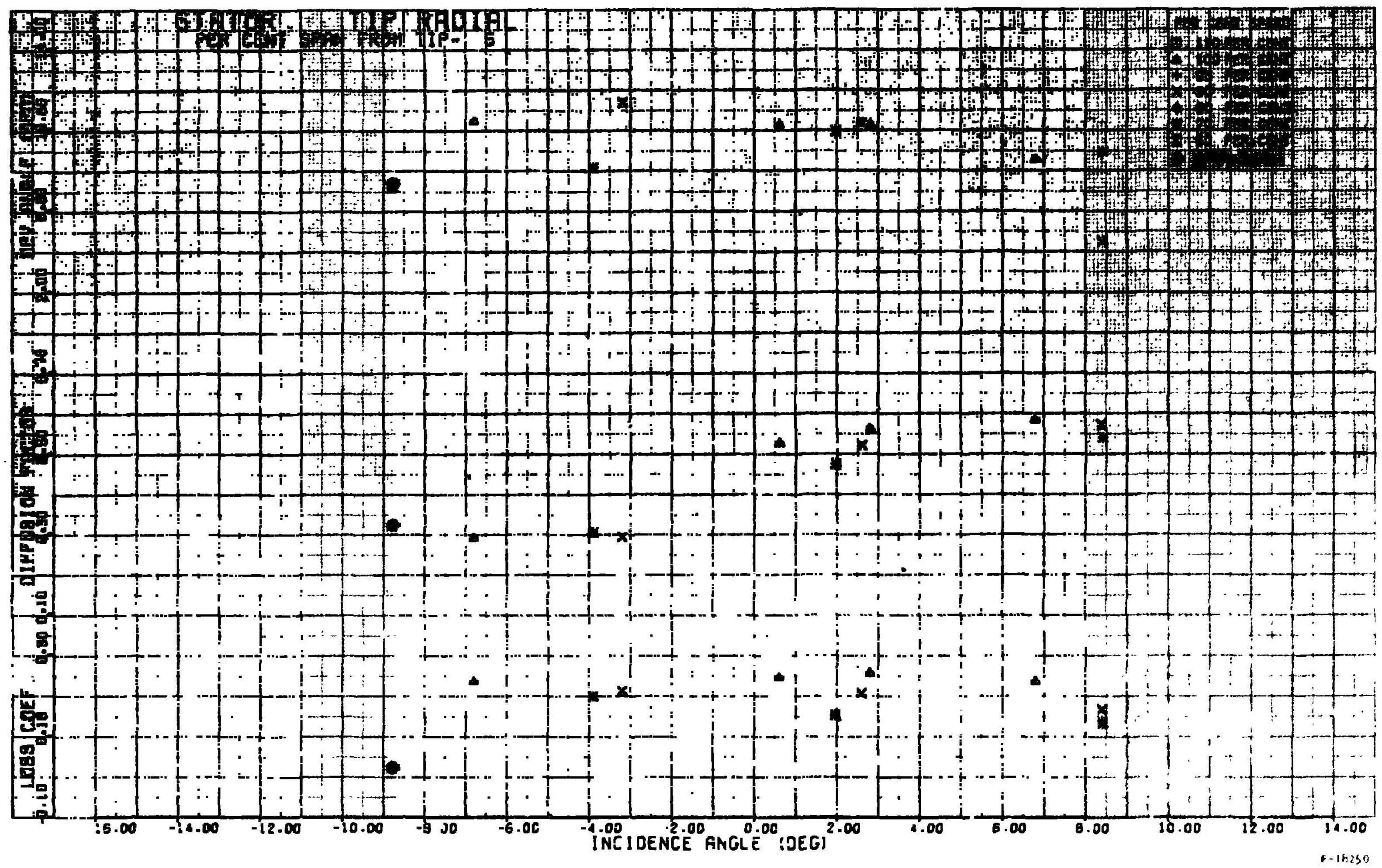

Figure 54a.--Stator Vane Element Performance, Tip-Radially Distorted Inlet Flow, 5 Percent Span from Tip.

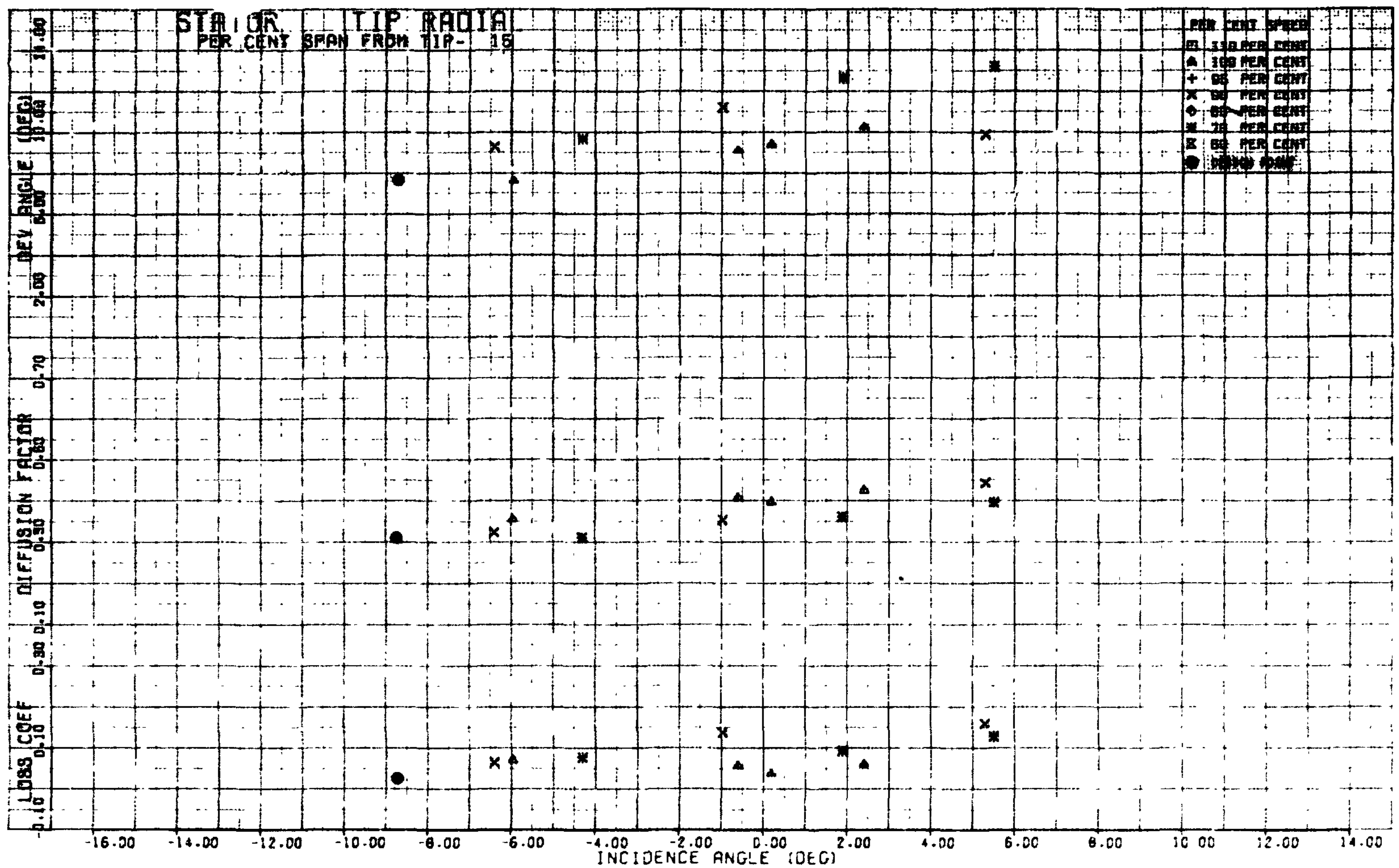

Figure 54b.--Stator Vane Element Performance, Tip-Radially Distorted Inlet Flow, 10 Percent Span from Tip.

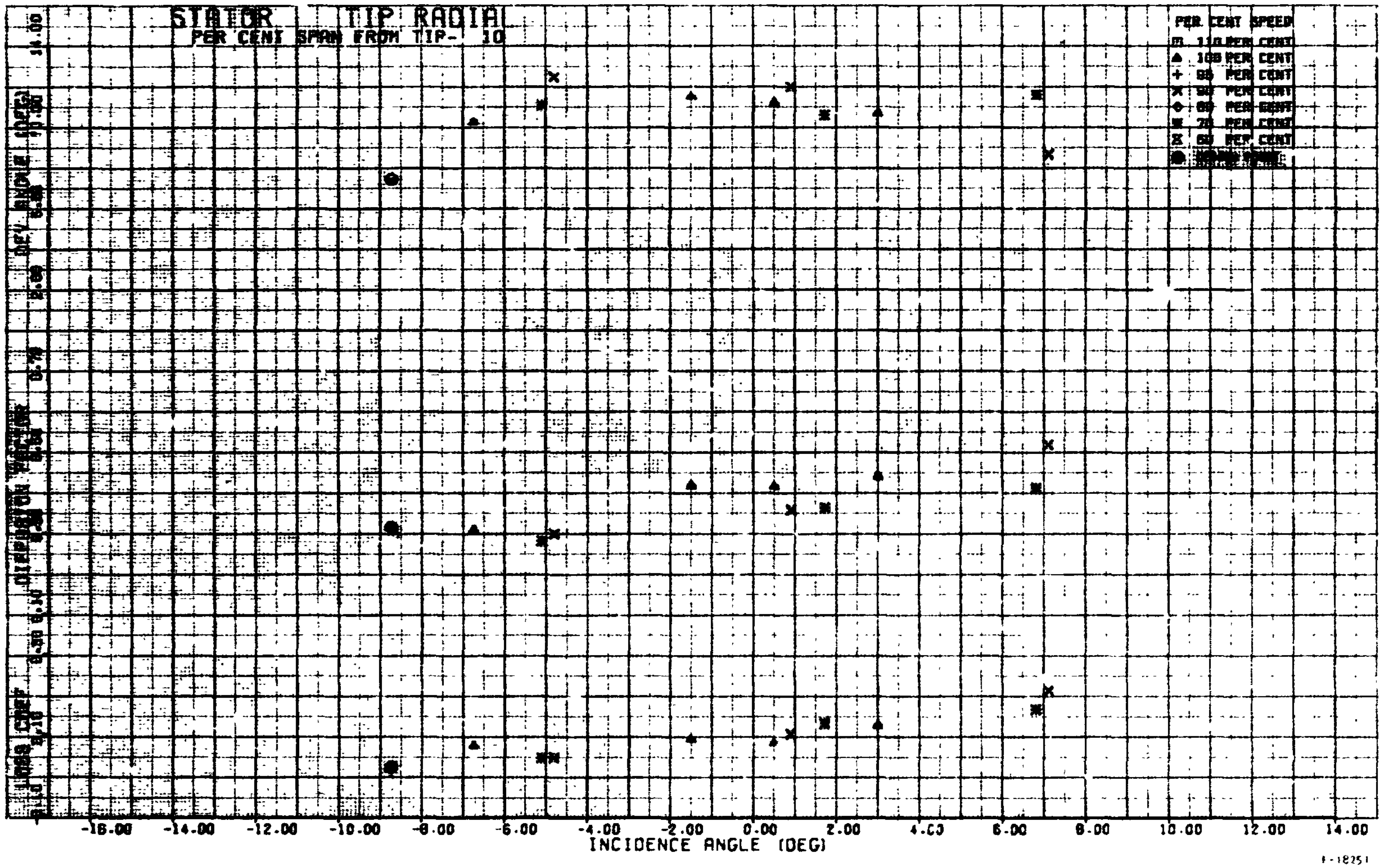

Figure 54c.--Stator Vane Element Performance, Tip-Radially Distorted Inlet Flow, 15 Percent Span from Tip.

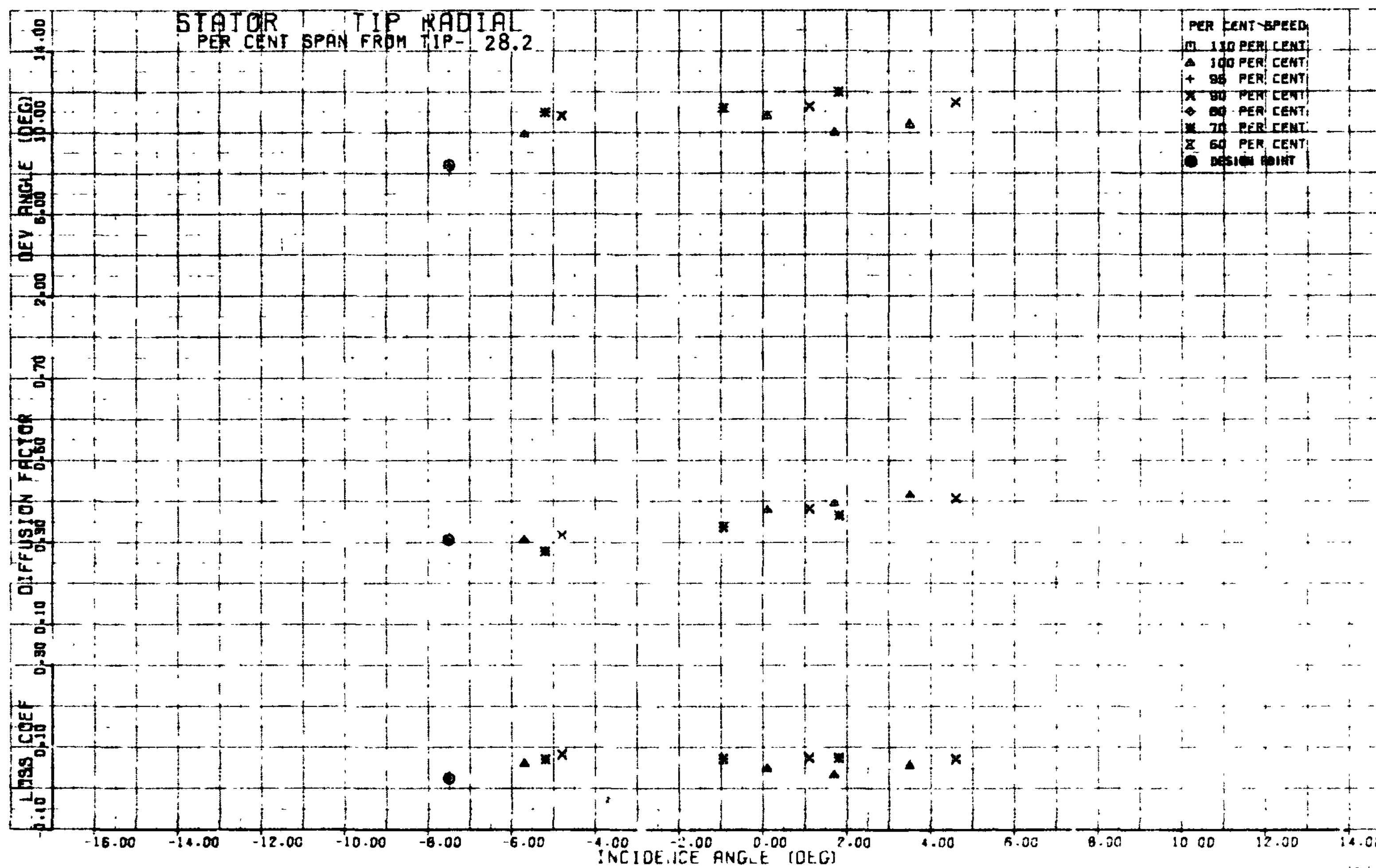

Figure 54d.--Stator Vane Element Performance, Tip-Radially Distorted Inlet Flow, 28.2 Percent Span from Tip.

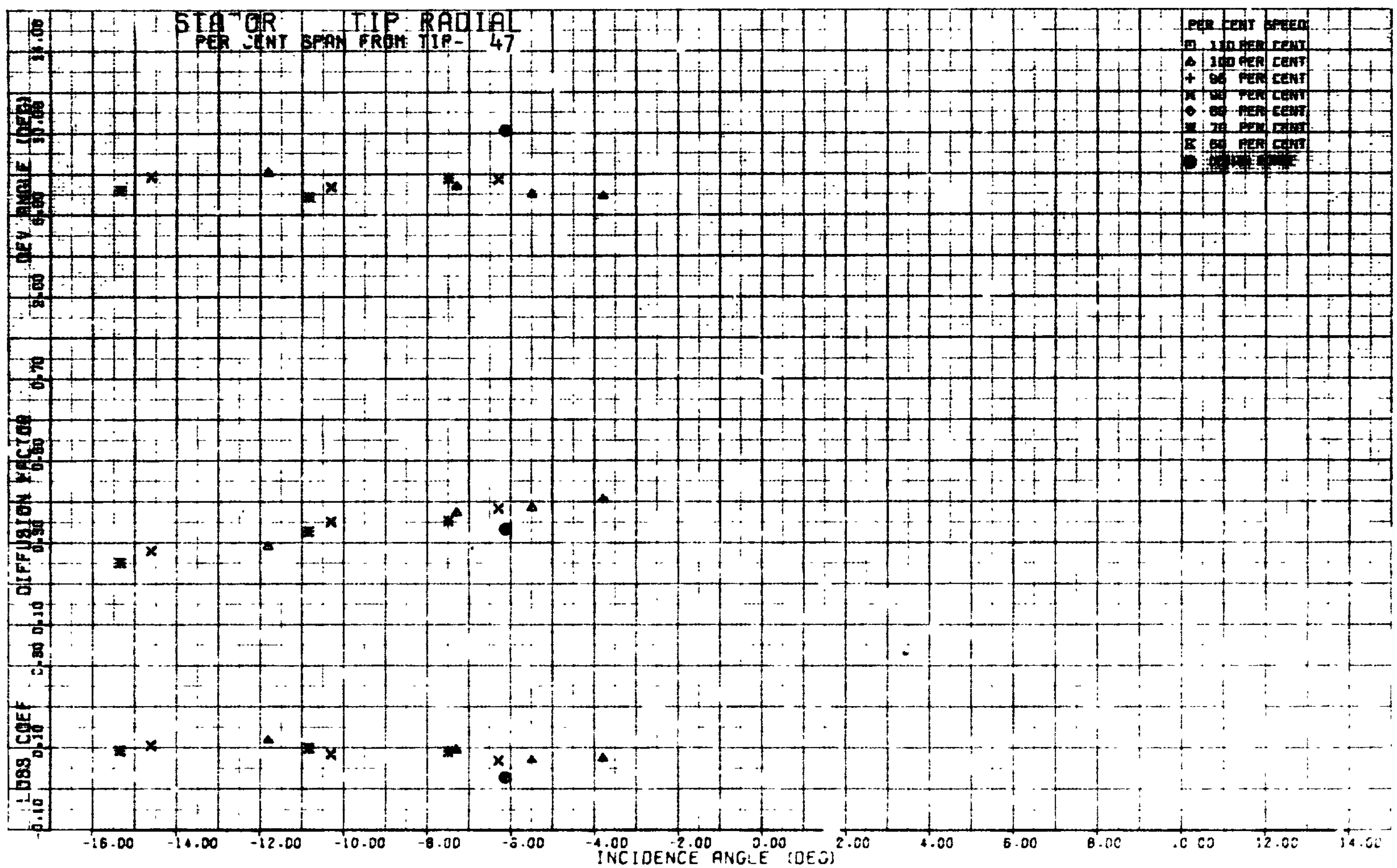

Figure 54e.--Stator Vane Element Performance, Tip-Radially Distorted Inlet Flow, 47 Percent Span from Tip.

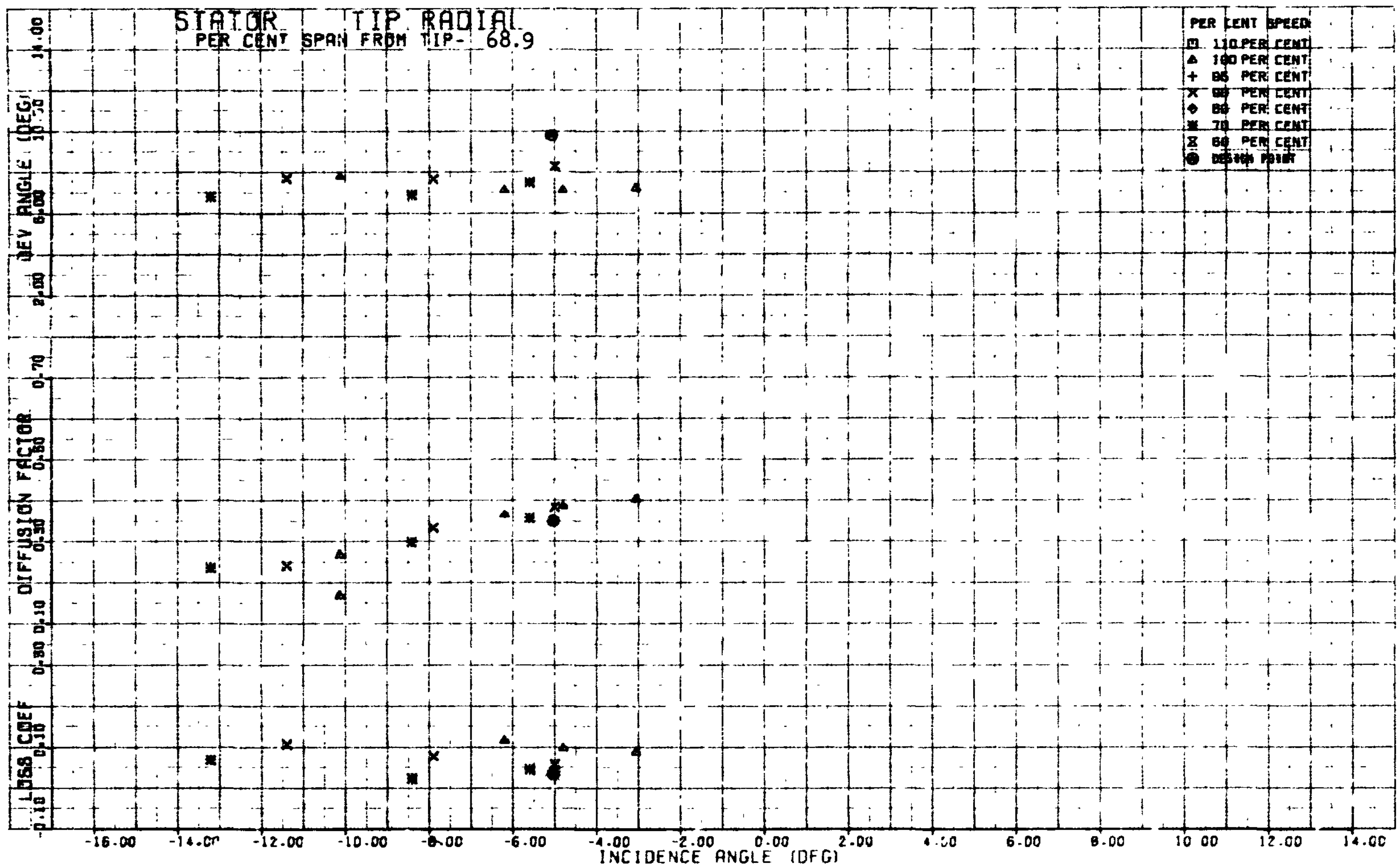

Figure 54f.--Stator Vane Element Performance, Tip-Radially Distorted Inlet Flow, 68.9 Percent Span from Tip.

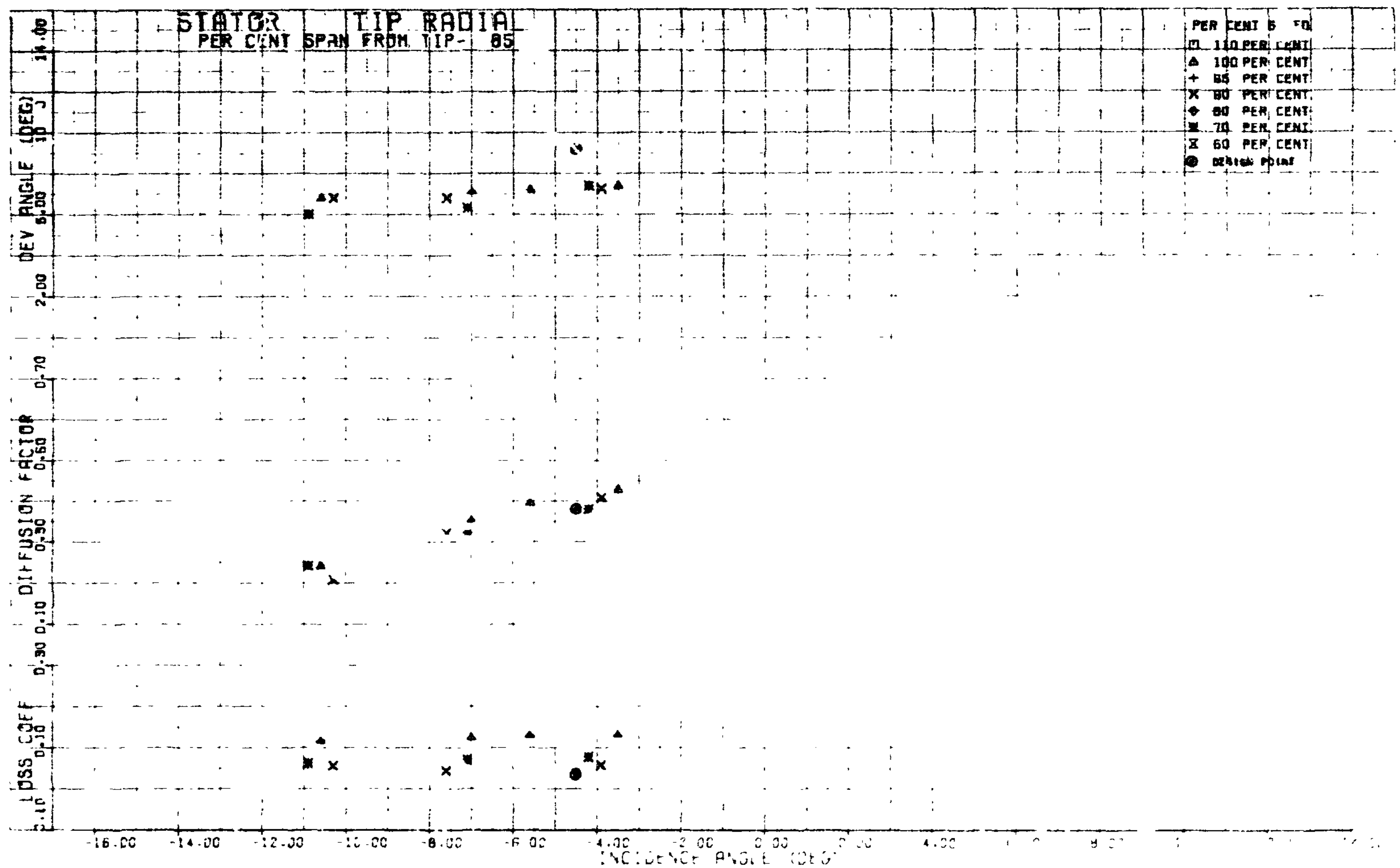

Figure 54g.--Stator Vane Element Performance, Tip-Radially Distorted Inlet Flow, 85 Percent Span from Tip.

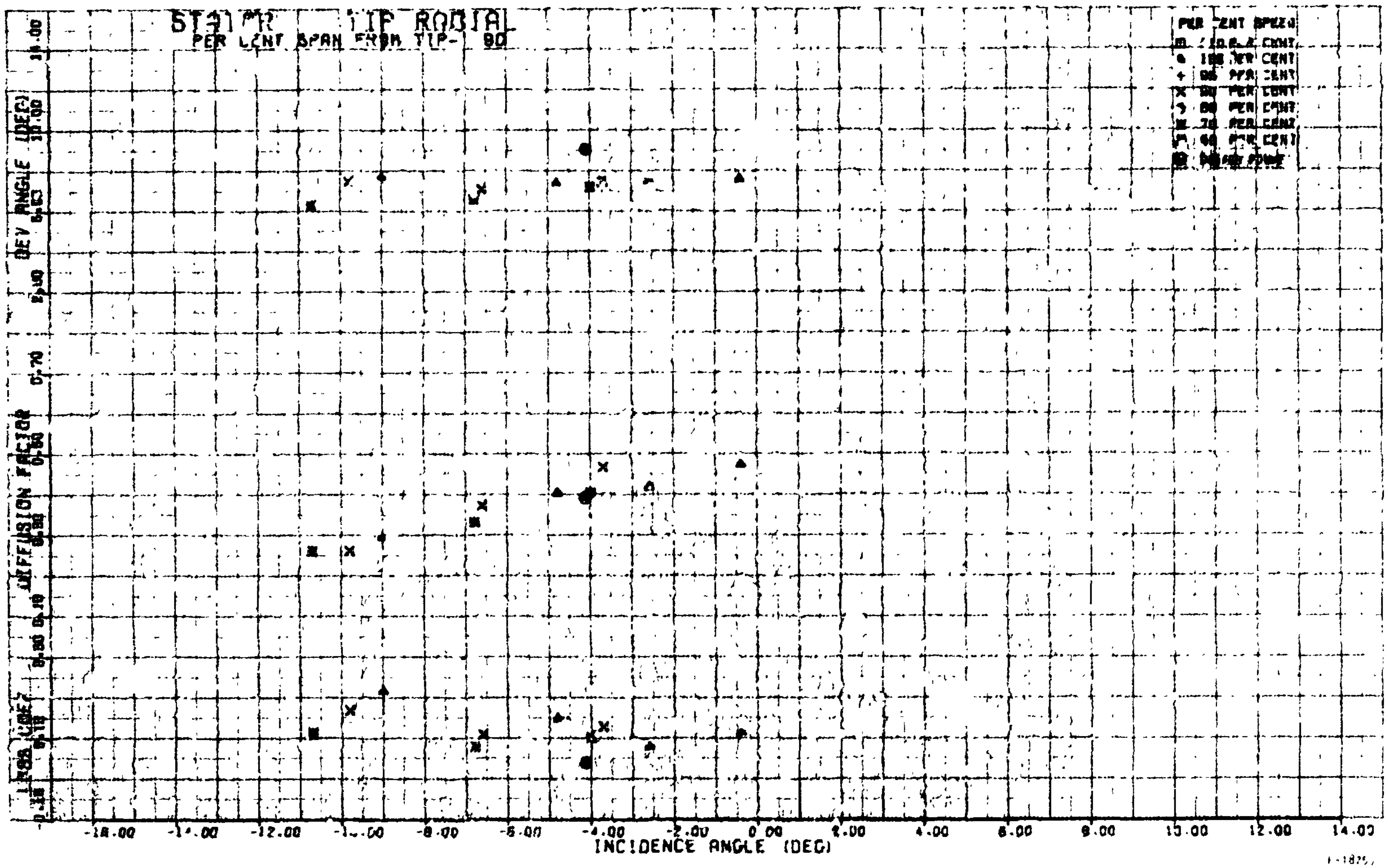

Figure 54h.--Stator Vane Element Perf>rmance, Tip-Radially Distorted Inlet Flow, 90 Percent Span from Tip.

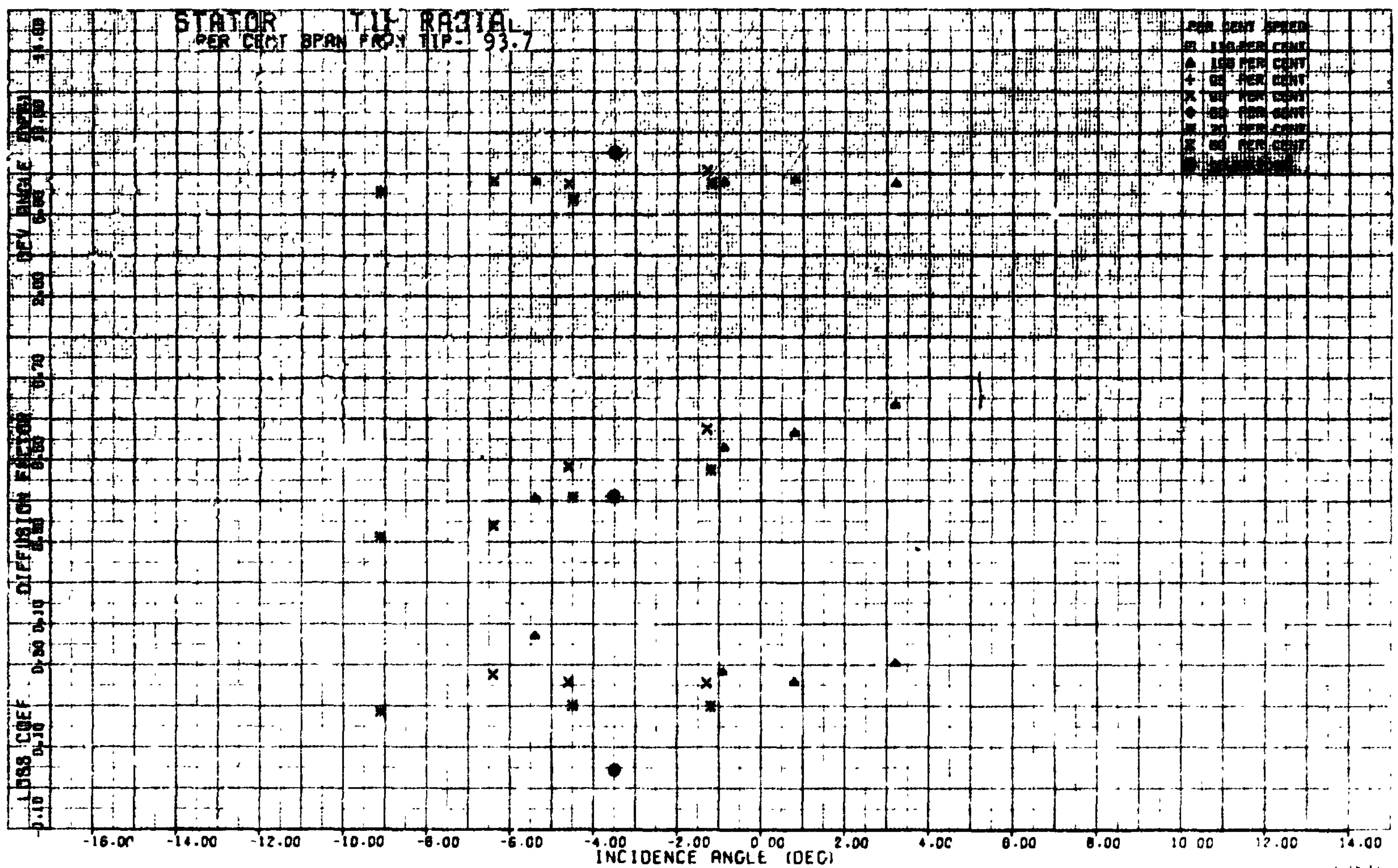

Figure 54i.--Stator Vane Element Performance, Tip-Radially Distorted Inlet Flow, 93.7 Percent Span from Tip.

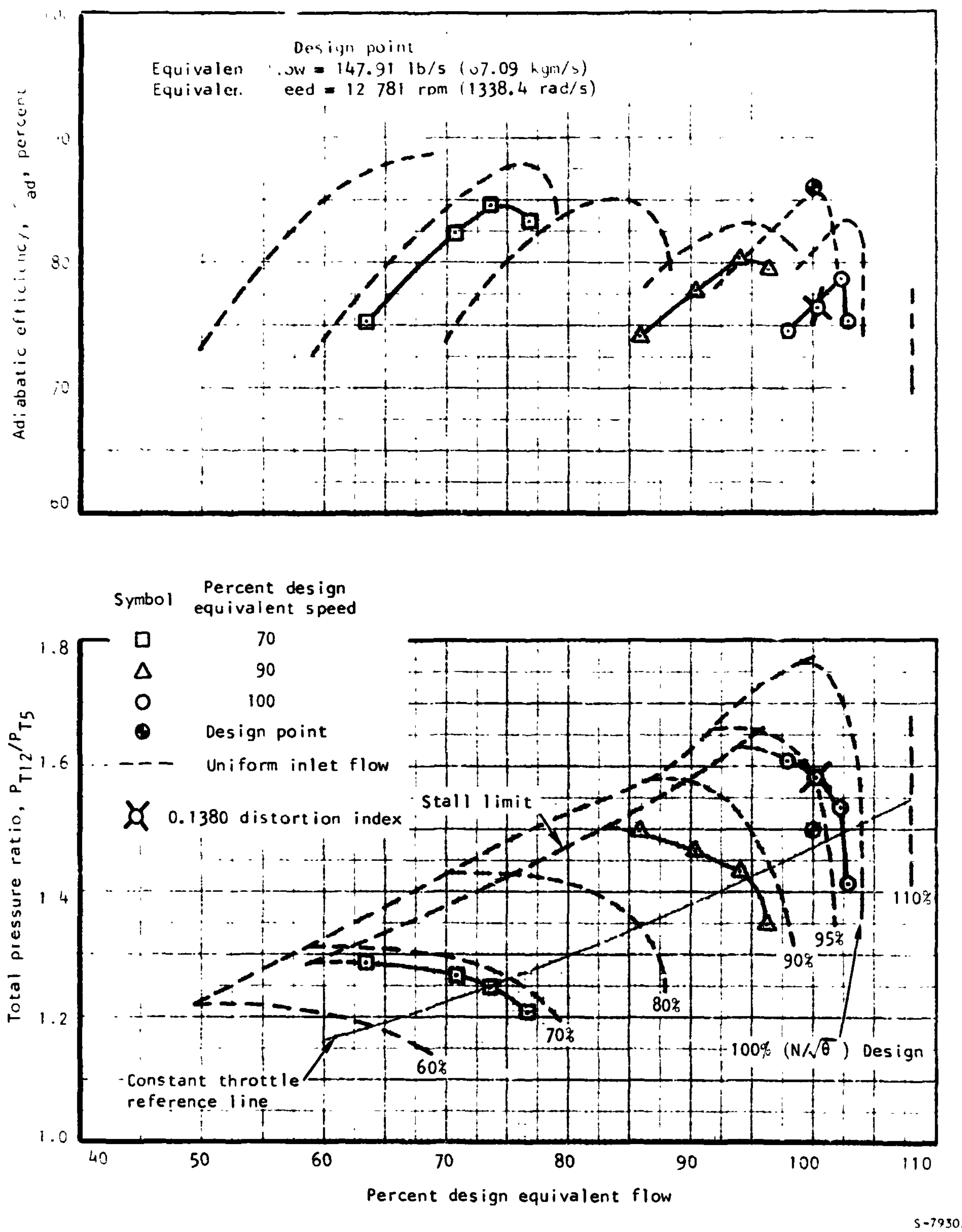

Figure 55.--Stage Performance, Circumferential Inlet Distortion.

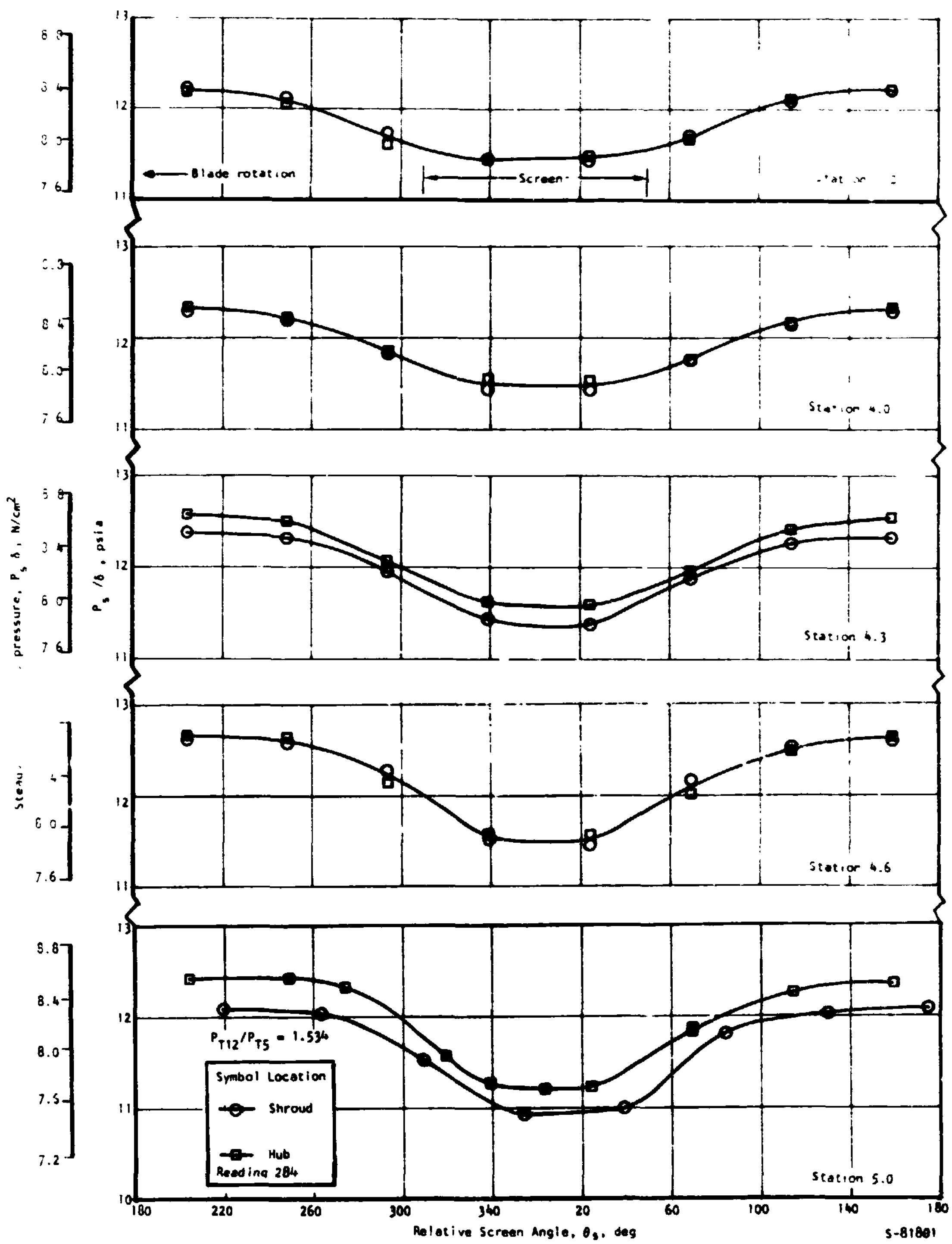

Figure 56.--Circumferential Distribution of Rotor Upstream Static Pressures at Design Speed with Circumferential Inlet Distortion.

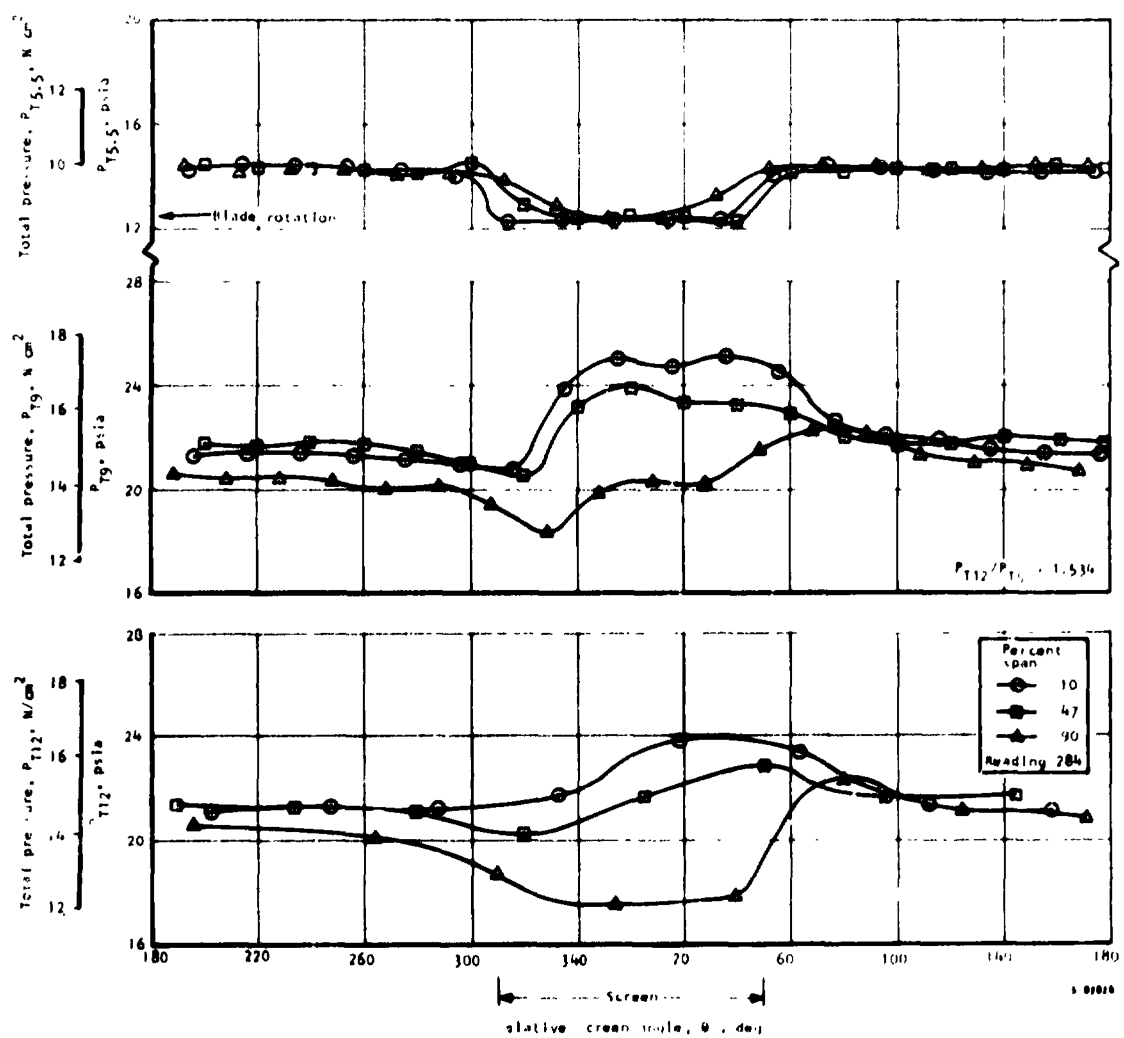

Figure 57.--Circumferential Distribution of Total Pressure at Design Speed with Circumferential Inlet Distortion.

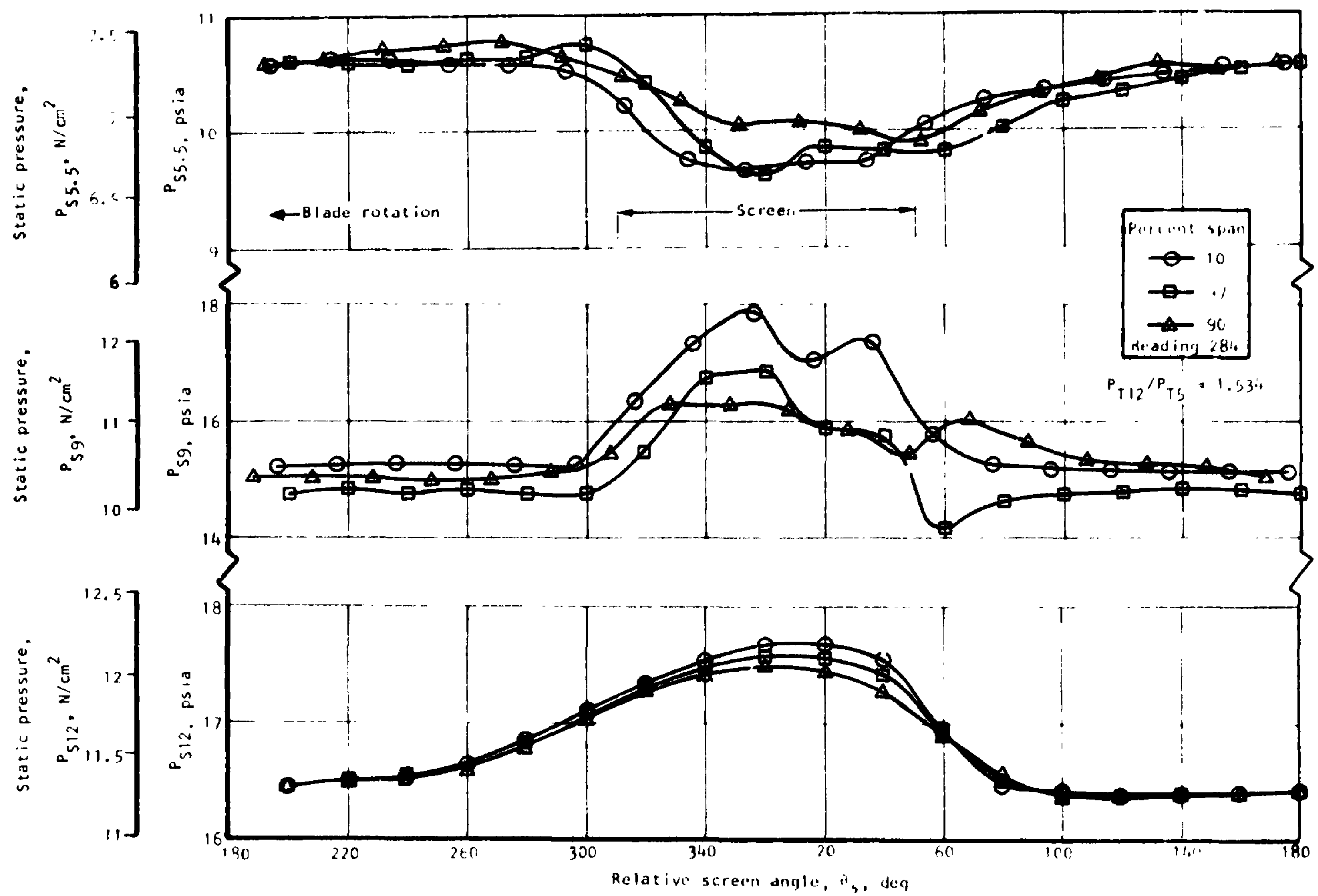

Figure 58.--Circumferential Distribution of Static Pressure at Design Speed with Circumferential Inlet Distortion.

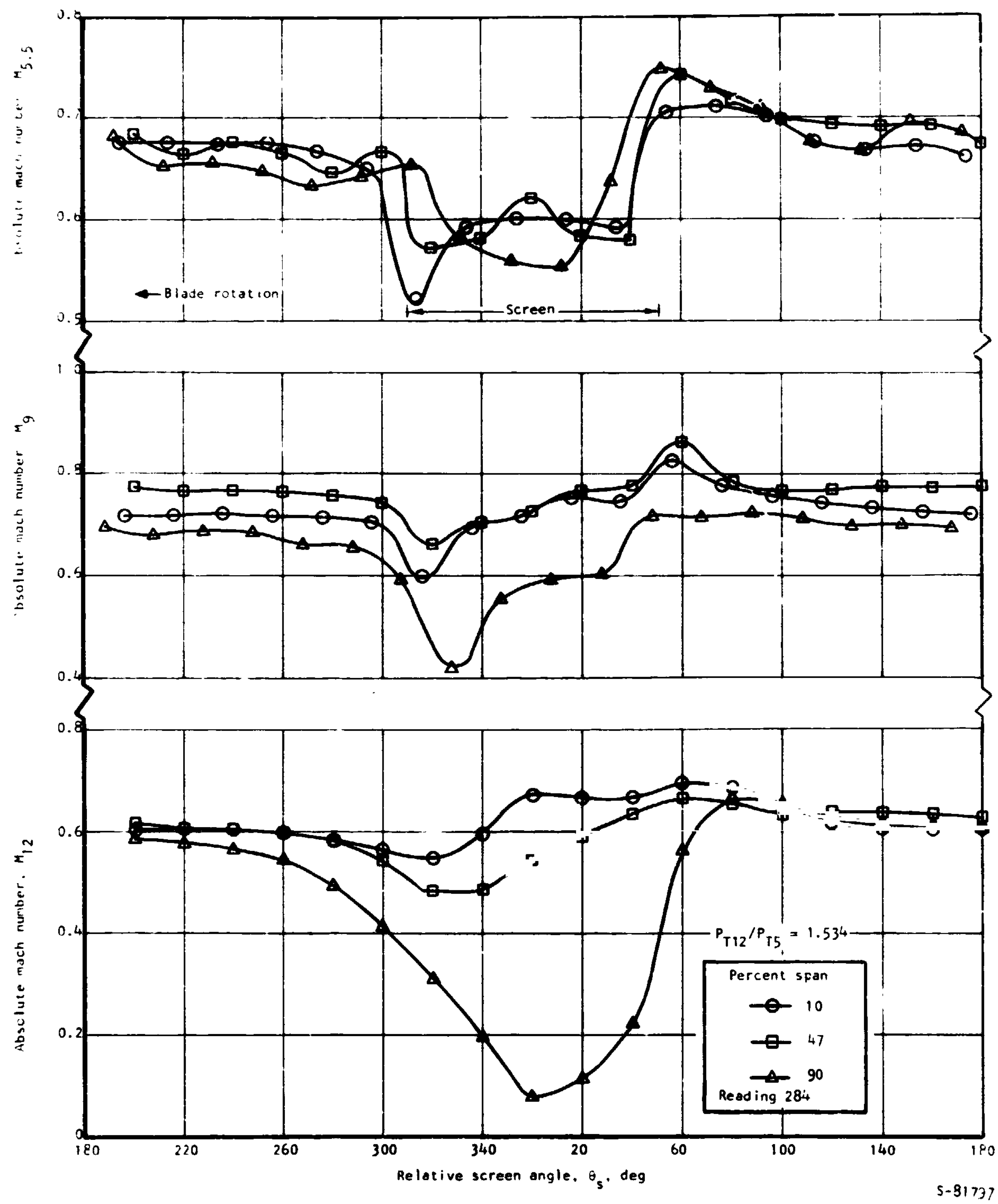

Figure 59.--Circumferential Distribution of Absolute Mach Number at Design Speed with Circumferential Inlet Distortion.

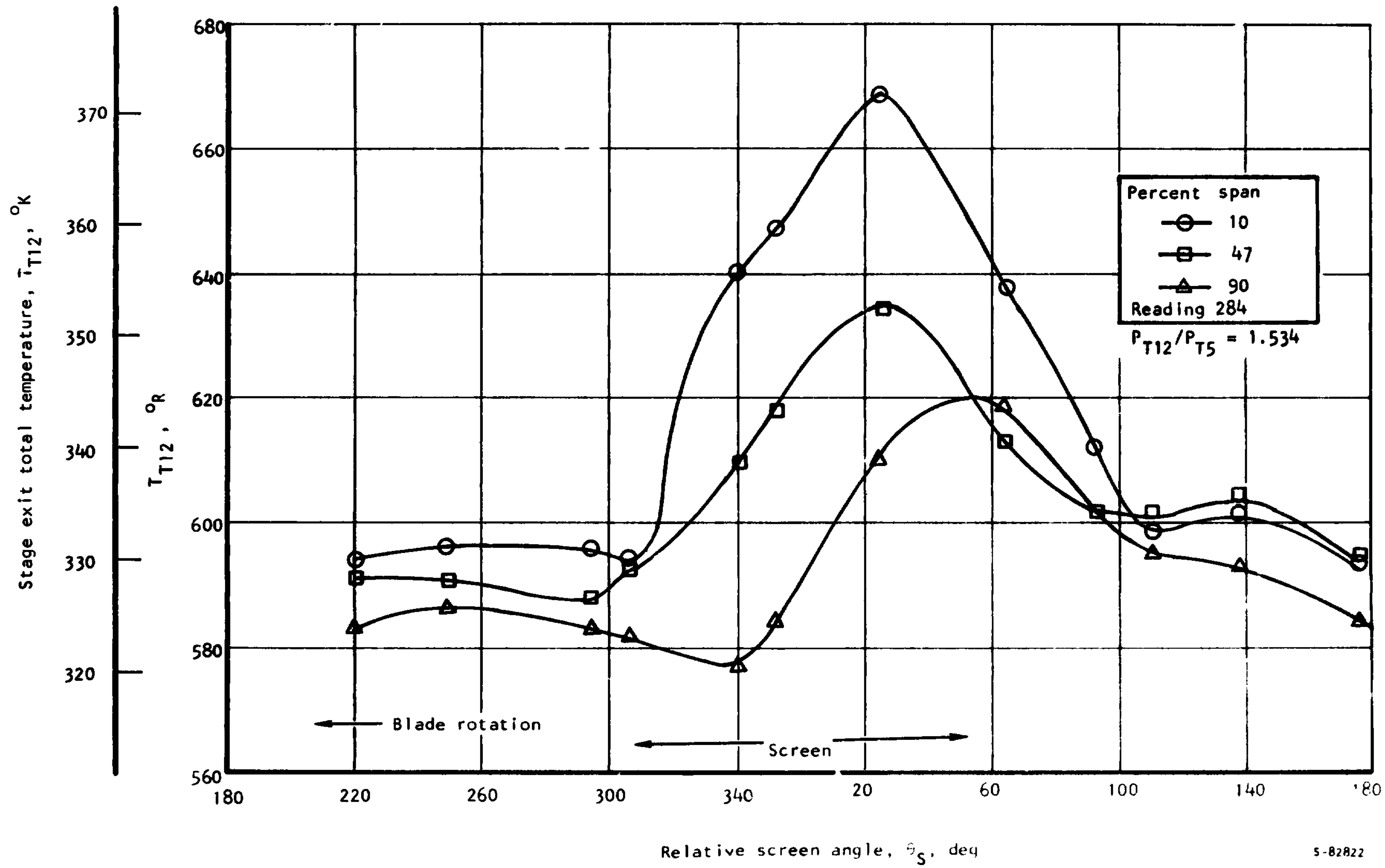

Figure 60.--Circumferential Distribution of Stage Exit Total Temperature at Design Speed with Circumferential Inlet Distortion.

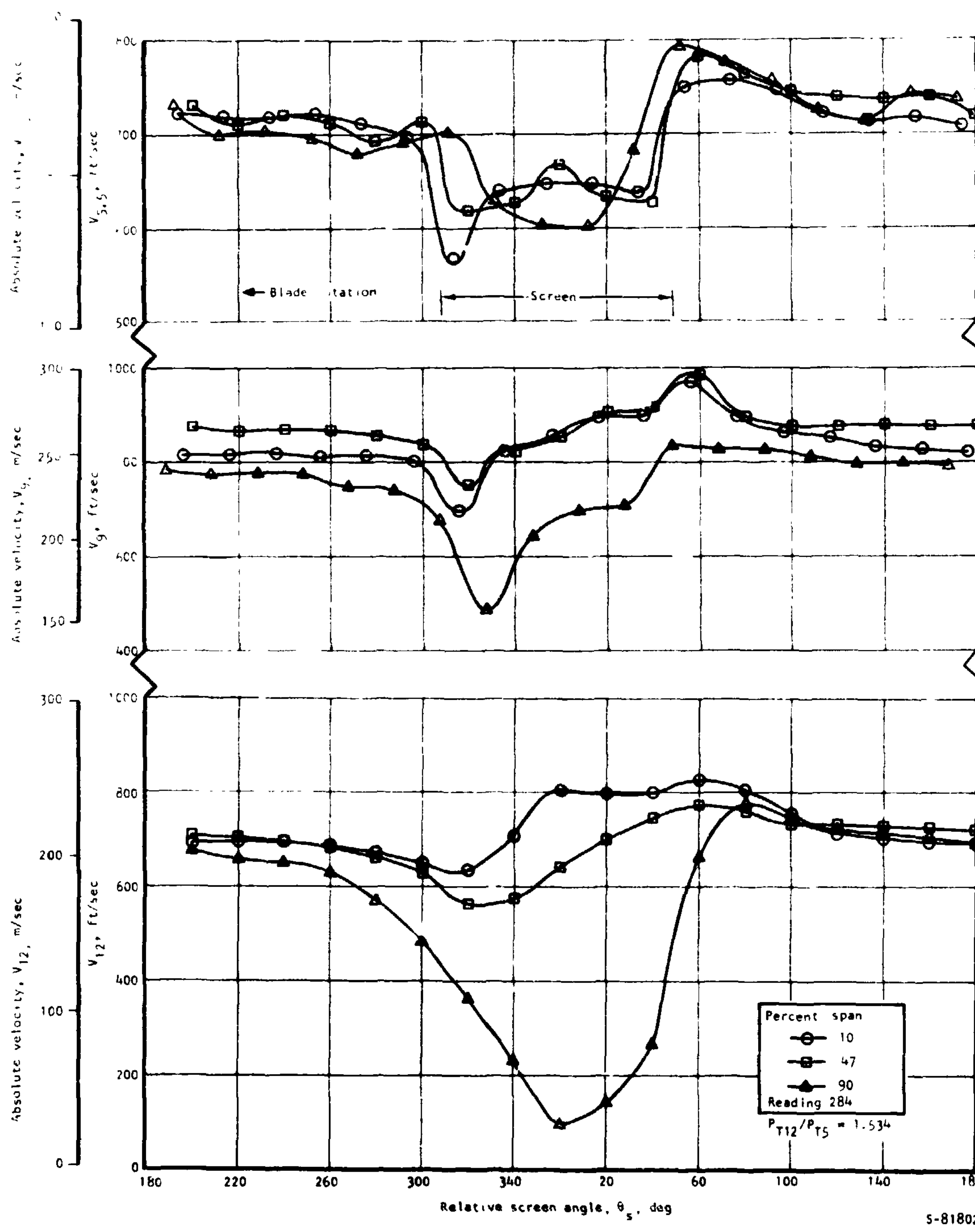

Figure 61.--Circumferential Distribution of Absolute Mach Number at Design Speed with Circumferential Inlet Distortion.

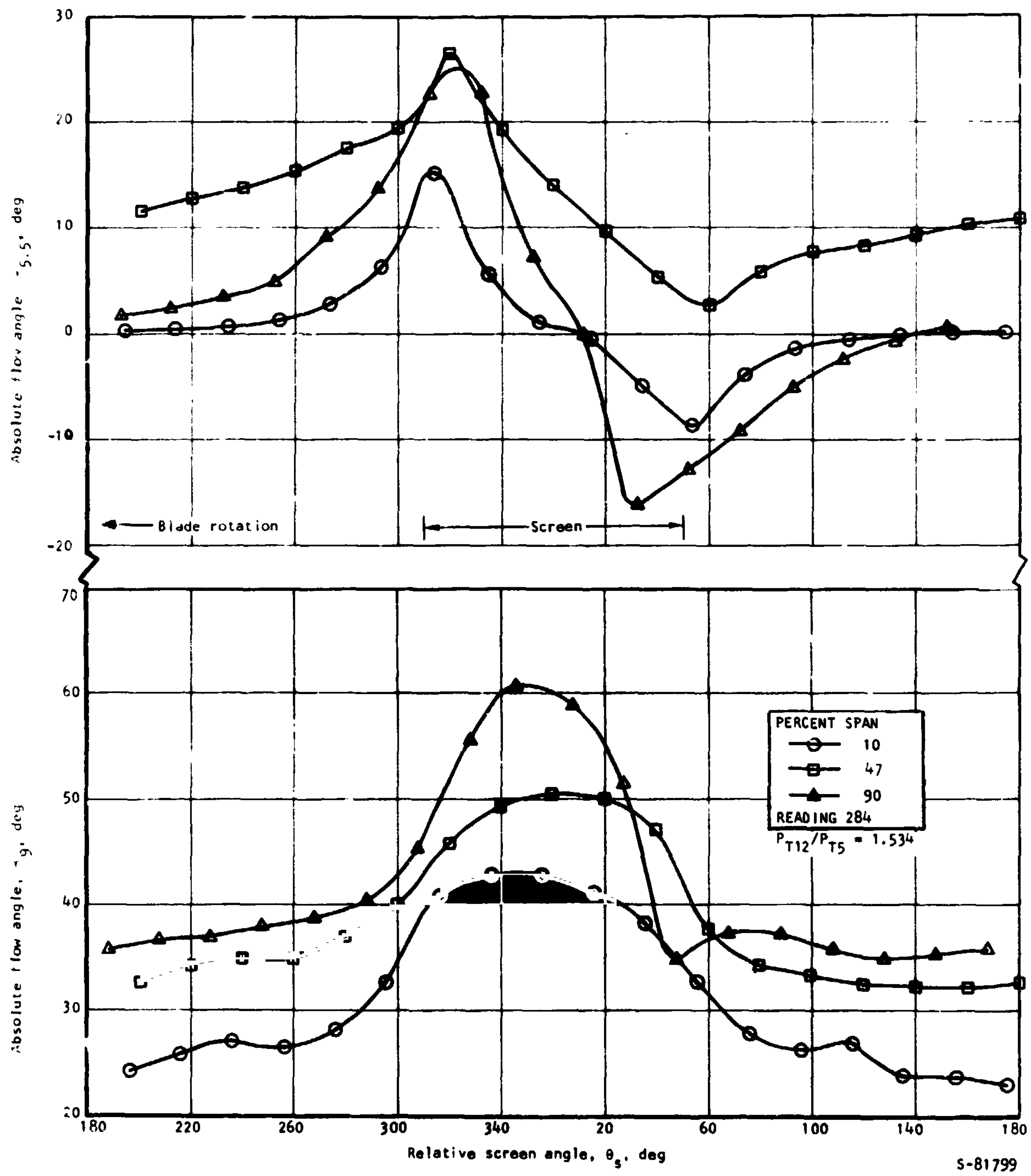

Figure 62.--Circumferential Distribution of Absolute Flow Angle at Design Speed with Circumferential Inlet Distortion.

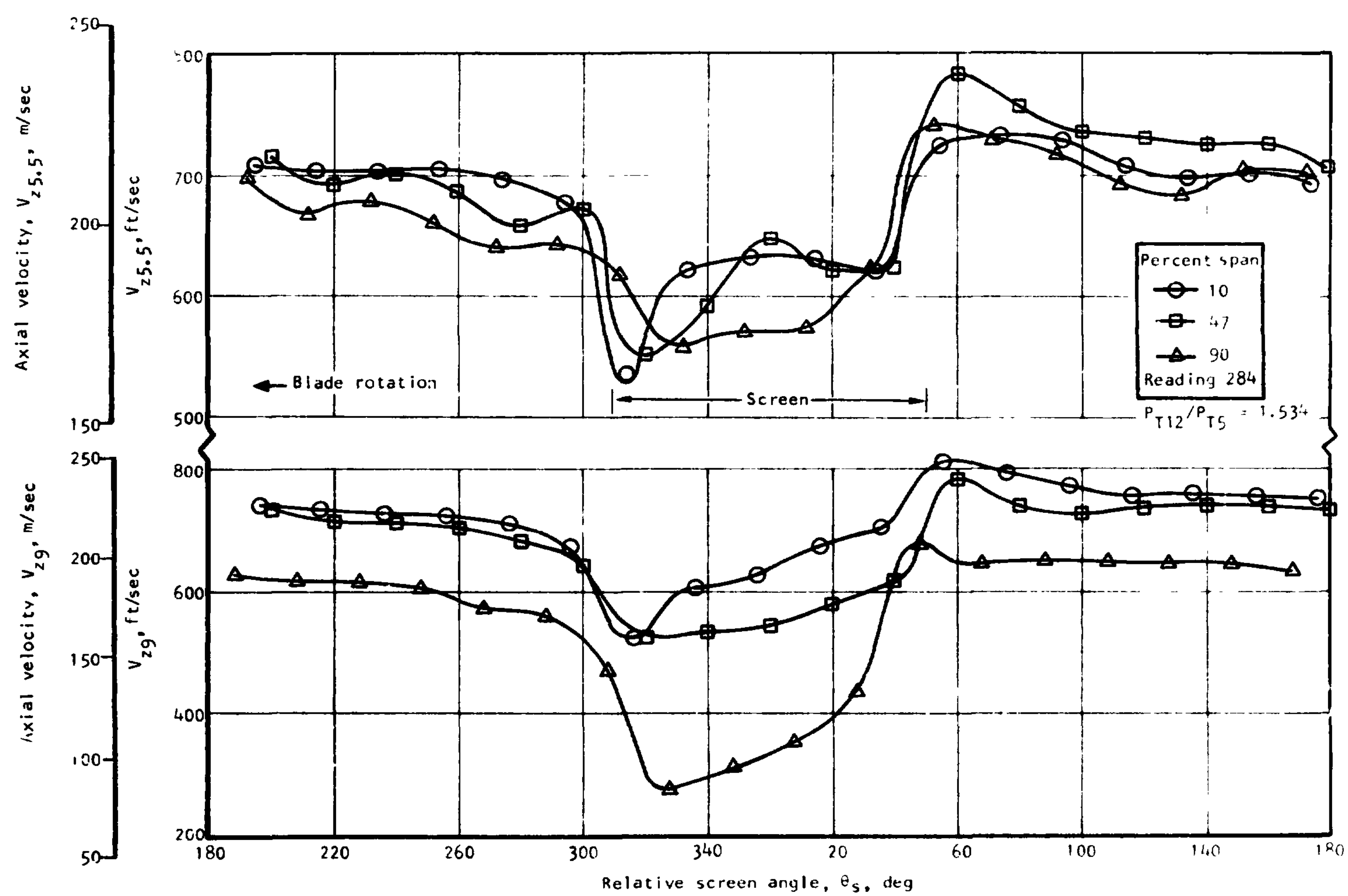

Figure 63.--Circumferential Distribution of Axial Velocity at Design Speed with Circumferential Inlet Distortion.

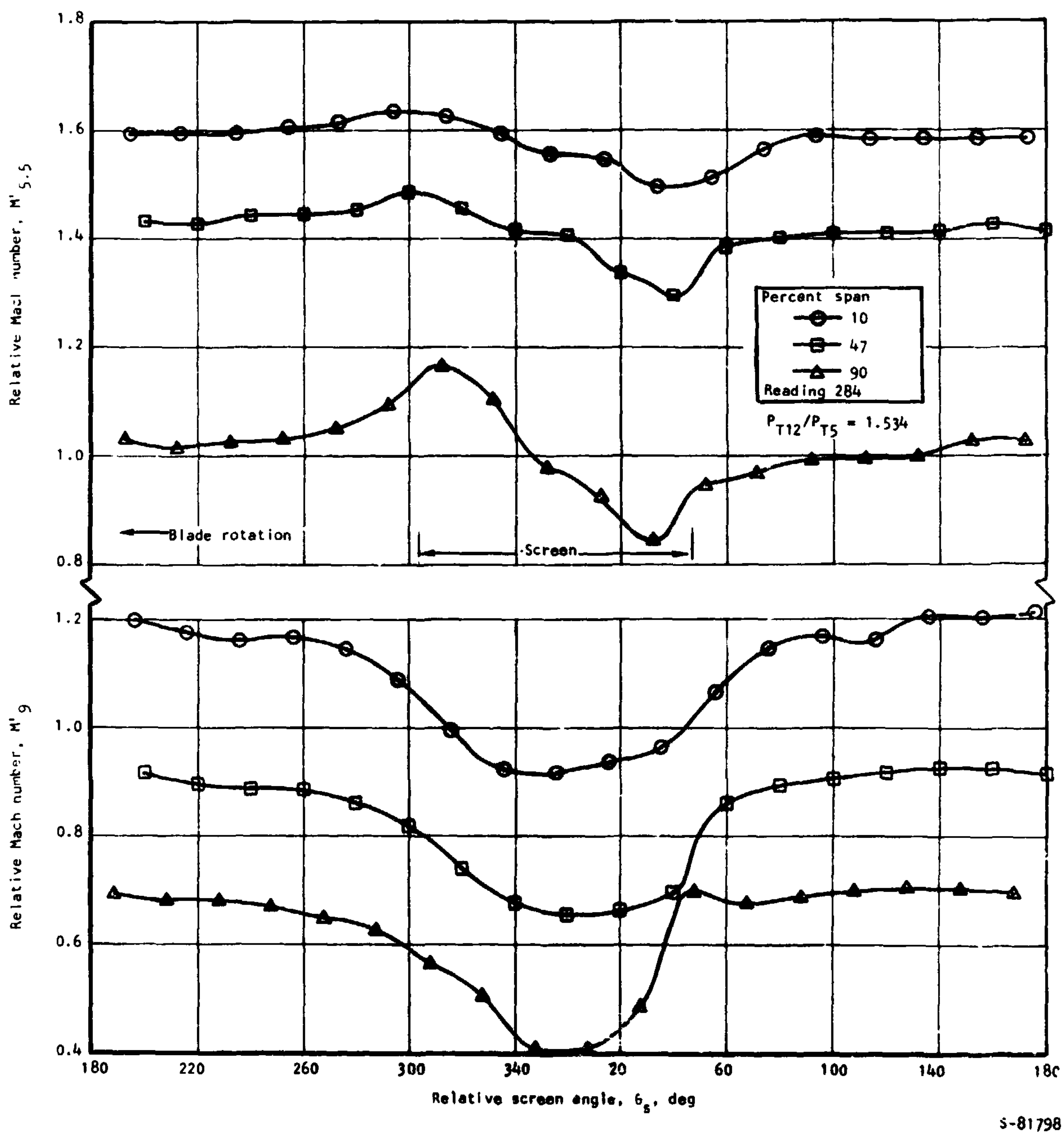

Figure 64.--Circumferential Distribution of Relative Mach Number at Design Speed with Circumferential Inlet Distortion.

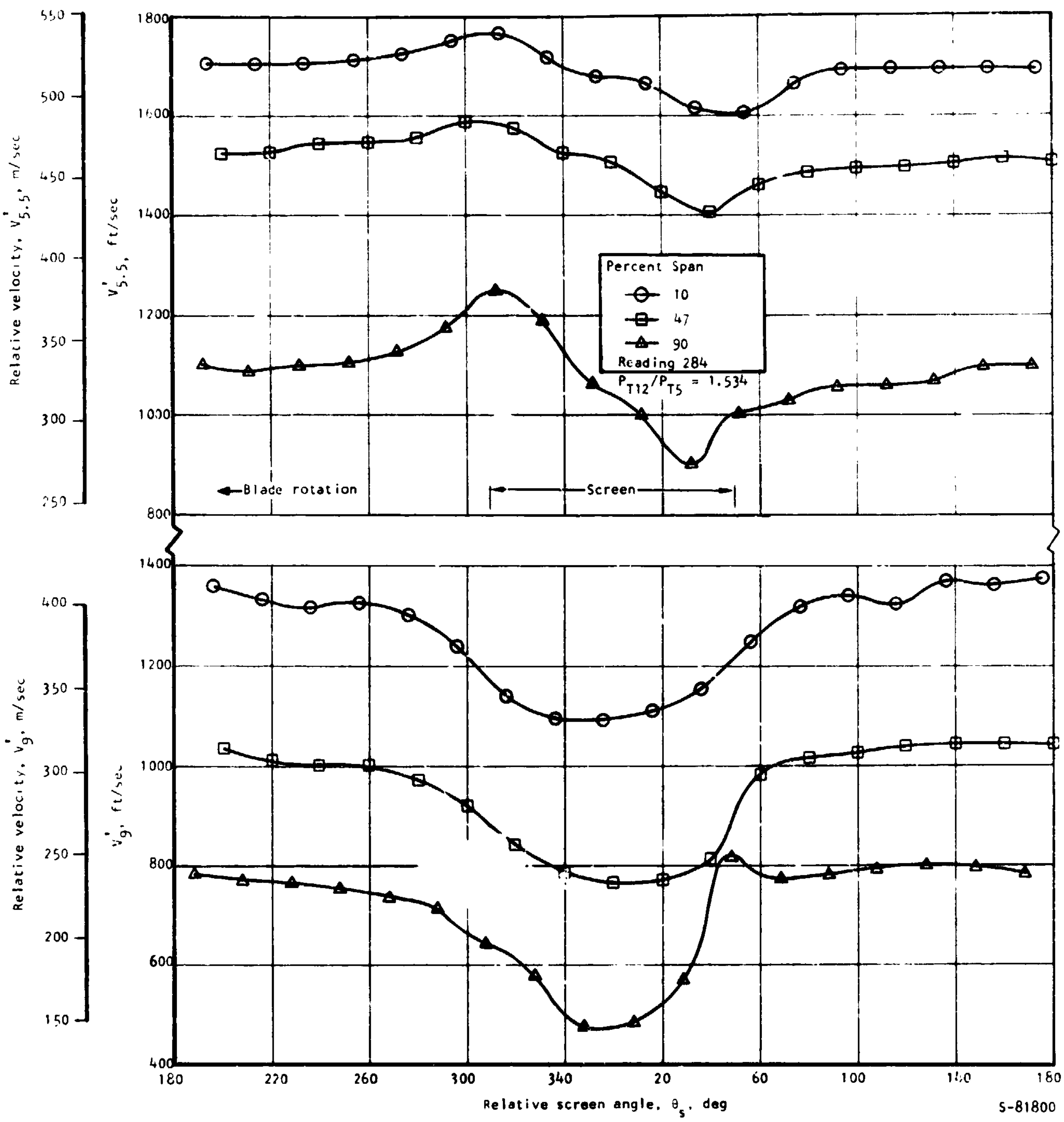

Figure 65.--Circumferential Distribution of Relative Velocity at Design Speed with Circumferential Inlet Distortion.

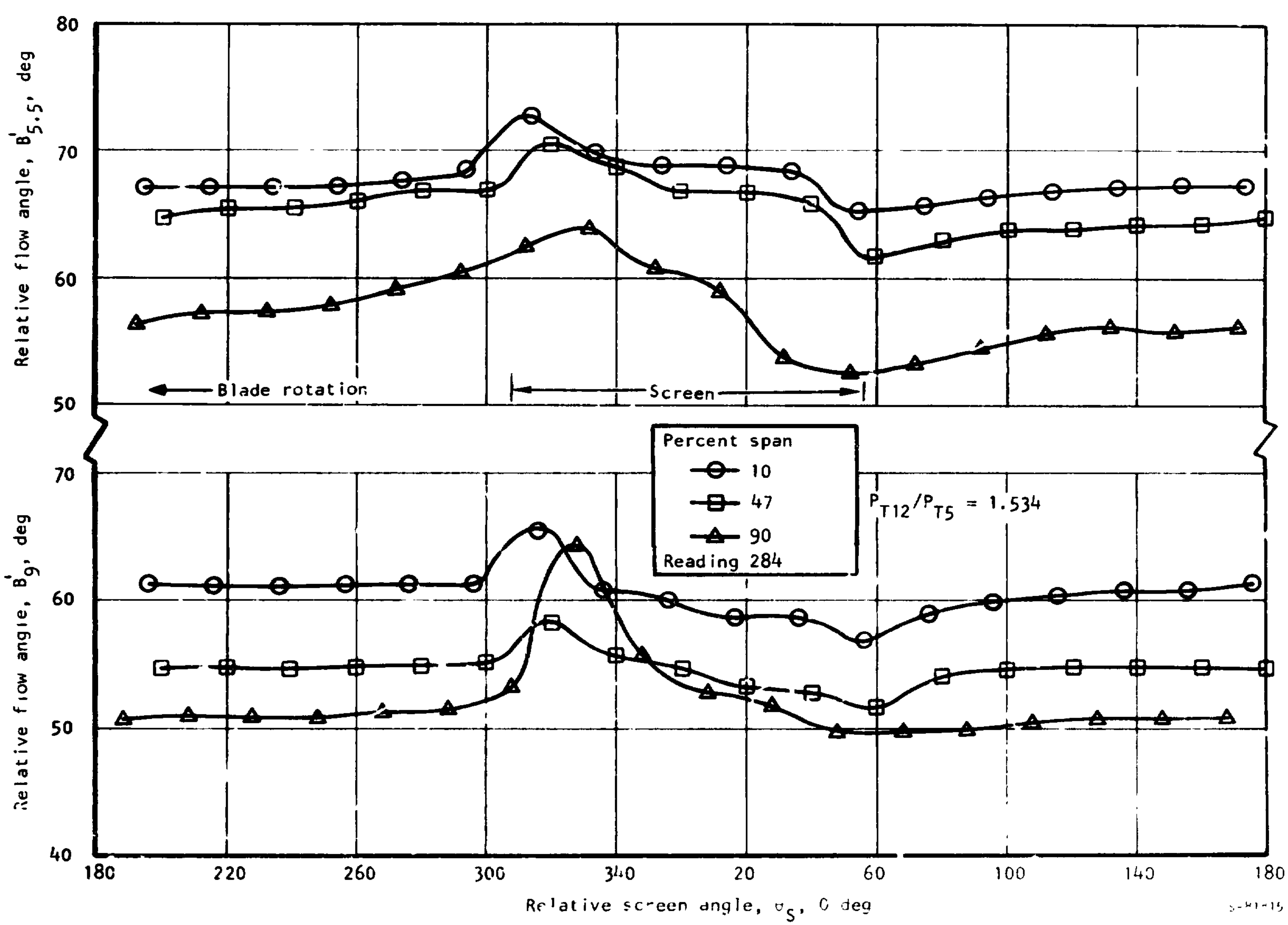

Figure 66.--Circumferential Distribution of Relative Flow Angle at Design Speed with Circumferential Inlet Distortion.

APPENDIX A

REDESIGNED ROTOR FOR TRANSONIC FAN STAGE

The original design detailed in ref. 1 exhibited an aerodynamic instability phenomenon (flutter), which resulted in high cycle fatigue failure of the midspan dampers during initial testing to 110 percent of design speed. The flutter phenomenon was concluded to be a coupled bending-torsion mode instability. The performance data obtained at design speed from this test were encouraging, and it was felt that modifications to the midspan dampers (thickness, contact angle, and contact surface shape) would be sufficient to relieve the structural problem. However, to further ensure structural integrity of the redesigned rotor without sacrificing the original aerodynamic features, the torsional flutter parameter was increased by thickening blade sections immediately adjacent to the damper.

Aerodynamic

The redesign of the rotor followed the procedures detailed in ref. 1, which consist of sequential running of the axisymmetric stream filament computer program for velocity diagrams the blade design calculation program for blade sections on conical surfaces, and the blade stacking program for definition of sections on cylindrical surface tangent planes. The original stage design objectives were retained.

Overall total pressure ratio	1.5
Flow per unit annulus area	42 lb/sec-ft^2 (205.1 kgm/sec-m^2)
Equivalent total flow	148 lb/sec (67.1 kgm/sec)
Equivalent tip speed	1600 ft/sec (488.6 m/sec)
Equivalent speed	12 781 rpm (1338.4 rad/sec)
Adiabatic efficiency	86 percent

Also retained from the original design were the flow path, streamline work and loss distributions, number blades, and approximately the same solidity distribution and aspect ratio. The redesign was initiated by revising the axisymmetric stream filament computer program to reflect the lade thickness distribution of fig. A-1 as dictated by mechanical design requirements. The resulting velocities and angles at the blade inlet and outlet are shown in table A-1 as a function of streamline number. The incidence angle rules used for the original design were maintained for the supersonic and transonic region of the redesigned blade. The incidence angles of the subsonic (inboard) sections of the original blade were thought to be low, however, and were increased for the redesign. The deviation rules applied to the redesigned blade were the same as those used for the original blade. The resulting incidence angles, deviation angles, and Carter's rule additive are tabulated in table A-1.

The blade design program does not provide a precise quantitive definition of the input changes required to generate a blade of the desired thickness. The effective, available methods of implementing thickness changes required an increase in both the leading and trailing edge radii as shown in fig. A-2, coupled with an increase in trailing edge shock strength via the specification of an increase in D-shock (the trailing edge shock strength minus the leading edge shock strength) as shown in fig. A-3. The resulting conical developments for typical streamlines 1, 3, 5, 7, and 12 are shown in fig. A-4. Streamline 5 is the closest streamline to the midspan damper and is where the greatest increase in thickness from the original design was required.

The 12 conical blade sections resulting from the blade design program were then used to establish the 14 manufacturing section coordinates as described in the paragraphs that follow.

Mechanical

A geometric summary of the redesigned rotor blade is presented in table A-2. The rotor airfoil coordinates of the resulting 14 rotor blade sections incorporating both axial and tangential tilt and allowance for blade untwist are presented in table A-3. The coordinates are plane blade sections defined by the intersection of the blade with planes tangent to the cylindrical surfaces. A typical section is presented in fig. A-5. The materials selected for the critical components have not changed from the original design. The fan blade and disc material is Ti-6Al-4V (AMS 4928), and the stator vane material is 17-4 PH (AMS 5643).

The fan blade thickness was increased by approximately 45 percent at the midspan damper to increase the blade natural frequency, thereby raising the flutter parameter to a more stable regime. Both torsional flutter and coupled flexural torsional flutter modes were examined. Fig. A-6 shows the torsional flutter parameter ($\omega_T C_T/V_T'$) versus rotor speed for the original and redesigned blade, where ω_T is the torsional natural frequency, C_T is the blade tip chord and V_T' is the relative fluid velocity at the blade tip. The redesigned blade shows a 45 percent increase in the torsional flutter parameter over the original. From an analysis of the data obtained with the original rotor blade, the threshold of flutter, as indicated in fig. A-6, was thought to occur at approximately 93 percent of design speed. At 110 percent of design speed, the redesigned blade has a 20 percent margin over the value of the flutter parameter at which the original blade fluttered at 93 percent of design speed.

A flutter parameter for coupled flexural-torsional flutter, based on the stability criteria established in ref. 7 is shown in fig. A-7. Using the theoretical approach outlined in Ref. 7, the stability boundary was located based on the results of the original test. Fig. A-7 compares this coupled flutter parameter ($V_T'/C_T\ f_B$) (arbitrary scale) with the rotation-to-translation ratio ($\phi_T C_T/2h_T$) for both the original and redesigned blade, where f_B is the first flexure natural frequency of the blade, h_T is the relative deflection (translation) of the blade tip midchord point in the first flexural mode, and ϕ_T is the relative angular deflection of the blade tip in the first flexural mode.

The redesigned blade is well within the stable region and should be aeroelastically stable, with respect to this mode of flutter, over the operating speed range.

The blade natural frequencies were calculated using a finite element program in which the blade is modeled as a curved variable thickness plate. The blade was assumed to be built-in (clamped at the root and supported in the axial and tangential directions at the midspan damper. The damper is assumed to be locked up at zero speed for nominal blade dimensions. The first three natural frequencies are shown as a function of rotor speed on the excitation diagram given in fig. A-8. No serious resonant conditions are shown in the operating range.

The first three mode shapes at zero speed are shown in fig. A-9. The location of the maximum vibratory stress in each mode, as well as the relative values (in percent) of the vibratory stress at other critical points, also are shown.

Fig. A-10 is a modified Goodman diagram showing the allowable vibratory stress as a function of steady stress. The allowable vibratory stress is 50 percent of the 10^7 cycle endurance strength. The airfoil mid-chord at the midspan damper has been chosen as a critical point for vibratory stress. The allowable vibratory stress at this location is ±30 ksi (207×10^6 N/m^2) at design speed.

The airfoil was tilted 0.010 in./in. (cm/cm) in the tangential direction and 0.0035 in./in. (cm/cm) in the axial direction to allow centrifugal loads to counteract the aerodynamic loads. The airfoil suction and pressure surface design speed stress distributions due to centrifugal, untwist, and aerodynamic loads are shown in fig. A-11. The steady stresses at 110 percent speed will be 1.21 times those shown. Thus, the maximum equivalent calculated airfoil stress at 110 percent speed is 78.6 ksi (543×10^6 N/m^2).

The airfoil will untwist due to both centrifugal and aerodynamic loads. The untwist versus radius at the design point is shown in fig. A-12. The untwist at the midspan damper is approximately 0.5 deg. The nominal midspan damper blade-to-blade spacing will increase with speed and thereby allow the midspan damper to untwist the 0.5 deg at design speed.

The midspan damper stress distribution is shown in fig. A-13. The redesigned damper has a smaller interface angle (15 deg) and has no grind relief notch, which was the origin of failure on the original blade. The maximum midspan damper equivalent stress is 80 ksi (551×10^6 N/m^2) and is very localized. This stress is slightly less than the allowable 82 ksi (566×10^6 N/m^2).

The disc stresses with the redesigned blade are slightly higher than those in the original design because of the small increase in blade weight. The disc tangential and radial stresses at critical locations at 110 percent design speed are listed on the next page.

Location	Type of Stress	Calculated Stress Ksi	(N/m²)	Allowable Stress Ksi	(N/m²)
Disc	Avg. tangential	67.6	(465×10^6)	67.5	(465×10^6)
Bore	Max. tangential	88.0	(607×10^6)	91.0	(926×10^6)
Web	Max. radial	30.0	(207×10^6)	85.5	(590×10^6)

The bore and web stresses are within the allowables. The average tangential stress is equal to the allowable, indicating the burst criteria has just been met.

The minimum shedding speeds for the airfoil and dovetail were determined using 90 percent of the minimum natural ultimate stress at the maximum temperature conditions.

Blade airfoil	18 090 rpm (1892 rad/sec)
Blade shank	21 900 rpm (2295 rad/sec)
Disc shank	17 800 rpm (1864 rad/sec)
Disc burst	17 600 rpm (1843 rad/sec)

The minimum burst and shedding speed is 17 600 rpm (1843.1 rad/sec), which is 138 percent of the design speed.

The dovetail stresses in the blade and disc are slightly higher than those of the original design because of the heavier airfoil and midspan damper on the redesigned blade. The neck, tang, and combined stresses at 110 percent speed are listed in table A-4 along with the allowable stresses. All margins of safety are positive. The combined fillet stress is a combination of tang bending and neck tension, excluding the stress concentration effects. The maximum fillet stress, which determines the low-cycle fatigue life of the attachment, includes the stress concentration factor. All calculated stresses show a positive margin of safety.

TABLE A-1
ROTOR AERODYNAMIC SUMMARY

P_{T1} = 14.696 psia 10.133 N/cm^2
T_{T1} 518.69 °R 288.16°K
$N/\sqrt{\theta}$ = 12 78[illegible] rpm 1338.4 rad/sec
$W\sqrt{\theta}/\delta$ 147.91 lbm/s 67.09 kg/sec
U_{T1} = 1603.0 ft/sec = 488.594 m/sec
r_{T1} 14.370 in. 36.50 cm

Blockage factor = 0.960

Inlet (station 6)

Streamline	1	2	3	4	5	6	7	8	9	10	11	12
r/r_{T6}	1.0000	0.9638	0.9274	0.8897	0.8501	0.8081	0.7638	0.7161	0.6644	0.6077	0.5432	.4622
Flow	0.0	9.09	18.18	27.27	36.36	45.45	54.55	63.64	72.73	81.82	[illegible]	100.00
P_T/P_{T1}	1.0	1.0	1.0	1.0	1.0	1.0	1.0	1.0	1.0	1.0	1.0	1.0
T_T/T_{T0}	1.0	1.0	1.0	1.0	1.0	1.0	1.0	1.0	1.0	1.0	1.0	1.0
U/U_{T6}	1.0000	0.9638	0.9274	0.8897	0.8501	0.8081	0.7638	0.7161	0.6644	0.6077	0.5432	0.4622
V_a/U_{T6}	1.0000	0.9638	0.9274	0.8897	0.8501	0.8081	0.7638	0.7161	0.6644	0.6077	0.5432	0.4622
β	-13.00	-9.26	-5.42	-2.29	-0.63	-0.05	2.03	3.37	4.36	7.53	13.76	23.30
V/U_{T6}	0.4318	0.4567	0.4594	0.4555	0.4486	0.4440	0.4406	0.4313	0.4242	0.4170	0.3955	0.3374
V'/U_{T6}	0.4318	0.4567	0.4594	0.4555	0.4486	0.4440	0.4406	0.4313	0.4242	0.4170	0.3955	0.3374
β'	66.64	64.64	63.64	62.88	62.17	61.21	60.01	58.93	57.44	55.54	53.94	54.35
β	0.0	0.0	0.0	0.0	0.0	0.0	0.0	0.0	0.0	0.0	0.0	0.0
i_{MCL}	2.791	2.797	2.839	3.130	3.675	3.623	3.670	3.908	4.341	5.266	5.856	6.086
i_{ss}	0.721	0.801	0.847	1.000	1.300	1.220	1.216	1.355	1.620	2.136	2.100	1.160
M'	1.619	1.593	1.547	1.493	1.434	1.374	1.313	1.243	1.170	1.093	0.992	0.837
M	0.642	0.682	0.687	0.681	0.669	0.662	0.656	0.641	0.630	0.618	0.584	0.485

Overall parameters

	1	2	3	4	5	6	7	8	9	10	11	12
$\bar{r}/r_{T6}$	0.9848	0.9523	0.9187	0.8835	0.8461	0.8063	0.7638	0.7180	0.6685	0.6151	0.5565	0.4863
T/T_{T0}	0.1470	0.1419	0.1400	0.1400	0.1410	0.1439	0.1485	0.1499	0.1439	0.1400	0.1369	0.1390
$\bar{\omega}$	0.0785	0.0642	0.0596	0.0620	0.0688	0.0840	0.1096	0.1202	0.0978	0.0831	0.0714	0.0910
D	0.2150	0.2340	0.2520	0.2685	0.2903	0.3191	0.3558	0.3879	0.4033	0.4126	0.3878	0.2410
η_{ad}	0.851	0.875	0.891	0.893	0.887	0.867	0.841	0.837	0.870	0.900	0.920	0.928
σ	1.622	1.644	1.668	1.679	1.693	1.706	1.724	1.752	1.781	1.805	1.885	2.098

Exit (station 8)

Blockage factor = 0.955

	1	2	3	4	5	6	7	8	9	10	11	12
r/r_{T6}	0.9694	0.9407	0.9101	0.8771	0.8421	0.8041	0.7635	0.7199	0.6724	0.6224	0.5696	0.5144
P_T/P_{T1}	1.512	1.510	1.509	1.509	1.509	1.510	1.511	1.512	1.513	1.514	1.517	1.528
T_T/T_{T0}	1.147	1.142	1.140	1.140	1.141	1.144	1.149	1.150	1.144	1.140	1.137	1.139
U/U_{T6}	0.9694	0.9407	0.9101	0.8771	0.8421	0.8041	0.7635	0.7199	0.6724	0.6224	0.5696	0.5144
V_θ'/U_{T6}	0.7835	0.7554	0.7217	0.6824	0.6375	0.5850	0.5251	0.4649	0.4097	0.3475	0.2742	0.1840
V_M/U_{T6}	0.4666	0.4371	0.4129	0.3954	0.3805	0.3692	0.3600	0.3543	0.3590	0.3729	0.4078	0.4807
β	-11.50	-9.69	-8.42	-7.79	-6.22	-3.54	-2.15	-1.18	3.19	7.96	12.99	17.70
V/U_{T6}	0.5024	0.4746	0.4538	0.4408	0.4320	0.4294	0.4319	0.4364	0.4449	0.4633	0.5036	0.5832
V'/U_{T6}	0.9114	0.8727	0.8315	0.7885	0.7423	0.6918	0.6359	0.5845	0.5447	0.5097	0.4915	0.5147
β'	59.21	59.95	60.22	59.90	59.16	57.74	55.57	52.69	48.77	42.98	33.92	20.95
β	21.75	22.93	24.51	26.24	28.26	30.71	33.54	35.72	36.21	36.40	35.91	34.50
M'	1.275	1.217	1.156	1.094	1.028	0.956	0.878	0.807	0.755	0.710	0.691	0.736
M	0.703	0.662	0.631	0.612	0.598	0.594	0.596	0.602	0.617	0.645	0.708	0.834
δ^o	3.778	3.788	3.933	5.753	7.869	7.727	7.930	8.191	8.370	8.533	8.914	10.277
x	3.14	3.01	3.09	4.80	6.74	5.96	5.40	5.31	5.50	5.43	4.81	2.49

TABLE A-2
ROTOR GEOMETRIC SUMMARY

[Blade sections, defined by the intersection of the blade with planes tangent to cylindrical surfaces]

Blade height = 7.728 in. (19.63 cm)
Hub tip ratio = 0.462

Number of blades = 40
Aspect ratio = 2.76

L = plane radius															
	in.	14.370	13.800	13.100	12.750	12.400	12.000	11.700	11.000	10.300	9.600	8.900	8.200	7.500	6.642
	cm	36.500	35.052	33.274	32.385	31.496	30.480	29.718	27.940	26.162	24.384	22.606	20.828	19.050	16.871
Blade height from tip, percent		0	7.7	16.7	20.9	25.4	30.6	34.8	44.0	52.9	61.9	71.0	80.0	89.0	100.0
β_6^* design		65.01	62.43	61.01	60.30	59.54	58.41	57.92	56.65	55.42	53.88	51.89	50.23	48.87	49.85
β_8^* design		56.91	57.09	56.89	56.20	54.24	51.59	50.54	48.20	44.82	40.35	34.06	24.11	10.08	-4.26
β_M design		62.02	60.36	58.85	57.51	55.82	54.06	53.48	52.06	49.77	46.38	41.70	36.11	30.85	25.43
Protwist		1.050	0.960	0.860	0.740	0.750	1.030	0.810	0.830	0.980	0.900	0.500	0.160	0.0	0.0
β_6^* static		66.06	63.39	61.87	61.04	60.29	58.44	58.73	57.48	56.40	54.78	52.39	50.39	48.87	49.85
β_8^* static		57.96	58.05	57.75	56.94	54.99	52.62	51.35	49.03	45.80	44.26	34.56	24.27	10.08	-4.26
β_M static		63.05	61.32	59.71	58.25	56.57	55.09	54.29	52.89	50.75	47.28	42.20	36.27	30.65	25.48
Camber		8.10	5.34	4.12	4.10	5.30	6.82	7.38	8.45	10.60	13.52	17.83	26.12	38.79	54.11
Chord	in.	3.660	3.577	3.477	3.421	3.351	3.274	3.194	3.026	2.882	2.728	2.558	2.414	2.303	2.191
	cm	9.296	9.086	8.832	8.689	8.512	8.316	8.113	7.686	7.320	6.929	6.497	6.132	5.850	5.565
Solidity		[illegible]	1.650	1.690	1.708	1.720	1.737	1.738	1.751	1.781	1.809	1.830	1.874	1.955	2.100
T_{max}/c		0.0235	0.0264	0.0324	0.0412	0.0520	0.0567	0.0545	0.0532	-0.0560	0.0611	0.0679	0.0740	0.0803	0.0875
r_{LE}/c[a]		0.0015	0.0017	0.0020	0.0024	0.0032	0.0036	0.0032	0.0029	0.0032	0.0037	0.0044	0.0052	0.0059	0.0065
r_{TE}/c[a]		0.0014	0.0016	0.0019	0.0032	0.0054	0.0074	0.0035	0.0034	0.0035	0.0042	0.0052	0.0063	0.0072	0.0080

[a]Leading and trailing edge radii are defined to be the semi-minor axes of 2-to-1 ellipses.

TABLE A-3
ROTOR AIRFOIL COORDINATES

ROTOR AIRFOIL COORDINATES
SECTION NO. 1 RADIUS 14.370 IN. (36.500 CM.)

SUCTION SURFACE X,IN.	Y,IN.	X,CM.	Y,CM.	PRESSURE SURFACE X,IN.	Y,IN.	X,CM.	Y,CM.
-.8820	-1.7139	-2.2404	-4.3534	-.8820	-1.7159	-2.2404	-4.3534
-.8820	-1.7135	-2.2404	-4.3523	-.8818	-1.7160	-2.2396	-4.3587
-.8817	-1.7106	-2.2394	-4.3449	-.8810	-1.7179	-2.2374	-4.3635
-.8807	-1.7075	-2.2370	-4.3371	-.8798	-1.7190	-2.2346	-4.3663
-.8647	-1.6668	-2.1963	-4.2337	-.8781	-1.7192	-2.2303	-4.3668
-.8213	-1.5579	-2.0861	-3.9572	-.8762	-1.7185	-2.2255	-4.3650
-.7779	-1.4508	-1.9758	-3.6851	-.8742	-1.7169	-2.2205	-4.3610
-.7345	-1.3456	-1.8656	-3.4174	-.8703	-1.7110	-2.2105	-4.3458
-.6911	-1.2420	-1.7554	-3.1547	-.8542	-1.6773	-2.1698	-4.2605
-.6477	-1.1407	-1.6452	-2.[illegible]974	-.8109	-1.5866	-2.0597	-4.0300
-.6043	-1.0413	-1.5350	[illegible].6449	-.7676	-1.4958	-1.9497	-3.7994
-.5609	-.9433	-1.4248	[illegible].3960	-.7242	-1.4050	-1.8396	-3.5687
-.5176	-.8464	-1.3146	-2.1499	-.6809	-1.3142	-1.7295	-3.3381
-.4742	-.7502	-1.2044	-1.9054	-.6376	-1.2235	-1.6195	-3.1077
-.4308	-.6547	-1.0942	-1.6630	-.5943	-1.1329	-1.5094	-2.8775
-.3874	-.5604	-.9840	-1.4234	-.5509	-1.0424	-1.3994	-2.6476
-.3440	-.4671	-.8738	-1.1865	-.5076	-.9520	-1.2893	-2.4181
-.3006	-.3747	-.7636	-.9516	-.4643	-.8618	-1.1792	-2.1890
-.2572	-.2829	-.6534	-.7186	-.4210	-.7718	-1.0692	-1.9604
-.2138	-.1917	-.5432	-.4869	-.3776	-.6821	-.9592	-1.7324
-.1705	-.1011	-.4330	-.2568	-.3343	-.5926	-.8491	-1.5056
-.1271	-.0113	-.3228	-.0286	-.2910	-.5034	-.7390	-1.2786
-.0837	.0779	-.2126	.1979	-.2476	-.4145	-.6290	-1.0529
-.0403	.1664	-.1024	.4226	-.2043	-.3260	-.5189	-.8281
.0031	.2541	.0078	.6455	-.1610	-.2379	-.4089	-.6044
.0465	.3413	.1181	.8668	-.1176	-.1503	-.2988	-.3817
.0899	.4277	.2283	1.0864	-.0743	-.0631	-.1887	-.1604
.1332	.5135	.3385	1.3043	-.0310	.0235	-.0787	.0596
.1766	.5987	.4487	1.5206	.0123	.1095	.0314	.2781
.2200	.6831	.5589	1.7352	.0557	.1949	.1414	.4951
.2634	.7669	.6691	1.9480	.0990	.2796	.2515	.7103
.3068	.8500	.7793	2.1589	.1423	.3636	.3615	.9236
.3502	.9323	.8895	2.3681	.1857	.4468	.4716	1.1349
.3936	1.0139	.9997	2.5754	.2290	.5292	.5817	1.3441
.4370	1.0915	1.1099	2.7725	.2723	.6106	.6917	1.5509
.4804	1.1625	1.2201	2.9527	.3157	.6910	.8018	1.7551
.5237	1.2288	1.3303	3.1211	.3590	.7703	.9118	1.9566
.5671	1.2941	1.4405	3.2870	.4023	.8485	1.0219	2.1553
.6105	1.3586	1.5507	3.4508	.4456	.9293	1.1320	2.3604
.6539	1.4224	1.6609	3.6128	.4890	1.0172	1.2420	2.5837
.6973	1.4854	1.7711	3.7730	.5323	1.1094	1.3521	2.8179
.7407	1.5476	1.8813	3.9310	.5756	1.1995	1.4621	3.0466
.7435	1.5517	1.8886	3.9413	.6190	1.2878	1.5722	3.2710
.7456	1.5541	1.8937	3.9475	.6623	1.3742	1.6822	3.4905
.7477	1.5559	1.8993	3.9521	.7056	1.4584	1.7923	3.7043
.7499	1.5569	1.9047	3.9546	.7490	1.5405	1.9024	3.9129
.7517	1.5570	1.9094	3.9548	.7518	1.5458	1.9096	3.9264
.7531	1.5561	1.9130	3.9526	.7534	1.5493	1.9136	3.9353
.7539	1.5544	1.9149	3.9483	.7540	1.5521	1.9151	3.9423
.7540	1.5531	1.9153	3.9448	.7540	1.5531	1.9153	3.9446

TABLE A-3.--Continued

ROTOR AIRFOIL COORDINATES
SECTION NO. 2 RADIUS 13.800 IN. (35.052 CM.)

SUCTION SURFACE				PRESSURE SURFACE			
X,IN.	Y,IN.	X,CM.	Y,CM.	X,IN.	Y,IN.	X,CM.	Y,CM.
-.9345	-1.6420	-2.3736	-4.1708	-.9345	-1.6420	-2.3736	-4.1708
-.9344	-1.6409	-2.3735	-4.1679	-.9344	-1.6437	-2.3733	-4.1749
-.9338	-1.6378	-2.3720	-4.1599	-.9336	-1.6457	-2.3714	-4.1802
-.9326	-1.6345	-2.3689	-4.1517	-.9323	-1.6470	-2.3680	-4.1834
-.9150	-1.5978	-2.3260	-4.0583	-.9305	-1.6473	-2.3635	-4.1842
-.8702	-1.4993	-2.2102	-3.8083	-.9284	-1.6467	-2.3581	-4.1825
-.8246	-1.4021	-2.0944	-3.5614	-.9261	-1.6451	-2.3524	-4.1785
-.7789	-1.3061	-1.9785	-3.3176	-.9215	-1.6387	-2.3405	-4.1622
-.7333	-1.2115	-1.8627	-3.0772	-.9046	-1.6077	-2.2976	-4.0835
-.6877	-1.1184	-1.7469	-2.8408	-.8590	-1.5239	-2.1819	-3.8707
-.6421	-1.0267	-1.6310	-2.6077	-.8135	-1.4399	-2.0662	-3.6574
-.5965	-.9359	-1.5152	-2.3771	-.7679	-1.3558	-1.9505	-3.4437
-.5509	-.8457	-1.3994	-2.1482	-.7224	-1.2715	-1.8348	-3.2297
-.5053	-.7559	-1.2835	-1.9201	-.6768	-1.1872	-1.7191	-3.0155
-.4597	-.6666	-1.1677	-1.6932	-.6313	-1.1029	-1.6034	-2.8013
-.4141	-.5780	-1.0519	-1.4681	-.5857	-1.0185	-1.4877	-2.5871
-.3685	-.4900	-.9360	-1.2446	-.5402	-.9342	-1.3720	-2.3729
-.3229	-.4025	-.8202	-1.0224	-.4946	-.8500	-1.2563	-2.1591
-.2773	-.3155	-.7044	-.8014	-.4491	-.7659	-1.1406	-1.9455
-.2317	-.2289	-.5885	-.5813	-.4035	-.6820	-1.0249	-1.7324
-.1861	-.1427	-.4727	-.3624	-.3580	-.5983	-.9092	-1.5197
-.1405	-.0570	-.3569	-.1447	-.3124	-.5148	-.7935	-1.3076
-.0949	.0283	-.2410	.0718	-.2668	-.4315	-.6778	-1.0961
-.0493	.1131	-.1252	.2873	-.2213	-.3486	-.5621	-.8854
-.0037	.1976	-.0094	.5018	-.1757	-.2659	-.4464	-.6754
.0419	.2817	.1065	.7155	-.1302	-.1836	-.3307	-.4663
.0875	.3654	.2223	.9281	-.0846	-.1017	-.2150	-.2582
.1331	.4488	.3381	1.1399	-.0391	-.0201	-.0993	-.0511
.1787	.5317	.4540	1.3506	.0065	.0610	.0164	.1549
.2243	.6143	.5698	1.5603	.0520	.1417	.1322	.3599
.2699	.6964	.6856	1.7690	.0976	.2219	.2479	.5637
.3155	.7781	.8015	1.9765	.1431	.3017	.3636	.7662
.3611	.8594	.9173	2.1829	.1887	.3809	.4792	.9674
.4067	.9401	1.0331	2.3879	.2342	.4594	.5950	1.1670
.4523	1.0161	1.1490	2.5808	.2798	.5374	.7107	1.3649
.4980	1.0862	1.2648	2.7589	.3253	.6146	.8264	1.5611
.5436	1.1530	1.3806	2.9287	.3709	.6911	.9421	1.7553
.5892	1.2195	1.4965	3.0976	.4165	.7694	1.0578	1.9544
.6348	1.2854	1.6123	3.2650	.4620	.8550	1.1735	2.1718
.6804	1.3510	1.7281	3.4315	.5075	.9467	1.2892	2.4045
.7260	1.4160	1.8440	3.5967	.5531	1.0374	1.4049	2.6350
.7716	1.4806	1.9598	3.7606	.5987	1.1269	1.5206	2.8625
.7747	1.4849	1.9677	3.7717	.6442	1.2153	1.6363	3.0870
.7770	1.4877	1.9735	3.7787	.6898	1.3024	1.7520	3.3082
.7795	1.4897	1.9798	3.7838	.7353	1.3882	1.8677	3.5260
.7819	1.4908	1.9859	3.7866	.7809	1.4726	1.9834	3.7405
.7840	1.4908	1.9913	3.7867	.7840	1.4783	1.9913	3.7550
.7855	1.4899	1.9952	3.7843	.7857	1.4822	1.9958	3.7648
.7864	1.4880	1.9974	3.7794	.7864	1.4853	1.9976	3.7727
.7865	1.4865	1.9978	3.7756	.7865	1.4865	1.9978	3.7756

TABLE A-3.--Continued

ROTOR AIRFOIL COORDINATES
SECTION NO. 3 RADIUS 13.100 IN. (33.274 CM.)

SUCTION SURFACE X,IN.	Y,IN.	X,CM.	Y,CM.	PRESSURE SURFACE X,IN.	Y,IN.	X,CM.	Y,CM.
-.9574	-1.5712	-2.4319	-3.9908	-.9574	-1.5712	-2.4319	-3.9908
-.9573	-1.5695	-2.4317	-3.9867	-.9573	-1.5727	-2.4316	-3.9947
-.9566	-1.5659	-2.4297	-3.9774	-.9565	-1.5752	-2.4296	-4.0010
-.9551	-1.5622	-2.4259	-3.9679	-.9550	-1.5767	-2.4258	-4.0048
-.9389	-1.5293	-2.3848	-3.8843	-.9530	-1.5771	-2.4205	-4.0058
-.8924	-1.4353	-2.2666	-3.6457	-.9505	-1.5764	-2.4142	-4.0040
-.8458	-1.3425	-2.1484	-3.4100	-.9478	-1.5746	-2.4075	-3.9996
-.7993	-1.2509	-2.0302	-3.1773	-.9421	-1.5672	-2.3930	-3.9807
-.7528	-1.1606	-1.9120	-2.9480	-.9260	-1.5394	-2.3520	-3.9101
-.7062	-1.0718	-1.7938	-2.7224	-.8795	-1.4594	-2.2339	-3.7070
-.6597	-.9841	-1.6756	-2.4997	-.8330	-1.3796	-2.1159	-3.5041
-.6131	-.8973	-1.5574	-2.2792	-.7865	-1.2998	-1.9978	-3.3015
-.5666	-.8110	-1.4392	-2.0600	-.7400	-1.2202	-1.8797	-3.0992
-.5201	-.7251	-1.3210	-1.8417	-.6936	-1.1407	-1.7617	-2.8973
-.4735	-.6398	-1.2028	-1.6250	-.6471	-1.0613	-1.6436	-2.6956
-.4270	-.5551	-1.0846	-1.4100	-.6006	-.9822	-1.5255	-2.4948
-.3805	-.4711	-.9664	-1.1965	-.5541	-.9033	-1.4075	-2.2943
-.3339	-.3875	-.8482	-.9841	-.5076	-.8245	-1.2894	-2.0943
-.2874	-.3043	-.7300	-.7728	-.4612	-.7460	-1.1713	-1.8948
-.2409	-.2216	-.6118	-.5628	-.4147	-.6676	-1.0533	-1.6956
-.1943	-.1393	-.4935	-.3539	-.3682	-.5895	-.9352	-1.4974
-.1478	-.0576	-.3753	-.1464	-.3217	-.5117	-.8171	-1.2997
-.1012	.0237	-.2571	.0602	-.2752	-.4342	-.6991	-1.1028
-.0547	.1046	-.1389	.2658	-.2287	-.3569	-.5810	-.9066
-.0082	.1852	-.0207	.4705	-.1823	-.2800	-.4629	-.7113
.0384	.2655	.0975	.6743	-.1358	-.2034	-.3449	-.5167
.0849	.3454	.2157	.8773	-.0893	-.1272	-.2268	-.3230
.1314	.4250	.3339	1.0794	-.0428	-.0512	-.1087	-.12[illegible]
.1780	.5043	.4521	1.2808	.0037	.0244	.0093	.062[illegible]
.2245	.5833	.5703	1.4816	.0501	.0997	.1274	.2531
.2711	.6621	.6885	1.6817	.0966	.1746	.2454	.4434
.3176	.7406	.8067	1.8811	.1431	.2491	.3635	.6328
.3641	.8178	.9249	2.0773	.1896	.3233	.4816	.8212
.4107	.8898	1.0431	2.2600	.2361	.3971	.5996	1.0085
.4572	.9569	1.1613	2.4306	.2826	.4704	.7177	1.1949
.5037	1.0227	1.2795	2.5977	.3290	.5434	.8358	1.3801
.5503	1.0883	1.3977	2.7643	.3755	.6178	.9538	1.5693
.5968	1.1537	1.5159	2.9305	.4220	.7000	1.0719	1.7781
.6434	1.2190	1.6341	3.0963	.4685	.7902	1.1900	2.0070
.6899	1.2841	1.7523	3.2617	.5150	.8801	1.3080	2.2356
.7364	1.3491	1.8706	3.4267	.5615	.9696	1.4261	2.4628
.7830	1.4138	1.9888	3.5912	.6079	1.0583	1.5442	2.6880
.7867	1.4190	1.9981	3.6042	.6544	1.1461	1.6622	2.91[illegible]
.7894	1.4221	2.0050	3.6122	.7009	1.2332	1.7803	3.1323
.7923	1.4244	2.0124	3.6181	.7474	1.3193	1.8984	3.3511
.7951	1.4257	2.0195	3.6213	.7939	1.4046	2.0164	3.5677
.7975	1.4258	2.0257	3.6214	.7976	1.4113	2.0258	3.5848
.7993	1.4246	2.0303	3.6185	.7996	1.4157	2.0309	3.5958
.8003	1.4224	2.0328	3.6129	.8004	1.4193	2.0330	3.6050
.8005	1.4207	2.0332	3.6086	.8005	1.4207	2.0332	3.6086

TABLE A-3.--Continued

ROTOR AIRFOIL COORDINATES
SECTION NO. 4 RADIUS 12.750 IN. (32.385 CM.)

SUCTION SURFACE X,IN.	SUCTION SURFACE Y,IN.	SUCTION SURFACE X,CM.	SUCTION SURFACE Y,CM.	PRESSURE SURFACE X,IN.	PRESSURE SURFACE Y,IN.	PRESSURE SURFACE X,CM.	PRESSURE SURFACE Y,CM.
-.9760	-1.5335	-2.4792	-3.8951	-.9760	-1.5335	-2.4792	-3.8951
-.9759	-1.5314	-2.4788	-3.8897	-.9759	-1.5351	-2.4789	-3.8993
-.9749	-1.5271	-2.4763	-3.8788	-.9750	-1.5381	-2.4766	-3.9067
-.9731	-1.5227	-2.4717	-3.8676	-.9733	-1.5399	-2.4722	-3.9113
-.9572	-1.4914	-2.4314	-3.7881	-.9708	-1.5404	-2.4659	-3.9126
-.9097	-1.3983	-2.3107	-3.5518	-.9679	-1.5396	-2.4584	-3.9106
-.8622	-1.3064	-2.1900	-3.3184	-.9647	-1.5376	-2.4504	-3.9054
-.8147	-1.2157	-2.0694	-3.0878	-.9578	-1.5288	-2.4328	-3.8833
-.7672	-1.1261	-1.9487	-2.8604	-.9419	-1.5026	-2.3925	-3.8166
-.7197	-1.0378	-1.8280	-2.6361	-.8944	-1.4239	-2.2717	-3.6167
-.6722	-.9506	-1.7073	-2.4146	-.8468	-1.3454	-2.1508	-3.4173
-.6247	-.8643	-1.5866	-2.1954	-.7992	-1.2671	-2.0300	-3.2185
-.5771	-.7787	-1.4659	-1.9780	-.7516	-1.1892	-1.9092	-3.0205
-.5296	-.6939	-1.3453	-1.7624	-.7041	-1.1115	-1.7884	-2.8233
-.4821	-.6099	-1.2246	-1.5491	-.6565	-1.0342	-1.6675	-2.6268
-.4346	-.5267	-1.1039	-1.3379	-.6089	-.9572	-1.5467	-2.4313
-.3871	-.4443	-.9832	-1.1285	-.5614	-.8805	-1.4259	-2.2366
-.3396	-.3624	-.8625	-.9206	-.5138	-.8043	-1.3050	-2.0429
-.2921	-.2812	-.7418	-.7142	-.4662	-.7284	-1.1842	-1.8501
-.2445	-.2006	-.6212	-.5095	-.4187	-.6529	-1.0634	-1.6583
-.1970	-.1207	-.5005	-.3066	-.3711	-.5777	-.9425	-1.4675
-.1495	-.0414	-.3798	-.1051	-.3235	-.5030	-.8217	-1.2777
-.1020	.0374	-.2591	.0949	-.2759	-.4287	-.7009	-1.0890
-.0545	.1156	-.1384	.2937	-.2284	-.3549	-.5800	-.9013
-.0070	.1934	-.0178	.4912	-.1808	-.2814	-.4592	-.7148
.0405	.2707	.1029	.6875	-.1332	-.2084	-.3384	-.5294
.0880	.3475	.2236	.8826	-.0856	-.1358	-.2175	-.3450
.1355	.4239	.3443	1.0767	-.0381	-.0637	-.0967	-.1618
.1831	.5000	.4650	1.2699	.0095	.0079	.0241	.0202
.2306	.5757	.5857	1.4623	.0571	.0792	.1450	.2011
.2781	.6511	.7063	1.6537	.1046	.1499	.2658	.3807
.3256	.7242	.8270	1.8395	.1522	.2202	.3866	.5592
.3731	.7920	.9477	2.0117	.1998	.2900	.5075	.7365
.4206	.8556	1.0684	2.1732	.2474	.3593	.6283	.9126
.4681	.9183	1.1891	2.3325	.2949	.4281	.7491	1.0875
.5157	.9809	1.3098	2.4915	.3425	.4965	.8699	1.2611
.5632	1.0434	1.4305	2.6502	.3901	.5647	.9906	1.4345
.6107	1.1058	1.5512	2.8088	.4377	.6397	1.1116	1.6249
.6582	1.1682	1.6718	2.9672	.4852	.7254	1.2325	1.8425
.7057	1.2305	1.7925	3.1255	.5328	.8137	1.3533	2.0667
.7532	1.2929	1.9132	3.2839	.5804	.9020	1.4741	2.2910
.8007	1.3552	2.0339	3.4423	.6279	.9905	1.5949	2.5156
.8050	1.3609	2.0448	3.4566	.6755	1.0785	1.7158	2.7393
.8095	1.3658	2.0561	3.4693	.7231	1.1660	1.8366	2.9617
.8143	1.3695	2.0682	3.4785	.7706	1.2532	1.9575	3.1830
.8188	1.3714	2.0799	3.4833	.8182	1.3398	2.0783	3.4032
.8228	1.3714	2.0899	3.4834	.8225	1.3476	2.0892	3.4230
.8257	1.3695	2.0973	3.4786	.8260	1.3551	2.0980	3.4420
.8273	1.3659	2.1013	3.4694	.8274	1.3609	2.1015	3.4566
.8275	1.3632	2.1019	3.4626	.8275	1.3632	2.1019	3.4626

TABLE A-3.--Continued

ROTOR AIRFOIL COORDINATES
SECTION NO. 5 RADIUS 12.400 IN. (31.496 CM.)

SUCTION SURFACE				PRESSURE SURFACE			
X,IN.	Y,IN.	X,CM.	Y,CM.	X,IN.	Y,IN.	X,CM.	Y,CM.
-.9921	-1.4870	-2.5199	-3.7770	-.9921	-1.4870	-2.5199	-3.7770
-.9919	-1.4841	-2.5193	-3.7695	-.9920	-1.4889	-2.5196	-3.7818
-.9905	-1.4786	-2.5160	-3.7556	-.9909	-1.4926	-2.5168	-3.7913
-.9881	-1.4729	-2.5099	-3.7412	-.9886	-1.4950	-2.5111	-3.7973
-.9729	-1.4435	-2.4711	-3.6666	-.9855	-1.4957	-2.5031	-3.7992
-.9245	-1.3513	-2.3484	-3.4324	-.9817	-1.4948	-2.4934	-3.7967
-.8762	-1.2602	-2.2256	-3.2010	-.9776	-1.4922	-2.4830	-3.7902
-.8279	-1.1702	-2.1029	-2.9723	-.9686	-1.4813	-2.4602	-3.7625
-.7796	-1.0813	-1.9802	-2.7466	-.9533	-1.4569	-2.4214	-3.7005
-.7313	-.9936	-1.8575	-2.5238	-.9048	-1.3795	-2.2982	-3.5040
-.6830	-.9069	-1.7348	-2.3036	-.8563	-1.3025	-2.1749	-3.3084
-.6347	-.8212	-1.6121	-2.0860	-.8077	-1.2260	-2.0516	-3.1139
-.5864	-.7365	-1.4894	-1.8707	-.7592	-1.1498	-1.9284	-2.9205
-.5380	-.6527	-1.3666	-1.6579	-.7107	-1.0741	-1.8051	-2.7283
-.4897	-.5700	-1.2439	-1.4477	-.6621	-.9989	-1.6818	-2.5371
-.4414	-.4881	-1.1212	-1.2399	-.6136	-.9241	-1.5586	-2.3472
-.3931	-.4071	-.9985	-1.0341	-.5651	-.8498	-1.4353	-2.1585
-.3448	-.3269	-.8758	-.8304	-.5165	-.7760	-1.3120	-1.9710
-.2965	-.2476	-.7531	-.6288	-.4680	-.7027	-1.1887	-1.7848
-.2482	-.1691	-.6304	-.4294	-.4195	-.6299	-1.0655	-1.5999
-.1999	-.0914	-.5076	-.2321	-.3709	-.5576	-.9422	-1.4163
-.1516	-.0144	-.3849	-.0366	-.3224	-.4859	-.8189	-1.2341
-.1032	.0619	-.2622	.1572	-.2739	-.4147	-.6957	-1.0532
-.0549	.1375	-.1395	.3491	-.2254	-.3440	-.5724	-.8738
-.0066	.2124	-.0168	.5394	-.1768	-.2739	-.4491	-.6957
.0417	.2867	.1059	.7281	-.1283	-.2044	-.3259	-.5190
.0900	.3603	.2286	.9153	-.0798	-.1354	-.2026	-.3439
.1383	.4335	.3513	1.1011	-.0312	-.0670	-.0793	-.1701
.1866	.5061	.4741	1.2855	.0173	.0008	.0439	.0022
.2349	.5778	.5968	1.4676	.0658	.0681	.1672	.1729
.2833	.6447	.7195	1.6376	.1144	.1347	.2905	.3422
.3316	.7067	.8422	1.7949	.1629	.2008	.4137	.5099
.3799	.7658	.9649	1.9451	.2114	.2662	.5370	.6761
.4282	.8245	1.0876	2.0943	.2599	.3310	.6603	.8407
.4765	.8830	1.2103	2.2428	.3085	.3952	.7835	1.0038
.5248	.9412	1.3330	2.3905	.3570	.4588	.9068	1.1653
.5731	.9991	1.4558	2.5377	.4055	.5217	1.0301	1.3251
.6214	1.0568	1.5785	2.6842	.4541	.5865	1.1533	1.4898
.6698	1.1143	1.7012	2.8303	.5026	.6610	1.2766	1.6790
.7181	1.1716	1.8239	2.9759	.5511	.7463	1.3999	1.8956
.7664	1.2288	1.9466	3.1212	.5997	.8319	1.5231	2.1130
.8147	1.2859	2.0693	3.2662	.6482	.9182	1.6464	2.3323
.8197	1.2918	2.0821	3.2812	.6967	1.0042	1.7697	2.5507
.8272	1.2993	2.1011	3.3003	.7453	1.0900	1.8930	2.7685
.8350	1.3046	2.1208	3.3136	.7938	1.1754	2.0162	2.9854
.8423	1.3073	2.1395	3.3205	.8423	1.2604	2.1395	3.2015
.8486	1.3070	2.1554	3.3198	.8473	1.2692	2.1522	3.2238
.8531	1.3038	2.1668	3.3118	.8531	1.2811	2.1670	3.2541
.8555	1.2981	2.1729	3.2971	.8555	1.2903	2.1730	3.2773
.8558	1.2943	2.1737	3.2876	.8558	1.2943	2.1737	3.2876

TABLE A-3.--Continued

ROTOR AIRFOIL COORDINATES
SECTION NO. 6 RADIUS 12.000 IN. (30.480 CM.)

SUCTION SURFACE				PRESSURE SURFACE			
X,IN.	Y,IN.	X,CM.	Y,CM.	X,IN.	Y,IN.	X,CM.	Y,CM.
-1.0030	-1.4452	-2.5476	-3.6707	-1.0030	-1.4452	-2.5476	-3.6707
-1.0027	-1.4416	-2.5469	-3.6617	-1.0029	-1.4470	-2.5474	-3.6753
-1.0012	-1.4355	-2.5430	-3.6462	-1.0017	-1.4512	-2.5444	-3.6859
-.9984	-1.4293	-2.5360	-3.6304	-.9993	-1.4538	-2.5382	-3.6927
-.9838	-1.4021	-2.4988	-3.5612	-.9958	-1.4547	-2.5294	-3.6948
-.9351	-1.3121	-2.3753	-3.3329	-.9916	-1.4537	-2.5186	-3.6923
-.8865	-1.2231	-2.2517	-3.1066	-.9870	-1.4509	-2.5069	-3.6853
-.8379	-1.1349	-2.1282	-2.8826	-.9768	-1.4389	-2.4810	-3.6547
-.7892	-1.0475	-2.0046	-2.6607	-.9621	-1.4162	-2.4438	-3.5973
-.7406	-.9609	-1.8811	-2.4408	-.9131	-1.3408	-2.3193	-3.4056
-.6919	-.8753	-1.7575	-2.2233	-.8641	-1.2656	-2.1947	-3.2150
-.6433	-.7906	-1.6340	-2.0082	-.8150	-1.1912	-2.0702	-3.0256
-.5946	-.7069	-1.5104	-1.7957	-.7660	-1.1171	-1.9457	-2.8375
-.5460	-.6242	-1.3869	-1.5855	-.7170	-1.0435	-1.8211	-2.6505
-.4974	-.5425	-1.2633	-1.3779	-.6679	-.9704	-1.6966	-2.4648
-.4487	-.4616	-1.1398	-1.1726	-.6189	-.8978	-1.5721	-2.2804
-.4001	-.3818	-1.0162	-.9697	-.5699	-.8257	-1.4475	-2.0972
-.3514	-.3029	-.8927	-.7693	-.5209	-.7541	-1.3230	-1.9154
-.3028	-.2250	-.7691	-.5714	-.4718	-.6831	-1.1984	-1.7350
-.2542	-.1480	-.6456	-.3758	-.4228	-.6125	-1.0739	-1.5559
-.2055	-.0718	-.5220	-.1824	-.3738	-.5426	-.9494	-1.3782
-.1569	.0035	-.3985	.0089	-.3247	-.4732	-.8248	-1.2020
-.1082	.0780	-.2749	.1981	-.2757	-.4044	-.7003	-1.0272
-.0596	.1517	-.1514	.3852	-.2267	-.3361	-.5757	-.8536
-.0109	.2245	-.0278	.5703	-.1776	-.2684	-.4512	-.6818
.0377	.2966	.0957	.7533	-.1286	-.2013	-.3267	-.5114
.0863	.3679	.2193	.9345	-.0796	-.1348	-.2021	-.3424
.1350	.4384	.3428	1.1135	-.0306	-.0689	-.0776	-.1750
.1836	.5048	.4664	1.2822	.0185	-.0036	.0470	-.0092
.2322	.5658	.5899	1.4371	.0675	.0610	.1715	.1550
.2809	.6229	.7135	1.5823	.1165	.1250	.2960	.3175
.3295	.6792	.8370	1.7253	.1656	.1883	.4206	.4784
.3782	.7350	.9606	1.8669	.2146	.2510	.5451	.6375
.4268	.7903	1.0841	2.0073	.2636	.3129	.6696	.7946
.4755	.8450	1.2077	2.1463	.3127	.3741	.7942	.9502
.5241	.8993	1.3312	2.2841	.3617	.4346	.9187	1.1038
.5727	.9530	1.4548	2.4207	.4107	.4942	1.0433	1.2553
.6214	1.0064	1.5783	2.5562	.4598	.5534	1.1678	1.4055
.6700	1.0592	1.7019	2.6905	.5088	.6179	1.2924	1.5694
.7187	1.1117	1.8254	2.8237	.5578	.6925	1.4169	1.7589
.7673	1.1637	1.9490	2.9558	.6069	.7746	1.5414	1.9674
.8159	1.2154	2.0725	3.0870	.6559	.8563	1.6660	2.1749
.8219	1.2217	2.0876	3.1030	.7049	.9377	1.7905	2.3819
.8322	1.2309	2.1138	3.1266	.7539	1.0190	1.9150	2.5882
.8428	1.2373	2.1406	3.1428	.8030	1.1000	2.0396	2.7939
.8526	1.2403	2.1655	3.1503	.8520	1.1807	2.1641	2.9990
.8607	1.2395	2.1862	3.1484	.8580	1.1905	2.1792	3.0238
.8665	1.2351	2.2009	3.1372	.8657	1.2053	2.1989	3.0616
.8694	1.2274	2.2083	3.1177	.8691	1.2172	2.2076	3.0917
.8697	1.2234	2.2090	3.1076	.8697	1.2234	2.2090	3.1076

TABLE A-3.--Continued

ROTOR AIRFOIL COORDINATES
SECTION NO. 7 RADIUS 11.700 IN. (29.718 CM.)

SUCTION SURFACE X,IN.	Y,IN.	X,CM.	Y,CM.	PRESSURE SURFACE X,IN.	Y,IN.	X,CM.	Y,CM.
-1.0005	-1.4010	-2.5413	-3.5585	-1.0005	-1.4010	-2.5413	-3.5585
-1.0002	-1.3977	-2.5406	-3.5501	-1.0004	-1.4024	-2.5411	-3.5621
-.9988	-1.3924	-2.5369	-3.5366	-.9995	-1.4061	-2.5386	-3.5714
-.9963	-1.3869	-2.5306	-3.5228	-.9973	-1.4084	-2.5333	-3.5774
-.9822	-1.3615	-2.4949	-3.4581	-.9943	-1.4092	-2.5255	-3.5794
-.9336	-1.2740	-2.3712	-3.2360	-.9906	-1.4084	-2.5160	-3.5773
-.8849	-1.1873	-2.2476	-3.0157	-.9865	-1.4060	-2.5057	-3.5713
-.8362	-1.1013	-2.1240	-2.7974	-.9773	-1.3955	-2.4825	-3.5445
-.7876	-1.0160	-2.0004	-2.5807	-.9633	-1.3743	-2.4467	-3.4907
-.7389	-.9315	-1.8768	-2.3659	-.9143	-1.3011	-2.3224	-3.3047
-.6902	-.8477	-1.7532	-2.1533	-.8654	-1.2284	-2.1981	-3.1201
-.6416	-.7650	-1.6296	-1.9431	-.8164	-1.1562	-2.0738	-2.9367
-.5929	-.6832	-1.5060	-1.7354	-.7675	-1.0846	-1.9495	-2.7548
-.5442	-.6023	-1.3824	-1.5299	-.7186	-1.0134	-1.8252	-2.5742
-.4956	-.5223	-1.2587	-1.3268	-.6696	-.9429	-1.7008	-2.3949
-.4469	-.4433	-1.1351	-1.1261	-.6207	-.8728	-1.5765	-2.2169
-.3982	-.3653	-1.0115	-.9278	-.5717	-.8032	-1.4522	-2.0403
-.3496	-.2882	-.8879	-.7321	-.5228	-.7342	-1.3279	-1.8649
-.3009	-.2121	-.7643	-.5387	-.4739	-.6656	-1.2036	-1.6908
-.2522	-.1369	-.6407	-.3476	-.4249	-.5976	-1.0793	-1.5179
-.2036	-.0625	-.5171	-.1588	-.3760	-.5300	-.9550	-1.3463
-.1549	.0110	-.3935	.0278	-.3270	-.4629	-.8307	-1.1759
-.1062	.0836	-.2699	.2123	-.2781	-.3963	-.7063	-1.0067
-.0576	.1554	-.1463	.3946	-.2291	-.3302	-.5820	-.8357
-.0089	.2263	-.0227	.5749	-.1802	-.2645	-.4577	-.6718
.0398	.2965	.1010	.7531	-.1313	-.1993	-.3334	-.5062
.0884	.3658	.2246	.9290	-.0823	-.1345	-.2091	-.3417
.1371	.4307	.3482	1.0941	-.0334	-.0702	-.0848	-.1783
.1858	.4904	.4718	1.2457	.0156	-.0064	.0395	-.0162
.2344	.5464	.5954	1.3878	.0645	.0570	.1639	.1449
.2831	.6015	.7190	1.5278	.1134	.1200	.2882	.3047
.3317	.6560	.8426	1.6663	.1624	.1825	.4125	.4634
.3804	.7100	.9662	1.8033	.2113	.2445	.5368	.6210
.4291	.7634	1.0898	1.9389	.2603	.3060	.6611	.7773
.4777	.8162	1.2135	2.0731	.3092	.3671	.7854	.9324
.5264	.8685	1.3371	2.2060	.3582	.4277	.9097	1.0863
.5751	.9203	1.4607	2.3375	.4071	.4877	1.0340	1.2388
.6237	.9715	1.5843	2.4677	.4560	.5473	1.1583	1.3901
.6724	1.0223	1.7079	2.5966	.5050	.6094	1.2826	1.5479
.7211	1.0725	1.8315	2.7242	.5539	.6787	1.4070	1.7239
.7697	1.1222	1.9551	2.8505	.6029	.7555	1.5313	1.9190
.8184	1.1715	2.0787	2.9756	.6518	.8330	1.6556	2.1158
.8249	1.1780	2.0952	2.9921	.7007	.9104	1.7799	2.3124
.8335	1.1854	2.1170	3.0108	.7497	.9877	1.9042	2.5089
.8422	1.1904	2.1392	3.0235	.7986	1.0649	2.0285	2.7050
.8502	1.1926	2.1596	3.0291	.8476	1.1420	2.1529	2.9007
.8569	1.1918	2.1764	3.0271	.8541	1.1522	2.1693	2.9266
.8615	1.1881	2.1883	3.0177	.8604	1.1638	2.1854	2.9562
.8637	1.1818	2.1939	3.0017	.8634	1.1734	2.1924	2.9805
.8639	1.1790	2.1943	2.9947	.8639	1.1790	2.1943	2.9947

TABLE A-3.--Contin.ed

ROTOR AIRFOIL COORDINATES
SECTION NO. 8 RADIUS 11.000 IN. (27.940 CM.)

SUCTION SURFACE X,IN.	Y,IN.	X,CM.	Y,CM.	PRESSURE SURFACE X,IN.	Y,IN.	X,CM.	Y,CM.
-.9868	-1.3093	-2.5064	-3.3256	-.9868	-1.3093	-2.5064	-3.3256
-.9864	-1.3062	-2.5056	-3.3178	-.9867	-1.3102	-2.5063	-3.3279
-.9852	-1.3018	-2.5023	-3.3065	-.9860	-1.3133	-2.5043	-3.3356
-.9830	-1.2972	-2.4967	-3.2949	-.9842	-1.3153	-2.4999	-3.3409
-.9705	-1.2757	-2.4651	-3.2404	-.9817	-1.3160	-2.4934	-3.3428
-.9223	-1.1930	-2.3425	-3.0302	-.9785	-1.3154	-2.4854	-3.3412
-.8740	-1.1109	-2.2200	-2.8216	-.9750	-1.3135	-2.4766	-3.3363
-.8258	-1.0293	-2.0975	.6145	-.9670	-1.3047	-2.4563	-3.3139
-.7775	-.9483	-1.9750	[illegible]	-.9546	-1.2869	-2.4246	-3.2686
-.7293	-.8679	-1.8524	-2.2046	-.9064	-1.2183	-2.3022	-3.0945
-.6810	-.7884	-1.7299	-2.0025	-.8582	-1.1503	-2.1798	-2.9218
-.6328	-.7096	-1.6073	-1.8024	-.8100	-1.0829	-2.0573	-2.7505
-.5846	-.6315	-1.4848	-1.6041	-.7617	-1.0160	-1.9348	-2.5807
-.5363	-.5543	-1.3623	-1.4079	-.7135	-.9497	-1.8124	-2.4123
-.4881	-.4781	-1.2397	-1.2143	-.6653	-.8839	-1.6900	-2.2451
-.4395	-.4030	-1.1172	-1.0235	-.6171	-.8186	-1.5675	-2.0792
-.3916	-.3288	-.9947	-.8353	-.5689	-.7537	-1.4451	-1.9145
-.3434	-.2557	-.8722	-.6495	-.5207	-.6894	-1.3226	-1.7510
-.2951	-.1835	-.7496	-.4660	-.4725	-.6254	-1.2002	-1.5886
-.2469	-.1122	-.6271	-.2850	-.4243	-.5619	-1.0777	-1.4272
-.1986	-.0418	-.5045	-.1061	-.3761	-.4988	-.9553	-1.2669
-.1504	.0277	-.3820	.0704	-.3279	-.4360	-.8328	-1.1075
-.1022	.0964	-.2595	.2448	-.2797	-.3736	-.7104	-.9490
-.0539	.1642	-.1370	.4170	-.2315	-.3116	-.5880	-.7914
-.0057	.2295	-.0144	.5830	-.1833	-.2498	-.4655	-.6345
.0426	.2895	.1081	.7352	-.1351	-.1884	-.3431	-.4785
.0908	.3448	.2307	.8759	-.0869	-.1272	-.2206	-.3230
.1390	.3983	.3532	1.0116	-.0386	-.0662	-.0982	-.1683
.1873	.4511	.4757	1.1457	.0096	-.0055	.0243	-.0141
.2355	.5032	.5982	1.2782	.0578	.0549	.1467	.1395
.2838	.5548	.7208	1.4092	.1060	.1152	.2692	.2927
.3320	.6058	.8433	1.5387	.1542	.1754	.3916	.4454
.3803	.6562	.9659	1.6667	.2024	.2353	.5140	.5977
.4285	.7060	1.0884	1.7933	.2506	.2951	.6365	.7497
.4767	.7553	1.2109	1.9185	.2988	.3549	.7590	.9013
.5250	.8040	1.3334	2.0423	.3470	.4145	.8814	1.0528
.5732	.8522	1.4560	2.1647	.3952	.4740	1.0038	1.2039
.6215	.8999	1.5785	2.2857	.4434	.5339	1.1263	1.3560
.6697	.9470	1.7010	2.4055	.4916	.5962	1.2487	1.5144
.7179	.9937	1.8236	2.5239	.5398	.6617	1.3712	1.6807
.7662	1.0398	1.9461	2.6410	.5880	.7289	1.4936	1.8513
.8144	1.0854	2.0687	2.7569	.6362	.7962	1.6161	2.0223
.8221	1.0926	2.0881	2.7752	.6844	.8638	1.7385	2.1940
.8267	1.0963	2.0998	2.7845	.7327	.9316	1.8610	2.3662
.8313	1.0987	2.1116	2.7907	.7809	.9997	1.9834	2.5391
.8355	1.0997	[illegible]	2.7933	.8291	1.0680	2.1058	2.7127
.8390	1.0992	[illegible]	2.7919	.8367	1.0789	2.1253	2.7403
.8413	1.0972	2.1370	2.7868	.8402	1.0846	2.1340	2.7548
.8423	1.0938	2.1395	2.7784	.8419	1.0895	2.1385	2.7674
.8424	1.0930	2.1396	2.7761	.8424	1.0950	2.1396	2.7761

TABLE A-3.--Continued

ROTOR AIRFOIL COORDINATES
SECTION NO. 9 RADIUS 10.300 IN. (26.162 CM.)

SUCTION SURFACE X,IN.	Y,IN.	X,CM.	Y CM.	PRESSURE SURFACE X,IN.	Y,IN.	X,CM.	Y,CM.
-.9752	-1.2190	-2.4770	-3.0962	-.9752	-1.2190	-2.4770	-3.0962
-.9748	-1.2155	-2.4760	-3.0873	-.9752	-1.[illegible]97	-2.4770	-3.0979
-.9734	-1.2108	-2.4724	-3.0754	-.9744	-1[illegible]50	-2.4750	-3.1064
-.9710	-1.2060	-2.4662	-3.0632	-.9726	-1[illegible]51	-2.4705	-3.1119
-.9601	-1.1881	-2.4388	-3.0177	-.9699	-1.2260	-2.4656	-3.1140
-.9119	-1.1085	-2.3164	-2.8156	-.9666	-1.2254	-2.4551	-3.1124
-.8638	-1.0296	-2.1940	-2.6152	-.9628	-1.2234	-2.4456	-3.1075
-.8156	-.9512	-2.0715	-2.4161	-.9541	-1.2142	-2.4235	-3.0840
-.7674	-.8734	-1.9491	-2.2185	-.9433	-1.1994	-2.3960	-3.0464
-.7192	-.7963	-1.8267	-2.0227	-.8952	-1.1340	-2.2739	-2.8804
-.6710	-.7199	-1.7043	-1.8285	-.8471	-1.0695	-2.1517	-2.7165
-.6228	-.6440	-1.5819	-1.6357	-.7990	-1.0057	-2.0295	-2.5545
-.5746	-.5689	-1.4595	-1.4450	-.7509	-.9426	-1.9073	-2.3943
-.5264	-.4951	-1.3371	-1.2576	-.7028	-.8805	-1.7852	-2.2359
-.4782	-.4225	-1.2147	-1.0733	-.6547	-.8186	-1.6630	-2.0792
-.4301	-.3511	-1.0923	-.8919	-.6066	-.7575	-1.5408	-1.9241
-.3819	-.2809	-.9699	-.7134	-.5585	-.6970	-1.4186	-1.7705
-.3337	-.2117	-.8475	-.5377	-.5104	-.6371	-1.2965	-1.6183
-.2855	-.1436	-.7251	-.3648	-.4623	-.5777	-1.1743	-1.4674
-.2373	-.0766	-.6027	-.1947	-.4142	-.5188	-1.0521	-1.3178
-.1891	-.0107	-.4803	-.0271	-.3661	-.4604	-.9299	-1.1693
-.1409	.0537	-.3579	.1364	-.3180	-.4023	-.8078	-1.0218
-.0927	.1132	-.2355	.2877	-.2699	-.3446	-.6856	-.8754
-.0445	.1681	-.1131	.4269	-.2218	-.2873	-.5634	-.7297
.0037	.2199	.0093	.5586	-.1737	-.2302	-.4412	-.5848
.0518	.2709	.1317	.6881	-.1256	-.1734	-.3191	-.4405
.1000	.3212	.2541	.8157	-.0775	-.1168	-.1969	-.2968
.1482	.3707	.3765	.9416	-.0294	-.0604	-.0747	-.1535
.1964	.4195	.4989	1.0655	.0187	-.0041	.0474	-.0105
.2446	.4676	.6213	1.1877	.0668	.0520	.1696	.1322
.2928	.5156	.7437	1.3082	.1149	.1082	.2918	.2748
.3410	.5617	.8661	1.4268	.1630	.1643	.4140	.4173
.3892	.6078	.9885	1.5439	.2111	.2204	.5361	.5599
.4374	.6532	1.1109	1.6593	.2592	.2767	.6583	.7027
.4856	.6980	1.2333	1.7730	.3073	.3330	.7805	.8458
.5337	.7422	1.3557	1.8852	.3554	.3895	.9027	.9894
.5819	.7857	1.4781	1.9958	.4035	.4463	1.0248	1.1337
.6301	.8287	1.6005	2.1049	.4516	.5035	1.1470	1.2790
.6783	.8710	1.7229	2.2125	.4997	.5612	1.2692	1.4254
.7265	.9128	1.8453	2.3186	.5478	.6192	1.3914	1.5729
.7747	.9540	1.9677	2.4232	.5959	.6777	1.5135	1.7214
.8229	.9947	2.0901	2.5265	.6440	.7366	1.[illegible]57	1.8710
.8318	1.0022	2.1129	2.5455	.6921	.7959	1.7579	2.0217
.8365	1.0055	2.124[illegible]	2.5539	.7402	.8557	1.8801	2.1735
.8412	1.0076	2.[illegible]366	2.5594	.7883	.9159	2.0022	2.3264
.8454	1.0084	2.1472	2.5612	.8364	.9765	2.1244	2.4804
.8487	1.0076	2.1557	2.5594	.8453	.9874	2.1472	2.5092
.8509	1.0055	2.1612	2.5541	.8490	.9933	2.1566	2.5[illegible]
.8517	1.0022	2.1632	2.5457	.8510	.9980	2.1616	
.8517	1.0020	2.1632	2.5451	.8517	1.0020	2.1632	

TABLE A-3.--Continued

ROTOR AIRFOIL COORDINATES
SECTION NO. 10 RADIUS 9.600 IN. (24.384 CM.)

SUCTION SURFACE X, IN.	Y, IN.	X, CM.	Y, CM.	PRESSURE SURFACE X, IN.	Y, IN.	X, CM.	Y, CM.
-.9827	-1.1152	-2.4962	-2.8327	-.9827	-1.1152	-2.4962	-2.8327
-.9822	-1.1110	-2.4949	-2.8220	-.9827	-1.1156	-2.4962	-2.8336
-.9805	-1.1059	-2.4905	-2.8091	-.9820	-1.1192	-2.4943	-2.8429
-.9777	-1.1008	-2.4835	-2.7960	-.9801	-1.1217	-2.4895	-2.8490
-.9683	-1.0860	-2.4594	-2.7584	-.9772	-1.1227	-2.4821	-2.8516
-.9219	-1.0138	-2.3417	-2.5751	-.9735	-1.1221	-2.4727	-2.8502
-.8756	-.9424	-2.2240	-2.3938	-.9694	-1.1201	-2.4622	-2.8451
-.8292	-.8718	-2.1063	-2.2143	-.9595	-1.1102	-2.4371	-2.8199
-.7829	-.8018	-1.9885	-2.0367	-.9500	-1.0981	-2.4130	-2.7891
-.7365	-.7326	-1.8708	-1.8608	-.9010	-1.0359	-2.2886	-2.6312
-.6902	-.6639	-1.7531	-1.6862	-.8520	-.9749	-2.1641	-2.4763
-.6438	-.5958	-1.6354	-1.5134	-.8030	-.9150	-2.0396	-2.3240
-.5975	-.5289	-1.5177	-1.3435	-.7540	-.8561	-1.9152	-2.1745
-.5512	-.4633	-1.3999	-1.1768	-.7050	-.7982	-1.7907	-2.0274
-.5048	-.3988	-1.2822	-1.0130	-.6560	-.7412	-1.6662	-1.8827
-.4585	-.3356	-1.1645	-.8524	-.6070	-.6851	-1.5417	-1.7403
-.4121	-.2737	-1.0468	-.6951	-.5580	-.6299	-1.4173	-1.5999
-.3658	-.2130	-.9291	-.5411	-.5090	-.5753	-1.2928	-1.4613
-.3194	-.1536	-.8113	-.3901	-.4600	-.5215	-1.1683	-1.3246
-.2731	-.0953	-.6936	-.2421	-.4110	-.4684	-1.0438	-1.1897
-.2267	-.0402	-.5759	-.1022	-.3620	-.4159	-.9194	-1.0563
-.1804	.0110	-.4582	.0281	-.3130	-.3639	-.7949	-.9244
-.1340	.0591	-.3404	.1500	-.2639	-.3125	-.6704	-.7938
-.0877	.1056	-.2227	.2684	-.2150	-.2616	-.5460	-.6643
-.0413	.1514	-.1050	.3845	-.1659	-.2110	-.4215	-.5359
.0050	.1962	.0127	.4984	-.1169	-.1600	-.2970	-.4064
.0513	.2402	.1303	.6102	-.0679	-.1109	-.1725	-.2816
.0977	.2834	.2482	.7199	-.0189	-.0612	-.0481	-.1554
.1441	.3258	.3659	.8276	.0301	-.0116	.0764	-.0296
.1904	.3674	.4836	.9332	.0791	.0378	.2009	.0959
.2367	.4082	.6013	1.0369	.1281	.0871	.3253	.2213
.2831	.4483	.7190	1.1386	.1771	.1365	.4498	.3467
.3294	.4876	.8368	1.2385	.2261	.1860	.5743	.4723
.3758	.5261	.9545	1.3364	.2751	.2355	.6988	.5982
.4221	.5640	1.0722	1.4325	.3241	.2853	.8232	.7246
.4685	.6011	1.1899	1.5268	.3731	.3355	.9477	.8521
.5148	.6375	1.3077	1.6193	.4221	.3861	1.0722	.9806
.5612	.6732	1.4254	1.7101	.4711	.4371	1.1966	1.1103
.6075	.7083	1.5431	1.7991	.5201	.4887	1.3211	1.2412
.6539	.7427	1.6608	1.8864	.5691	.5407	1.4456	1.3733
.7002	.7764	1.7785	1.9721	.6181	.5932	1.5701	1.5067
.7466	.8095	1.8963	2.0561	.6671	.6462	1.6945	1.6413
.8391	.8736	2.1313	2.2190	.7161	.6997	1.8190	1.7771
.8494	.8806	2.1574	2.2367	.7651	.7537	1.9435	1.9143
.8548	.8837	2.1713	2.2445	.8141	.8082	2.0679	2.0528
.8601	.8855	2.1846	2.2491	.8631	.8632	2.1924	2.1926
.8647	.8858	2.1963	2.2500	.8676	.8691	2.2038	2.2074
.8682	.8847	2.2053	2.2471	.8701	.8740	2.2101	2.2200
.8704	.8822	2.2108	2.2408	.8711	.8785	2.2125	2.2315
.8711	.8789	2.2125	2.2325	.8711	.8789	2.2125	2.2325

TABLE A-3.--Continued

ROTOR AIRFOIL COORDINATES
SECTION NO. 11 RADIUS 8.900 IN. (22.606 CM.)

SUCTION SURFACE				PRESSURE SURFACE			
X,IN.	Y,IN.	X,CM.	Y,CM.	X,IN.	Y,IN.	X,CM.	Y,CM.
-.9976	-.9789	-2.5340	-2.4863	-.9976	-.9789	-2.5340	-2.4863
-.9976	-.9787	-2.5340	-2.4859	-.9970	-.9828	-2.5323	-2.4962
-.9969	-.9737	-2.5320	-2.4731	-.9950	-.9855	-2.5272	-2.5032
-.9948	-.9681	-2.5267	-2.4590	-.9918	-.9868	-2.5191	-2.5064
-.9915	-.9625	-2.5184	-2.4448	-.9877	-.9863	-2.5087	-2.5053
-.9440	-.8943	-2.3979	-2.2716	-.9830	-.9843	-2.4968	-2.5002
-.8966	-.8273	-2.2773	-2.1014	-.9715	-.9739	-2.4677	-2.4736
-.8491	-.7616	-2.1568	-1.9344	-.9626	-.9635	-2.4451	-2.4474
-.8017	-.6969	-2.0362	-1.7702	-.9133	-.9069	-2.3197	-2.3036
-.7542	-.6334	-1.9157	-1.6087	-.8645	-.8525	-2.1959	-2.1653
-.7068	-.5707	-1.7952	-1.4495	-.8158	-.7993	-2.0721	-2.0303
-.6593	-.5092	-1.6746	-1.2933	-.7671	-.7475	-1.9484	-1.8987
-.6118	-.4493	-1.5541	-1.1411	-.7183	-.6969	-1.8246	-1.7701
-.5644	-.3909	-1.4336	-.9928	-.6696	-.6474	-1.7008	-1.6445
-.5169	-.3339	-1.3130	-.8482	-.6209	-.5991	-1.5771	-1.5216
-.4695	-.2786	-1.1925	-.7076	-.5722	-.5517	-1.4533	-1.4014
-.4220	-.2246	-1.0719	-.5705	-.5234	-.5054	-1.3295	-1.2836
-.3746	-.1720	-.9514	-.4370	-.4747	-.4599	-1.2058	-1.1681
-.3271	-.1209	-.8309	-.3071	-.4260	-.4153	-1.0820	-1.0548
-.2797	-.0725	-.7103	-.1841	-.3773	-.3714	-.9582	-.9434
-.2322	-.0269	-.5898	-.0682	-.3285	-.3280	-.8344	-.8330
-.1847	.0163	-.4692	.0413	-.2798	-.2858	-.7107	-.7258
-.1373	.0580	-.3487	.1474	-.2311	-.2438	-.5869	-.6193
-.0898	.0987	-.2282	.2508	-.1823	-.2024	-.4631	-.5142
-.0424	.1384	-.1076	.3516	-.1336	-.1615	-.3394	-.4102
.0051	.1772	.0129	.4500	-.0849	-.1210	-.2156	-.3074
.0525	.2149	.1335	.5459	-.0362	-.0807	-.0918	-.2051
.1000	.2517	.2540	.6393	.0126	-.0408	.0319	-.1036
.1475	.2876	.3745	.7305	.0613	-.0010	.1557	-.0027
.1949	.3226	.4951	.8193	.1100	.0386	.2795	.0980
.2424	.3567	.6156	.9059	.1587	.0781	.4032	.1985
.2898	.3899	.7361	.9903	.2075	.1177	.5270	.2990
.3373	.4223	.8567	1.0726	.2562	.1574	.6506	.3997
.3847	.4538	.9772	1.1527	.3049	.1972	.7745	.5009
.4322	.4846	1.0978	1.2308	.3537	.2374	.8983	.6031
.4796	.5145	1.2183	1.3069	.4024	.2781	1.0221	.7065
.5271	.5437	1.3389	1.3810	.4511	.3193	1.1458	.8110
.5746	.5721	1.4594	1.4532	.4998	.3610	1.2696	.9169
.6220	.5998	1.5799	1.5235	.5486	.4031	1.3934	1.0240
.6695	.6266	1.7005	1.5917	.5973	.4459	1.5171	1.1325
.7169	.6526	1.8210	1.6577	.6460	.4891	1.6409	1.2423
.7644	.6779	1.9416	1.7218	.6948	.5328	1.7647	1.3534
.8649	.7287	2.1969	1.8509	.7435	.5770	1.8885	1.4657
.8761	.7341	2.2253	1.8647	.7922	.6217	2.0122	1.5791
.8826	.7367	2.2417	1.8712	.8409	.6669	2.1360	1.6938
.8886	.7378	2.2570	1.8741	.8897	.7125	2.2598	1.8098
.8937	.7375	2.2699	1.8732	.8951	.7184	2.2737	1.8246
.8974	.7357	2.2795	1.8688	.8984	.7236	2.2818	1.8380
.8995	.7326	2.2849	1.8609	.8999	.7285	2.2857	1.8504
.9000	.7300	2.2859	1.8541	.9000	.7300	2.2859	1.8541

TABLE A-3.--Continued

ROTOR AIRFOIL COORDINATES
SECTION NO. 12 RADIUS 8.200 IN. (20.828 CM.)

SUCTION SURFACE X, IN.	Y, IN.	X, CM.	Y, CM.	PRESSURE SURFACE X, IN.	Y, IN.	X, CM.	Y, CM.
-1.0131	-.8556	-2.5732	-2.1731	-1.0131	-.8556	-2.5732	-2.1731
-1.0131	-.8549	-2.5732	-2.1716	-1.0125	-.8594	-2.5717	-2.1829
-1.0121	-.8495	-2.5707	-2.1577	-1.0104	-.8625	-2.5665	-2.1908
-1.0096	-.8435	-2.5644	-2.1425	-1.0069	-.8640	-2.5576	-2.1946
-1.0059	-.8375	-2.5549	-2.1272	-1.0024	-.8637	-2.5461	-2.1939
-.9573	-.7720	-2.4316	-1.9608	-.9972	-.8618	-2.5330	-2.1889
-.9088	-.7084	-2.3083	-1.7994	-.9842	-.8508	-2.4999	-2.1611
-.8602	-.6469	-2.1849	-1.6431	-.9756	-.8417	-2.4781	-2.1379
-.8116	-.5872	-2.0616	-1.4915	-.9261	-.7898	-2.3524	-2.0060
-.7631	-.5292	-1.9383	-1.3442	-.8762	-.7391	-2.2255	-1.8772
-.7145	-.4729	-1.8149	-1.2012	-.8263	-.6899	-2.0988	-1.7523
-.6660	-.4183	-1.6916	-1.0625	-.7764	-.6423	-1.9720	-1.6313
-.6174	-.3654	-1.5683	-.9281	-.7264	-.5960	-1.8452	-1.5140
-.5689	-.3142	-1.4450	-.7980	-.6765	-.5512	-1.7184	-1.4001
-.5203	-.2645	-1.3216	-.6718	-.6266	-.5077	-1.5916	-1.2896
-.4718	-.2163	-1.1983	-.5493	-.5767	-.4655	-1.4647	-1.1823
-.4232	-.1694	-1.0750	-.4303	-.5267	-.4244	-1.3379	-1.0781
-.3747	-.1241	-.9516	-.3151	-.4768	-.3845	-1.2111	-.9766
-.3261	-.0808	-.8283	-.2051	-.4269	-.3456	-1.0844	-.8779
-.2775	-.0396	-.7050	-.1007	-.3770	-.3078	-.9576	-.7817
-.2290	-.0006	-.5816	-.0017	-.3271	-.2708	-.8306	-.6879
-.1804	.0367	-.4583	.0932	-.2771	-.2348	-.7039	-.5963
-.1319	.0727	-.3350	.1846	-.2272	-.1995	-.5771	-.5068
-.0833	.1073	-.2117	.2726	-.1773	-.1650	-.4503	-.4191
-.0348	.1407	-.0883	.3574	-.1274	-.1312	-.3235	-.3331
.0138	.1728	.0350	.4390	-.0775	-.0979	-.1967	-.2487
.0623	.2037	.1583	.5175	-.0275	-.0652	-.0700	-.1656
.1109	.2335	.2817	.5930	.0224	-.0330	.0568	-.0837
.1595	.2620	.4050	.6655	.0723	-.0011	.1837	-.0028
.2080	.2895	.5283	.7352	.1222	.0304	.3105	.0771
.2566	.3159	.6517	.8023	.1722	.0616	.4373	.1565
.3051	.3412	.7750	.8667	.2221	.0927	.5641	.2354
.3537	.3655	.8983	.9283	.2720	.1237	.6909	.3142
.4022	.3887	1.0217	.9873	.3219	.1548	.8177	.3933
.4508	.4109	1.1450	1.0437	.3716	.1862	.9445	.4730
.4993	.4320	1.2683	1.0974	.4218	.2178	1.0713	.5532
.5479	.4522	1.3916	1.1486	.4717	.2496	1.1981	.6341
.5964	.4714	1.5150	1.1973	.5216	.2817	1.3249	.7155
.6450	.4896	1.6383	1.2435	.5715	.3139	1.4517	.7974
.6936	.5068	1.7616	1.2872	.6214	.3464	1.5785	.8799
.7421	.5231	1.8850	1.3286	.6714	.3791	1.7053	.9629
.7907	.5384	2.0083	1.3675	.7213	.4119	1.8321	1.0463
.8977	.5689	2.2802	1.4450	.7712	.4450	1.9589	1.1303
.9096	.5720	2.3104	1.4529	.8211	.4782	2.0857	1.2147
.9172	.5733	2.3297	1.4563	.8710	.5117	2.2125	1.2996
.9240	.5733	2.3470	1.4561	.9210	.5453	2.3393	1.3850
.9295	.5718	2.3609	1.4524	.9275	.5504	2.3559	1.3981
.9332	.5691	2.3704	1.4455	.9320	.5556	2.3673	1.4111
.9349	.5655	2.3748	1.4358	.9345	.5606	2.3737	1.4240
.9350	.5639	2.3750	1.4324	.9350	.5639	2.3750	1.4324

TABLE A-3.--Continued

ROTOR AIRFOIL COORDINATES
SECTION NO. 13 RADIUS 7.500 IN. (19.050 CM.)

SUCTION SURFACE X,IN.	Y,IN.	X,CM.	Y,CM.	PRESSURE SURFACE X,IN.	Y,IN.	X,CM.	Y,CM.
-1.0067	-.7599	-2.5570	-1.9301	-1.0067	-.7599	-2.5570	-1.9301
-1.0067	-.7589	-2.5569	-1.9277	-1.0061	-.7637	-2.5556	-1.9396
-1.0055	-.7531	-2.5540	-1.9130	-1.0040	-.7671	-2.5501	-1.9483
-1.0028	-.7468	-2.5471	-1.8969	-1.0003	-.7688	-2.5408	-1.9528
-.9987	-.7405	-2.5367	-1.8808	-.9955	-.7686	-2.5286	-1.9523
-.9527	-.6806	-2.4199	-1.7287	-.9900	-.7667	-2.5145	-1.9475
-.9067	-.6228	-2.3031	-1.5819	-.9756	-.7556	-2.4782	-1.9192
-.8607	-.5671	-2.1863	-1.4405	-.9672	-.7472	-2.4566	-1.8979
-.8147	-.5135	-2.0694	-1.3043	-.9175	-.6989	-2.3304	-1.7752
-.7687	-.4617	-1.9526	-1.1726	-.8667	-.6512	-2.2014	-1.6540
-.7228	-.4117	-1.8358	-1.0458	-.8159	-.6050	-2.0725	-1.5366
-.6768	-.3635	-1.7190	-.9234	-.7652	-.5604	-1.9435	-1.4235
-.6308	-.3169	-1.6022	-.8049	-.7144	-.5173	-1.8146	-1.3139
-.5848	-.2719	-1.4854	-.6906	-.6636	-.4756	-1.6856	-1.2080
-.5388	-.2284	-1.3685	-.5802	-.6128	-.4353	-1.5566	-1.1057
-.4928	-.1864	-1.2517	-.4735	-.5621	-.3963	-1.4277	-1.0067
-.4468	-.1458	-1.1349	-.3704	-.5113	-.3587	-1.2987	-.9111
-.4008	-.1067	-1.0181	-.2709	-.4605	-.3223	-1.1698	-.8186
-.3548	-.0691	-.9013	-.1755	-.4098	-.2870	-1.0408	-.7290
-.3088	-.0332	-.7844	-.0844	-.3590	-.2529	-.9119	-.6424
-.2628	.0010	-.6676	.0026	-.3082	-.2199	-.7829	-.5585
-.2168	.0335	-.5508	.0850	-.2575	-.1879	-.6539	-.4773
-.1709	.0645	-.4340	.1639	-.2067	-.1569	-.5250	-.3985
-.1249	.0942	-.3172	.2392	-.1559	-.1268	-.3960	-.3221
-.0789	.1224	-.2003	.3110	-.1051	-.0976	-.2671	-.2478
-.0329	.1494	-.0835	.3793	-.0544	-.0692	-.1381	-.1757
.0131	.1750	.0333	.4444	-.0036	-.0415	-.0091	-.1054
.0591	.1992	.1501	.5060	.0472	-.0146	.1198	-.0370
.1051	.2222	.2669	.5645	.0979	.0117	.2488	.0296
.1511	.2440	.3838	.6197	.1487	.0374	.3777	.0951
.1971	.2644	.5006	.6717	.1995	.0626	.5067	.1589
.2431	.2837	.6174	.7205	.2502	.0872	.6356	.2215
.2891	.3017	.7342	.7663	.3010	.1114	.7646	.2831
.3351	.3185	.8510	.8089	.3518	.1355	.8935	.3441
.3810	.3340	.9679	.8485	.4026	.1593	1.0225	.4046
.4270	.3484	1.0847	.8850	.4533	.1829	1.1515	.4645
.4730	.3616	1.2015	.9184	.5041	.2062	1.2804	.5237
.5190	.3735	1.3183	.9487	.5549	.2292	1.4094	.5822
.5650	.3842	1.4351	.9759	.6056	.2518	1.5383	.6397
.6110	.3937	1.5520	1.0001	.6564	.2741	1.6673	.6963
.6570	.4020	1.6688	1.0212	.7072	.2960	1.7963	.7518
.7030	.4091	1.7856	1.0391	.7580	.3174	1.9252	.8062
.8255	.4218	2.0969	1.0714	.8087	.3384	2.0542	.8594
.9360	.4255	2.3775	1.0807	.8595	.3587	2.1831	.9111
.9483	.4254	2.4087	1.0806	.9103	.3785	2.3121	.9615
.9564	.4248	2.4292	1.0789	.9610	.3985	2.4410	1.0121
.9632	.4229	2.4466	1.0741	.9668	.4026	2.4558	1.0226
.9684	.4199	2.4597	1.0666	.9707	.4071	2.4655	1.0342
.9715	.4161	2.4675	1.0570	.9722	.4118	2.4695	1.0459
.9723	.4125	2.4696	1.0479	.9723	.4125	2.4696	1.0479

TABLE A-3.--Concluded

ROTOR AIRFOIL COORDINATES
SECTION NO. 14 RADIUS 6.642 IN. (16.871 CM.)

SUCTION SURFACE X,IN.	Y,IN.	X,CM.	Y,CM.	PRESSURE SURFACE X,IN.	Y,IN.	X,CM.	Y,CM.
-.9750	-.6839	-2.4765	-1.7372	-.9750	-.6839	-2.4765	-1.7372
-.9750	-.6634	-2.4764	-1.7360	-.9743	-.6883	-2.4747	-1.7483
-.9740	-.6775	-2.4740	-1.7210	-.9720	-.6917	-2.4689	-1.7569
-.9714	-.6710	-2.4674	-1.7044	-.9682	-.6934	-2.4593	-1.7612
-.9674	-.6644	-2.4573	-1.6876	-.9633	-.6932	-2.4469	-1.7609
-.9216	-.6009	-2.3408	-1.5264	-.9577	-.6913	-2.4326	-1.7559
-.8757	-.5403	-2.2243	-1.3723	-.9438	-.6805	-2.3972	-1.7284
-.8298	-.4826	-2.1078	-1.2257	-.9356	-.6724	-2.3764	-1.7078
-.7840	-.4276	-1.9913	-1.0861	-.8876	-.6256	-2.2546	-1.5890
-.7381	-.3752	-1.8748	-.9529	-.8369	-.5780	-2.1258	-1.4682
-.6922	-.3253	-1.7583	-.8263	-.7862	-.5323	-1.9970	-1.3519
-.6464	-.2779	-1.6418	-.7058	-.7355	-.4883	-1.8682	-1.2403
-.6005	-.2327	-1.5253	-.5910	-.6848	-.4461	-1.7394	-1.1331
-.5546	-.1898	-1.4088	-.4821	-.6341	-.4056	-1.6106	-1.0303
-.5088	-.1491	-1.2923	-.3787	-.5834	-.3669	-1.4818	-.9318
-.4629	-.1106	-1.1758	-.2809	-.5327	-.3297	-1.3530	-.8375
-.4170	-.0741	-1.0593	-.1883	-.4820	-.2942	-1.2242	-.7472
-.3712	-.0396	-.9427	-.1007	-.4313	-.2602	-1.0954	-.6609
-.3253	-.0070	-.8263	-.0178	-.3806	-.2278	-.9666	-.5785
-.2794	.0238	-.7098	.0605	-.3299	-.1968	-.8378	-.4998
-.2336	.0529	-.5932	.1345	-.2792	-.1672	-.7090	-.4248
-.1877	.0804	-.4768	.2043	-.2285	-.1391	-.5803	-.3533
-.1418	.1063	-.3602	.2700	-.1777	-.1123	-.4515	-.2853
-.0960	.1305	-.2437	.3315	-.1270	-.0868	-.3227	-.2206
-.0501	.1531	-.1272	.3890	-.0763	-.0626	-.1939	-.1591
-.0042	.1742	-.0107	.4425	-.0256	-.0397	-.0651	-.1008
.0416	.1938	.1058	.4921	.0251	-.0179	.0637	-.0456
.0875	.2118	.2223	.5379	.0758	.0027	.1925	.0068
.1334	.2283	.3388	.5799	.1265	.0221	.3213	.0562
.1792	.2433	.4553	.6181	.1772	.0406	.4501	.1031
.2251	.2569	.5718	.6525	.2279	.0581	.5789	.1477
.2710	.2690	.6883	.6833	.2786	.0750	.7077	.1906
.3168	.2797	.8048	.7103	.3293	.0914	.8365	.2322
.3627	.2889	.9213	.7337	.3800	.1073	.9653	.2725
.4086	.2966	1.0378	.7534	.4307	.1225	1.0941	.3112
.4544	.3029	1.1543	.7694	.4814	.1370	1.2229	.3480
.5003	.3078	1.2708	.7817	.5321	.1508	1.3517	.3831
.5462	.3112	1.3873	.7903	.5828	.1639	1.4804	.4163
.5920	.3131	1.5038	.7952	.6336	.1761	1.6092	.4474
.6379	.3135	1.6203	.7964	.6843	.1876	1.7380	.4764
.6838	.3125	1.7368	.7938	.7350	.1981	1.8668	.5032
.7296	.3100	1.8533	.7873	.7857	.2077	1.9956	.5277
.8558	.2952	2.1737	.7498	.8364	.2164	2.1244	.5497
.9697	.2717	2.4630	.6900	.8871	.2241	2.2532	.5691
.9824	.2684	2.4952	.6819	.9378	.2307	2.3820	.5860
.9906	.2656	2.5162	.6747	.9885	.2370	2.5108	.6020
.9973	.2618	2.5332	.6651	.9957	.2398	2.5290	.6090
1.0019	.2574	2.5450	.6538	1.0009	.2435	2.5423	.6184
1.0042	.2526	2.5506	.6417	1.0038	.2479	2.5497	.6296
1.0043	.2509	2.5510	.6372	1.0043	.2509	2.5510	.6372

TABLE A-4

BLADE-TO-DISC ATTACHMENT STRESSES

	Blade				Disc			
	Allowable	Nominal	Peak	Margin of safety	Allowable	Nominal	Peak	Margin of safety
Neck tension or tang bending	87.4 (603×10^6)	39.9 (275×10^6)	50.7 (350×10^6)	0.72	87.4 (603×10^6)	66.2 (457×10^6)	82.8 (571×10^6)	0.06
Combined fillet	127.6 (875×10^6)	75.7 (522×10^6)	94.7 (654×10^6)	0.35	127.6 (875×10^6)	102.7 (708×10^6)	124.2 (857×10^6)	0.02
Maximum fillet	130.0 (897×10^6)	0. (0.)	139.3 (961×10^6)	0.87	130.0 ($897 . 10^6$)	0. (0.)	192.0 (1325×10^6)	0.35
Bearing	121.3 (838×10^6)	52.2 (360×10^6)	78.6 (542×10^6)	0.54	121.3 (838×10^6)	51.8 (357×10^6)	77.9 (537×10^6)	0.56
Shear	50.7 (350×10^6)	25.3 (174×10^6)	29.6 (204×10^6)	0.67	50.7 (350×10^6)	23.8 (164×10^6)	27.8 (192×10^6)	0.77

Notes:

1. All stresses are in ksi (N/m^2).
2. All stresses are calculated at 110 percent design speed (14 100 rpm or 1477 rad/sec).
3. Margin of safety is based on the larger of 1.2 times the nominal stress or the calculated peak stress.
4. Margin of safety = (allowable stress/calculated stress) - 1.
5. Allowable stresses include:

   5 percent reduction for surface finish and loading rate (except for combined fillet).
   4.5 percent reduction for broach angle.
6. Allowable maximum fillet stress is 1/2 amplitude equivalent elastic stress.

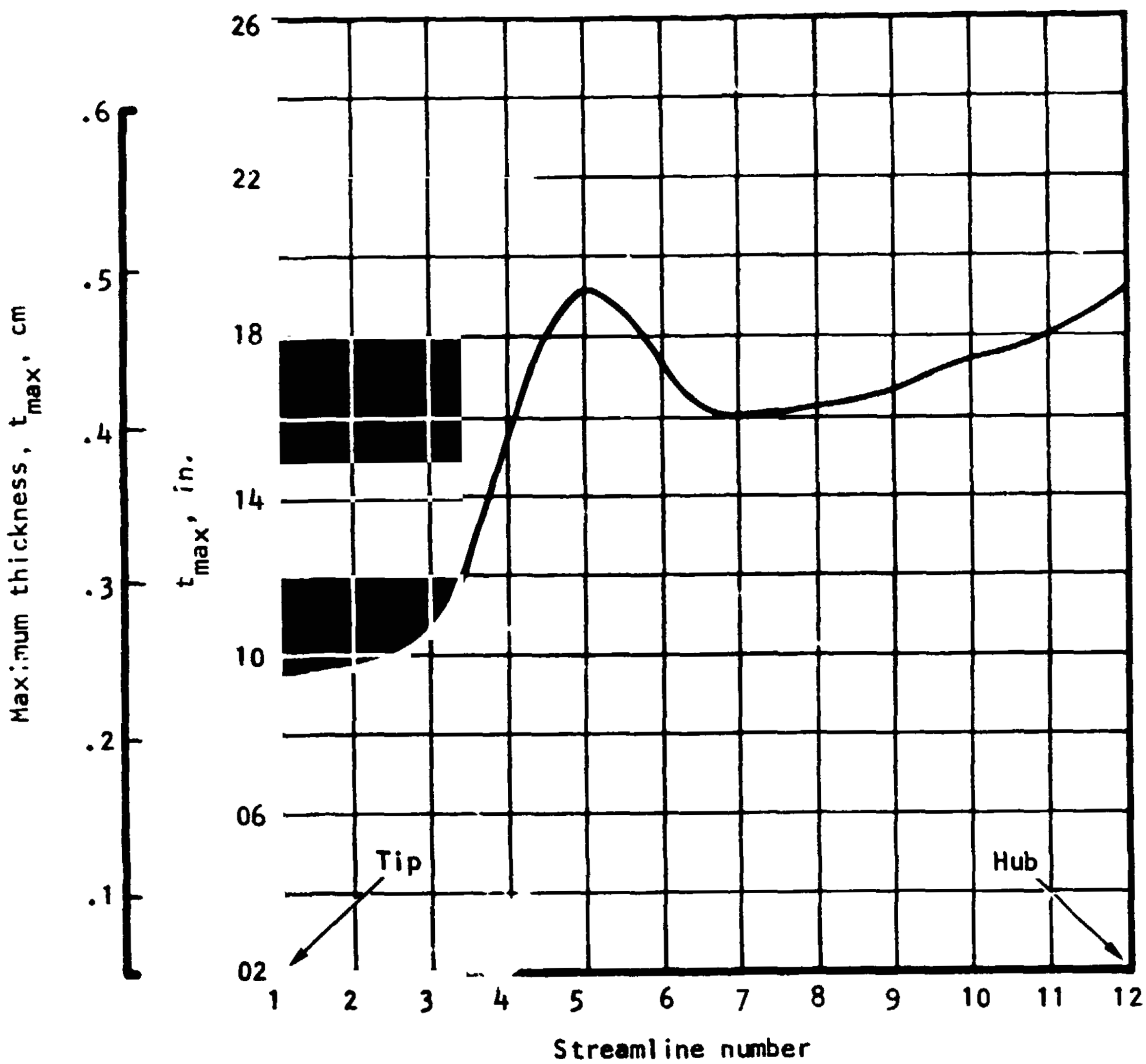

S-80697

Figure A-1.--Rotor Blade Maximum Thickness Distribution.

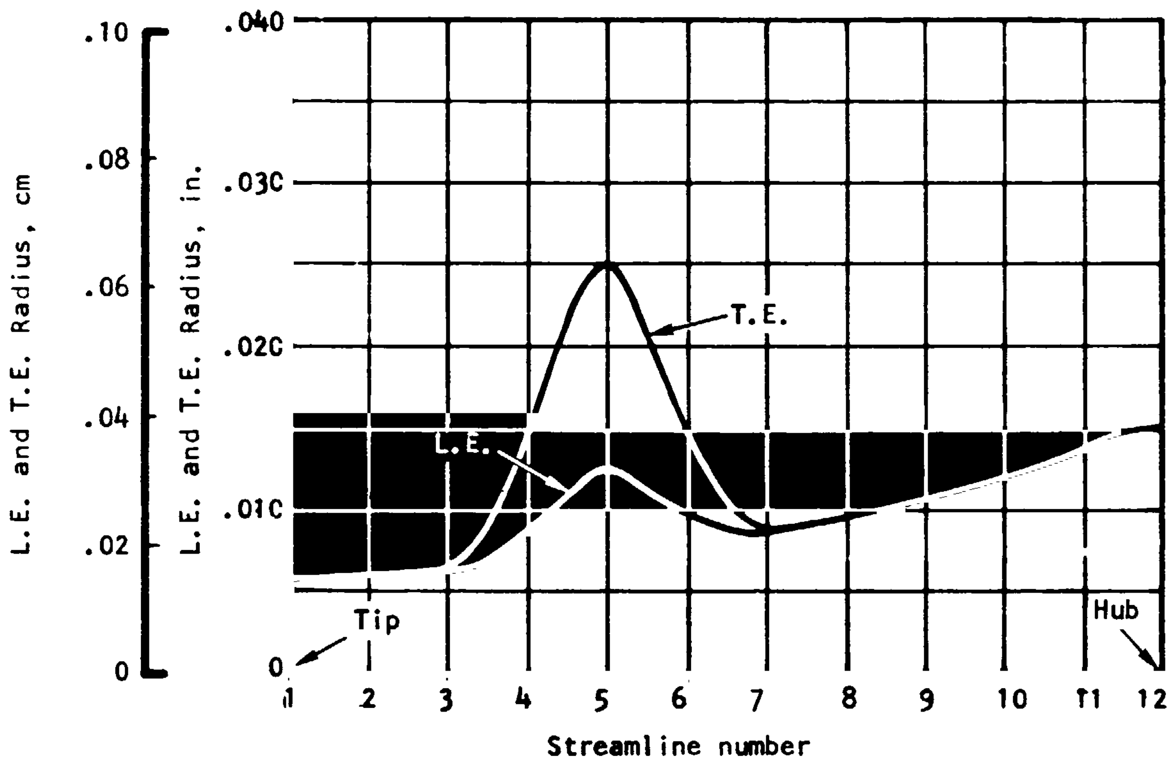

Figure A-2.--Rotor Blade Leading- and Trailing-Edge Radii.

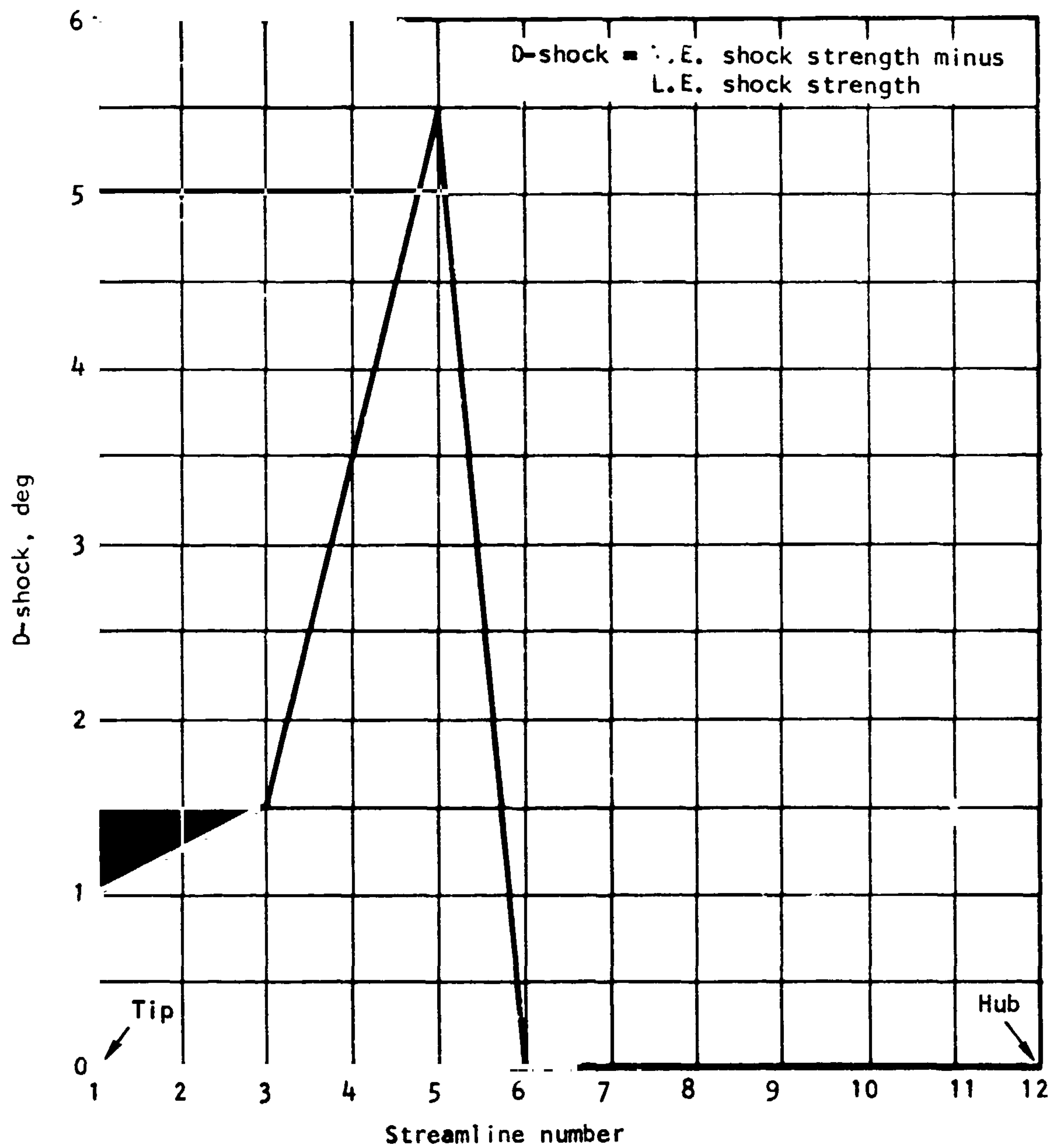

S-80558

Figure A-3.--Rotor Blade Trailing-Edge Shock Strength Minus Leading-Edge Shock Strength.

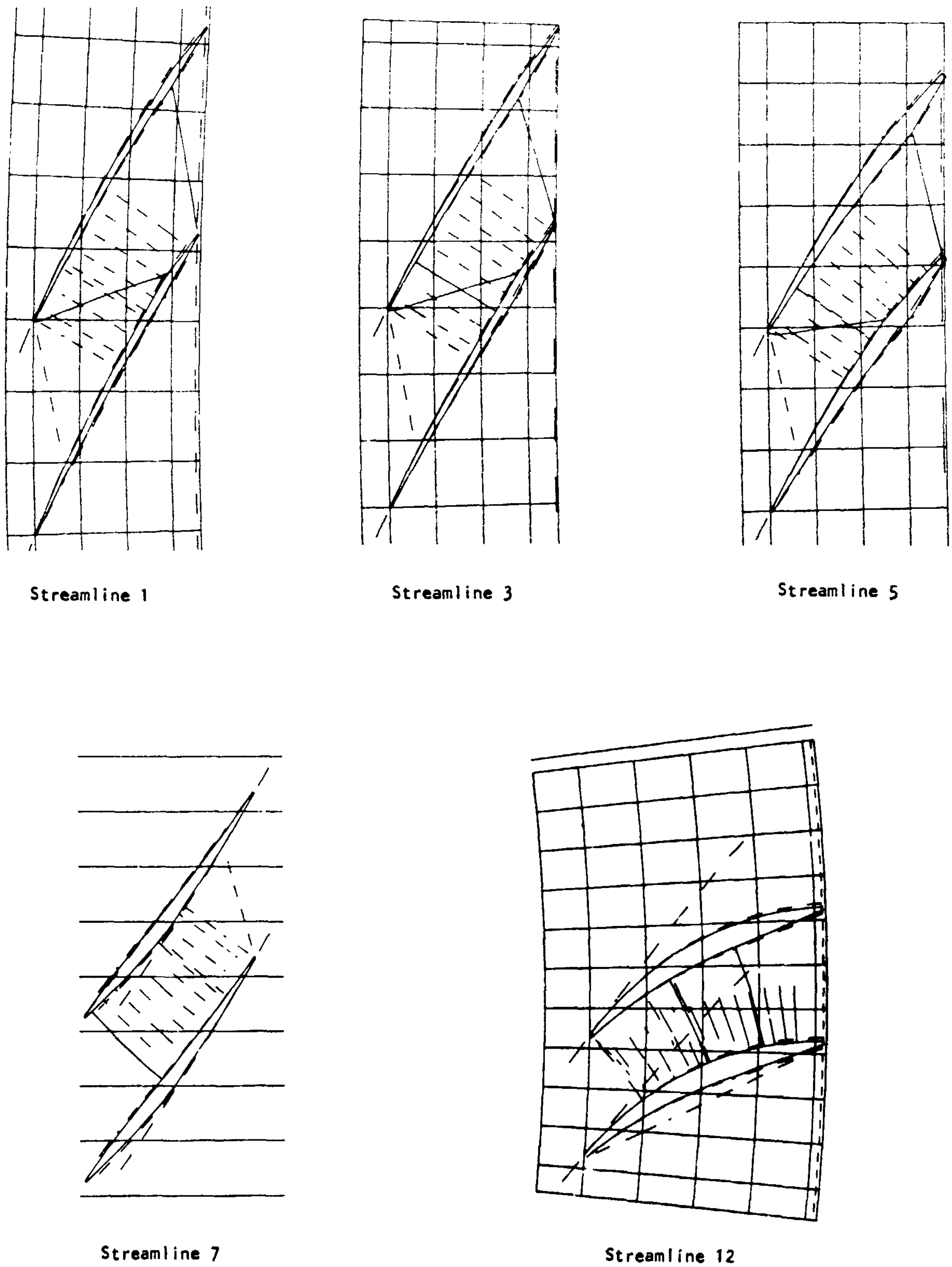

S-82824

Figure A-4.--Rotor Blade Conical Development.

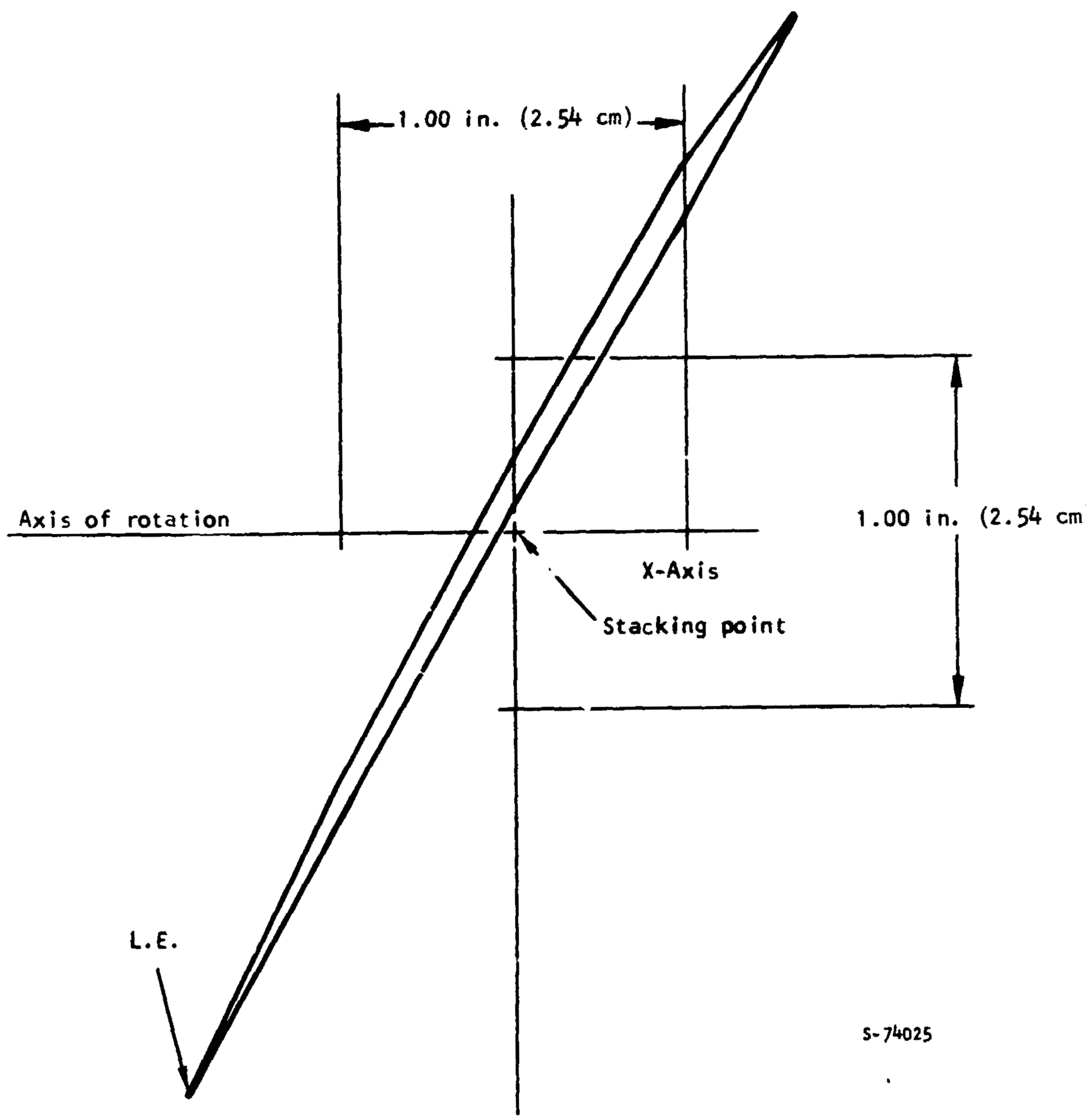

Figure A-5.--Typical Rotor Blade Section.

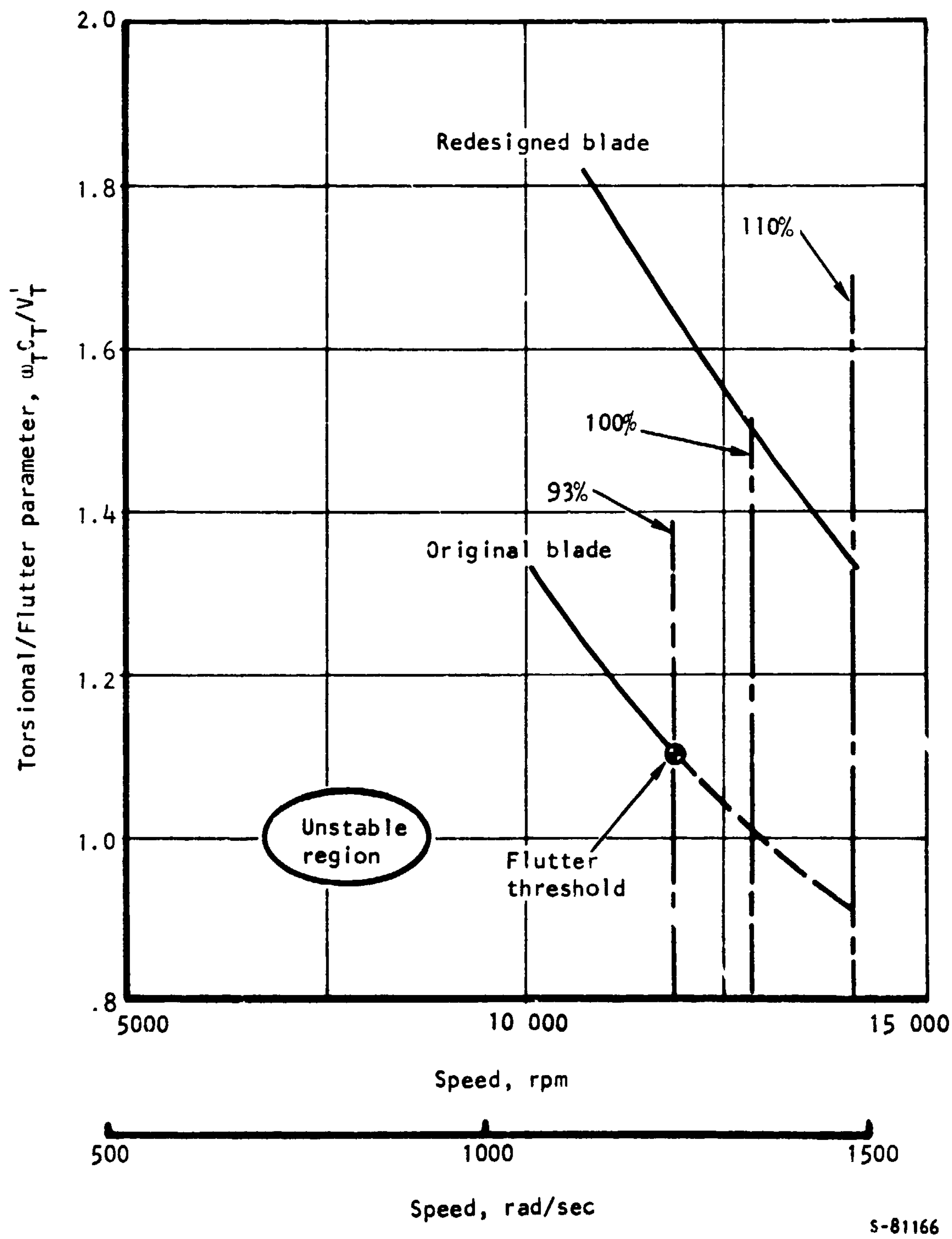

Figure A-6.--Fan Blade Torsional Flutter Parameter.

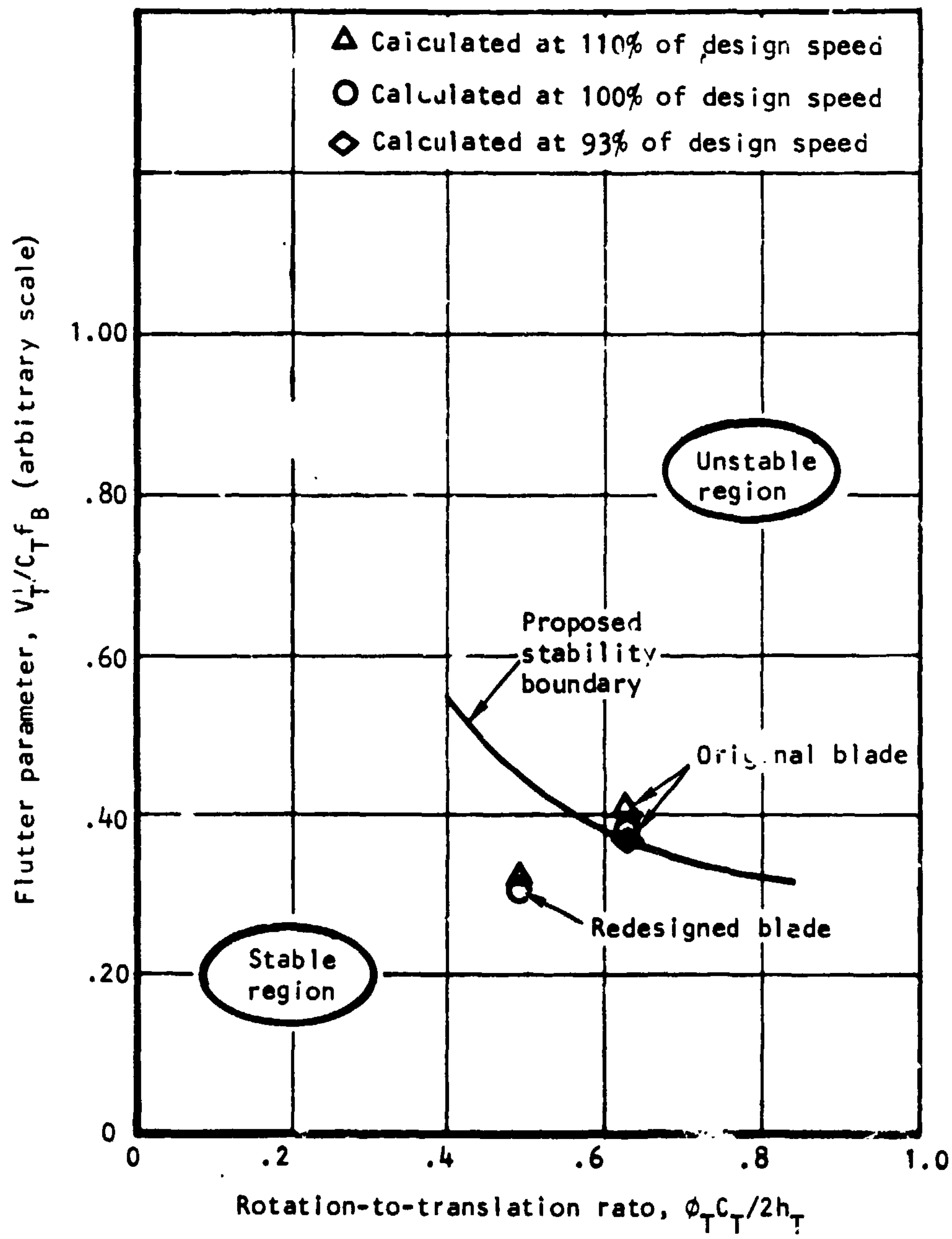

S-806?9

Figure A-7.--Fan Blade Coupled Flexural-Torsional Flutter Parameter.

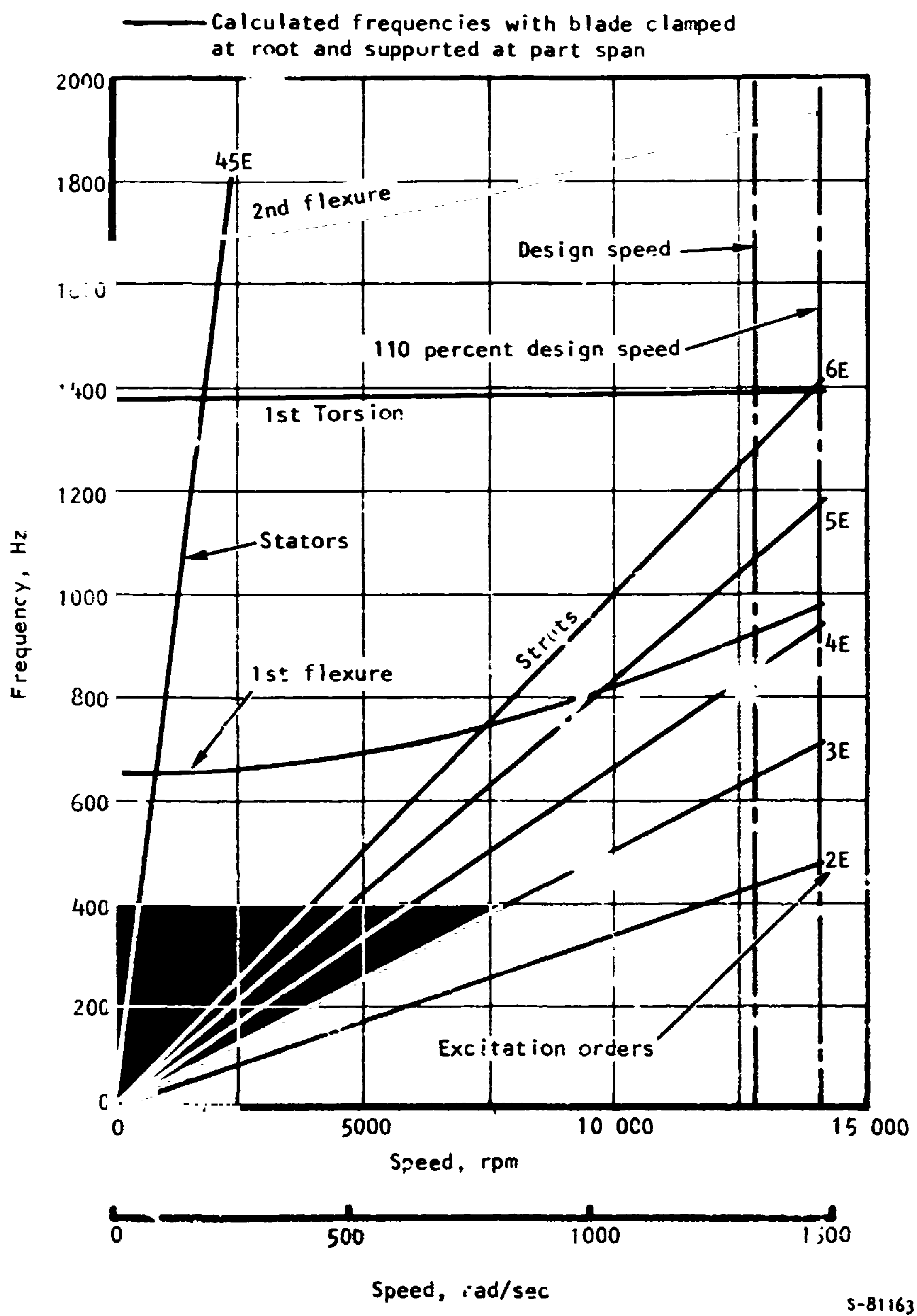

Figure A-8.--Fan Blade Excitation Diagram.

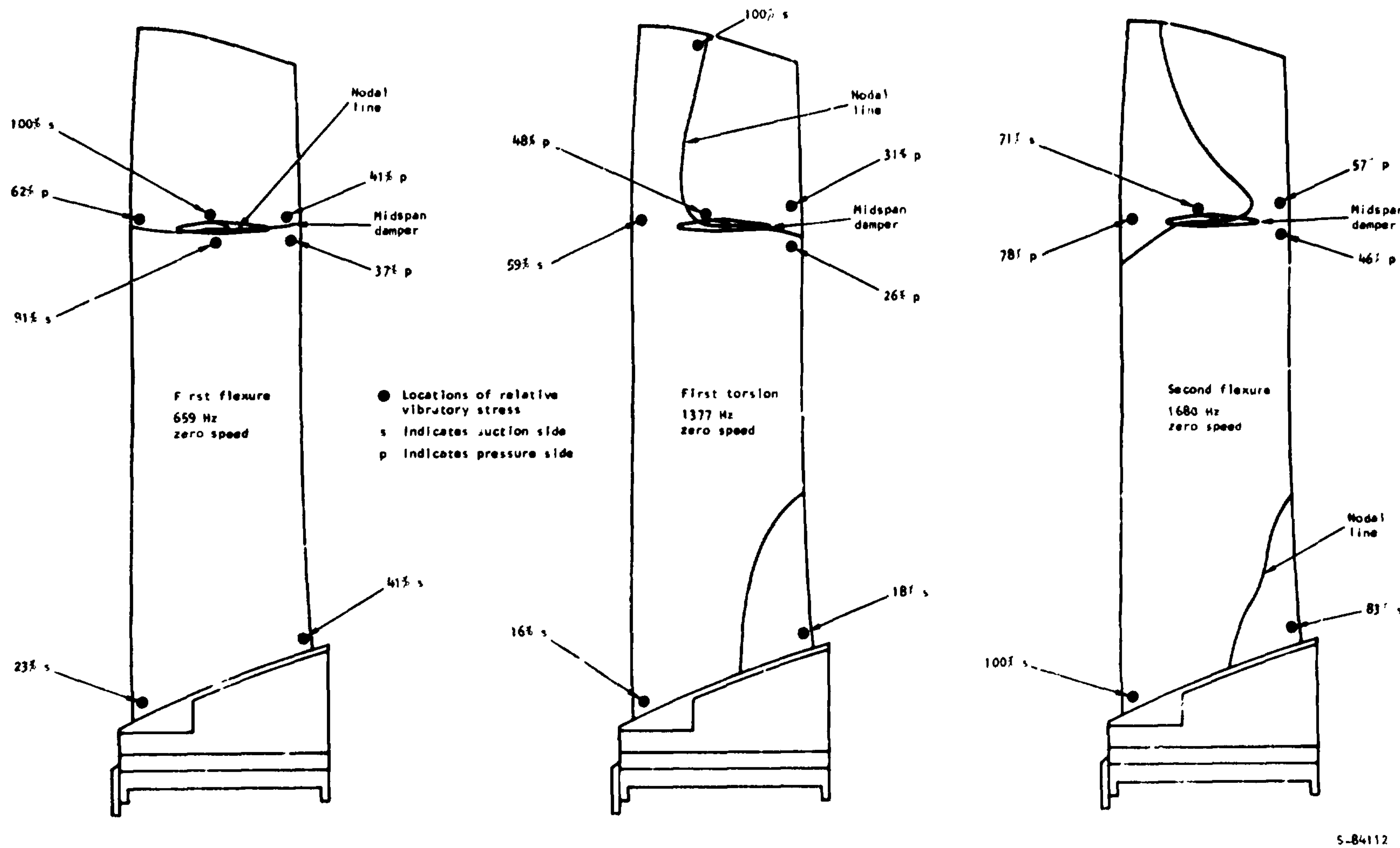

Figure A-9.--Fan Blade Mode Shapes and Relative Vibratory Stress.

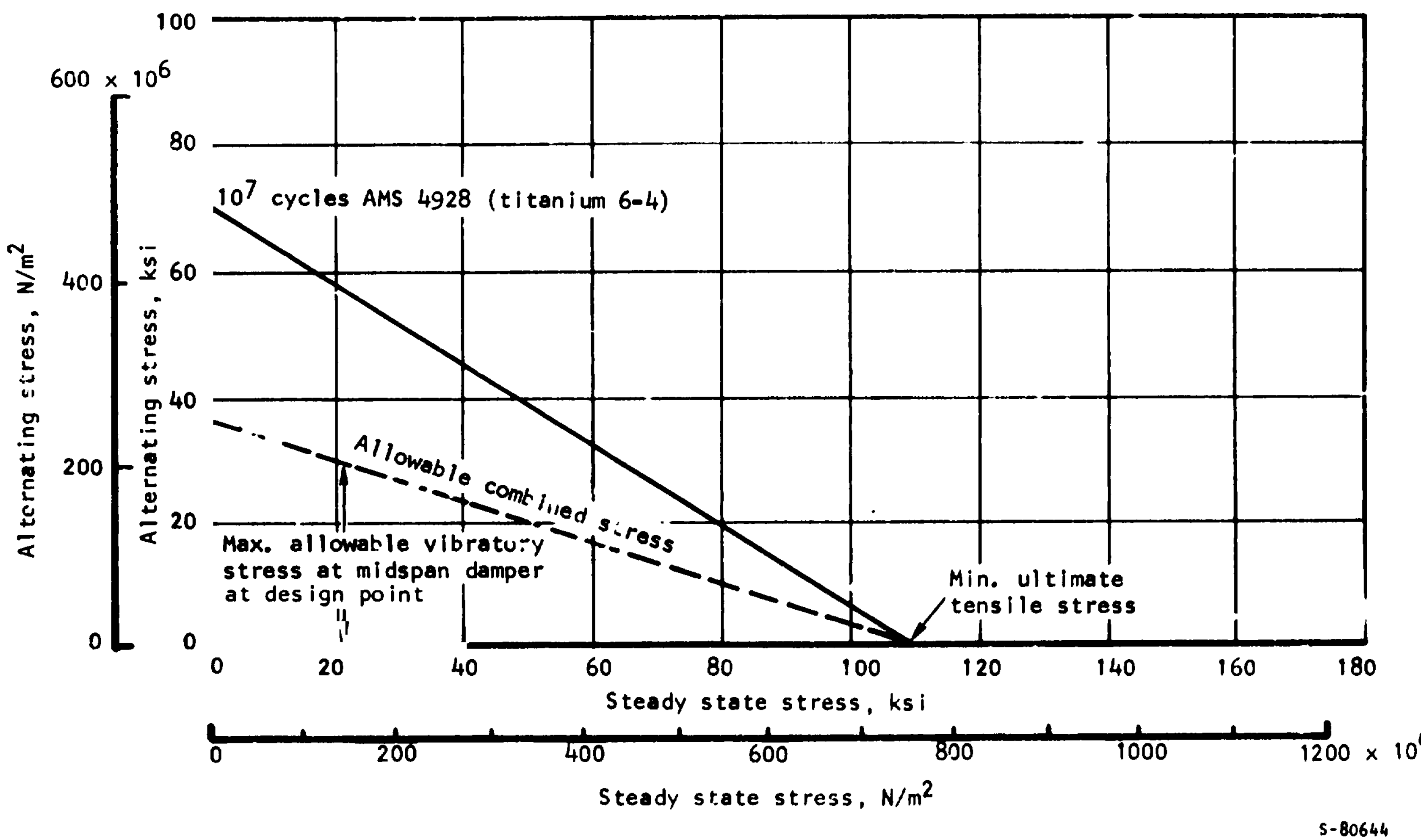

Figure A-10.--Blade Goodman-Solderburg Diagram.

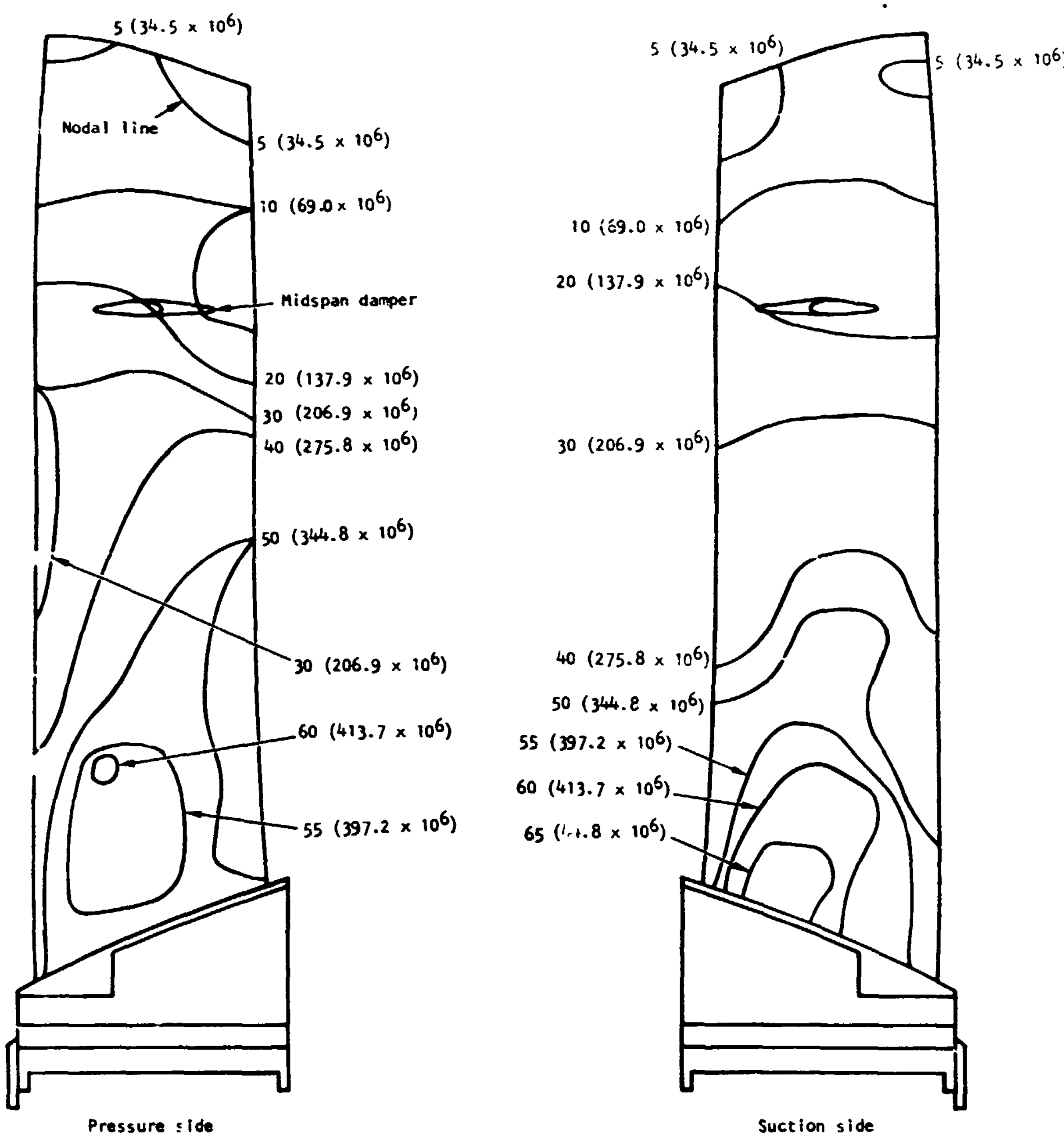

Stresses in ksi (N/m^2)
N = 12 800 rpm (1340.5 rad/sec)
(100%)
Aerodynamic design point loads included

S-71157

Figure A-11.--Fan Blade Equivalent Steady Stress Distribution.

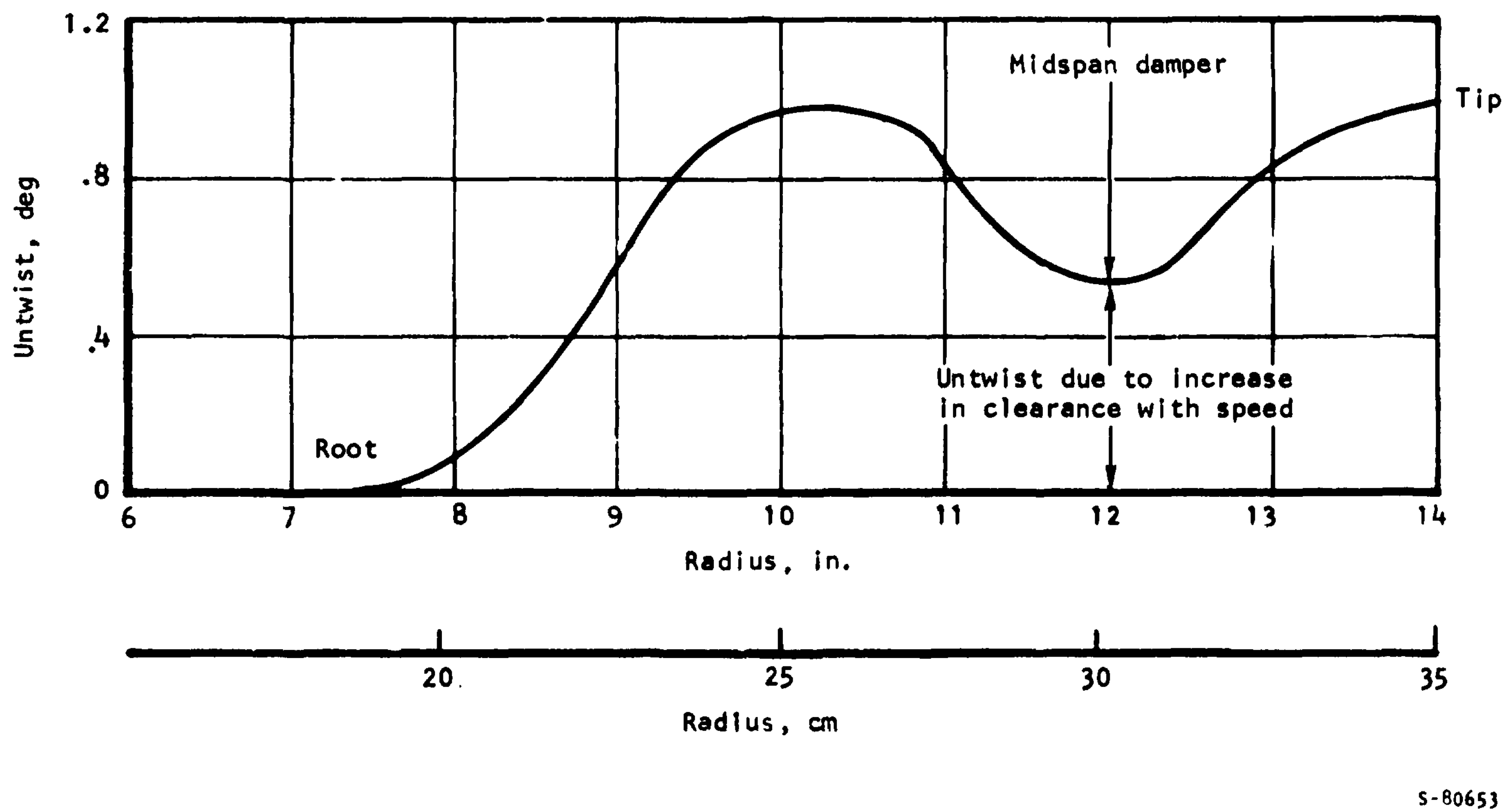

Figure A-12.--Airfoil Untwist at Design Speed.

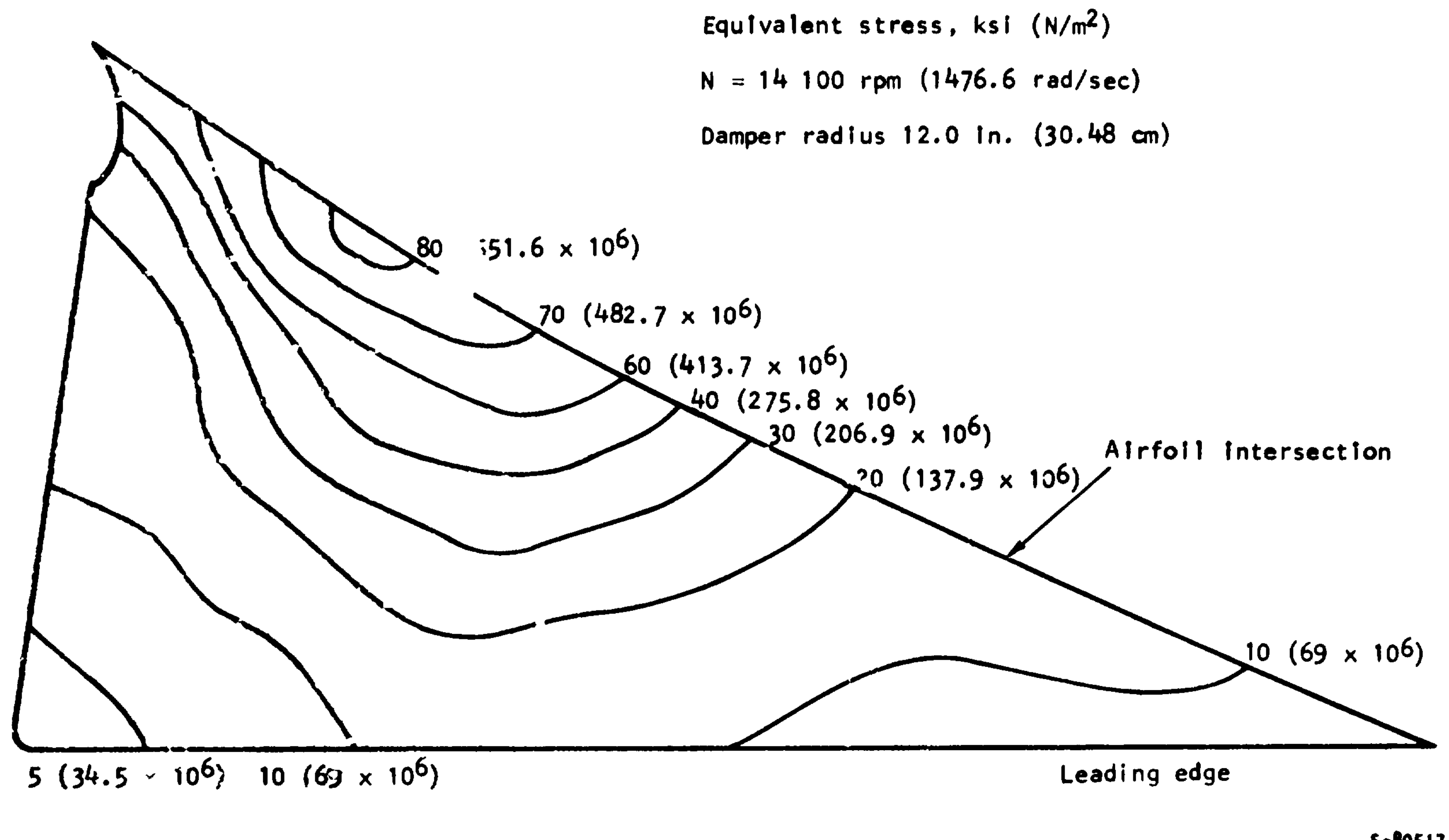

Figure A-13.--Midspan Damper Stress Distribution.

APPENDIX B

SYMBOLS AND PERFORMANCE PARAMETER DEFINITIONS

Symbols

AR	aspect ratio
c	chord, in. (cm)
C_T	blade tip chord, in. (cm)
D	diffusion factor
D-shock	T.E. shock strength - L.E. shock strength, deg
D.I.	distortion index, $(P_{Tmax} - P_{Tmin})/P_{Tmax}$
f_B	first flexure natural frequency, Hz
h_T	relative deflection (translation) of the blade tip mid-chord point in the first flexural mode
i	incidence angle, angle between inlet air direction and line tangent to blade or vane at leading edge, deg
M	Mach number
N	rotational speed, rpm (rad/sec)
P	total pressure, psia (N/cm^2)
p	static pressure, psia (N/cm^2)
r	radius, in. (cm)
SL	streamline number
SM	stall margin, percent
T	total temperature, ^oR (^oK)
t	static temperature, ^oR (^oK)
t_{max}	blade maximum thickness, in. (cm)
U	rotor speed, ft/sec (m/sec)
V	air velocity, ft/sec (m/sec)
V'_T	relative fluid velocity at blade tip, ft/sec (m/sec)

W	weight flow rate, lbm/sec (kg/sec)
X	Carter's rule additive to deviation angle, deg
Z	axial distance, in. (cm)
β	air angle $\left[\cot^{-1}(V_m/V_\theta)\right]$, deg
β^*	metal angle on conical surface between tangent to mean camber line and axial direction at leading and trailing edge, deg
β_M	stagger or chord angle, angle between a chord line and axial direction (measured in a plane parallel to Z-axis), deg
$\Delta\beta$	camber or turning angle, deg
γ	ratio of specific heats for air
δ	ratio of mass average inlet total pressure to standard pressure of 14.696 psia (10.133 N/cm^2)
δ^0	deviation angle, angle between exit air direction and tangent to blade mean camber line at trailing edge, deg
η	efficiency, percent
θ	ratio of inlet total temperature to standard temperature of 518.69^{0}R (288.16^{0}K)
θ_S	circumferential distortion screen relative angle, deg
σ	solidity, ratio of chord to spacing
ϕ	angle between tangent to streamline projected on meridional plane and axial direction, deg
ϕ_T	relative angular deflection of blade tip in first flexural mode, rad
$\bar{\omega}$	total pressure loss coefficient
ω_T	blade tip torsional natural frequency, Hz

Superscripts:

'	relative to moving blades
*	designates blade metal angle

Subscripts:

ad	adiabatic
id	ideal

L.E.	leading edge
M	meridional component
max	maximum
MCL	mean camber line
min	minimum
poly	polytropic
r	radial direction
ss	suction surface
T	denotes stagnation conditions
T.E.	trailing edge
Z	axial direction
θ	tangential component
0	inlet bellmouth screen plane
1	bellmouth instrumentation plane
5	rotor inlet instrumentation plane
5.5	rotor inlet traverse plane
6	rotor leading edge
8	rotor trailing edge
9	rotor exit traverse plane
10	stator leading edge
11	stator trailing edge
12	stage exit plane

Performance Parameter Definitions

i_m incidence angle based on mean camber line

$$i_m = \beta_6' - \beta_6'^{*} \quad \text{(rotor)}$$

$$i_m = \beta_{10} - \beta_{10}^{*} \quad \text{(stator)}$$

δ^o deviation

$$\delta^o = \beta_8' - \beta_8'^* \quad \text{(rotor)}$$

$$\delta^o = \beta_{11} - \beta_{11}^* \quad \text{(stator)}$$

D diffusion factor

$$D = 1 - \frac{V_8'}{V_6'} + \frac{r_8 V_{\theta 8} - r_6 V_{\theta 6}}{(r_6 + r_8)\, \sigma V_6'} \quad \text{(rotor)}$$

$$D = 1 - \frac{V_{11}}{V_{10}} + \frac{r_{10} V_{\theta 10} - r_{11} V_{\theta 11}}{(r_{10} + r_{11})\, \sigma V_{10}} \quad \text{(stator)}$$

$\bar{\omega}$ loss coefficient

$$\bar{\omega} = \frac{\left(P_8'\right)_{id} - P_8'}{P_6' - P_6} \quad \text{(rotor)}$$

where $\left(P_8'\right)_{id} = P_6' \left\{\left[1 + \left(\frac{\gamma - 1}{2}\right)\left(\frac{U_8^2}{a_{01}^2}\right)\right]\left[1 - \left(\frac{r_6}{r_8}\right)^2\right]\right\}^{\gamma/(\gamma-1)}$

and a_{01} = upstream total acoustic velocity

$$\bar{\omega} = \frac{P_{10} - P_{11}}{P_{10} - P_{10}} \quad \text{(stator)}$$

loss parameter

$$\frac{\bar{\omega} \cos \beta_8'}{2\sigma} \quad \text{(rotor)}$$

$$\frac{\bar{\omega} \cos \beta_{11}}{2\sigma} \quad \text{(stator)}$$

η_{poly} polytropic efficiency

$$\eta_{poly} = \frac{\frac{\gamma - 1}{\gamma} \ln\left[\frac{P_8}{P_6}\right]}{\ln\left[\frac{T_8}{T_6}\right]} \qquad \text{(rotor)}$$

$$\eta_{poly} = \frac{\frac{\gamma - 1}{\gamma} \ln\left[\frac{P_{11}}{P_{10}}\right]}{\ln\left[\frac{t_{11}}{t_{10}}\right]} \qquad \text{(stator)}$$

$$\eta_{poly} = \frac{\frac{\gamma - 1}{\gamma} \ln\left[\frac{P_{12}}{P_5}\right]}{\ln\left[\frac{T_{12}}{T_5}\right]} \qquad \text{(stage)}$$

η_{ad} adiabatic efficiency

$$\eta_{ad} = \frac{\left[\frac{P_8}{P_6}\right]^{\frac{\gamma-1}{\gamma}} - 1}{\left[\frac{T_8}{T_6}\right] - 1} \qquad \text{(rotor)}$$

$$\eta_{ad} = \frac{\left[\frac{P_{12}}{P_5}\right]^{\frac{\gamma-1}{\gamma}} - 1}{\left[\frac{T_{12}}{T_5}\right] - 1} \qquad \text{(stage)}$$

SM stall margin

$$SM = \left[\frac{\left(\dfrac{P_{12}/P_5}{W\sqrt{\theta}/\delta}\right)_{\text{at stall}}}{\left(\dfrac{P_{12}/P_5}{W\sqrt{\theta}/\delta}\right)_{\text{at reference point}}} - 1 \right] \times 100\% \qquad N/\sqrt{\theta} = \text{constant}$$

For absolute values of stall margin, the reference point at any speed and inlet flow condition (whether uniform or distorted) is defined as the intersection of a particular speed line with the constant throttle line passing through design pressure ratio at design speed obtained with uniform inlet flow.

REFERENCES

1. Wright, L. C.; Vitale, N. G.; Ware, T. C.; and Erwin, J. R.: High-Tip-Speed, Low-Loading Transonic Fan Stage (Part I-Aerodynamic and Mechanical Design). NASA CR-121095, AiResearch 72-8421, April 1973.

2. Bailey, E. E.: Preliminary Performance of a Low Loading High Tip Speed Fan Stage. NASA TMX-68027, March 1972.

3. Erwin, J. R., and Vitale, N. G., Rotor Design of a High-Tip-Speed Low-Loading Transonic Fan. AIAA Paper No. 72-83, January 1972.

4. Ware, T. C.; Kobayashi, R. J.; and Jackson, R. J.: High-Tip-Speed, Low-Loading Transonic Fan Stage (Part 2-Data Compilation). NASA CR-121262, AiResearch 73-9487, Feburary 1974.

5. Wuerker, R. F.; Kobayashi, R. J.; Heflinger, L. O.; and Ware, T. C.: Application of Holography to Flow Visualization within Rotating Compressor Blade Row, Final Report. NASA CR-121264, AiResearch 73-9489, February 1974.

6. ASME Research Committee of Fluid Meters: Fluid Meters - Their Theory and Application. Fifth Edition, American Society of Mechanical Engineers, New York, N.Y., 1959, p. 47.

7. Carta, F. O.: Coupled Blade-Disk-Shroud Flutter Instabilities in Turbojet Engine Rotors. ASME Paper No. 66-WA/GT-6, December 1966.